
GCOS Reference Upper-Air Network

*GRUAN Technical Document 8*

# GRUAN characterisation and data processing of the Vaisala RS41 radiosonde

Michael Sommer, Christoph von Rohden, Tzvetan Simeonov, Peter Oelsner, Tatjana Naebert, Gonzague Romanens, Hannu Jauhiainen, Petteri Survo, Ruud Dirksen

***Publisher***

GRUAN Lead Centre

***Number & Version***

GRUAN-TD-8
1.0.0 (2023-06-28)

# Document info

*Title:* GRUAN characterisation and data processing of the Vaisala RS41 radiosonde

*Topic:* Radiosonde

*Authors:* Michael Sommer[1], Christoph von Rohden[1], Tzvetan Simeonov[1], Peter Oelsner[1], Tatjana Naebert[1], Gonzague Romanens[2], Hannu Jauhiainen[3], Petteri Survo[3], Ruud Dirksen[1]

*Affiliations:*
[1] GRUAN Lead Centre, Lindenberg Meteorological Observatory, Deutscher Wetterdienst, 15848 Tauche, Germany
[2] MeteoSwiss, Payerne, Switzerland
[3] Vaisala Oyj, 01670 Vantaa, Finland

*Publisher:* GRUAN Lead Centre, DWD

*Document type:* Technical Document

*Document number:* GRUAN-TD-8

*Page count:* 206

*Version:* 1.0.0 (2023-06-28)

# Abstract

The Vaisala RS41 radiosonde is used for operational atmospheric observations within the Global Climate Observing System (GCOS) Reference Upper-Air Network (GRUAN). It is in use since 2014 and currently in operation at more than 15 GRUAN sites with approximately 800 soundings per month, and thus contributes significantly to the volume of GRUAN observational data. The network was established with the ambition to provide atmospheric measurements of Essential Climate Variables (ECVs) and other variables with reference quality. Beside the use of appropriate instruments that are capable of meeting the reference criteria, data products are developed in GRUAN (GRUAN Data Products, GDPs) which are based on raw data and include high quality, reference-level product data of the variables measured by the instrument together with uncertainty estimates.

This document collects technical information on the construction and working principles of the RS41 radiosonde and its sensors, provides information on the software and hardware equipment, and provides guidance on the practice for the routine preparation and conduction of soundings with attention to the requirements in GRUAN. The pre-launch procedures at the ground include the full implementation of manufacturer-prescribed ground checks before per-

forming independent checks of humidity, temperature and pressure in stabilised environments (Standard Humidity Chamber, SHC) as part of a GRUAN sounding preparation to verify the manufacturer calibration. No corrections are applied based on these GRUAN ground checks. However, the results may contribute to the uncertainty budget.

Furthermore, comprehensive information is presented on the GRUAN-developed processing of the raw data coming from the sensors for temperature, water vapour, pressure, and GPS, and leading to the final product variables (air temperature, relative humidity, pressure, altitude, wind speed and wind direction, and further derived variables) in its first version (RS41-GDP.1). The information applies to all sub-variants of the RS41 radiosonde, as the types of installed sensors are the same. The processing includes algorithms based on results from extensive laboratory experiments that have been performed to characterise the physical sensors with respect to the quantification of systematic biases. The most important of these biases are the solar radiative warming of the temperature sensor and the strong increase of relative humidity sensor response time at low temperature. The current data product version (RS41-GDP.1) focuses on the ascent part of radiosoundings until the balloon bursts, i.e. descent data are not included in the GRUAN Data Product (GDP).

An important component of the processing and therefore of the RS41-GDP.1 is the estimation of uncertainties which is done for each measured variable, vertically resolved, and combining them in a consistent way following the guidelines in the Guide to the Expression of Uncertainty in Measurement (GUM) when deriving final magnitudes (*JCGM*, 2008).

Each uncertainty component contributing to the combined final uncertainty of the actual variable is assigned a correlation property. Three correlation types are used, namely ‘uncorrelated’, ‘spatially correlated’, and ‘temporally correlated’. Although the strength of correlations is generally variable, a simplistic approach assigns a complete degree of correlation for the two correlated types, i.e. corresponding to a correlation coefficient of $r = 1$, and no correlation ($r = 0$) for the uncorrelated. This assignment is based on assumptions rather than on substantial covariance analyses. The correlated and uncorrelated uncertainties are, together with the product variables and their combined estimated uncertainties, stored in the provided GDP files. With this concept, the user is offered the way to include the effect of correlations of uncertainties on a rough level according to specific needs of an analysis or study using the RS41 data.

The GRUAN data processing system (GDPS) for radiosondes ingests calibrated raw data together with a set of metadata. It is clearly structured, easily configurable and modular, and as such also designed to be adaptable to other radiosonde models. This document summarises information on the format and extent of the input data, the processing steps, and some basic information on the composition of the RS41-GDP.1 output files in NetCDF format.

# Editor Remarks

Reference herein to any specific commercial product, process, or service by trade name, trademark, manufacturer, or otherwise, does not constitute or imply its endorsement by GRUAN.

## Acknowledgements

A big thank you to Alessandro Fassò, Bruce Ingleby, and Daniel Brewer for the comprehensive and very helpful reviews of the document. The authors also wish to thank the technical staff at Lindenberg Meteorological Observatory (Rico Tietz, Susanne Körner, Helge Friedrich, and Marion Fiedler-Krüger) for their tireless support with building and operating the experimental setups and carrying out numerous measurements which were essential for the GRUAN RS41 data product development.

## Contacting GRUAN Lead Centre

Please contact the GRUAN Lead Centre (gruan.lc@dwd.de) in case of questions or comments in relation to this document, or in relation to GRUAN's use of Vaisala RS41 Radiosonde data. If appropriate, the Lead Centre will redirect requests to the Task Team Radiosondes (tt-radiosondes@gruan.org).

## Revision history

| Version | Author / Editor | Description |
|---|---|---|
| 1.0.0 (2023-06-28) | Michael Sommer,<br>Christoph von Rohden,<br>Tzvetan Simeonov,<br>Peter Oelsner,<br>Tatjana Naebert,<br>Gonzague Romanens,<br>Hannu Jauhiainen,<br>Petteri Survo,<br>Ruud Dirksen | First published version as GRUAN Technical Document 8 (GRUAN-TD-8) |

# Table of contents

## Appendix

# 1 Introduction

## 1.1 Motivation

The great scientific need for long-term and regular global observations of Essential Climate Variables (ECVs) of high quality in the troposphere and lower stratosphere led to the establishment of GCOS Reference Upper-Air Network (GRUAN) (*Seidel et al.*, 2009; *Bodeker et al.*, 2016). Temperature, pressure and water vapour concentration at altitudes between (0 to 40) km belong to the priority-1 ECVs, as defined in the GRUAN Implementation Plan (*GCOS-134*, 2009), while wind speed and wind direction are defined as priority-2 ECVs.

The Vaisala RS41 radiosonde is, similar to most other recent models, designed to measure temperature and relative humidity with dedicated sensors, as well as height, wind direction, wind speed, and pressure using the on-board GPS receiver. The model variant RS41-SGP is equipped with a pressure sensor for direct pressure measurements. The RS41 has been in operational use for several years at a number of GRUAN stations, at some of them as the successor of the Vaisala RS92 model.

GRUAN measurement sites aim to provide measurements with reference quality using radiosondes and other in-situ and remote sensing instruments. GRUAN aims at meeting the following criteria by the data products for each of the instruments used in the network (*GCOS-226*, 2019):

- Extensive collection of metadata,
- Use of well-documented and open processing and correction algorithms,
- Comprehensive estimates of the measurement uncertainty for each data point, i.e. vertically resolved,
- Traceability to SI-units or internationally accepted standards.

High temporal and thus vertical resolution is necessary to fulfil the requirements for long-term trend analyses in a reference network. Together with observations from aircraft and drop sonde measurements, radiosonde balloon launches are the only in-situ measurement with the advantage of high vertical resolution and close-to-real-time data availability.

The RS41 has become an important instrument for the GRUAN, since it complies fully with all of the above criteria. The GRUAN Lead Centre (LC) developed an automatic processing routine, the output of which is a GRUAN data product (GDP), containing reference quality profiles for temperature, humidity, pressure, altitude, and wind, further derived magnitudes, as well as comprehensive metadata. It is intended that all RS41 launches performed by any GRUAN station can be fully processed as RS41-GDP.

The RS41-GDP is a purely bottom-up approach, which means that the final results do not rely on comparisons to other instruments. The product has reference quality in the sense that it only relies on SI-traceable calibration and corrections with specified uncertainties. The product is

subject to ongoing extensive validation, e.g. by comparison with other reference data, as a basis for further development and improvement.

This document is intended as description and reference for the GRUAN-processing and the algorithms used therein including the uncertainty evaluation. The document furthermore represents a source for general technical information and provides background documentation and guidance for the operational use of the sonde in GRUAN.

Chapter 2 provides information on the RS41 radiosonde system hardware, the sensors working principles and construction, as well as the Vaisala Sounding System MW41. Chapters 3 and 4 are specifically dedicated to the description of GRUAN activities such as experimental work to characterise the instrument and determine systematic sensor effects and corrections, the results of which are quantitatively implemented in the GDP. Chapter 5 summarises the traceability chains for the temperature, relative humidity, pressure, and Global Positioning System (GPS) measurements done with the RS41. Chapter 6 outlines the concept of estimation and propagation of measurement uncertainties related to the GRUAN processing of the radiosonde raw data, which are described in detail in the respective Chapters 3 and 4. Sources and combination pathways of uncertainty components are presented in detailed graphical charts, individually for the most important variables temperature, relative humidity, and pressure. An important new feature is a simple but consistent scheme of assigning correlation properties (either no correlation or 'complete' correlation) to the main uncertainty components, which are also provided in the product files. Chapter 7 provides technical and background information on the data processing system and the data management. A more detailed description of the structure and contents of the GDP data files is available in *Sommer et al.* (2022) which can be downloaded from the GRUAN web site (https://www.gruan.org).

## 1.2 Instrument heritage

In the early 1930's, Vilho Väisälä has done pioneering work in the development of radiosonde technology. He launched the first Finnish radiosonde in December 1931. Continuing with his work, he founded the Vaisala company in 1936, and started production of the world's first commercial radiosonde. Later in 1981 the RS80 radiosonde was introduced with major breakthroughs in the design. It was small, lightweight, and used a compact sensor boom with integrated small-size temperature sensor and polymer humidity sensor with purely electrical measurement technology, i.e. without any mechanical parts (*Jauhiainen et al.*, 2014).

After the introduction of the RS80 model, a further major step in Vaisala's continuous work on radiosondes was the development of the RS90 up to the RS92 generation models, the latter of which introduced in 2003. It was equipped with a thin-wire capacitive temperature sensor, a silicon pressure sensor, and a twin humidity sensor, which was capable of preventing sensor icing in freezing sounding conditions with the help of an active sensor heating. The RS92 radiosonde was the first using a GPS receiver for position and wind measurements. The RS92 was used as the benchmark radiosonde model within the GRUAN since its establishment in 2007. The first radiosonde GRUAN data product (GDP) was published for the RS92 in 2012 (*Dirksen et al.*, 2014). Almost 65 000 RS92 launches were performed at GRUAN sites, and are stored in the GRUAN data archive.

The most recent model RS41 was introduced by Vaisala in 2013. The RS41 in recent years

largely replaced its RS92 predecessor model and is currently a market leader. It uses state-of-the-art sensor technology and advanced correction methods (Section 2.1.3): platinum resistor based technology for the temperature sensor, humidity sensor chip which combines a capacitive polymer sensor with a temperature sensor and a continuously active heating element, GPS single-frequency receiver for height, wind and pressure derivation, silicon-based pressure sensor (in case of the RS41-SGP model variant), high level of quality control throughout manufacturing and calibration and pre-launch automatic ground checks (*Vaisala*, 2017c).

## 1.3 The role of the RS41 radiosonde in GRUAN

To date, radiosounding is the most significant and widespread measurement method in GRUAN. Many GRUAN sites have chosen the RS41 as their operational radiosonde, and the measurement data (manufacturer product) are delivered to the WMO data network in near real time. The RS41 measurements are often embedded in WMO-schedules for regular messages to Global Telecommunication System (GTS) for National Weather Forecast (NWF).

The sounding programs vary in scope among the GRUAN sites. Regular flights are performed at least weekly and up to 4 times daily (and up to 8 times daily during intensive campaigns). Section 3.3 provides more information about scheduling.

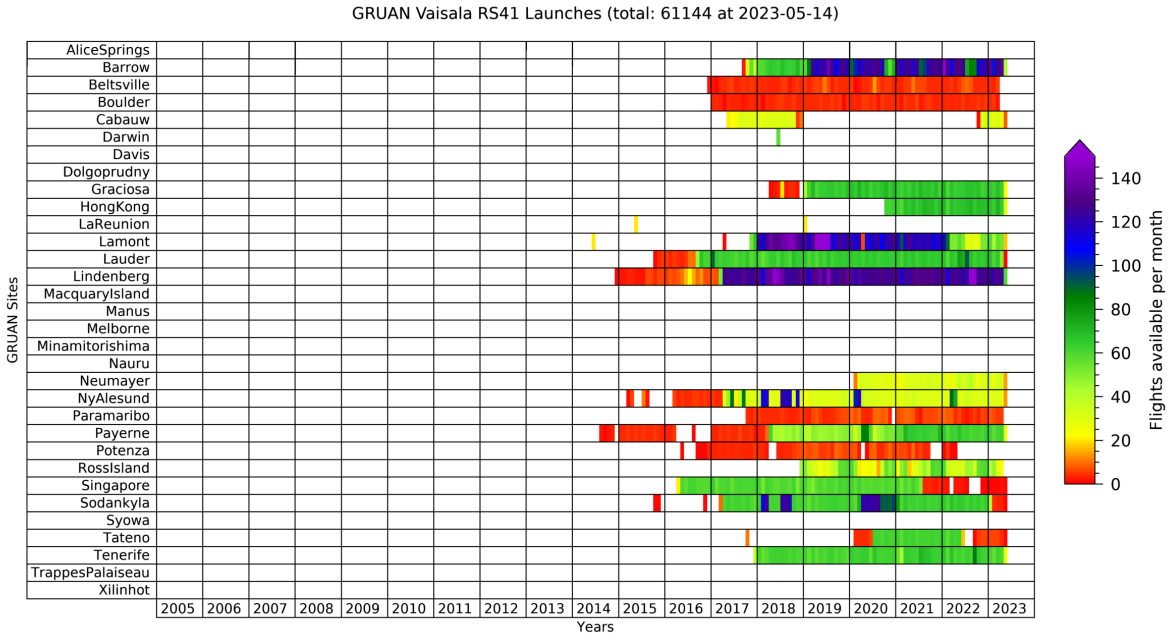


**Figure 1.1:** GRUAN-archived RS41-soundings by 14 May 2023

Currently (Spring 2023), the RS41 model family is the most frequently used radiosonde in GRUAN (see Figure 1.1). Approximately 800 out of 1200 soundings per month, i.e. about two thirds of all radiosoundings, are performed using the RS41. The RS41 thus takes over the role of its predecessor, the RS92, as a benchmark sonde.

The RS41 is used in most regions worldwide as operational radiosonde at GRUAN sites in the Arctic (e.g. Barrow, Ny-Ålesund), northern mid-latitude (e.g. Lamont, Lindenberg, Tateno), the

tropics (e.g. Hong Kong, Singapore), southern mid-latitude (e.g. Lauder), and the Antarctic (e.g. Neumayer, Ross Island). A certification of further measurement sites for GRUAN is intended, especially in Africa and South America, for better global coverage on all continents.

GRUAN data management is largely determined by the extensive radiosonde measurement programme. The data flow structures for the RS41 radiosonde are fully implemented and have been in operation for years. The data flow can therefore be integrated easily into the existing data management in GRUAN.

After an RS41 sounding has been performed at a GRUAN station, a complete set of measurement data (including raw data) and metadata is transmitted operationally to the Lead Centre (LC). The Lead Centre (LC) makes technical documentation, instructions and guidelines available to the sites and provides software tools for data upload to GRUAN (RsLaunchClient, gtRsl). The Lead Centre (LC) is responsible for the data storage and management including data dissemination. Due to its function as a processing centre for the RS41, the Lead Centre (LC) also takes care of QC/QA as part of the GRUAN processing. See Chapter 7 for more information about data management and data processing related to the RS41.

At present, the RS41-GDP.1 is the third GRUAN data product (GDP) for a radiosonde following those for the Vaisala RS92 (RS92-GDP.2) (*Dirksen et al.*, 2014) and the Meisei RS-11G (RS-11G-GDP.1) (*Kizu et al.*, 2018).

GRUAN RS41 data have been used in a considerable number of scientific studies and applications, see e.g. https://www.gruan.org/documentation/articles:

- Climatological time series in the upper atmosphere
- Comparisons with satellite measurements and data products
- Comparisons with ground based measurement systems
- Comparisons with other radiosonde models
- (and much more).

The RS41 is also widely used in other measurement networks such as GCOS Upper-Air Network (GUAN) and therefore generally takes a correspondingly large share of available radiosonde measurement data.

## 1.4 Terminology

The following list reflects some general definitions of relevant metrological terms from the International Vocabulary of Metrology (VIM) (*JCGM*, 2012) to which this document refers.

**True value**: Value consistent with the definition of a quantity that would be obtained by an imaginary perfect measurement. In practice, true values are unknowable.

**Measurement accuracy**: Closeness of agreement between a measurement result and a true quantity value of the measurand as a result of the always existing imperfections of measurement. Note that measurement accuracy is a concept, not a quantity with a given numerical quantity value. A measurement is said to be more accurate when it offers a smaller deviation from a reference (measurement error).

**Measurement precision**: The closeness of agreement between values obtained by replicate

measurements on the same measurand under specified conditions. It is used to define measurement repeatability, intermediate measurement precision, and measurement reproducibility and is usually expressed numerically by measures of imprecision, such as standard deviation, variance, or coefficient of variation.

**Repeatability**: Measurement precision under conditions of measurement that involves the same measurement procedure, same operators, same measuring system, same operating conditions and same location, and replicate measurements on the same measurand over a short period of time.

**Reproducibility**: The measurement precision under conditions of measurement of the same measurand that includes different locations, times, operators, measurement procedures and measuring systems. A specification should give the conditions changed and unchanged, to the extent practical.

**Measurement uncertainty**: A parameter, associated with the result of a measurement, which characterises the dispersion of the values attributed to the measurand. In general it is a combination of many components which are either of statistical nature (Type A evaluation), or come from other – also systematic – sources (Type B evaluation). That is, it is a stated quantity which can be reasonably attributed the resulting value of a measurement.

**Measurement error**: Difference of a measurement result and a reference quantity value. The measurement error is known when the measured quantity value is compared to calibrated reference quantity value with negligible measurement uncertainty or if compared to a conventional quantity value.

**Systematic measurement error**: Component of measurement error that in replicate measurements remains constant or varies in a predictable manner. It results from systematic effects that do not average to zero as the number of measurements increases. If a systematic measurement error is known, a correction can be applied. The term 'bias' is often used for a systematic measurement error.

**Random measurement error**: Component of measurement error that in replicate measurements varies in an unpredictable manner. A reference quantity value for a random measurement error is the average that would ensue from an infinite number of replicate measurements of the same measurand. Random measurement errors of a set of replicate measurements form a distribution that is characterised by its expectation, which is generally assumed to be zero, and its variance. Random measurement error and systematic measurement sum up to the overall measurement error.

**Stability**: Stability refers to the consistency of random measurement errors and systematic measurement errors with time. Undetected changes in systematic measurement errors induce artificial trends in measurement time series.

**Coverage factor**: Combined standard uncertainties $u_c(y)$ can in principle be used universally to express the uncertainty of a measurement result. In a number of areas of life there is the requirement to give a measure of uncertainty that defines an interval about the measurement result that may be expected to encompass a larger fraction of the distribution of values that could reasonably be attributed to the measurand (Chapter 6 in *JCGM*, 2008). To account for this, the term *expanded uncertainty* ($U$) is introduced, calculated by multiplying the combined

standard uncertainty $u_c(y)$ by a *coverage factor* $k$:

$$U = k u_c(y). \tag{1.1}$$

The measurement result is then $Y = y \pm U$, with $y - U \leq Y \leq y + U$ an interval that may be expected to encompass a large(r) fraction of the distribution of values for $Y$. The value of $k$ is chosen on the basis of the required application dependent level of confidence of the interval $y - U$ to $y + U$. In general, $k$ will be in the range 1 to 3. For GRUAN the use of $k = 2$, according to a confidence level of 95.45 % for normally distributed measurement errors, is advised for uncertainties in product data and metadata files of GDPs, as well as in product documentation (*GCOS-171*, 2013). Wherever it helps to avoid confusion, $k$-values should be indicated when reporting uncertainties. To avoid further confusion when dealing with relative humidity, which is designated in this document with the symbol $U$, the lower-case letter $u$ is also used for the *expanded uncertainty*.

# 2 Instrumentation

This chapter discusses the RS41 radiosonde system hardware. Section 2.1 describes the sensors on board the radiosonde and Section 2.2 describes the Vaisala Sounding System MW41.

## 2.1 RS41 radiosonde

The Vaisala RS41 is a family of closely related radiosondes. The **RS41-SG** is the base model and is the most commonly used within GRUAN. The SG model is equipped with a sensor boom for measuring temperature (see Section 2.1.3.1) and humidity (see Section 2.1.3.2), while pressure and location-derived observations are acquired using the on board GPS antenna and receiver (see Section 2.1.3.4), situated within the radiosonde housing.

The **RS41-SGP** is an extended version of the RS41-SG with an included dedicated pressure sensor (described in Section 2.1.3.3).

The **RS41-SGM** is another version of the RS41-SG model, where the start of the radiosonde transmission is from a specifically defined height. Further on, the transmitted data from the radiosonde is encrypted. These features follow guidelines of specialised customers with higher security requirements. The RS41-SGM doesn't include a pressure sensor.

The **RS41-D** is a version of the RS41-SGP model, designed to work in synergy with the Vaisala RT20 Radiotheodolite. The RS41-D variant lacks the GPS antenna and receiver, which are standard for the other radiosondes on the RS41 platform. Its main purpose is passive windfinding for artillery and other tactical operations.

Additionally, any of the above-mentioned models of radiosondes on the RS41 platform can be connected to additional sensors through the XData protocol for reference measurements of humidity, ozone or other atmospheric parameters (described in Section 2.1.2).

All models within the RS41 radiosonde platform share the same sensor boom and housing.

### 2.1.1 Sonde construction

The RS41 radiosonde consists of a sensor boom connected to an electronic board, which is powered by an attached Li-battery pack, and mechanically and thermally protected by an EPS foam housing. The antenna, connected to the opposite end of the board, consists of a trailing thin wire (see Fig. 2.1). The radiosonde is suspended to the unwinder string in such a way that the sensor boom points sideways up from the body when the radiosonde is ascending. The standard unwinder is equipped with a 55 m long thin non-UV treated polypropylene string.

Figure 2.1 shows the RS41-SGP in the two existent hard plastic cover and soft shell versions

(see below). Table 2.1 lists basic technical specifications as given in the data sheets for RS41-SGP.

Further manufacturer specifications on the measurement performance (uncertainties) are given in Table 2.2 in Section 2.1.4.


**Figure 2.1:** RS41-SGP radiosonde. Model with hard-plastic cover (back), and Soft & Light version with EPS foam material housing (since October 2017) (front).

The sensor boom (see Fig. 2.2) is around 11 cm long and 1.5 cm wide. It contains the temperature (Section 2.1.3.1) and humidity (Section 2.1.3.2) sensors of the radiosonde. Except for the humidity sensor chip, the entire sensor boom including the temperature sensing element is covered with a highly reflective aluminium coating to minimise undesired thermal effects, especially warming by short-wave solar radiation or IR radiative cooling. The coating also has hydrophobic properties. Especially in terms of the temperature sensor element, this lowers the risk for wetting during passage of water clouds and a subsequent temperature 'contamination' due to evaporative cooling.

During soundings, the boom is bent at an angle of about 45° away from the sonde body, with the sensitive side of the humidity chip pointing downwards against the direction of the air flow. The angle is intended to optimise the measurement performance with regard to two opposing effects: On the one hand the surface of the sonde housing as seen from the sensors should be as low as possible to minimise radiative effects that are connected with the sonde housing. On the other hand, an effective ventilation of the sensors should be ensured especially for humidity.

The housing of the radiosonde is approximately 15 cm long, 6 cm wide, and 4.5 cm thick. It contains the main integrated board of the radiosonde, as well as the battery pack and the optional pressure sensor board. The data logger, radio transmitter and antenna and the GPS antenna and receiver are directly soldered to the main integrated board of the radiosonde. The sensor boom is attached to the main board through a detachable connector. The trailing side of the housing has an opening for the XData port of the radiosonde and for the circa 13 cm long telemetry antenna. The LED indicator light is situated at the bottom of the front panel of the radiosonde along with the power button.

In 2017 Vaisala modified the casing of the RS41 radiosonde by changing from a hard-plastic

**Table 2.1:** Basic technical specification as given in Vaisala data sheets for RS41-SGP (*Vaisala*, 2015b, 2020e).

| RS41-SGP | Hard plastic cover | Soft shell |
|---|---|---|
| **Telemetry** | | |
| Transmitter type | Synthesised | |
| Tuning range | (400.15 to 405.99) MHz | |
| Maximum transmitting range | up to 350 km | |
| Frequency stability, 90 % probability | ±2 kHz | |
| Deviation, peak-to-peak | 4.8 kHz | |
| Emission bandwidth | According to EN 302 054 | |
| Output power (high-power mode) | min. 60 mW | |
| Sideband radiation | According to EN 302 054 | |
| Data downlink | 4800 bit/s | |
| Frequency setting | Wireless with ground check device | |
| **GPS receiver (SA Off, PDOP<4)** | | |
| Number of channels | ≤48 | |
| Frequency | 1575.42 mHz, L1 C/A code | |
| Cold start acquisition time | 35 s (nominal) | |
| Reacquisition time | 1 s (nominal) | |
| Correction | Differential | |
| Reporting resolution of lat, lon pos. values | $(1.0 \times 10^{-8})°$ | |
| **Operational Data** | | |
| Power-up | Wireless with ground check device or switch | |
| Factory calibration | Stored on Flash memory | |
| Battery | 2 pcs. AA-size Lithium cells | |
| Operating time | >240 min | |
| Weight | 113 g | 84 g |
| Dimensions (without wire antenna, L×W×H) | | |
| Body | (145 × 63 × 46) mm | (155 × 63 × 46) mm |
| Sensor boom bent | (272 × 63 × 104) mm | |
| **Add-on Sensor Support** | | |
| Protocol support | XData to connect several sensors in the same chain, data transferred either directly or via OIF411 to RS41 | |
| Transfer rate | max. 200 byte/s | |

cover to a purely EPS foam material housing (see Fig. 2.1). The intention was to make the sonde body softer (lower risk of injury for people during landing), lighter (less balloon payload, slight reduction of required filling gas; weight reduction is 27 %), and less environmental impact (47 % reduction in the amount of hard plastic). Vaisala states that the change does not have any impact on the measurement performance of the RS41 (*Vaisala*, 2017b). An independent investigation (*NOAA*, 2017), where 10 functional precision tests were conducted with the soft model compared to 33 tests with the hard cover model, found slight differences in the closeness of the sondes to the RS41 specification with regard to pressure, height, and humidity, whereas they were found to be similar when comparing temperature and wind group statistics.

### 2.1.2 Additional sensor support (Xdata)

The RS41-SG and RS41-SGP radiosondes are capable of transmitting data for 'external' sensors or instruments that support the Xdata (data) protocol (*Vaisala*, 2015a; *Wendell and Jordan*, 2016). When connected to the RS41 Additional Sensor Interface, data of the auxiliary sensors are sent to the ground system via the radiosonde telemetry, and the transmitted data are stored in the radiosonde's sounding archive file.

In this way, measurement data can be obtained with instruments for example for ozone partial pressure, particle back-scatter ratio or frost point temperature together with radiosonde profiles. As far as known, the InterMet iMet-1-RSB was the first Xdata-compatible radiosonde. Xdata is one of the iMet-1 external command definitions.

Xdata allows simultaneous operation of one or more additional sensors in an open chain topology where binary data packets in ASCII and hexadecimal ASCII format are handed over to the radiosonde for transmission by chain links from one additional sensor to the next towards the sonde. The bandwidth available with RS41 is 200 B $s^{-1}$ (9600 baud) shared by all connected sensors.

The mechanical interface is a 10-pin double row connector header with 2 mm pin spacing.

In addition to data transmission, the connector also allows the radiosonde be powered externally (*Vaisala*, 2015a; *Oelsner and Tietz*, 2021).

Conversely, connected sensors can also be powered from the radiosonde batteries, e.g. used

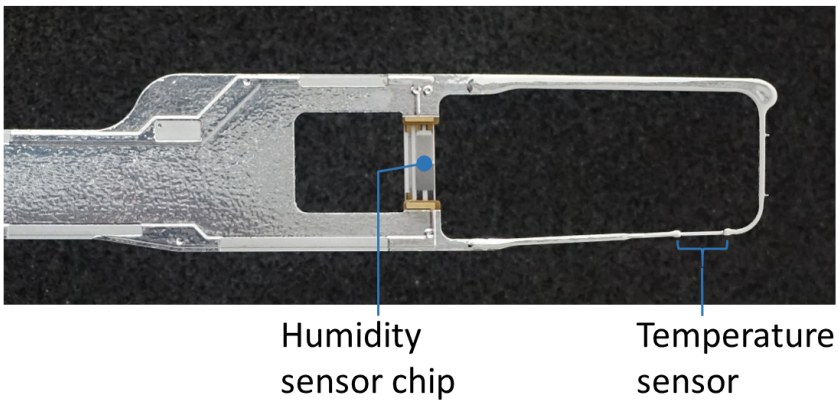


**Figure 2.2:** Sensor boom of RS41 radiosonde.

by the Vaisala Ozone Interface RS41 (OIF411) included in the Vaisala Ozone Interface Kit RS41 (RSA411) for ECC ozone sondes, released and offered in parallel to the RS41 radiosonde family (*Vaisala*, 2019). The OIF411 is equipped with this connector type for additional sensors supporting the iMet-1 connector type because additional sensors may be compatible only with the iMet-1 connector type (4-pin single row, 2.54 mm pin spacing). That is, the OIF411 acts as an adaptor and chain link by forwarding received Xdata packets to the radiosonde in addition to interfacing an ECC.

## 2.1.3 Sensor technology

### 2.1.3.1 Temperature

The Vaisala RS41 temperature sensor is designed and manufactured in-house and uses resistive platinum technology (Pt1000). The measurement signal is the electrical resistance which increases linearly with temperature. The sensor element has dimensions of about 5 mm length and 0.25 mm thickness (see Fig. 2.3). Its response time to changes in temperature is generally a function of ambient pressure, sensor ventilation, and thermal properties of the sensor. Vaisala states 63 %-response times as (0.5, 1.2 and 2.5) s for (1000, 100 and 10) hPa, respectively (*Vaisala*, 2017c). This time-lag is corrected for in the manufacturer's temperature data product by the DigiCORA® Sounding System MW41 with neglectable remaining uncertainty from this effect claimed by Vaisala.

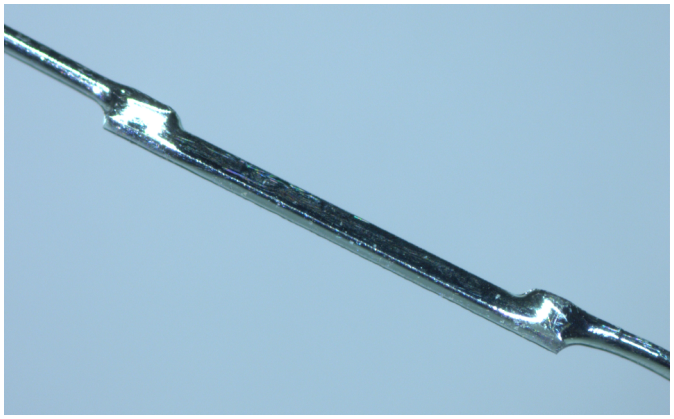

**Figure 2.3:** Macro photo of the Pt1000 platinum resistance temperature sensor of the RS41 radiosonde. The length of the sensor element is about 5 mm.

Vaisala investigated the linearity of the RS41 temperature sensor in laboratory tests (*Vaisala*, 2017c). As a result, an uncertainty related to non-linearity of 0.05 K ($k = 2$) is stated, with no systematic bias in sensor calibration. During these tests, the uncertainty of the reference temperature measurement was 0.04 K ($k = 2$). The results are valid for the temperature range of −98 °C to 39 °C and indicate a strong linearity.

Similar tests have been conducted by Vaisala for temporal sensor stability (*Survo et al.*, 2014; *Vaisala*, 2017c). After calibration and shipment packaging according to standard manufacturing procedures, several sondes were stored under different temperature and humidity conditions and for different time periods up to three years. No systematic drifts were found within the uncertainty related to the drift tests.

Due to the good linearity characteristics and long-term stability, Vaisala claims that a check against an external reference sensor in conjunction with the sounding preparation is not necessary, and accordingly a correction to the temperature during the ground preparation phase does not need to be applied (see also Section 2.2).

#### 2.1.3.2 Humidity

The humidity sensor is based on the widely used capacitive polymer technology. It is developed by the manufacturer and produced in own clean-room facilities.

Capacitive humidity sensors essentially consist of a hydrophilic porous polymer material that is arranged as thin film (thickness $d$) between two flat electrodes (surface area $A$) which form a plate capacitor. These layers are arranged on a glass or ceramic substrate. The polymer exchanges water molecules with the surrounding moist air by diffusion. Depending on the amount of adsorbed water, the effective dielectric constant $\epsilon_r$ of the polymer and therefore the capacitance changes sensitively due to the high relative permittivity (or dielectric constant) of water:

$$C = \epsilon_r \frac{A}{d}. \tag{2.1}$$

This capacity change can be measured as frequency change which serves as a measure for the water vapour content in the air. The capacitance of the polymer measures the relative humidity rather than the absolute water content, because the adsorption-desorption equilibrium changes with relative humidity.

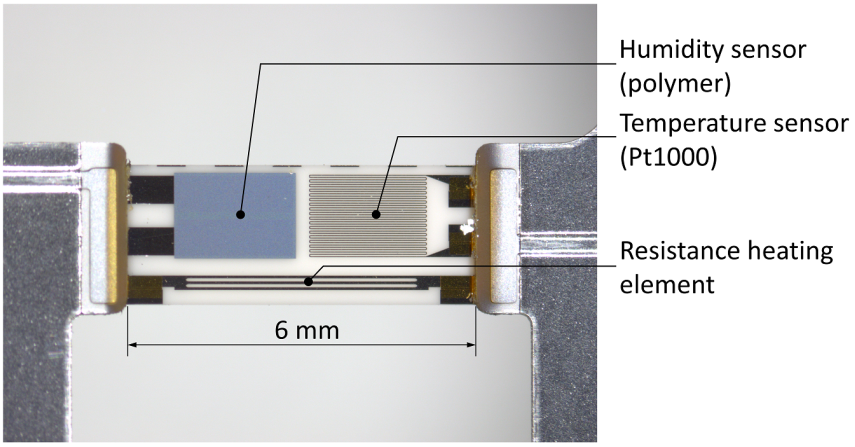


**Figure 2.4:** Humidity sensor chip (Humicap®) of the RS41 radiosonde.

The humidity sensor of the RS41 radiosonde is permanently heated so that its temperature $T_\mathrm{i}$ is kept above the ambient air temperature $T_\mathrm{a}$ at a constant offset of about 5 K. $T_\mathrm{i}$ is measured by a separate temperature sensor. Both the resistance heating element and the temperature sensor are integrated on the humidity sensor chip next to the polymer (see Fig. 2.4). $T_\mathrm{a}$ is measured by the Pt1000 sensor near the tip of the sensor boom. The water vapour partial pressure directly above the surface of humidity sensor, $e_\mathrm{i} = U_\mathrm{i} \cdot e_\mathrm{s}(T_\mathrm{i})$, with $e_\mathrm{s}(T_\mathrm{i})$ the saturation vapour pressure, cannot directly be measured. However, by definition there is saturation at the dew point, i.e. $e_\mathrm{d} = e_\mathrm{s}(T_\mathrm{d})$, and the dew point $T_\mathrm{d}$ of an air parcel does not change with temperature as long as

there are no phase transitions. That is, with the definition of relative humidity,

$$e_{\mathrm{s}}(T_{\mathrm{d}}) = U_{\mathrm{i}} \cdot e_{\mathrm{s}}(T_{\mathrm{i}}). \tag{2.2}$$

The same applies to the environment:

$$e_{\mathrm{s}}(T_{\mathrm{d}}) = U_{\mathrm{a}} \cdot e_{\mathrm{s}}(T_{\mathrm{a}}). \tag{2.3}$$

The relative humidity in the ambient air is therefore

$$U_{\mathrm{a}} = U_{\mathrm{i}} \cdot e_{\mathrm{s}}(T_{\mathrm{i}})/e_{\mathrm{s}}(T_{\mathrm{a}}). \tag{2.4}$$

With the measured values for $T_{\mathrm{i}}$ and $T_{\mathrm{a}}$ and the measured relative humidity above the heated polymer $U_{\mathrm{i}}$ can be directly converted into the relative humidity for the ambient air without the need to determine the dew point $T_{\mathrm{d}}$. Vaisala uses the ITS-90 compatible form of Wexler's formula by *Hardy* (1998) for calculation of the saturation vapour pressure $e_{\mathrm{s}}(T_{\mathrm{i}})$ and $e_{\mathrm{s}}(T_{\mathrm{a}})$ (see Section 4.4.2.1).

This method ensures that the relative humidity detected by the sensor is always kept below the saturation level at which the polymer is potentially prone to 'contamination' with liquid water, and where the calibration is most difficult. Further advantages are the performance improvement at low ambient temperatures with respect to the response time, as well as less susceptibility to direct solar irradiation (no dry bias).

#### 2.1.3.3 Pressure

The pressure sensor directly measures the atmospheric pressure at the current height in a sounding. The RS41 is equipped with a shock-resistant single crystal capacitive silicon sensor element designed by Vaisala (see Fig. 2.6). It is basically the same as used since the Vaisala RS90 series radiosondes, with revised electronics and calibration. A thin pliable silicon diaphragm covering an evacuated cavity is deflected dependent on air pressure and serves as sensing element (*Vaisala*, 2014). A metal coated diaphragm forms a capacitor together with a fixed base electrode (see Fig. 2.5). The deflection is transduced in a capacity change which is calibrated to pressure.

The pressure calibration is dependent on temperature. The dependence of the pressure sensor measurement on temperature is compensated for by using measurement data of a separate temperature sensor on the pressure board.

The pressure sensor of the RS41-SGP radiosonde requires an adjustment against a well calibrated reference barometer during ground preparations (see Section 3.2.2).

#### 2.1.3.4 GPS

The GPS positioning, employed by the RS41/SPS311 system, consists of a base GPS antenna and receiver at the launch site and a rover GPS antenna and receiver on-board the radiosonde. The default GPS setup is designed to provide differential corrections for the positioning of the radiosonde.

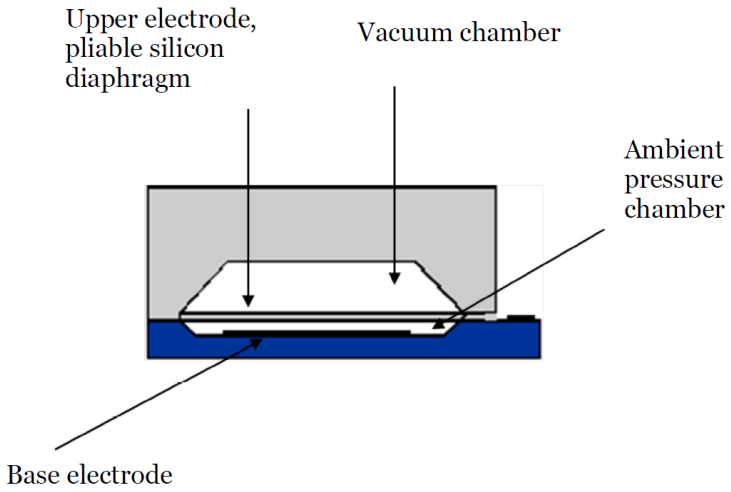


**Figure 2.5:** Pressure sensor construction in Vaisala radiosondes. Figure taken from *Vaisala* (2014).

The RS41-SGP radiosonde is equipped with a single frequency GPS-only u-blox 6 receiver, coupled with an omnidirectional passive patch antenna (*ublox*, 2013b, see also Fig. 2.6). The receiver uses the L1 C/A frequency for positioning and, according to the radiosonde technical documentation, provides vertical accuracy within 10 geopotential meters (*Vaisala*, 2013).

The GPS module used in the Vaisala Signal Processing System SPS311 consists of the same GPS-only u-blox 6 receiver as the one in the RS41 radiosonde, coupled with active single-frequency GPS-only antenna. The antenna is fixed on a mast with the exact position accounted for in the signal processing. The GPS setup of SPS311 is designed to provide differential corrections for the radiosonde. The differential corrections are implemented to the pseudorange measurements from each GPS satellite. The dynamics of the ground-based station coordinates are stored with a resolution of 1 m for the vertical position and 1 cm for the horizontal positioning components.

The GPS receiver on-board the RS41 radiosonde is used not only for positioning, but also for timekeeping. The measurements from the radiosonde are sent to the ground station every GPS second. The receiver stores measured data in a buffer, before outputting pseudorange, Doppler-shift, position and time measurements to the RS41 frame for each measurement instance (GPS epoch).

Key features and specifications of the Vaisala GPS receiver system are listed in the following (*Vaisala*, 2013):

Radiosonde GPS setup:

- The setup consists of the antenna, RF front-end, and the GPS chip. The GPS antenna is a robust, high-sensitive patch antenna,
- RS41 equipped with a u-blox 6 code-correlating GPS receiver; uses the public course acquisition code in the L1 frequency (L1C/A 1575.42 MHz),
- Typical time to first satellite tracking after cold start is 35 s.

Local GPS setup at ground station:

- The Vaisala DigiCora® Sounding System MW41 includes a GPS receiver with a local

GPS antenna at the station.

- The local receiver is a single-frequency code-correlating GPS receiver, similar to the receiver on-board the radiosonde.
- The antenna by default is a Vaisala GPS Antenna GA31.

### GPS-based height and pressure

*Height measurement* Each GPS satellite generates a unique pseudo-random (PRN) code containing the transmission time and satellite position. The GPS receiver calculates the time differences between the transmission and reception of the coded messages and, multiplying by the speed of light, determines the so-called 'pseudorange' distances between the radiosonde and satellites. Pseudoranges from four or more satellites are required to obtain the horizontal and vertical position of the radiosonde. Pseudoranges are not the true ranges, since they include inaccuracies, associated with the state of the neutral and the ionised atmosphere, as well as clock, orbit and relativistic errors.

Raw GPS height is expressed relative to the WGS84 reference ellipsoid model of the Earth. This value is then converted to express height from local Mean Sea Level (MSL), specified in WGS84 using an Earth geoid model. The Vaisala RS41 height above MSL is calculated against the EGM96 geoid, while the GDP for the RS41 radiosonde is calculated against the EGM2008 geoid. MSL height is also converted into geopotential height, which adjusts the MSL height to compensate for gravity variation with latitude and elevation. It is expressed in geopotential meters (gpm).

*Pressure measurement* This technique requires a reference pressure sensor at the sounding station. The pressure-sensor value calibrates all observations in the GPS-derived pressure profile. It is very important to use a properly calibrated reference pressure sensor. Station height parameters, including the height of the pressure sensor and the height of the ground-based GPS antenna, are also essential factors in the calculation. The MW41 system enables configuration of these height parameters. The pressure derivation from height is described in details in Section 4.4.2.1.

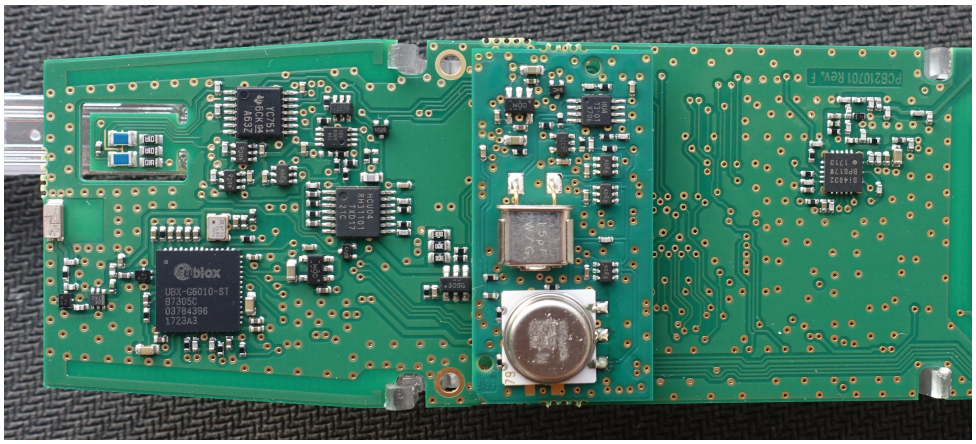


**Figure 2.6:** Back side of the RS41 circuit board, with the u-blox GPS receiver (large black squared chip on the lower left) and antenna and the pressure sensor board attached in the middle.

**Table 2.2:** Basic uncertainty specifications of the Vaisala RS41 radiosonde provided by the manufacturer. The table is reproduced from Table 1.1 in *Vaisala* (2017c). Data is given for $k = 2$ ($2\sigma$-confidence level). Humidity specifications are valid for $T >$–60 °C.

| **RS41 specification** | $p$ / hPa | $T$ / °C | $U$ / % |
|---|---|---|---|
| Uncertainty after ground preparation | | 0.2 | 3.0 |
| Uncertainty in sounding | | | |
| >100 hPa | 1.0 | | |
| 100 hPa to 10 hPa | 0.3 | | |
| <10 hPa | 0.04 | | |
| <16 km | | 0.3 | 4.0 |
| >16 km | | 0.4 | 4.0 |
| Reproducibility in sounding | | | |
| >100 hPa | 0.5 | 0.15 | 2.0 |
| 100 hPa to 10 hPa | 0.2 | 0.3 | 2.0 |
| <10 hPa | 0.04 | 0.3 | 2.0 |

Vaisala states an uncertainty for geopotential height derived from GPS measurements of 10 gpm. For pressure, the values are (1.0, 0.3 and 0.04) hPa for pressure levels of (>100, 100 to 10 and <10) hPa (*Vaisala*, 2013). Both are given for $k = 2$.

#### GPS wind measurement

Apart from the pseudorange observations used for the determination of the location of the radiosonde, the u-blox chip is also observing the Doppler shift of the GPS frequency for every satellite and transmitting these observations to the ground station. These observations are then used by the Vaisala MW41 software for the calculation of horizontal speed of the radiosonde in conjunction with the pseudorange observations, determining location.

Unlike the Vaisala data product, the wind speed in the GDP is based exclusively upon location observations. The procedure is done in two steps:

- Smoothing of obtained latitude/longitude coordinates,
- Calculating the coordinate difference between the measuring instances.

### 2.1.4 Manufacturer calibration and uncertainty specifications

Basic specifications for measurement uncertainties of the key parameters temperature, relative humidity, and pressure (in case of RS41-SGP with installed pressure sensor) are given in Table 2.2. The measurement uncertainty for GPS-derived wind speed is specified as 0.15 m s$^{-1}$, and 2° for wind direction ($k = 2$). Information on manufacturer calibration and the traceability chain can be found in Chapter 5.

More details about the measurement performance are listed in the Vaisala data sheets (*Vaisala*, 2015b, 2020e). They are essentially identical for the hard plastic cover and soft shell sonde

versions. The technical specifications are reproduced in Table 2.1.

## 2.2 Sounding system

The Vaisala Sounding System MW41 (*Vaisala*, 2021c) is designed for receiving sonde data transmitted by telemetry, data processing, data analysis and presentation, archiving, report generation and message distribution (Fig. 2.7). The MW41 system supports all sonde models of the RS41 family (RS41-SG, -SGP, -SGM, -D) as well as the previous generation model RS92-SGP (until software version 2.15). The sounding system for civilian usage consists of:

- The MW41 sounding software that runs on a standard PC with Microsoft Windows® operating system.
- The Vaisala Sounding Processing Subsystem SPS311G including a GPS module, e.g. a u-blox 6 single-frequency module, connected to the PC over Local Area Network (LAN).
- A radiosonde telemetry antenna, e.g. the directional type Vaisala RB31 or the omnidirectional types Vaisala RM31N or RM32.
- A GPS antenna, e.g. Vaisala GA31 or GA41 enhanced multi-path rejection antenna.
- A RI41 radiosonde interface for applying sonde checks and initialisation, including a variant RI41-B equipped with a pressure reference sensor (*Vaisala*, 2021b). Any model is connected to the PC using a Universal Serial Bus (USB) link.

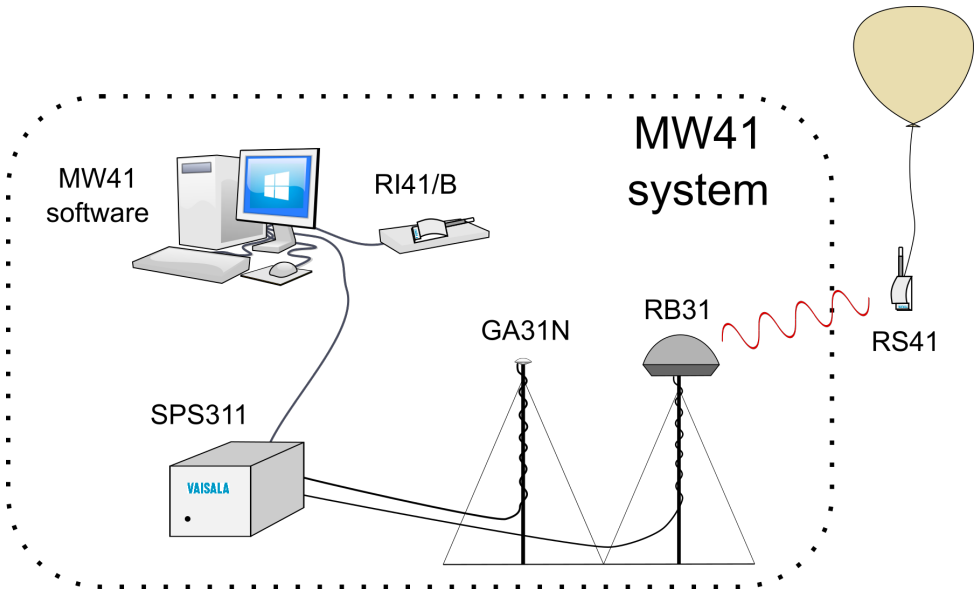


**Figure 2.7:** Example scheme of a RS41/MW41 system. The RS41 radiosonde signals are received by the Signal Processing System (SPS) through the RB31 telemetry antenna. The differential GPS receiver inside the SPS receives data through the GA31N antenna. Both the SPS and the RI41 ground check device are connected to a Windows®-PC, running the MW41 software.

The MW41 sounding software is a multi-service application using an IBM solidDB database for sounding data and application state storage. Depending on the MW41 sounding software version the graphical user interface is either a website hosted by an local Apache Tomcat web

server or an standalone executable. The software comes with standard features and can be supplemented with licensed options, e.g. the Advanced Option and therein the report template editor and generator, scripting with IronPython and descending sounding storage, or the Special Sensor Option including ozone calculation plus graphics and the additional sensor interface feature (Section 2.1.2). A product description and a full list of operational features can be found in *Vaisala* (2020c) that refers to the software version 2.17. Since software version 2.11 the GRUAN support is added to the standard features and makes RS41 humidity and temperature readings of the humidity sensor accessible through the sounding archive file (MWX). See Section 7.2.1 for details about the MWX format.

For individual data processing and formatting tasks, e.g. real time decoding of additional sensor data, an IronPython version 2.7 script interpreter (*Vaisala*, 2020a) with access to data, event and message services of the MW41 sounding software is implemented as licensed option. Such scripts are called automatically by the MW41 sounding system startup, per sounding or as external calls from users or batch processes. The ECC ozone sonde processing functionality of the MW41 sounding software is relying on that feature and is invoked per sounding.

The SPS311G Sounding Processing Subsystem is the hardware hub of the MW41 sounding system. It is connected to the radiosonde telemetry and GPS antennas and is receiving radiosonde transmissions and GPS satellite signals, while providing GPS differential corrections. The GPS system within the MW41 is described in more detail in Section 4.4.

Ground preparation and the available autolauncher system are shortly described in the following Sections 2.2.1 and 3.1.2.

### 2.2.1 Ground preparation

**Manual launches** The manufacturer prescribed manual ground preparation is performed by the operator on the RI41/RI41-B ground-check device and is therefore also part of a proper GRUAN sounding (see Chapter 3). The RI41-B device is equipped with a barometer module. It is operated with the MW41 sounding system. For the check, the sonde is placed onto the RI41 device (see Fig. 2.8). The MW41 sounding system then detects and automatically powers up the radiosonde. It communicates with the sonde using a wireless short-range data link at 13.56 MHz.

The steps during the check period include basic sensor functionality checks and enable the setting of desired options for in-flight operational parameters, as for example a timer to power off the radiosonde at predefined time, pressure, or altitude, as well as the transmitter frequency.

More detailed information on the Vaisala ground check is given in *Vaisala* (2016), and the Vaisala ground check steps are described in Section 3.2.2.

**Automatic launches** For RS41 soundings launched with the Vaisala unmanned sounding system AUTOSONDE® AS15, automatic ground check procedures are performed in a similar manner to manual launches.


**Figure 2.8:** A RS41-SGP is placed onto a RI41-B ground-check device to perform the ground preparation steps.

### 2.2.2 Autosonde sounding station

The Vaisala Autosonde® AS15 sounding station provides full automation for upper-air soundings with the Vaisala RS41 radiosonde (*Vaisala*, 2017a). It is built into a sandwich-wall container with dimensions 4.9 m × 2.4 m × 2.5 m (L×W×H) and a total weight of approximately 3000 kg (see Fig. 2.9). A fiber-glass launcher vessel for balloon filling is mounted on one end. The vessel has movable cover lids that allow for a hands-free balloon release. The interior of the container is divided into two equal compartments:

- **Operator room:** the working space for tray loading, inspection and maintenance work. The control computer, uninterruptible power supply (UPS), and sounding subsystems are installed in this compartment.
- **Robot room:** the location of the robotic system and pneumatic circuit that drive a 24-tray rotating table used to store radiosondes, and subsequently feed them to the preparation module.

We refer the reader to the detailed product description of the AS15 sounding station for further details on its assembly/content (*Vaisala*, 2018a).

A photograph of the AS15 at the GRUAN station in Payerne (Switzerland) is shown in Fig. 2.10.

The system currently sold by Vaisala is the AUTOSONDE® AS41. Vaisala AUTOSONDE® AS41 is an upper-air observation system for synoptic and adaptive use. With a loading capacity of 60 radiosondes, site visits and reloading is only required once every four weeks (*Vaisala*, 2021a).

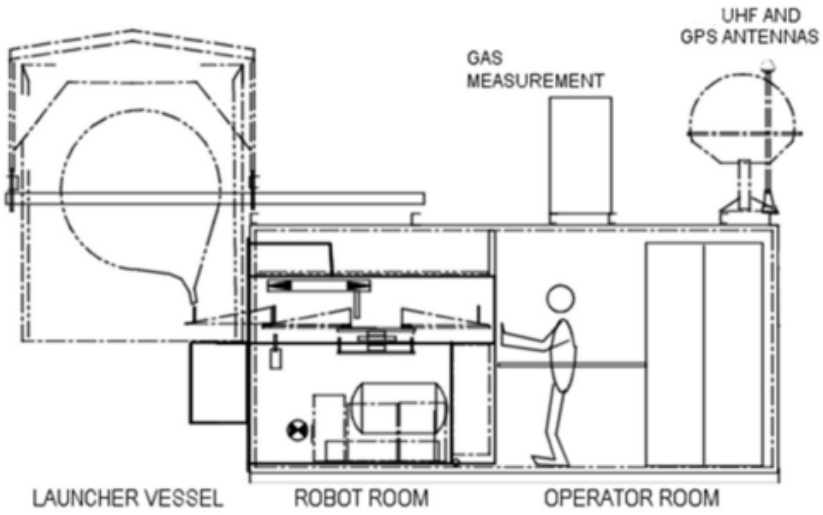


**Figure 2.9:** Side-cut schematic of the Vaisala Autosonde® AS15 sounding station (taken from *Vaisala*, 2018a).


**Figure 2.10:** Vaisala Autosonde® AS15 sounding station during launch of a RS41, installed at the GRUAN site of Payerne (PAY), Switzerland.

# 3 Measurement practice

This chapter provides information on the steps in the practical conduct of soundings with the RS41. This includes overviews of the procedures for manual soundings and when using automatic launchers (Section 3.1). Section 3.2 provides information on the manufacturer's calibration of the measurement sensors and the passed on measurement uncertainties. As part of the GRUAN procedures, the calibrations are checked at individual points, in particular using the Standard Humidity Chamber (SHC) developed in GRUAN. The last Section 3.3 highlights some aspects of sounding planning at the stations and in the network.

## 3.1 Process of a GRUAN RS41 sounding

### 3.1.1 Manual soundings

This section describes the main steps and activities when performing a manual RS41 sounding in GRUAN. The activities can be divided into three areas:

1. MW41 sounding software configuration (to be carried out once for the same type of soundings).
2. Regular equipment maintenance tasks prior to sounding preparation, see flow chart in Fig. 3.1.
3. Tasks related to the individual sounding preparation and implementation, see Fig 3.2.

The specifications and recommendations described hereinafter originate from the best-practice at the GRUAN site Lindenberg (LIN). The activities of the operators are potentially influenced by subjectivity. This plays a key role for manual sounding preparations and is therefore briefly discussed at the end of this section. Section 3.1.2 summarises the current practice for RS41 soundings with the Vaisala Autosonde in GRUAN.

The MW41 sounding software requires configuration in terms of station-specific meta data. Configuration instructions are available in *Vaisala* (2020b), or can be accessed for the current version via the sounding software graphical user interface. Important meta data are the station and launch site WGS84-coordinates and altitudes (above MSL). The altitude of the location of the radiosonde ground check place (RI41/RI41-B) is taken as the station reference altitude, with associated relative altitudes (offsets) of the station barometer, the GPS-antenna and the launch site. All values for altitudes or altitude offsets fed in the MW41 should be related to the same MSL-reference avoiding inconsistencies and therefore potential negative impact on the quality of sounding data (see also Section 4.4 for more information on altitude reference systems).

Sounding at GRUAN data quality level requires regular maintenance of the ground check equipment. For basics about the pressure check see Section 3.2.1.3 and for the GRUAN ground check

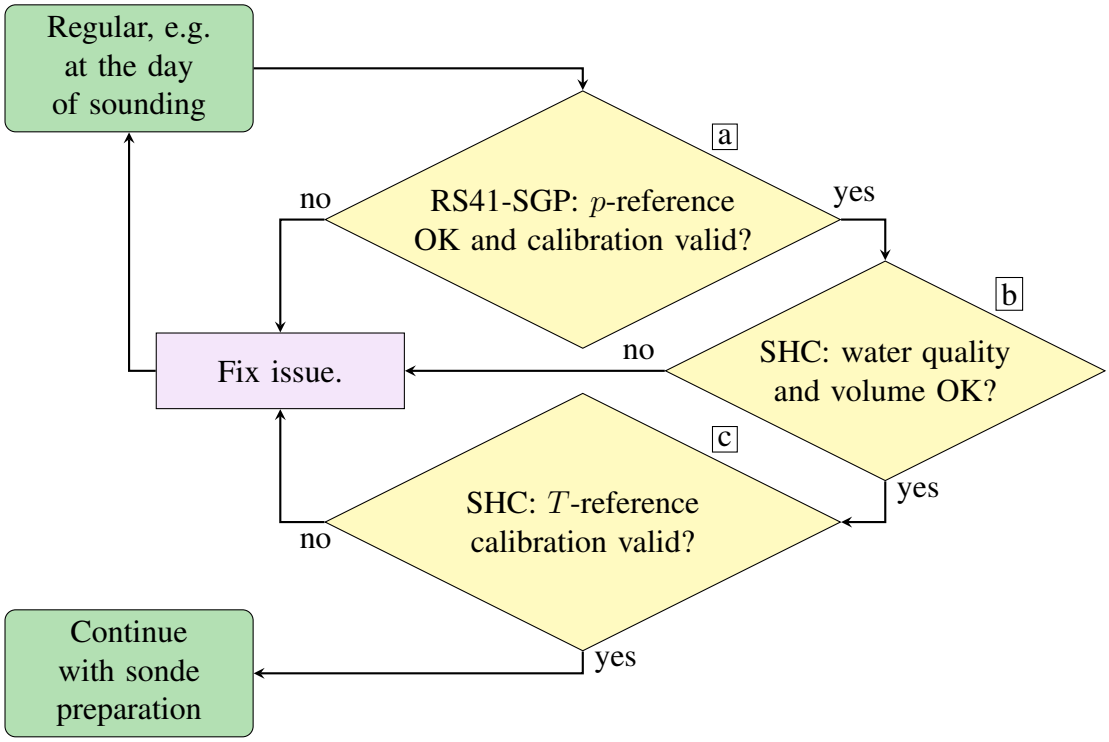


**Figure 3.1:** Regular GRUAN maintenance tasks for major components of the sounding preparation equipment. Calibration issues may be skipped until fixed. If so, a note should be added to the sounding META data. More details about nodes [a] to [c] are given in text.

in the Standard Humidity Chamber (SHC) see Section 3.2.3. The following list summarises the steps and recommendations for practice:

### Radiosonde pressure adjustment (RS41-SGP):

1. Fig. 3.1, task [a]: An external pressure reference sensor or the built-in barometer in RI41-B for the pressure check requires regular comparison with a pressure reference every six months or more frequently. Annual, SI-traceable (Section 5.3) re-calibration is recommended. The calibration date should be checked on each sounding day.
2. Fig. 3.2, task [a]: For the one-point adjustment of the RS41-SGP pressure sensor using a RI41-B with built-in, or a RI41 with an external pressure reference sensor, the sonde circuit should be in thermal equilibrium with lab conditions. Strong temperature drifts of the sonde circuit during the adjustment can lead to wrong pressure adjustment results.

### GRUAN ground check in SHC:

- Maintenance, Fig. 3.1, tasks [b] and [c]:
    1. The SHC should contain about 1 litre of double-distilled water (bottom of the 15 litre SHC covered with a $\sim$2 cm-water layer). The water should be changed every three months, or if any impurities are visible. Double-distilled water is preferable to single-distilled water. The water quality and volume should be visually checked before using the SHC.

2. A calibrated sensor should be installed in the air volume inside the SHC that can be used to continuously measure the temperature of the air above the bottom water layer in parallel to the 100 % relative humidity check of the radiosonde. It should be placed such that it samples the air under similar conditions as with the radiosonde under test.

- Operation, Fig 3.2 tasks [b], [d] and [e]:

1. Activate the SHC-heater at a time long enough before the actual ground check begins (e.g. 20 min), and for a period of time (about 10 min) so that the water is heated slightly above laboratory temperature (about 3 K to 4 K). The air in the SHC absorbs additional moisture during this process.
2. After the heating is switched off, the humid air in the SHC enters a slow cooling phase towards the slightly cooler laboratory temperature via radiation from the SHC surfaces and becomes saturated with moisture. The actual check of the radiosonde should not be started before the air is clearly saturated. This can take 10 min or more after switching off the heater. With the fan running during the whole process (continuous ventilation of the chamber volume), the time for establishing water vapour saturation can be significantly reduced to about 1 min.
3. Given that the laboratory temperature is reasonably stable, the closed SHC is then ready for one or more radiosonde humidity sensor checks for an interval of 1.5 h or longer. If significant amounts of saturated air inside the SHC is replaced by unsaturated room air, for example when keeping the openings for installation of the radiosonde sensor booms open too long, the heating procedure should be repeated to re-establish saturation conditions.
4. The 100 % SHC check should only take place if it is ensured that the temperature inside the chamber exceeds the room temperature by a few K and that there is a continuous decrease in SHC temperature with time by slow self-cooling towards room temperature.
5. Radiosondes should be plugged into the SHC using a customised sealing sonde adaptor. This helps to prevent exchange with ambient air during the check.
6. Tests have shown that the actual measured relative humidity of RS41 family radiosondes in the SHC varies slightly with the sensor boom orientation relative to the fan-driven air flow. As best practice approach, the orientation should be as similar to in-flight conditions as possible. That is, the sensitive side of the humidity sensor chip (see Fig. 2.4) should be oriented in downstream direction of the air flow.
7. Unstable laboratory temperature conditions or irradiation with sun light during the check period may lower or even reverse the temperature difference between chamber and room air. This shall be prevented. The use of the ground check in a room with air conditioning is preferred.
8. Reference temperature sensor, Fig. 3.1 task [c]: It is recommended to yearly calibrate or replace the reference air temperature sensors in the chamber. The calibration date should be checked at each sounding day. Traceability of the calibration to SI units must be ensured.

In manual soundings, care and circumspection on the part of the operators performing the

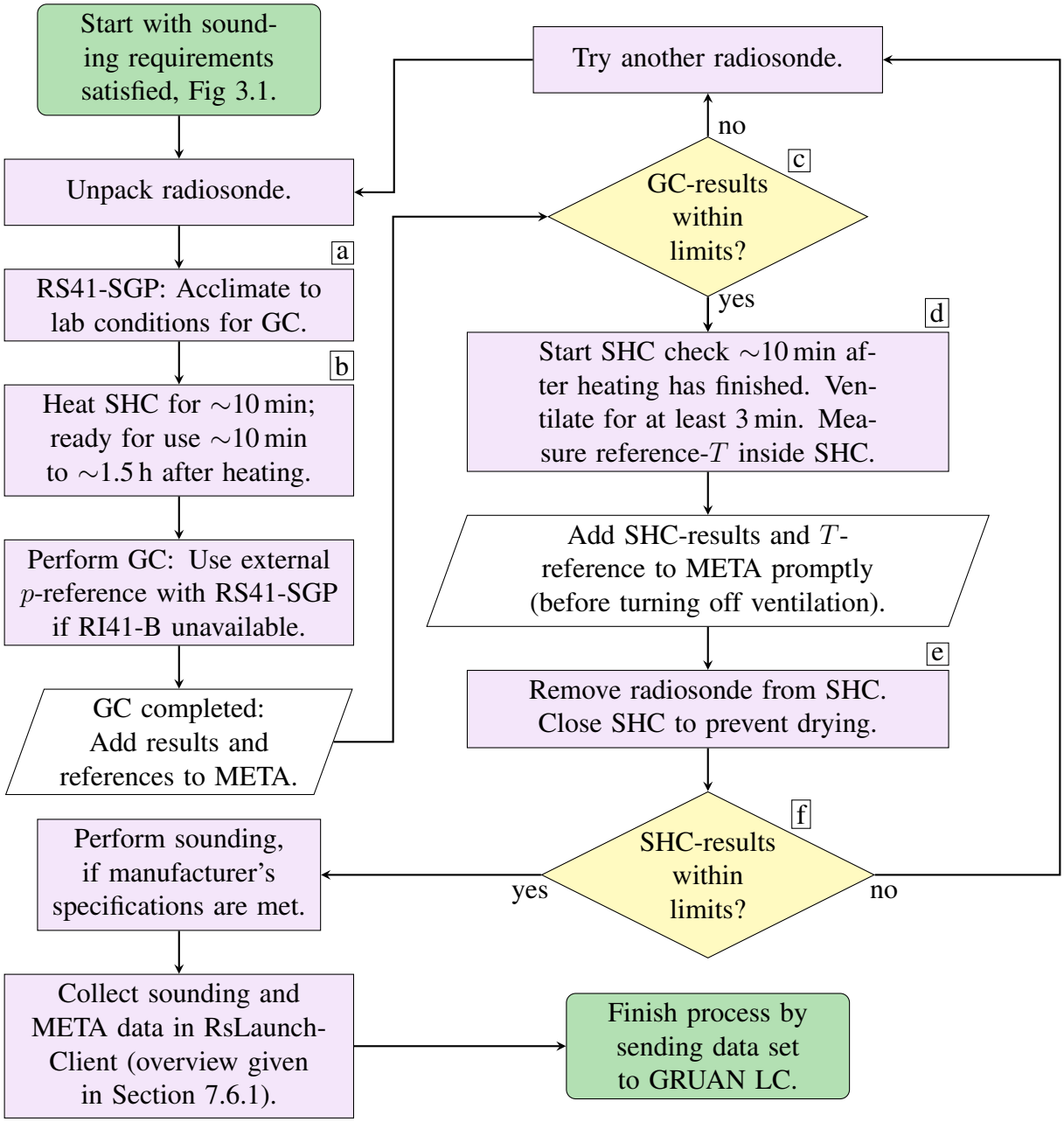


**Figure 3.2:** Sequence of tasks for manual GRUAN soundings. Additional information on some of the nodes is given in the text and linked by labels (e.g. a). Accepted limits of GC-results for the decision c are summarised in Table 3.1. In addition, accepted limits of SHC can be defined for the decision f related to full GRUAN (topic is in discussion) or a specific site (e.g. 2 %RH is used as limit for $\Delta U_{\mathrm{GC}}$ at Lindenberg site).

soundings are crucial for consistently high quality and reproducibility of the measurements. It is important that all operators are aware of the guidelines in GRUAN and that pre-launch preparations are carried out according to these guidelines. This means that the operators should be trained in performing the quality-relevant checks in order to avoid technical errors or problems, and to be able to carry out the soundings completely on one's own responsibility. The GRUAN site manager is responsible for instructing and appropriate training of the operators.

**Table 3.1:** Acceptance limits of ground check results for RS41 family radiosondes defined by the manufacturer ($\Delta p_{GC}$ applies only to RS41-SGP). Units with check results beyond these limits are considered defective and should not be launched. Note that the symbol $\Delta$ is used throughout the document in the sense of a simple difference between two values.

| Manufacturer GC | | |
|---|---|---|
| $\Delta p_{GC}$ | $\Delta T_{GC}$ | $\Delta U_{GC}$ |
| 3 hPa | 3 K | 2 %RH |

The daily maintenance tasks are often the responsibility of the operators (see Fig. 3.1), but this may vary between stations.

## 3.1.2 Autosonde sounding station

### 3.1.2.1 Basic principles of operation

**Tray loading** The AS15 sounding station automates the "launching" of radiosondes. The assembly of balloons and payload (comprised of a parachute, a valve, an unwinder, and a RS41 radiosonde), however, remains a manual process, together with their upload into the trays of the rotating table (see Fig. 3.3). This preparatory step is crucial, in that it directly impacts the flight performances. For example, to prevent any leakage of balloon gas during the ascent, care must be taken when inserting the valve (plastic part with a diameter similar to that of the balloon nozzle acting as sealing join and anti-backflow) into the balloon nozzle, with the subsequent attachment of the parachute string on it. A careful placement of the (deflated) balloon in the tray is paramount for a successful launch, as is the connection of the gas pipe to the valve.

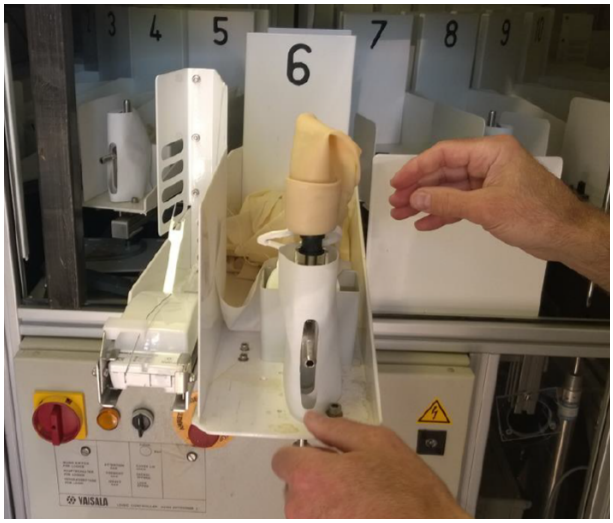


**Figure 3.3:** Finalisation of the balloon and payload assembly in tray 6 (out of 24) of the rotating table. A "pull-out" mechanism provides easy access to individual trays from the control room in the AS15 sounding station. Each payload is comprised of a balloon, parachute, a valve, an unwinder, and a RS41 radiosonde (photo taken from *Vaisala*, 2018a).

Upon the insertion of a loaded tray back in the robotic room, an articulated arm mounted with a

Near Field Communication (NFC) module automatically moves close to the RS41 radiosonde (see Fig. 3.4). A direct, wireless connection to the radiosonde is established, and a basic test of the RS41 performance is initiated. This test lasts a few seconds, during which temperature and relative humidity values of the sonde are compared with a Vaisala Humidity Temperature Transmitter HMT330-AS mounted directly in the robotic room. The maximum difference allowed when loading new radiosondes onto the rotating table is 3 °C for temperature, and 4 % for relative humidity.

**Figure 3.4:** View into the operator room of AS15. The robot room is behind the window (top right). The ground check device RI41-AS1 is marked with a red circle (top left). Bottom: view into the robot room, with the NFC module arm approaching the RS41 for wireless communication (from left to right).

**Flight initialisation** A launch can be triggered either autonomously by the AS15 sounding station as a scheduled event, or manually by a human operator via the AUTOSONDE software. In either case, the flight initialisation begins with the subsystem SPS311 switching on, followed by the robot spinning the rotating table until the appropriate tray is located near the Near Field Communication (NFC) module (Fig. 3.4). Next, a series of pre-launch checks are triggered via the MW41 software, in a manner similar to manual launches. This process starts with a reconditioning step via RI41-AS1 (similar to RI41 for manual flight with a NFC module). After the MW41 ground check is completed, checking the GPS receiver, and ensuring that the RS41 is transmitting via radio, the rotating table turns 180° and places the (automatically or manually) chosen tray into the launch vessel. The gas filling process is initiated, and typically lasts 300 s for a volume of 1.2 $m^3$ of He. The balloon is subsequently released by opening the cover doors of the launcher vessel.

#### 3.1.2.2 AS15 sounding station performance

**Burst altitudes** Parameters such as balloon type and filling volume, as well as the payload attachment technique, have significant impact on the altitude performance of radiosounding flights. If attention is being paid to these elements, automated releases do not lead to a decrease in performance (in terms of the balloon burst altitude) in comparison with traditional launches (*Madonna et al.*, 2020). Figure 3.5 shows a histogram of the altitude reached by radiosondes launched from the GRUAN site of Payerne (Switzerland) in 2021, both for traditional and automatic launches via the AS15 sounding station. All flights used an 800 g Totex (TX800) balloon with an internal parachute. One should note that TX800 balloons are being used only 2 times per week for traditional launches in Payerne, which results in a comparatively smaller number of traditional flights ($N = 114$) compared to automated ones ($N = 491$). Three of the weekly manual soundings use an Ozone sensor together with the RS41 radiosonde, which requires bigger balloons, and thus explains this population difference.

The automated soundings are found to have a median burst altitude of ≈37 000 m (above MSL), ≈2000 m more than traditional soundings. The turnover strategy for the radiosondes loaded in the AS15 sounding station in Payerne is such that the launch occurs rarely later than 8 days after tray loading. Up to this duration, no change of the burst altitude with storing time is observed (see Fig. 3.6).

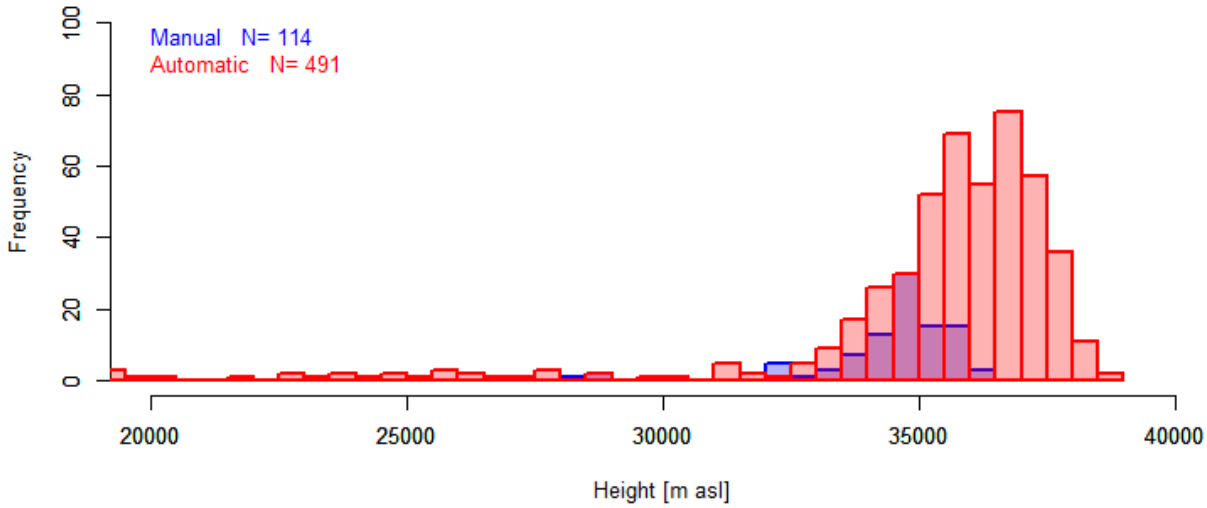


**Figure 3.5:** Histogram of the altitude reached with Totex 800 g (internal parachute) balloon launched manually (blue) and with the AS15 autosonde (red) at Payerne in 2021.

**Standard Humidity Chamber** At present, no manufacturer-independent ground check of the relative humidity sensor of radiosondes is implemented within the AS15 sounding station nominal operational procedure. The generation of GRUAN data products for the RS41 launched by the AS15 sounding station thus currently relies on a statistical analysis of large historical datasets of manual ground checks in Standard Humidity Chambers (SHCs), performed manually for traditional launches.

Dedicated investigations are required within the GRUAN framework to assess the feasibility of integrating a "SHC-100 %" manufacturer-independent ground-check for AS15 sounding sta-

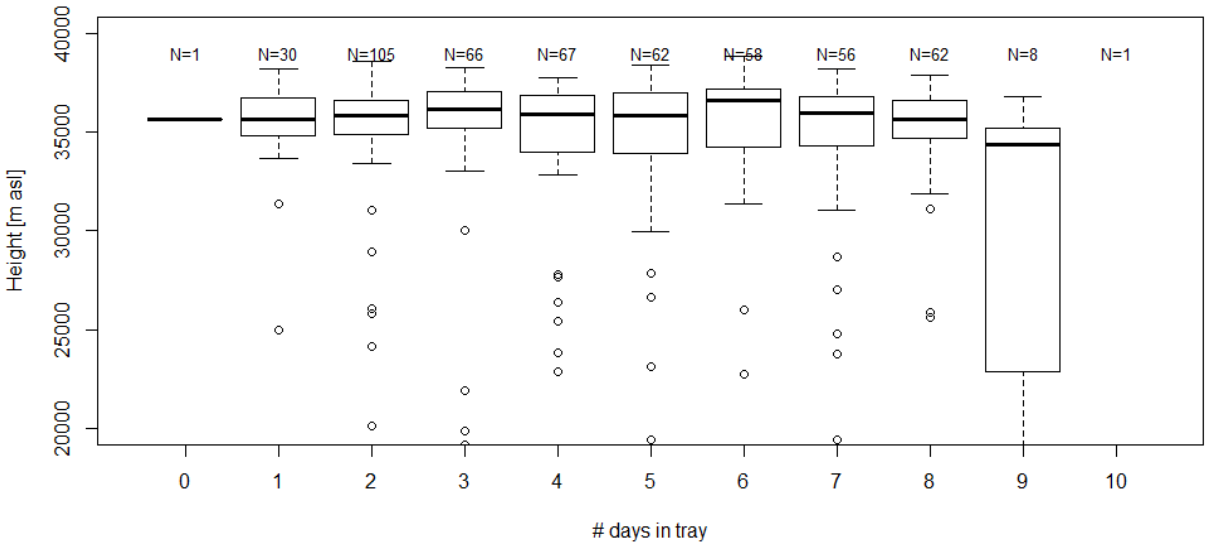


**Figure 3.6:** Boxplot of the altitude reached with TX800 balloons (with internal parachute) for automated launches, as a function of the number of days between the loading and the release in AS15 for 2021 at Payerne.

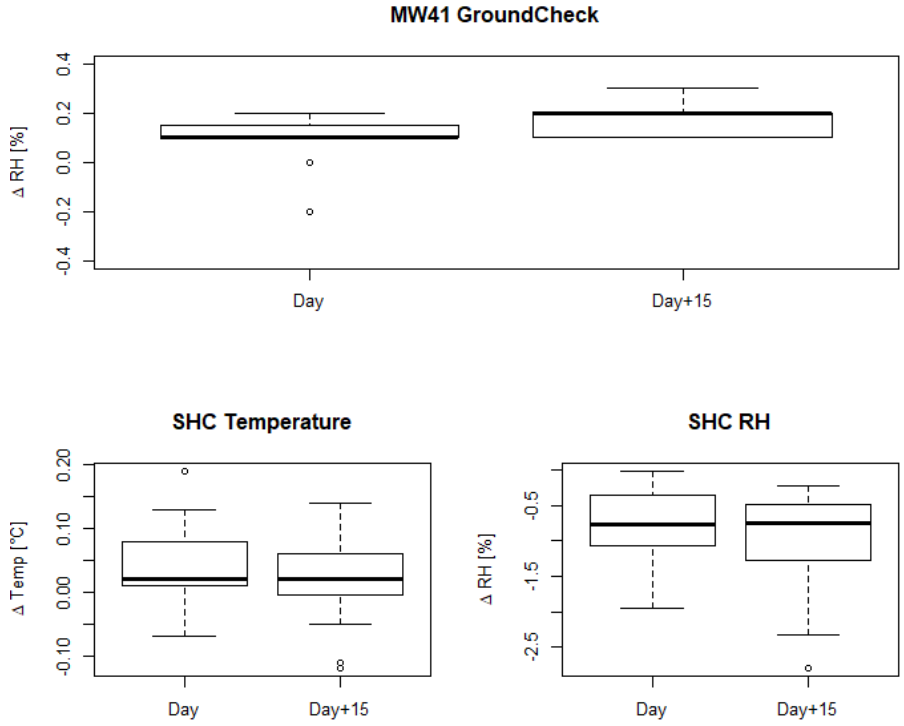


**Figure 3.7:** Top: boxplot of the relative humidity difference connected to the sensor reconditioning process (from MW41 software). Bottom left: boxplot of the temperature difference between the reference and the RS41 in the SHC. Bottom right: boxplot of the deviation of relative humidity of the RS41 from 100 % in the SHC.

tions. A priori, a SHC ground-check could be performed when loading RS41 radiosondes into the rotating table of the AS15 sounding station. Of course, this would differ from traditional flights where the SHC measurements are performed immediately before the launch. Adding a SHC-100% check to the loading procedure would also significantly extend its duration to a total of $\sim$2 hours for 10 RS41 radiosondes, compared to 40 minutes with the existing procedure.

One may argue that maintaining the RS41 sensor boom in open air for several days within the robot room of the AS15 sounding station, in the immediate vicinity of talcum powder from the balloon, may alter the sensitivity of the temperature and RH sensors – and thus void any ground check performed at loading time. To test this scenario, and evaluate whether a SHC ground check performed at loading time is equivalent (or not) to a SHC ground-check at launch time, a series of dedicated experiments are ongoing at several GRUAN sites. In Payerne, RS41 radiosondes were ground-checked first at their loading time into the auto-launcher, subsequently stored for 15 days within the trays of the AS15 sounding station rotating table, before being ground-checked a second time. One should note that a reconditioning via the MW41 software was performed prior to both SHC ground checks. The results of this experiment are shown in Figure 3.7. From the 28 radiosondes assessed in Payerne in 2021, there is no evidence of a difference between performing a SHC ground check immediately before launch, or 15 days earlier. This result, which requires further confirmation, indicates that the implementation of SHC ground checks as part of the loading procedure of RS41 radiosondes in the AS15 sounding station would not lead to erroneous outcomes for the generation of GRUAN data products.

## 3.2 Calibration and pre-launch procedures

This section describes the estimation and linkage of the uncertainty components of temperature and relative humidity that are associated with the GRUAN ground procedures during preparation of the radiosonde before launch. This includes information on the sensor calibration at the manufacturer's facilities, the manufacturer's prescribed ground check, which is always part of a GRUAN sounding, and the additional GRUAN ground check in the Standard Humidity Chamber. The result is a decision as to whether a radiosonde meets the criteria to be launched, and if so, a measurement uncertainty is assigned that applies to the current readings of the sonde in the state immediately prior to launch. This pre-launch uncertainty is a component of the total uncertainty budget. Detailed schematic overviews of the propagation of uncertainty components are given in the form of flowcharts in Chapter 6 in Fig. 6.1 for temperature and in Fig. 6.2 for relative humidity.

### 3.2.1 Calibration at manufacturer

Manufacturer calibrations are performed in automated calibration stations. Automation controls the devices under test through the calibration sequence and makes sure that each step of the process is completed, and that the devices under test meet their specifications. In the production, RS41 units are calibrated against production working standards (see Chapter 5 on traceability).

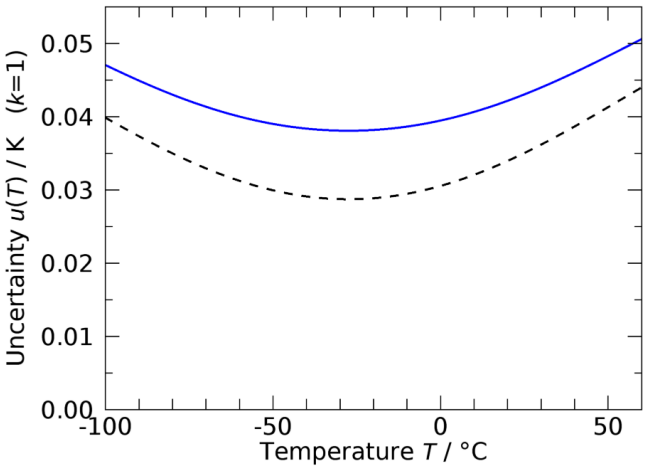


**Figure 3.8:** Vaisala specification of calibration-related uncertainty for the RS41 temperature measurement. Dashed black curve: Combined uncertainty after sensor calibration (reproduced from *Vaisala*, 2017d) for $k = 1$. Blue curve: Combined uncertainty after ground preparation (reproduced from *Vaisala*, 2017c) for $k = 1$.

#### 3.2.1.1 Temperature

In the manufacturer data sheet (*Vaisala*, 2015b, 2020e, see also Table 2.2), the calibration uncertainty of the temperature sensor is specified as 'Repeatability in calibration'. The value is 0.05 K ($k = 1$), and is described as the standard deviation of differences between successive calibrations. However, Vaisala provides more detailed information in the form of a combined uncertainty after sensor calibration in the temperature range of −100 °C to 60 °C in *Vaisala* (2017d). This combined uncertainty includes the uncertainty of the mathematically formulated sensor model, i.e. sensor linearity and sensor model fit to the calibration points. It is given in Eq. (A.1, Appendix A.1.1) and reproduced with the black curve in Fig. 3.8 for $k = 1$.

The blue curve in Fig. 3.8 is the combined uncertainty for temperature measurements after ground preparation for $k = 1$ (*Vaisala*, 2017c). It includes a constant component due to possible deterioration during storage a value of $u_{\mathrm{stor}} = 0.025\,\mathrm{K}$:

$$u_{\mathrm{gp}}(T_{\mathrm{s}}) = \sqrt{u_{\mathrm{cal}}^2 + u_{\mathrm{stor}}^2}, \tag{3.1}$$

with index 'gp' standing for 'after ground preparation', and 's' denoting 'sonde'. This uncertainty is used in the RS41-GDP as 'overall' calibration-related uncertainty provided by the manufacturer (see flow chart of uncertainties for temperature in Fig. 6.1).

The two apply to both the actual temperature sensor near the tip of the sensor boom and the sensor integrated on the humidity sensor chip. It is mentioned here again that other components arising during the later radiosounding, e.g. those associated with corrections of systematic errors, are not included in this uncertainty.

Information on the traceability of temperature is given in Section 5.1.

#### 3.2.1.2 Humidity

Humidity sensors for the RS41 radiosonde are calibrated at Vaisala's calibration facility in specially designed measurement chambers. Similar to temperature, Vaisala states an overall estimate of the humidity calibration as 'Repeatability in calibration', see Table 2.2. However, a combined uncertainty after sensor calibration is provided by Vaisala (*Vaisala*, 2017d) as a function of relative humidity at ambient temperature of 20 °C, including the sensor model uncertainty. It denotes the uncertainty of the basic sensor calibration. It is given in Eq. (A.2) and reproduced in Figure 3.9 for $k = 1$.

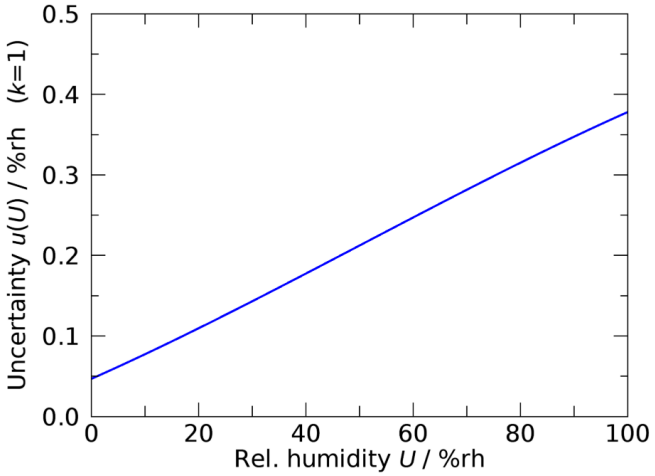


**Figure 3.9:** Combined factory calibration uncertainty of the RS41 humidity sensor ($k = 1$). Reproduced from *Vaisala* (2017d).

For the actual humidity measurement, the uncertainties of the measured air temperature and of the (heated) built-in temperature sensor on the integrated humidity chip have to be taken into account, because both are used for the derivation of the relative humidity. Together with uncertainty components from the sensor model, calibration, and storage, this leads to the combined uncertainty after ground preparation, $u_{\mathrm{gp}}(U_{\mathrm{s}})$, as function of relative humidity and air temperature, which is used in the GRUAN data processing. It is shown in Table A.1 and reproduced from Fig. 3.2 in *Vaisala* (2017c) in Fig. 3.10. Again, uncertainty factors related to dynamic sounding conditions are not included at that stage.

Further details on calibration of the humidity sensor is given in Section 5.2.

#### 3.2.1.3 Pressure

The pressure sensor of the RS41-SGP radiosonde is calibrated at the manufacturer (Section 5.3). The calibration uncertainty is given in the data sheet (*Vaisala*, 2015b) as 'Repeatability in calibration' – again to be considered as (conservative) overall estimate – as 0.15 hPa ($k = 1$) for $p =$ (100 to 3) hPa and 0.2 hPa for $p > 100$ hPa, respectively. A more representative estimate for the combined uncertainty, which applies after ground preparation and includes the factory calibration, is given in *Vaisala* (2017d) as function of pressure. It is reproduced for $k = 1$ in Fig. 3.11 (see also Eq. (A.3) in Section A.1). This component is included in the GRUAN uncertainty budget for the RS41-GDP.

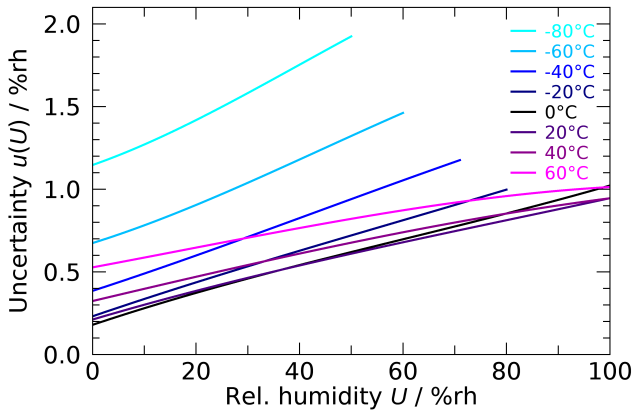


**Figure 3.10:** Combined calibration uncertainty for relative humidity measurement after ground preparation, reproduced from *Vaisala* (2017c) for $k = 1$.

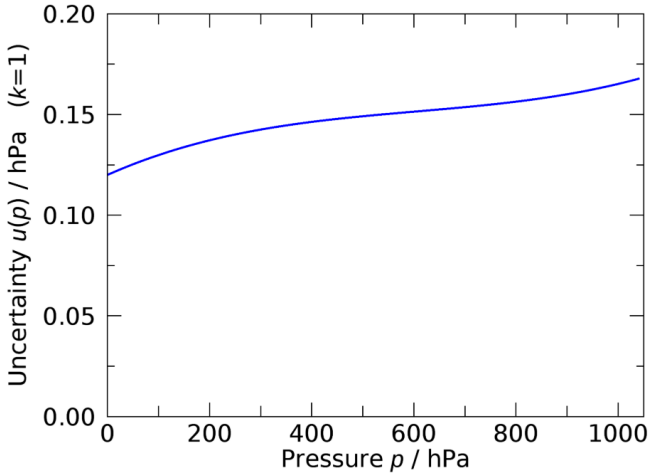


**Figure 3.11:** Combined calibration uncertainty for pressure measurement after ground preparation, reproduced from *Vaisala* (2017d) for $k = 1$.

## 3.2.2 Ground check prescribed by manufacturer

The RS41 sonde undergoes a manufacturer prescribed ground check using the RI41 or RI41-B ground check devices as part of the pre-launch procedures (*Vaisala*, 2016, 2021b). The check is done routinely before manual radiosonde launches as well as in an automated manner in Vaisala's AUTOSONDE® system.

### 3.2.2.1 Temperature

During the fully automated check, readings from the sonde's temperature sensor are compared with that integrated on the sonde's humidity sensor chip. The check result is reported as a status information for the operator. Vaisala claims a high accuracy of the temperature sensor (platinum resistor) as well as the absence of significant errors due to sensor drift during storage and transport. Therefore no correction or adjustment is applied or requested after the ground check,

i.e. the check is a basic test of the functionality of the sonde. In cases where the temperature readings deviate more than a pre-set limit (±3 K), the MW41 software assumes malfunction, terminates the preparation process and asks for a replacement radiosonde.

#### 3.2.2.2 Relative humidity

The humidity sensor is reconditioned during the check by controlled heating. During that, the integrated humidity sensor chip is heated to about 150 °C for 3 min. With this, potential chemical contaminants are removed, and practically dry conditions (0 % relative humidity) are established around the humidity sensor (physical principle). The sonde then detects possible deviations of the sensor reading from zero humidity. An offset type correction is applied, and it is assumed that the sensor is re-set according to the factory calibration.

If under stable indoor conditions a deviation exceeding ±2 % relative humidity is detected, there is a pre-flight failure under warranty (*Vaisala*, 2018b). The preparation procedure is terminated and the operator is asked to change the radiosonde.

#### 3.2.2.3 Pressure

For the RS41-SGP sonde model, which is equipped with a pressure sensor, the actual pressure reading is compared to the built-in barometer module if the RI41-B ground check device is used. With the RI41, which has no internal pressure sensor, an external barometer can be used for the comparison, and the pressure value can be entered into the MW41 software manually. After the ground check, a relative correction is applied to the sonde's pressure measurements in sounding according to the ratio between reference and radiosonde pressure readings measured during the ground check. For further information on this and especially on uncertainties, see Section 4.3.

If the ground check result of the sonde's pressure sensor exceeds ±3 hPa relative to the Vaisala RI41-B or another precision barometer, there is a pre-flight failure under warranty (*Vaisala*, 2018b). If using the RI41-B, the preparation procedure is then terminated and the operator is asked to change the radiosonde. If an external barometer is used as reference, the operator is asked to check the reference value, and then either to correct the reference value, or to terminate the sounding preparations.

### 3.2.3 GRUAN ground check in the Standard Humidity Chamber (SHC)

A proper GRUAN radiosounding includes a pre-launch ground check of each sonde unit using the Standard Humidity Chamber (SHC) after the manufacturer prescribed checks have been passed (Section 3.2.2). Besides a check of relative humidity at $U = 100\,\%$, GRUAN recommends a simultaneous check of the chamber air temperature during that procedure by comparing the temperature sensor of the sonde with a metrologically traceable reference sensor installed inside the SHC. These readings represent an additional manufacturer-independent ground check, ensure traceability, and help to track instrument changes. They are included in the uncertainty budget and as a quality criterion.

The SHC (MLP-Prozessleittechnik GmbH Berlin, Germany) is a closed pot-like cylindrical chamber with the bottom covered by a 2 cm-layer of distilled water (Fig. 3.12. Before the check procedure, the chamber bottom is heated such that the water temperature rises slightly above ambient laboratory temperature. After switching off the heating, the air inside the chamber slowly adjusts to the laboratory temperature, thus permanent saturation (100 % relative humidity) is achieved. Because of the presence of condensation nuclei in the air, supersaturation is not expected. A fan provides a proper mixing to ensure a homogeneous temperature and humidity field inside the chamber. After plugging the sensor boom into the saturated air flow in the chamber using a sealed adaptor, the check period of several minutes is started. If a reference temperature sensor is installed as recommended by GRUAN, the temperature can be tracked in parallel. Further details on how operators should perform the SHC ground check are summarised in Section 3.1.

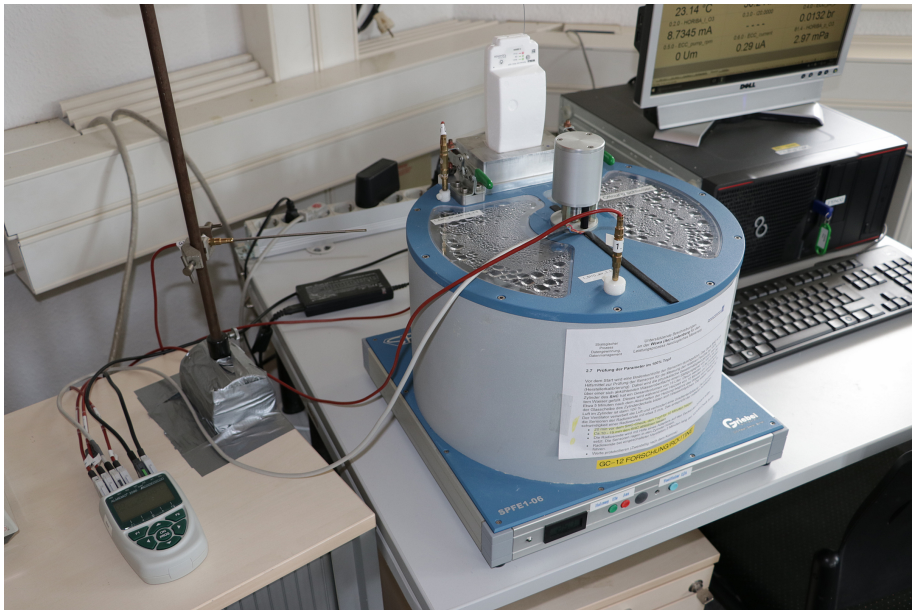

**Figure 3.12:** Standard Humidity Chamber (SHC) in operation at the GRUAN site Lindenberg checking a RS41 radiosonde plugged in vertically at the back side. The SHC vessel stands on an electronically controlled heating plate. The fan motor is attached at the centre of the SHC cover and drives the fan inside around the vertical axis. Water droplets on the inner side of the cover windows indicate water vapour saturation of the air inside the chamber. The temperature of the mixed air is measured by sensors opposite the RS41 inside the chamber linked to a data logger system.

#### 3.2.3.1 Temperature check in the SHC

Although primarily designed for ground checks of the humidity sensor, the SHC can in parallel be used for a check of the temperature sensor at laboratory conditions. The check compares the temperature displayed by the radiosonde with a calibrated reference sensor. The reference sensor is installed in the chamber such that it samples the ventilated air above the bottom water layer similar to the radiosonde. The difference of the measured temperatures averaged over at

least 3 min is evaluated as the results of the check:

$$\Delta T_{\mathrm{SHC}} = \overline{T_{\mathrm{s}}} - \overline{T_{\mathrm{ref}}}. \tag{3.2}$$

Note that the symbol $\Delta$ here and in the rest of the document means a simple difference between two values.

Active ventilation with a fan ensures that the air temperature inside the chamber is spatially uniform. A slow temperature decrease due to the slow self-cooling of the chamber may occur. This, however, should not affect the (possible) measured difference, assuming that the response times of the sensors are similar and in particular small compared to the temperature changes.

The uncertainty $u(\Delta T_{\mathrm{SHC}})$ associated with the check result consists of the uncertainty after ground preparation, $u_{\mathrm{gp}}(T_{\mathrm{s}})$ (which includes the manufacturer calibration and any uncertainty source until the manufacturer-prescribed ground check is finished, see Section 3.2.1), the calibration uncertainty of the reference sensor, as well as contributions from the SHC check procedure itself, $u\left(\overline{T_{\mathrm{s}}}\right)$ and $u\left(\overline{T_{\mathrm{ref}}}\right)$. The latter two are determined as follows:

**Radiosonde, $u(\overline{T_{\mathrm{s}}})$:** During the SHC check, the temperature inside the chamber is recorded with the sampling rate of the sonde (1 s). The averaging interval for calculation of $\overline{T_{\mathrm{s}}}$ starts after a settling phase upon insertion of the sonde's sensor boom into the ventilated chamber. It is assumed that possible condensation and evaporation on the radiosonde and reference sensor surfaces are in equilibrium and therefore do not distort the measurement because the chamber air is well mixed and kept in saturation during the check. $\overline{T_{\mathrm{s}}}$ is taken as measurement result for the tested sonde. Existing temperature variations during that period are separated into a linear trend and a random component. The resulting (formal) standard uncertainty for $\overline{T_{\mathrm{s}}}$ is then taken as the combination of the standard deviation of the mean of the residual $\sigma(T_{\mathrm{s}})/\sqrt{N}$ after subtracting the linear trend, and the manufacturer-provided uncertainty $u_{\mathrm{gp}}(T_{\mathrm{s}})$ (Eq. 3.1):

$$u\left(\overline{T_{\mathrm{s}}}\right) = \sqrt{\frac{\sigma^2(T_{\mathrm{s}})}{N} + u^2_{\mathrm{gp}}(T_{\mathrm{s}})}. \tag{3.3}$$

$N$ is the number of data points included in the mean, and the residual is assumed uncorrelated. Note that a possible trend does not contribute to the uncertainty of the difference to the reference. The uncertainties of the fit parameters of the trend are assumed to be small and are not taken into account.

**Reference sensor, $u\left(\overline{T_{\mathrm{ref}}}\right)$:** The temperature inside the SHC is measured with a reference sensor in one of the following ways, depending on the practice at the actual GRUAN-station:

a) simultaneously with the radiosonde as continuous record, preferably with the same sampling rate,

b) with a single manual reading by the operator in case the data are not automatically logged,

c) not measured (reference measurement not implemented).

*Case a):* In analogy to the sensor of the radiosonde, the standard uncertainty of the reference

sensor is

$$u\left(\overline{T_{\mathrm{ref}}}\right) = \sqrt{\frac{\sigma^2(T_{\mathrm{ref}})}{N} + u^2_{\mathrm{cal}}(T_{\mathrm{ref}})}, \tag{3.4}$$

with $u_{\mathrm{cal}}(T_{\mathrm{ref}})$ the calibration uncertainty of the reference sensor (available from calibration certificate). Consistently, a trend is not included in the uncertainty of $\overline{T_{\mathrm{ref}}}$.

*Case b):* It is assumed that in practice the single reading of the reference temperature takes place at some unknown point in time during the time of the check in the SHC. A possible temperature trend is recorded with the radiosonde, and can be taken into account as an uncertainty component for the reference measurement. Thus, Eq. (3.4) is modified by substituting the random term:

$$u\left(\overline{T_{\mathrm{ref}}}\right) = \sqrt{\left(\frac{T_{\mathrm{s,max}} - T_{\mathrm{s,min}}}{2\sqrt{3}}\right)^2 + u^2_{\mathrm{cal}}(T_{\mathrm{ref}})}, \tag{3.5}$$

with $T_{\mathrm{s,max}}$ and $T_{\mathrm{s,min}}$ the maximum and minimum radiosonde temperatures according to a (fitted) linear trend during the check interval.

Thus, the uncertainty of $\Delta T_{\mathrm{SHC}}$ is given for the cases a) and b) as

$$u\left(\Delta T_{\mathrm{SHC}}\right) = \sqrt{u^2\left(\overline{T_{\mathrm{s}}}\right) + u^2\left(\overline{T_{\mathrm{ref}}}\right)}. \tag{3.6}$$

*Case c):* If no reference temperature measurement is available during the SHC-check or no GRUAN ground check has been performed, a statistically evidenced uncertainty estimate based on existing SHC check results is assigned (see point 1 in the next subsection).

Similar ground check procedures can be carried out in a weather hut or shelter. However, the conditions are generally less controlled, and much higher fluctuations of the check variables are expected during the check time. Existing results from stations performing this (additional) check reveal that the uncertainty of the comparison $u\left(\Delta T_{\mathrm{SHC}}\right)$ may be considerably enhanced, which reduces the overall significance of the check.

#### 3.2.3.2 Combined GRUAN pre-launch uncertainty for temperature

The SHC-check is performed at room temperature. The result is not intended for correction or adjustment of the subsequently measured atmospheric temperature profile. Instead, it is used as a consistency check by comparing $\Delta T_{\mathrm{SHC}}$ with the manufacturer-given pre-launch uncertainty $u_{\mathrm{gp}}(T_{\mathrm{s}})$ (see Eq. 3.3). Depending on whether the GRUAN check is done, and if so, what the result is, $u_{\mathrm{gp}}(T_{\mathrm{s}})$ is passed on directly as overall pre-launch calibration uncertainty, or another component is added according to one of the following procedures (uncertainties given for $k = 1$):

1) At GRUAN sites that operate automatic launchers, and at some sites doing manual soundings, no independent SHC or comparable ground-check is routinely performed for temperature. Since no corresponding actual uncertainty can be determined in this case, a fixed uncertainty value is added to the radiosonde's pre-launch uncertainty $u_{\mathrm{gp}}(T_{\mathrm{s}})$ to take the absence of the check into account. This fixed component is determined to $\sigma_T = 0.113$ K, based on a one-time statistical analysis of available network-wide SHC ground check results over the period 2014 to 2020 ($N = 9269$). Thus, the overall pre-launch uncertainty

is calculated as

$$u_{\mathrm{cal}}(T_{\mathrm{s}}) = \sqrt{u_{\mathrm{gp}}^2(T_{\mathrm{s}}) + \sigma_T^2}. \tag{3.7}$$

The next two points apply when SHC ground checks are carried out:

2) If the check gives a deviation $\Delta T_{\mathrm{SHC}}$ smaller or equal to its uncertainty,

$$\frac{|\Delta T_{\mathrm{SHC}}|}{u(\Delta T_{\mathrm{SHC}})} \leq 1, \tag{3.8}$$

then the SHC-result is considered consistent with the manufacturer-provided pre-launch uncertainty. That is, $u_{\mathrm{gp}}(T_{\mathrm{s}})$, which is the uncertainty associated to all pre-launch activities including the manufacturer calibration, is passed on unchanged as overall uncertainty:

$$u_{\mathrm{cal}}(T_{\mathrm{s}}) = u_{\mathrm{gp}}(T_{\mathrm{s}}). \tag{3.9}$$

In practice, this is the case for the majority of temperature ground checks with the RS41.

3) If the check reveals that the radiosonde temperature is not consistent with the reference, i.e. the ratio in Eq. (3.8) exceeds unity, then it is the measured deviation $|\Delta T_{\mathrm{SHC}}|$ that is taken as pre-launch uncertainty:

$$u_{\mathrm{cal}}(T_{\mathrm{s}}) = |\Delta T_{\mathrm{SHC}}|\,. \tag{3.10}$$

However, an upper boundary is set according to the value calculated with Eq. (3.7), i.e.

$$u_{\mathrm{gp}}(T_{\mathrm{s}}) < u_{\mathrm{cal}}(T_{\mathrm{s}}) \leq \sqrt{u_{\mathrm{gp}}^2(T_{\mathrm{s}}) + \sigma_T^2}. \tag{3.11}$$

$\Delta T_{\mathrm{SHC}}$ discloses possible significant measurement deviations of the actual sonde's sensor. In practice, however, the reference sensor may also be biased to some extent, for example due to an unrecognised drift since the last routine calibration. Such reference sensor related errors are of systematic nature, which is less expected for the mean deviation of radiosondes (because of the random distribution of deviations and the large number of checked units). The upper limit is therefore introduced to avoid the assignment of unjustifiably large uncertainties, which would potentially persist in such cases over a longer period of soundings at a station. Furthermore the procedure ensures that the uncertainties assigned to the temperature measurement of SHC-checked sondes do not exceed those for sondes that do not undergo a check.

The 'overall' calibration uncertainty $u_{\mathrm{cal}}(T_{\mathrm{s}})$ applies uniformly to the temperature profile of the actual subsequent radiosounding, i.e. it is assumed fully correlated in the vertical, and is also considered correlated in time. Therefore it is stored in the GDP as correlated in time ('tcor') (see also Fig. 6.1 in Section 6.2.1).

#### 3.2.3.3 SHC-check for relative humidity

The uncertainty calculations for the humidity sensor with regard to the GRUAN SHC check procedure are to a large extent analogous to those for the temperature sensor. The ground check

result for relative humidity is

$$\Delta U_{\mathrm{SHC}} = \overline{U_{\mathrm{s}}} - U_{\mathrm{ref}}, \tag{3.12}$$

with $\overline{U_{\mathrm{s}}}$ the relative humidity displayed by the sonde under test as average over the time of the check, and $U_{\mathrm{ref}} = 100\,\%$ the relative humidity of the reference atmosphere in the SHC. Given the chamber is properly sealed during the check, no temporal trend should be present since the humidity is generated according to a physical principle. A constant value of $u\left(U_{\mathrm{ref}}\right) = 0.5\,\%$ ($k = 1$) is defined as uncertainty of the realisation of the 100 % relative humidity, which should cover possible humidity fluctuations in the chamber.

During the check, the relative humidity is continuously recorded by the sonde with a sampling rate of 1 $\mathrm{s}^{-1}$. Simultaneously with temperature, the averaging interval for $\overline{U_s}$ starts after a short equilibrating phase upon insertion of the sensor boom into the chamber. The uncertainty of the sonde measurement, $u\left(\overline{U_{\mathrm{s}}}\right)$, is determined as combination of the standard deviation of the mean and the manufacturer-provided pre-launch uncertainty $u_{\mathrm{gp}}(U_{\mathrm{s}})$:

$$u\left(\overline{U_{\mathrm{s}}}\right) = \sqrt{\frac{\sigma^2(U_{\mathrm{s}})}{N} + u^2_{\mathrm{gp}}(U_{\mathrm{s}})}. \tag{3.13}$$

Here, $\sigma(U_{\mathrm{s}})$ is the standard deviation of $U_{\mathrm{s}}$ over the sampling period, $N$ the number of data points, and $u_{\mathrm{gp}}(U_{\mathrm{s}})$ is the manufacturer-provided 'combined calibration uncertainty' (*Vaisala 2017c*; see also Fig. 3.10 and Table A.1). It is assumed that the 1 s sonde readings are uncorrelated.

#### 3.2.3.4 Combined GRUAN pre-launch uncertainty for relative humidity

The uncertainty of the SHC check result for relative humidity is

$$u\left(\Delta U_{\mathrm{SHC}}\right) = \sqrt{u^2\left(\overline{U_{\mathrm{s}}}\right) + u^2(U_{\mathrm{ref}})}. \tag{3.14}$$

As with temperature, the check result is used in the sense of a consistency check by comparison with the manufacturer-provided pre-launch uncertainty $u_{\mathrm{gp}}(U_{\mathrm{s}})$, and no correction is applied. Analogously the three cases apply (uncertainties for $k = 1$):

1) If no GRUAN SHC-check is performed, the pre-launch uncertainty is calculated as

$$u_{\mathrm{cal}}(U_{\mathrm{s}}) = \sqrt{u^2_{\mathrm{gp}}(U_{\mathrm{s}}) + \sigma^2_U}, \tag{3.15}$$

   with $\sigma_U$ the result of a statistical analysis of available GRUAN SHC ground check results for relative humidity: $\sigma_U = 0.84$ %RH; $N = 14545$.

2) If the measured mean deviation is smaller or equal to its uncertainty,

$$\frac{|\Delta U_{\mathrm{SHC}}|}{u(\Delta U_{\mathrm{SHC}})} \leq 1, \tag{3.16}$$

   then the SHC-result is consistent with the manufacturer-provided pre-launch uncertainty.

$u_{\mathrm{gp}}(U_{\mathrm{s}})$ is then passed on as overall pre-launch uncertainty:

$$u_{\mathrm{cal}}(U_{\mathrm{s}}) = u_{\mathrm{gp}}(U_{\mathrm{s}}). \tag{3.17}$$

3) If the ratio in Eq. (3.16) exceeds unity, $|\Delta U_{\mathrm{SHC}}|$ is taken instead as pre-launch humidity uncertainty, but limited upwards:

$$u_{\mathrm{cal}}(U_{\mathrm{s}}) = |\Delta U_{\mathrm{SHC}}|\,, \tag{3.18}$$

$$u_{\mathrm{gp}}(U_{\mathrm{s}}) < u_{\mathrm{cal}}(U_{\mathrm{s}}) \leq \sqrt{u^2_{\mathrm{gp}}(U_{\mathrm{s}}) + \sigma^2_U}). \tag{3.19}$$

## 3.3 Measurement scheduling

**Launch frequency** The daily launch times of the majority of the approximately 800 operating radiosonde stations worldwide adhere to some or all of the previously established synoptic times for ascents (00, 06, 12, 18 UTC). For GRUAN, a strict observance of this formal temporal scheme is not essential, and even potentially disadvantageous in some respects. A scheduling that meets the requirements of GRUAN shall be based on the following criteria:

- The routine launches should always take place at appropriate but fixed (local) times of the day, for example midnight or noon.
- To avoid issues connected with solar radiation, nighttime launches are preferred.
- Due to the particular radiation conditions, sunset and sunrise phases tend to bring increased uncertainties associated with data processing. If only one sounding is scheduled per day, the launch time should be set to exclusively either a night or daylight situation if possible.
- On occasion, launch times should be synchronised with other available measurement systems, whether on-site or with regularly passing satellites. Redundant measurements, i.e. observations of the same atmospheric state with different measurements systems, are important, and enables validation of systems.

GRUAN relies on long-term observations based on continuous measurements with sufficiently high sampling frequency. However, the number or frequency of soundings achievable at a station is usually limited by the available financial and human resources. These two aspects should be carefully weighed before determining the scope of measurements at a site, especially against the background that the extent of a programme should be changed as little as possible, reductions in the planned schedule should be particularly avoided. A daily radiosounding or more is a sound basis for analysing climate trends. If this exceeds a stations capacity, three soundings a week should be aimed for. An even lower frequency limits the usability of the data for trend analyses to certain altitude ranges (e.g. stratosphere) and variables (e.g. temperature), or requires observations over increased periods of time (e.g. 20 instead of 15 years) to enable the determination of significant trends.

**Re-launches** From GRUAN's point of view, immediate repetitions (re-launches) of occasionally failed soundings is not mandatory. However, it should be ensured that the targeted launch frequency is guaranteed for the vast majority of the soundings.

**Sounding altitudes** GRUAN targets to sounding altitudes of ∼30 km (pressure of ∼10 hPa) for daily radiosonde measurements (*GCOS-170*, 2013). That is, this height should be reached as frequently as possible, at least regularly, by using suitable balloon material. If this is impeded for superior reasons (e.g. ordered cost reductions) the following priorities should be considered as a basis for decision:

- Ozone soundings – Target altitude is ∼35 km (∼5 hPa); RS41 is the telemetry sonde
- Sounding of stratospheric water vapour – Target altitude is ∼30 km (10 hPa) (*GCOS-170*, 2013); RS41 is the telemetry sonde
- Intercomparisons with other radiosondes – Target pressure is <10 hPa
- Operational single soundings (at night) – Target pressure is <10 hPa
- Operational single soundings (daytime) – Target pressure is <10 hPa, but should be at least above the hygropause (about 18 km to 20 km at tropical latitudes).

**Reduction of the measurement programme** In the event of unavoidable adjustments to the current measurement programme, night flights should not be affected if possible, because they provide the most suitable basis for trend analyses. Comparison flights and multi-instrument flights with the RS41 serving as telemetry radiosonde should also be preferred using larger balloons if possible.

**Comparisons and redundant measurements** GRUAN sites are encouraged to perform long-term regular comparisons of their actual operational radiosonde with at least one other sonde, preferably a model from another manufacturer with existing or intended GRUAN Data Product (GDP). A weekly comparison with alternating daytime and nighttime flights is preferred.

Regular comparisons with sondes with existing GDPs are an important part of the GRUAN activities to evaluate and develop data products and to ensure data homogeneity. Even though it will certainly not be possible to include all GRUAN stations in such a measurement programme, care should be taken to cover all climate zones. This requires regular coordination within the network.

**Data submission** Measured data should be submitted to GRUAN in a timely manner after a sounding has been completed. Especially in the case of manually conducted soundings, the data submission to GRUAN (e.g. via RsLaunchClient) should be integral part of the operational sounding procedures. For the operational use of auto-launchers, a regular data transfer to GRUAN on a daily or weekly basis should take place.

A detailed description of the data flow can be found in Section 7.6.

# 4 Sensor characterisation and evaluation of GDP variables

This chapter describes experimental approaches to quantify the most important systematic biases in soundings with the RS41 radiosonde, namely the solar radiation error for the temperature sensor and the temperature-related time-lag for the humidity sensor. Corrections based on these experimental quantification are developed and implemented in the GRUAN data processing, including comprehensive uncertainty estimates, and summarised in this chapter. Furthermore, comprehensive analyses of the measurement uncertainties for all sensors including pressure (in case of the RS41-SGP model), and the position measurement (GPS), and for the derivation of pressure from GPS-related altitude measurements are carried out. The calculation and uncertainty estimates for other important product variables which are derived from the sensor measurements, especially position and humidity-related parameters, are presented.

## 4.1 Effect of solar radiation on RS41 temperature measurements

### 4.1.1 Solar heating of radiosonde temperature sensors

The heating of the temperature sensor by absorption of solar radiation is the most important error source for daytime radiosonde temperature measurements with the RS41. The effect may reach 1 K at 35 km altitude. A thorough quantification of the solar heating, and from that the derivation of a correction algorithm including uncertainty estimates, are essential for the quality of temperature in the GDP.

Within GRUAN, an experimental setup is developed called Simulator for Investigation of Solar Temperature Error of Radiosondes (SISTER) to quantify the heating. With this setup, the sensitivity to radiation is measured by exposing the radiosonde's sensor to light from an artificial source under controlled conditions. In a next step, an algorithm is developed and implemented in the GDP which calculates a correction of the radiation effect. For this, the experimental results are combined with modelled fluxes of shortwave solar radiation (Section 4.1.4). The correction is calculated as a function of the actual solar flux, air pressure, ventilation speed, and solar elevation. SISTER has the capability to take the effect of the changing sonde orientation into account, i.e. the radiative heating is averaged over the rotating movement of the sonde, which mimics the spinning around the vertical axis in ascents. A full description of the experiments and the radiation correction is presented in *von Rohden et al.* (2022). The results and some technical and practical aspects are summarised in the following.

## 4.1.2 Experimental approach

### 4.1.2.1 Setup and measurements

A laboratory setup (SISTER, Simulator for Investigation of Solar Temperature Error of Radiosondes) was developed at the Lindenberg Meteorological Observatory (Deutscher Wetterdienst) to quantify the sensitivity of the temperature measurement with radiosondes to solar radiation. It is designed to simulate conditions similar to those that a radiosonde is exposed during real ascents. This means that beside absolute pressure, the irradiation and flow conditions around the test sonde are reconstructed, including a simulation of the sonde's own rotational movements. The latter is important because the heating is sensitive to sonde's orientation relative to the Sun.

The setup has the following capabilities:

- Irradiation of a radiosonde with Sun-like light from an artificial source,
- Regulation of pressure according to the actual sounding altitude,
- Generation and control of air flow to ventilate the sonde,
- Variation of light incidence to mimic solar elevation,
- Simulation of orientation changes (sonde spinning) by rotation of the radiosonde during exposure,
- Installation of the radiosonde with angled sensor boom like in real ascents (important for ventilation).

All measurands are traceable to international standards and the results therefore comply with GRUAN's requirements of measurement traceability.

The facility is constructed as a wind tunnel with dimensions of approximately $(2 \times 1)$ m (Figure 4.1). It is assembled from 153 mm and 213 mm inner diameter metal tube sections. A 180 mm diameter quartz glass tube, integrated as one leg of the tunnel, serves as measuring chamber. The circuit board of the radiosonde is installed on a supporting rod in the central axis of the chamber. Radiation from a xenon arc lamp is applied from outside through the wall of the quartz tube, inducing shifts in the measured temperatures. The pressure can be controlled (see Table 4.2). At the same time, a uniform air flow is created at the position of the sonde, generated by a fan and a system of deflection units, and the air speed can be controlled as well. Before installation, the housing of the test sonde is removed to minimise the flow cross section and therefore minimise disturbances of the flow field. The sonde is installed in such a way that the air flow is similar to the situation of an ascending sonde in a real flight. In particular, the sensor boom of the RS41 radiosonde is bent at an angle of 45°, similar to a normal sounding.Technical information on the most important setup components is summarised in Table 4.1.

The rod carrying the radiosonde can be rotated using a stepper motor, so that the radiosonde spinning in soundings and therefore the changing illumination conditions can be recreated. The applied light spot is large enough so that the temperature sensor together with a sizeable part of the sensor boom are illuminated. In this way, the in-flight situation is approximated where the entire sensor boom is continuously exposed to sunlight, and the influence of the boom construction on the radiation error of the sensor is included. The angle of the incoming light can be varied by turning the entire setup relative to the fixed light source. This is used to mimic different solar elevation angles. The flux is varied by changing the distance between the chamber and the light source.

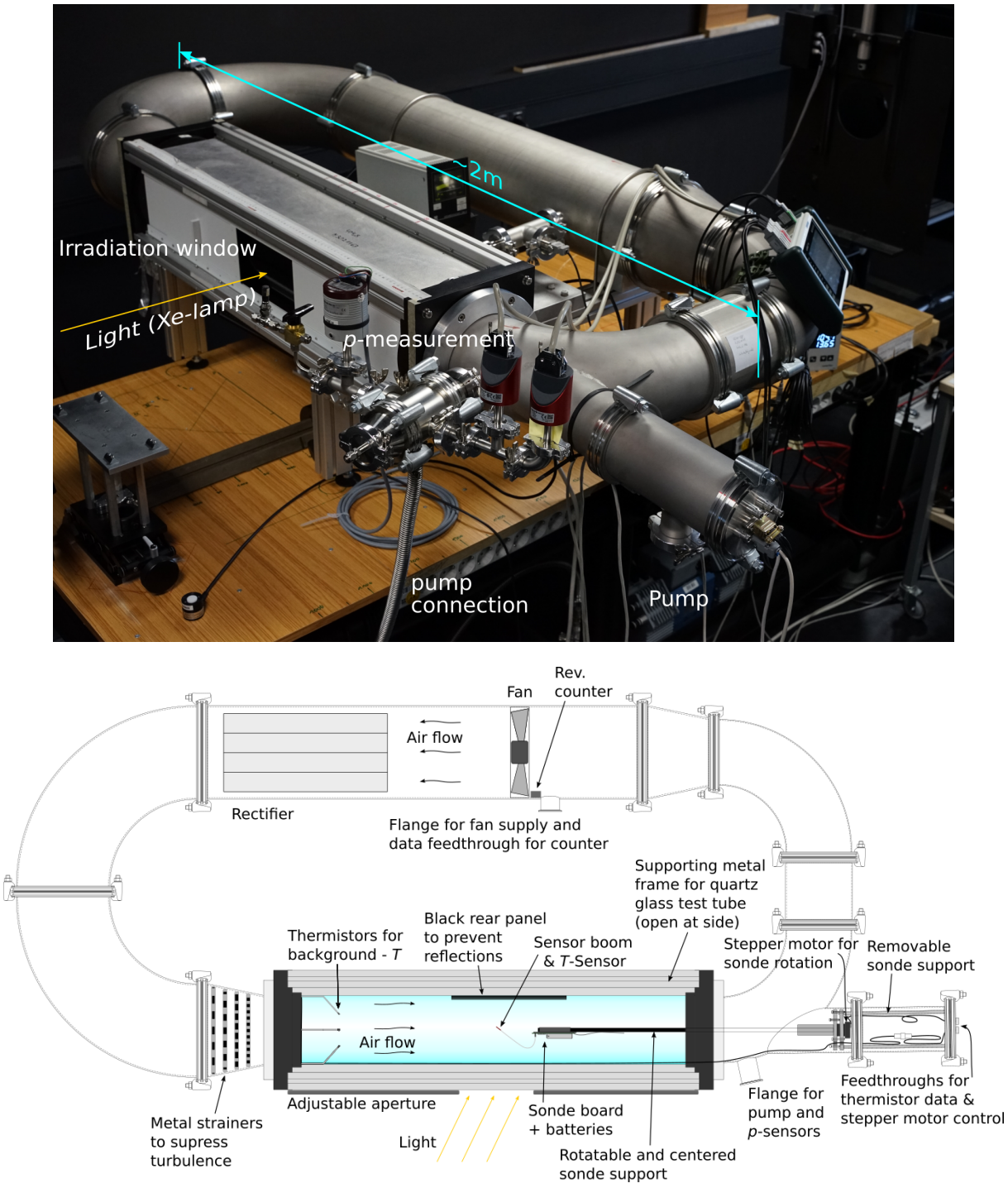


**Figure 4.1:** Photograph and schematic diagram of the experimental setup for the determination of the solar radiation bias in radiosonde temperature measurements.

**Table 4.1:** Specification of setup components.

| Component | Description / specification | Manufacturer |
|---|---|---|
| **Components** | | |
| Basic components (tubes, flanges, clamp screws, seals, etc.) | Standard components for vacuum technology (some parts as customisation) | Novotek Vakuumtechnik, Germany |
| Glass tube | $l$=1000 mm, 180 mm o.d., wall thickness 3.5 mm | QGT Quarzglastechnik, Germany |
| Glass tube connection | Al, FPM, DN 40 KF-26 | Inficon, Switzerland |
| Fan | Axial fan, mounted on DC-motor Faulhaber 3863H036C R, operating voltage and speed: 36 V, 5500 $\mathrm{min}^{-1}$ | Faulhaber, Germany |
| Pump | Diaphragm vacuum pump, MD 12 | Vacuubrand, Germany |
| Stepper motor | PD-1140 (PD42-1-1140-TMCL) with controller/driver, (0.22 to 0.7) N m, 24 V DC | Mocontronic Systems, Germany |
| Electrical feedthroughs | 9-pin Sub-D, 15-pin Sub-D (MIL-C-24308); BNC | VACOM, Germany |
| Light source | XBO 2500W/OFR, Xe-plasma lamp in LH-152N housing;<br>Power supply and control: TNX 4500<br>(Lamp at fixed position on optical bench) | OSRAM, Germany<br>Heinzinger Electronic, Germany |
| **Sensors** | | |
| Background temperature (4×) | Digital sensor N 801, FN0001K, NTC type N, cal. uncert. ($k$=2): 0.06 K, res.: 0.01 K | Ahlborn, Germany |
| Pressure(*) | Pressure sensor of RS41 sonde;<br>Ceram. capacit. gauges CMR 361 and 363 | Vaisala, Finland<br>Pfeiffer Vacuum, Germany |
| Irradiance | CMP22 pyranometer, (200 to 3600) nm, overall uncertainty $<$1 % | Kipp & Zonen B.V., The Netherlands |
| Revolution counter | FUA 919-3, retroreflective photoelectric sensor, 640 nm, unc.: 0.02 % of m.v. | Ahlborn, Germany |
| Measuring head for global radiation | FLA623GS, (400 to 1100) nm, (0 to 400) W $\mathrm{m}^{-2}$, absolute uncertainty $<$10 % (used for detection of irradiation periods) | Ahlborn, Germany |
| **Data aquisition** | | |
| Background thermistors, rev counter, FLA623GS | Multi-sensor data logger ALMEMO 710 | Ahlborn, Germany |
| Pressure(*) | Vaisala MW41 sounding system | Vaisala, Finland |
| Irradiance (CMP22) | Data logger Combilog 1022 | Theodor Friedrichs & Co., Germany |

(*) RS41 experiments with $p$ from sonde's own sensor (CMR $p$-gauges not yet installed at time of measurements)

The sensor boom is irradiated at limited time intervals. The duration of these intervals is such that the sensor temperature approaches a new thermal equilibrium (typically half a minute to three minutes, depending on the actual pressure and ventilation speed).

Due to the sonde rotation, the response shows an oscillating pattern on top of the main signal (see Section 4.1.3.2, Fig. 4.2). The actual radiation-induced temperature error is the time-averaged elevation relative to the temperature in the shade before and after the irradiation period. The new equilibrium temperature is estimated using a model fit to the sensor response data. The fit extends over an integer number of the oscillations which are associated with the rotation of the sonde. The background temperature is continuously recorded in parallel using thermistors at an upstream position relative to the sonde in the test chamber at the same sampling rate. Since the effective surface area of the sensor boom from the perspective of the sun also varies with sun elevation, measurements are performed for different angles of irradiation with respect to the central axis (see Table 4.3).

The data sets are recorded according to the following scheme:

- Set irradiance,
- Adjust pressure according to one of several predefined pressure levels,
- Adjust the ventilation speed according to pre-defined levels,
- Irradiate the rotating sonde long enough so that the sonde temperature reaches or at least converges to a quasi-constant value,
- Repeat the above scheme for different radiation incidence angles (sun elevation), and for a particular arrangement simulating the effect of diffuse radiation (see Section 4.1.2.2 below),

The solar temperature error $\Delta T$ is evaluated as the difference between effective indicated temperature and shade reference as a function of pressure, ventilation, and radiation incidence angle. The experimental parameter ranges and uncertainties are listed in Table 4.2.

**Table 4.2:** Adjustable ranges for parameters in experimental setup

| Quantity | Value | Typ. uncertainty |
|---|---|---|
| Pressure | Surf. to 3 hPa | (0.4 to 0.6) hPa |
| Ventilation | (0 to 6) m s$^{-1}$ | 0.5 m s$^{-1}$ |
| Irradiance | (0 to 2000) W m$^{-2}$ | 3.4 % |
| 'Sun elevation' | (0 to 90)°$^{(*)}$ | 2° |
| Sonde rotation | fixed at 16 s | – |

$^{(*)}$ (0 to 59)° continuously adjustable; 90° fixed

The pressure is measured with the sonde's own pressure sensor, because at that time the setup was not (yet) equipped with suitable pressure sensors. Pressure uncertainty includes the manufacturer's specification after ground preparation and a component derived from comparison tests with other pressure sensors. The velocity of the air flow (ventilation speed) was determined as function of the fan revolution at different pressures. This was carried out in extensive measurements using the Laser Doppler Anemometry (LDA) technique. With a dummy radiosonde installed in the same configuration as for the radiation tests, radial profiles of the axial flow speed were measured at a position close to the sensor boom. For further information, see *von*

*Rohden et al.* (2022). From the evaluation of the results, a constant overall uncertainty for the ventilation speed was estimated (Table 4.2). The uncertainty components for both pressure and ventilation are considered systematic (correlated).

The irradiance is controlled by the distance between the setup – more precise the position of the sensor – and the fixed light source, i.e. the setup was positioned along the beam direction according to an irradiance-distance relation, which was determined once before the experiments. The uncertainty estimate includes errors related to distance setting, temporal stability of the light source, and spatial homogeneity of the light spot directed to the sensor boom.

The radiation incidence angle is adjusted by moving the entire setup around a vertical axis through the position of the sonde sensor. In order to ensure a uniform irradiation over the entire cross-section covered by the rotating sensor boom, a correspondingly large light spot was projected (10 cm to 20 cm in diameter) through the adjustable aperture.

Besides the LDA-measurements for the determination of the air flow, a number of further experiments and investigations have been conducted, regarding the temporal stability and spatial homogeneity of the light source, the above mentioned derivation of a working relation between irradiance and distance from the light source, the light transmission (reflectivity and attenuation) through the wall of the quartz glass test chamber, and the relationship between irradiance and induced temperature error. More detailed information on this can be found in *von Rohden et al.* (2022).

#### 4.1.2.2 Key assumptions and limitations

Although the sonde spinning during ascents may be very unsteady it is presumed that it is on average reasonably reflected by the 16 s rotation period used. Tests have shown that the time-averaged bias does not significantly change for rotation periods between 4 s and 32 s. Further assumptions regarding the experimental design and the evaluation of the radiative heating of the temperature sensor $\Delta T$ are summarised in the following:

- Both sides of the sensor boom and the actual sensor are equally sensitive to irradiation.
- $\Delta T$ is proportional to irradiance $I$ (in W m$^{-2}$). This has been verified experimentally.
- Diffuse radiation generates the same $\Delta T$ as direct radiation given the same irradiance.To simulate the impact of the diffuse radiation, which makes up an essential part of the atmospheric short-wave radiation, direct radiation from the experimental light source was used. Due to the anisotropy of diffuse light, the sensor heating is essentially invariant with regard to the orientation, so that orientation-related averaging can be omitted, i.e. these tests were conducted without sonde rotation. The light was applied perpendicular to the boom surface. The overall $\Delta T$ in sounding is composed of the effects of both the direct and diffuse radiation components.
- It is assumed that existing spectral differences of the Xe-light source and sun do not introduce significant errors.
- The measurements are carried out at laboratory temperature only. Therefore the sensor heating is be investigated at low temperatures as present e.g. in the stratosphere or at the tropopause.

## 4.1.3 Data evaluation

### 4.1.3.1 Data sets

Table 4.3 summarises some parameters of the measured data sets. The overall number of data points for $\Delta T$ (see next Section 4.1.3.2) is 457. For further information on the different setup configurations we refer to *von Rohden et al.* (2022).

**Table 4.3:** Measured data sets, separated by incidence angle and irradiance.

| Angle / ° | $I$ / W m$^{-2}$ | Rot. period $T_R$ / s | N |
|---|---|---|---|
| 0 | 1142 | 16 | 55 |
| 20 | 1136 | 16 | 55 |
| 40 | 1111 | 16 | 54 |
| 59 | 1025 | 16 | 56 |
| 90 (a)$^{(*)}$ | 1142 | no rotation | 58 |
| 90 (b)$^{(*)}$ | 1142 | no rotation | 58 |
| 'diff' (a)$^{(*)}$ | 527 | no rotation | 61 |
| 'diff' (b)$^{(*)}$ | 527 | no rotation | 60 |

$^{(*)}$ (a) and (b) denote two realisations with 180° offset orientation in terms of the fixed angle of the sonde on the rotatable support rod.

### 4.1.3.2 Determination of solar temperature error

Figure 4.3 presents 1 s raw data of a measurement cycle of several hours. The four coloured solid lines are the shadow background temperatures from four thermistors installed at the upstream end of the test chamber (see Fig. 4.1) with a −1 K for better visibility. The curves in the upper panel are 1 s data of irradiance ($I_0$, orange), pressure (dark red) and ventilation speed (green). Over-plotted horizontal bars indicate values for these parameters averaged over the exposure periods. For irradiance, they are corrected for reflection and absorption at the wall of the quartz glass chamber ($I_{\mathrm{eff}}$).

Fig. 4.2 shows an example for the response of the RS41 temperature sensor to a ∼80 s light exposure at $v = 3.5\,\mathrm{m\,s^{-1}}$, $p = 6.9\,\mathrm{hPa}$, $I = 1111\,\mathrm{W\,m^{-2}}$,and an incidence angle of 40°. The plot shows radiosonde temperatures after subtraction of the shade temperature, which comes from the reference thermistor. When opening the aperture, the sensor temperature increases relative to the background, quickly in the initial phase, and then on average converging slower towards a quasi-constant value. With the sonde rotation, the actual amount of radiation absorbed by the sensor and sensor boom permanently changes, causing oscillating pattern on top of the mean signal.

The 1 s data of the sensor response are temporally averaged, i.e. over changes of the sonde orientation relative to the position of the light source. This is to reproduce averaging over the sonde's own spinning around the vertical in real soundings. The averaging is preformed by

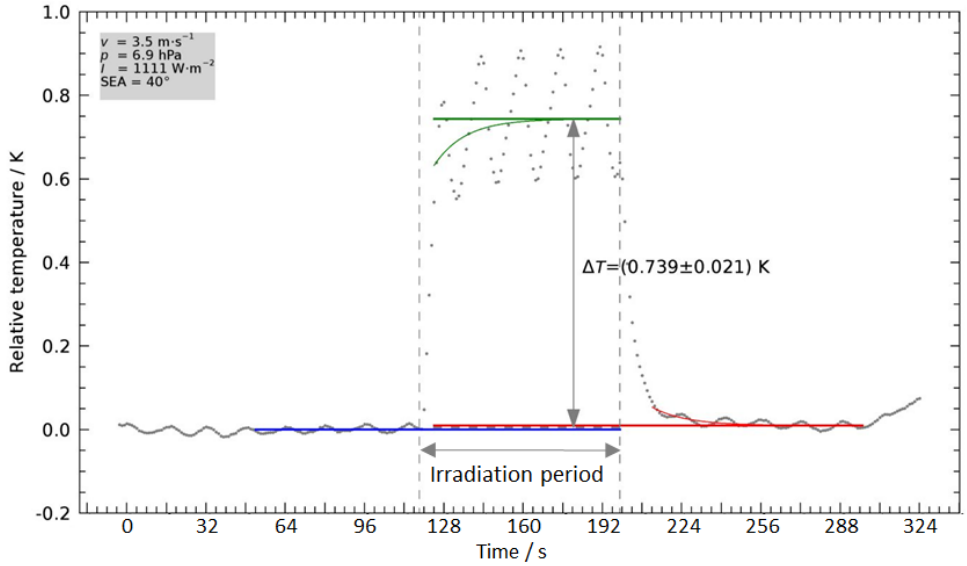


**Figure 4.2:** Example of the response of the RS41 temperature sensor to irradiation (dotted grey line) ($T$-peak at 25 000 s-time mark in Fig. 4.3). Straight blue line: $T$-mean in the shadow period $\sim$1 min before opening the shutter. Green curve: Fit to the $T$-response. Straight green line: $T$-response ($= c_0$) in equilibrium. Red curve: Equivalent fit after closing the shutter, with the straight red line indicating the re-established shadow-$T$. The shadow temperature (not shown) was subtracted from the sensor data before. The oscillations are due to the 16 s-rotation of the sonde.

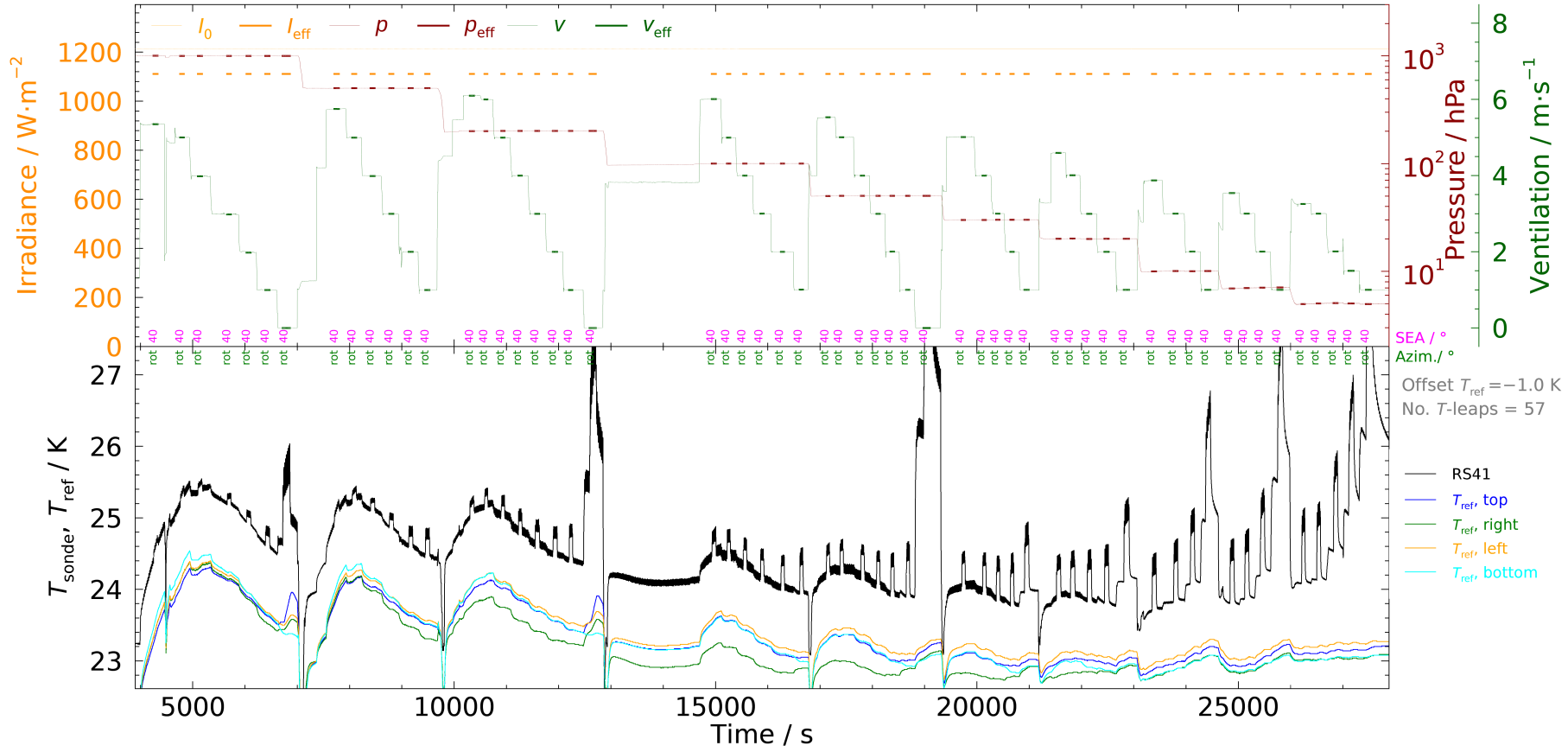


**Figure 4.3:** Example of a raw data including irradiance, pressure, and ventilation speed (upper panel), temperature of the radiosonde and shadow reference sensors (lower panel). The numbers in magenta denote the actual setting for the incidence angle (acc. to sun elevation), green labels indicate the angle of the sonde with respect to the central axis, in this case continuous rotation.

fitting a function of the form

$$\Delta T = c_0 + c_1 \exp(c_2 t) \tag{4.1}$$

to the data. The fit parameter $c_0$ represents the expected temperature equilibrium value. The data sections to be included in these fits are defined once and individually by hand for each illumination period.

After closing the shutter, the temperature declines back to the shadow level, following an equivalent convergent pattern. Therefore Eq. (4.1) is again used to re-determine the sonde temperature in shadow. The actual $\Delta T$ is determined by averaging the two differences between the temperature under illumination and the two shadow temperatures immediately before and after the exposure period.

#### 4.1.3.3 Data reduction and evaluation

Fig. 4.4 shows an example data set for an incidence of 59°, an irradiance of 1024 W m$^{-2}$, and a constant sonde rotation with $T_{\mathrm{R}}$ =16 s.

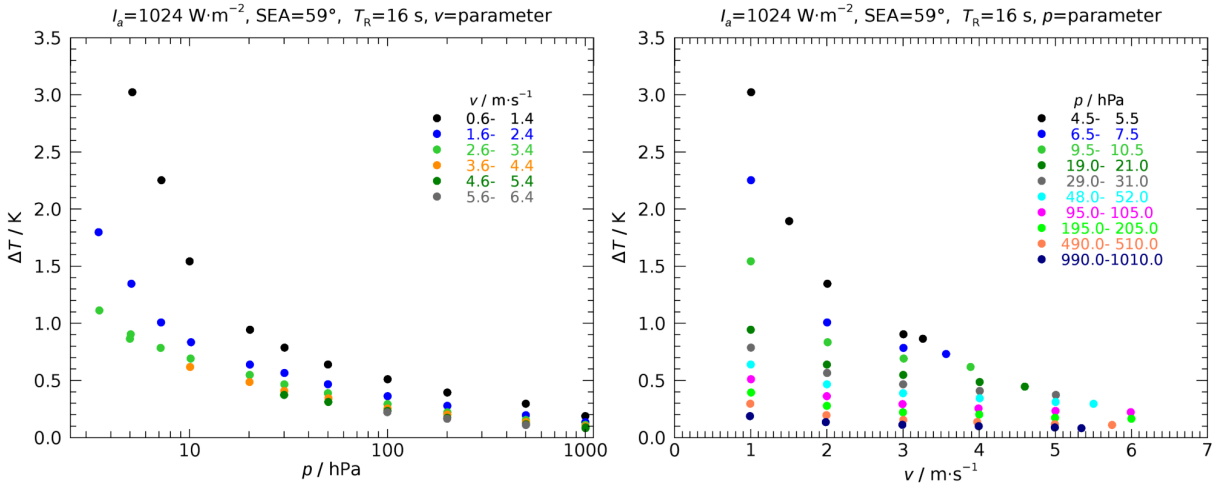


**Figure 4.4:** Example of measurement results. Left panel: $\Delta T$ vs. pressure, ventilation speed as parameter; logarithmic $p$-scale for better visibility. Right panel: $\Delta T$ vs. ventilation speed, pressure as parameter.

The change of $\Delta T$ with $p$ and $v$ can clearly be identified: for large values, the data points follow the expected convergence-like decrease towards zero; a strong increase is present on the other hand at low pressure and ventilation. This is consistent with the expectation of an inverse relation between radiative heating and cooling efficiency by the surrounding air flow at a given irradiance.

For each of the measurement runs (Table 4.3), i.e. for each setting of the incidence (angle and value of irradiance), a two-dimensional polynomial in terms of the square root of both $1/p$ and $1/v$ was fitted to the $\Delta T(p, v)$-data sets in the nonlinear least-squares sense to account for the

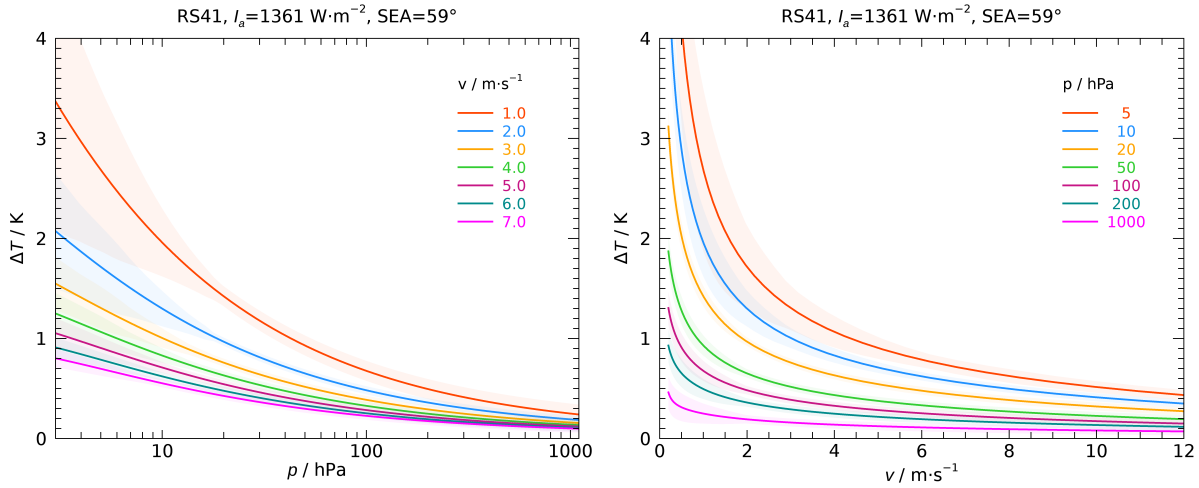


**Figure 4.5:** RS41 solar temperature error according to Eq. (4.2), scaled to an irradiance of 1361 W m$^{-2}$, and for an incidence angle ('SEA') of 59°. Shaded areas denote 1$\sigma$-uncertainty estimates.

combined effect of both quantities on the magnitude of radiative heating:

$$\Delta T(p, v) = \sum_{i,j} c_{ij} \left(\frac{1}{p^{1/2}}\right)^i \left(\frac{1}{v^{1/2}}\right)^j . \tag{4.2}$$

These expressions, together with uncertainty estimates (Section 4.1.3.4 and *von Rohden et al.*, 2022), are the experimental basis for the radiation correction (Section 4.1.5).

A comparison of the results from the different setup configurations calculated with Eq. (4.2) is shown in Fig. 4.5 – in a similar way to Fig. 4.4 – for $\Delta T(p)$ and $\Delta T(v)$ after correction to an (arbitrary chosen) irradiance of 1361 W m$^{-2}$. A comparison with regard to the incidence is shown in Fig. 4.6. Here, apart from the special configuration of the diffuse radiation measurements, $\Delta T$ deviates significantly at angles exceeding 59° (see 90°-curve at low $v$ in the right-hand panel of Fig. 4.6), which is why the angle-dependence (sun elevation) is taken into account in the creation of the radiation correction (see Section 4.1.5).

#### 4.1.3.4 Uncertainty estimates of experimental data

The overall uncertainty of the measured temperature error, $u(\Delta T)$, is a combination of four components:

- uncertainty associated with the determination of temperature differences, see Fig. 4.2,
- uncertainty connected to irradiation (3 %),
- uncertainty associated with pressure (0.4 hPa to 0.6 hPa),
- uncertainty associated with ventilation speed, set constant to 0.5 m s$^{-1}$ ($k = 1$).

The combined uncertainty is indicated as coloured shaded areas in Figs. 4.5 and 4.6. Before combination (sum of squares), the uncertainties of pressure and ventilation speed were converted to temperature uncertainty components via the local sensitivities $\frac{\partial(\Delta T)}{\partial p}$ and $\frac{\partial(\Delta T)}{\partial v}$ using

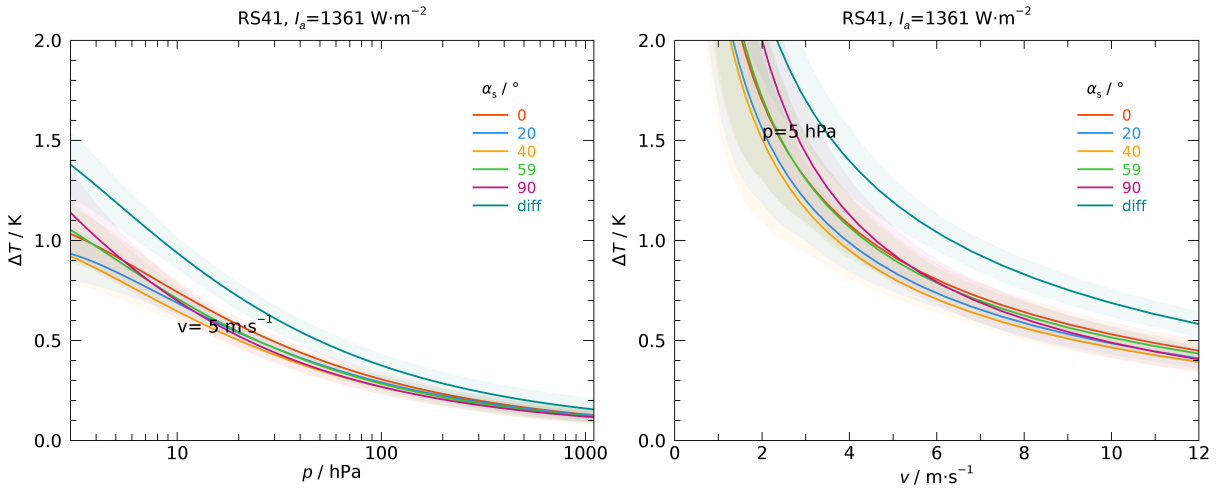


**Figure 4.6:** RS41 solar temperature error as function of pressure and ventilation for various radiation incidence angles ('SEA') and an irradiance of 1361 W m$^{-2}$. Shaded areas denote 1$\sigma$-uncertainty estimates. Left: Example for a ventilation of 5 m s$^{-1}$. Right: Example for a pressure of 5 hPa.

Eq. (4.2). The relative uncertainty of irradiation can directly be taken as relative uncertainty component for $\Delta T$ because of the proportionality. The ventilation is the largest contributor to the overall uncertainty.

Note that the above described uncertainties apply to the experimental results, not to the final radiation correction. The integration of the experimental results into the data processing, including the estimation of uncertainties, is outlined in Section 4.1.5.

### 4.1.4 Simulation of solar shortwave radiation using RTM Streamer

The radiative sensor heating varies with pressure, ventilation speed, position of the sun, and applied irradiance. The latter is not directly available from a radiosounding. Radiation fluxes are instead estimated during post-processing of the measured data using a radiation transfer model.

Within the development of the GRUAN Data Product (GDP) for the predecessor model Vaisala RS92 (*Dirksen et al.*, 2014) the Radiative Transfer Model (RTM) Streamer (*Key and Schweiger*, 1998) was chosen for radiation modelling. After review it was decided to use this model also for the RS41 processing because of the author's experience with the model software package and existing programming routines for integration in the GRUAN Data Processing System for radiosondes (GDPS). The information given in the following in this section essentially reproduces contents published in *von Rohden et al.* (2022).

In the RS92-GDP.2 the results for the radiation fluxes from the Streamer RTM simulations were stored in a predefined Look-Up Table (LUT) and were used as input for the radiation correction algorithm. However, the spatial grid was coarse, so that the following parameters and conditions were inadequately represented or covered:

- Actual atmospheric profile ($p$, $T$, $U$),

- Earth surface conditions (albedo),
- Height of clouds, and
- Cloud types.

For a more realistic representation of the radiation fluxes with better resolution, the existent simulation routine was largely redesigned. The atmospheric profile ($p$, $T$, $U$) measured by the radiosonde is directly used as input for the discrete layers of the RTM. The radiative properties of the earth's surface are reproduced in more detail from an existing global albedo data set, including seasonal variances at a monthly resolution (mean annual cycle). Additionally, cloud layers are defined relative to the height of the tropopause and the launch point.

The scenarios to be simulated are defined according to the sun position of the current radiosounding trajectory in order to achieve realistic results. At the same time the simulation depth or simulation accuracy is appropriately chosen to limit computational effort to a feasible level (usage of very fast, but slightly less precise, two-stream method). The LUTs contain a sufficient number of values so that linear interpolation between the discrete simulated points can be used to get the input values for the radiation correction procedure for each data point in the original sounding profile.

#### 4.1.4.1 Inclusion of the measured atmospheric profile

The number of levels or layers simulated with the RTM is limited to about 100. Therefore it is necessary to sample the measured atmospheric profile, which is available at a resolution of $\sim$5 m, onto a much coarser grid for input. This is realised by simply taking the closest value with respect to a defined altitude level, i.e. neither prominent points in the atmospheric profile nor interpolated values are used.

The layers are defined as follows:

- (0 to 5) km in 250 m steps,
- (5 to 21) km in 500 m steps,
- (21 to 36) km in 1000 m steps,
- (36 to 52) km in 2000 m steps.

Due to the variable altitudes of balloon burst points, a suitable reference radiosonde profile is defined which is used to fill layers at (higher) altitudes not covered by the actual profile. Such reference profiles are available for the following latitude ranges $\phi$:

- Tropics: $\phi < 23.43°$,
- Mid-latitudes (summer and winter): $23.43° \leq \phi < 66.56°$,
- Arctic: $\phi \geq 66.56°$.

#### 4.1.4.2 Surface albedo

The natural spatial and temporal variability of the surface albedo is significant and is represented in the simulation of the short-wave solar radiation at a global scale by using suitable available data sets.

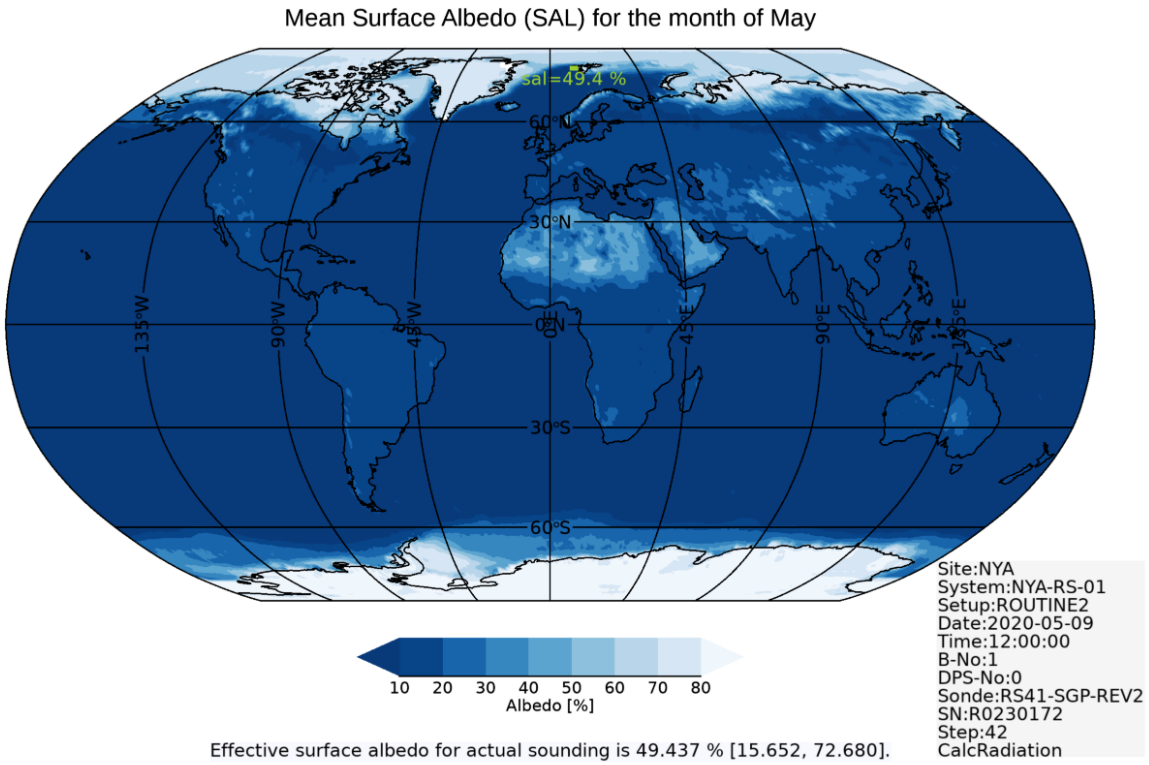


**Figure 4.7:** Example of the global mean surface albedo from the global CM-SAF data set (*Karlsson et al.*, 2017). The albedo is processed for the time of each radiosounding.

For the implementation in the GDPS a global data set of CM-SAF (CLARA_AVHRR_V002, *Karlsson et al.*, 2017) was chosen as a basis and optimised for this application. From this data set, an average working subset was generated for the surface albedo (SAL). It covers the period Jan 2005 to Dec 2015 including monthly means at a spatial resolution of 0.25°×0.25°. During the operational processing, a representative albedo is determined for each flight as arithmetic mean of all relevant data points (see Figure 4.7). Depending on the ascent date, the corresponding month is selected. Depending on the trajectory of the current sounding, a rectangle is determined, which encloses the trajectory's latitude-longitude space.

#### 4.1.4.3 Cloud simulation

Back-scatter from clouds is generally more variable in space and time than the earth's surface albedo. In principle, indications for the existence of cloud layers (and sometimes cloud types) can be retrieved to certain extent from the measured profile data, primarily by means of relative humidity. However, in most cases it is largely undefined to what extent these indications are representative for the cloud situation and its changes along the entire flight path. Therefore, it was decided not to operationally rely on such cloud detection. Also, the inclusion of external cloud information is in principle conceivable. However, real-time acquisition and evaluation of such information at sufficient spatial and temporal resolution seems too costly, or is even not available, for an integration into the operational processing.

Instead, a fixed cloud scenario was defined, which is used as a starting point for each radiosonde profile. The scenario includes two cloud layers: a water cloud comparatively close to the earth's surface, and a high altitude ice cloud below the tropopause. This means that tropopause height detection is a necessary preparatory step. In case the maximum height of a sounding is too low to determine the tropopause level, a standard altitude of 7.5 km is used. In Table 4.4 more details on the defined cloud layers are listed.

**Table 4.4:** Details for cloud layer scenario definitions.

| **Parameter** | Layer 1 | Layer 2 |
|---|---|---|
| Phase | liquid | ice solid col. |
| Optical thickness | 15.7 | 1.1 |
| Water content | 0.1 g/m$^3$ | 0.01 g/m$^3$ |
| Cloud top height | 3.0 km | tropopause |
| (if no tropopause) | | 7.5 km |
| Cloud thickness | 1.0 km | 2.0 km |

In addition to the cloud scenario, a clear-sky (cloudless) case is simulated with otherwise the same modelling settings.

#### 4.1.4.4 Position of the sun

For proper calculation of the solar radiation fluxes, the exact position of the sun relative to the radiosonde is required. Since the radiosonde follows a trajectory, where geographical position and altitude are changing with time, it is necessary to calculate the position of the sun individually for each data point. Furthermore it is important to make sure that the algorithm precisely calculates the altitude above the earth's surface – this is often not done in simpler algorithms.

The "NREL's Solar Position Algorithm (SPA)" is used, which is available as source code (in C), see *Reda and Andreas* (2004, 2003). It was transferred to IDL and adapted for use in the GDPS. Exact values for the sun position allow the detection of day, night and twilight conditions. An example is shown in Figure 4.8 for a twilight case at the Singapore GRUAN site.

#### 4.1.4.5 Horizon correction

The zenith angle of the horizon is not fixed at 90° during a radiosounding but slightly increasing (>90°) with altitude because of the curvature of the Earth. That is, situations may occur where the sonde at certain altitudes is affected by solar radiation while the sun, as seen from the ground, is still (or already) below the horizon. The RTM Streamer, however, assumes an atmosphere over an infinite flat surface without taking the curvature of the Earth into account, i.e. the zenith angle covers the range between exactly 0° and 90°. The effect is corrected for in the GRUAN RS41 processing (see *von Rohden et al.*, 2022). This zenith angle 'extension' beyond 90° is called horizon correction here.

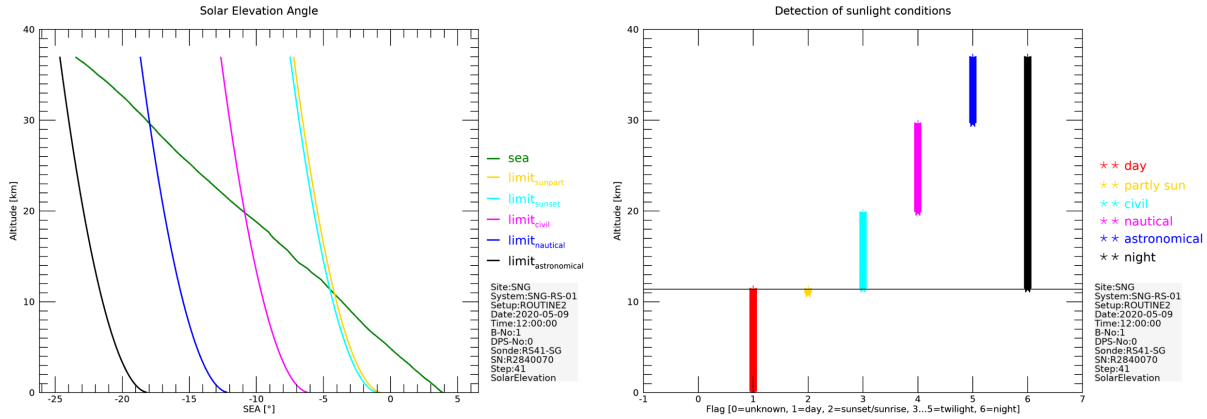


**Figure 4.8:** Example of calculated solar elevation angle and assignment to daylight phases (day, night, or twilight).

#### 4.1.4.6 Simulation runs and LUTs

Since a radiosonde flight is a trajectory rather than a vertical profile at a fixed time, the solar zenith angle varies during the flight. To account for this, a number of simulations are performed individually for each sounding for different zenith angles which cover the actual range. This is done for different zenith angles (with resolution 0.5°) which results in a flight-dependent number of required simulations (in the range between 5 and 50). This set of simulations is doubled for each sounding to account for both the cloudy (Section 4.1.4.3) and the clear-sky scenario.

The results of the simulations are temporarily stored, and for each of the two scenarios, Look-Up Tables (LUTs) are generated for three variables: $I_{\mathrm{SW,dir,down}}$, $I_{\mathrm{SW,dif,down}}$ and $I_{\mathrm{SW,dif,up}}$, with 'SW' denoting 'short-wave', 'dir'='direct', 'dif'='diffuse', respectively. The LUTs have two dimensions: altitude and solar zenith angle. The resolution of the LUTs is sufficiently high so that for the final radiation correction, linear interpolation between the grid points is used to extract the radiation fluxes according to the actual points in the radiosonde profile.

The RTM results refer to a plane horizontal surface. In order to retrieve the direct solar irradiance on the radiosonde, i.e. with vertical irradiation, the Streamer-calculated direct solar irradiance ($I_{\mathrm{SW,dir,down}}$) is divided by sinus of the solar elevation angle (SEA).

#### 4.1.4.7 Results and uncertainty estimates

After simulation runs and assignment to the actual radiosonde trajectory the following radiation profiles are available:

- $I_{\mathrm{dir,down,cs}}$ and $I_{\mathrm{dir,down,cl}}$ (also called $I_{\mathrm{dir,cs}}$ and $I_{\mathrm{dir,cl}}$),
- $I_{\mathrm{dif,up,cs}}$ and $I_{\mathrm{dif,up,cl}}$,
- $I_{\mathrm{dif,down,cs}}$ and $I_{\mathrm{dif,down,cl}}$,

with $I$ being radiances in $\mathrm{W\,m^{-2}}$, and with the subscripts "cl" and "cs" standing for "cloudy" and "clear sky" (=cloudless), respectively. With regard to the diffuse radiation components, no

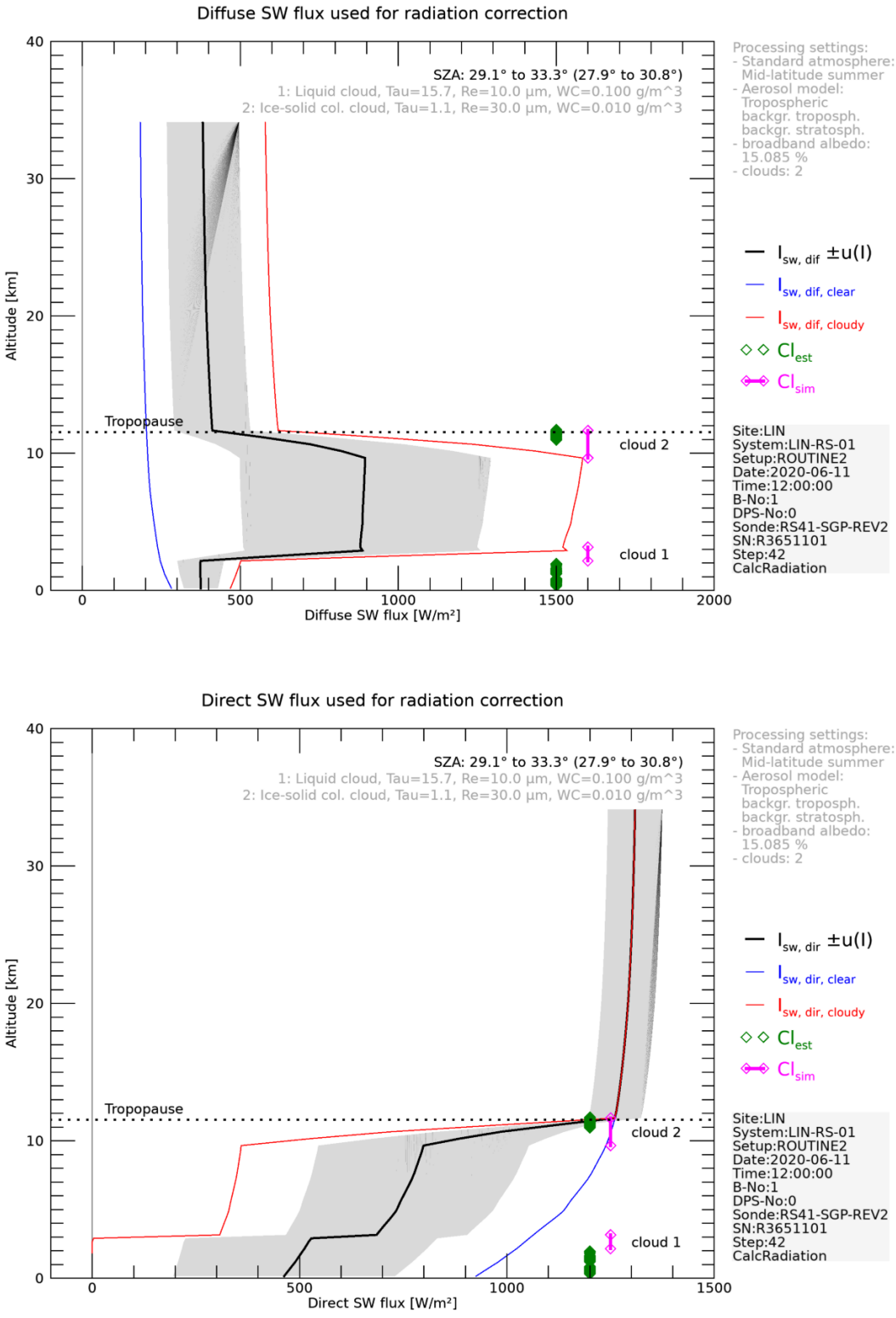


**Figure 4.9:** Example of simulated radiation fluxes including uncertainty estimates (traces and grey shaded area, respectively). Marks in magenta colour denote the cloud layers defined in the scenarios as used in all simulations ($Cl_{\mathrm{sim}}$); green symbols indicate heights with the potential presence of clouds based on the measured humidity profile ($Cl_{\mathrm{est}}$; $U > 97\,\%\mathrm{RH}$).

distinction between “up” and “down” is made for the radiation correction (see Section 4.1.5), which is why these components can be combined for the “cloudy” and “cloudless” scenarios, respectively:

$$\begin{aligned} I_{\mathrm{dif,cs}} &= I_{\mathrm{dif,down,cs}} + I_{\mathrm{dif,up,cs}} \\ I_{\mathrm{dif,cl}} &= I_{\mathrm{dif,down,cl}} + I_{\mathrm{dif,up,cl}}. \end{aligned} \tag{4.3}$$

From the two scenarios, average profiles of the two radiation quantities $I_{\mathrm{dir}}$ and $I_{\mathrm{dif}}$ are then calculated:

$$\begin{aligned} I_{\mathrm{dir}} &= \frac{1}{2}(I_{\mathrm{dir,cs}} + I_{\mathrm{dir,cl}}) \\ I_{\mathrm{dif}} &= \frac{1}{2}(I_{\mathrm{dif,cs}} + I_{\mathrm{dif,cl}}). \end{aligned} \tag{4.4}$$

The uncertainties for $I_{\mathrm{dir}}$ and $I_{\mathrm{dif}}$ are determined from the differences between the two scenarios:

$$\begin{aligned} u(I_{\mathrm{dir}}) &= \frac{|I_{\mathrm{dir,cs}} - I_{\mathrm{dir,cl}}|}{2\sqrt{3}} \\ u(I_{\mathrm{dif}}) &= \frac{|I_{\mathrm{dif,cs}} - I_{\mathrm{dif,cl}}|}{2\sqrt{3}}. \end{aligned} \tag{4.5}$$

In a second step, a lower limit (minimum) is for the uncertainty is defined, which is set relative (5 %) to the calculated average radiation. This lower limit is based on sensitivity tests, and it is introduced because the RTM is operated in the simple solution variant (two-stream method) for the sake of computing speed:

$$\begin{aligned} u_{\mathrm{min}}(I_{\mathrm{dir}}) &= 0.05 \cdot I_{\mathrm{dir}} \\ u_{\mathrm{min}}(I_{\mathrm{dif}}) &= 0.05 \cdot I_{\mathrm{dif}}. \end{aligned} \tag{4.6}$$

At low sun elevations between 0° and 5° significant refraction occurs in the curved atmosphere. Neither refraction nor earth curvature are taken into account in Streamer simulations. Therefore it was decided to double the minimum uncertainty $u_{\mathrm{min}}$ for solar elevations angles lower than 5°.

The final output of the RTM simulations are profiles of direct and diffuse radiation fluxes including uncertainty estimates (see example profiles in Figure 4.9) which are used for the solar radiation correction of the radiosonde’s temperature measurements in combination with the experimentally determined radiation sensitivities:

- $I_{\mathrm{dir}}$ and $u(I_{\mathrm{dir}})$
- $I_{\mathrm{dif}}$ and $u(I_{\mathrm{dif}})$.

### 4.1.5 Radiation correction and uncertainties

The experimental results from the radiation experiments are summarised in Look-Up Tables (LUTs) for both direct and diffuse light, and these tables are accessed during processing of the sounding raw temperature data. The LUTs contain the $\Delta T$ from the model fit to the experimental data (Eq. 4.2) after linear conversion ('normalisation') to an arbitrarily defined irradiance of $1000\,\mathrm{W\,m^{-2}}$, see also the second point in Section 4.1.2.2). The uncertainties (Section 4.1.3.3) are converted in the same way and stored as well. In the LUT for the direct light component, individual sets are stored for each experimental incidence angle. The LUTs also contain the normalised sensitivities $\frac{\partial(\Delta T)}{\partial p}$ and $\frac{\partial(\Delta T)}{\partial v}$, calculated from Eq. (4.2). The quantities normalised in this way are given the subscript "n" in the following.

Based on the LUTs and the values for $p$, $v$, and sun elevation in the measured profile, the actual final temperature correction $\Delta T_{\mathrm{rad}}$ and its uncertainty are calculated with the following steps for each data point in the profile:

1) Read out the "normalised" values of the experimentally measured radiation error $\Delta T_{\mathrm{n}}$ from the LUT by linear interpolation with respect to $p$, $v$, and Sun Zenith Angle (SZA); linearly convert these values according to the actual radiance output $I_{\mathrm{RTM}}$ from the Radiative Transfer Model (RTM) Streamer (see Section 4.1.4.7):

$$\Delta T'(p, v, \mathrm{SZA}) = \frac{I_{\mathrm{RTM}}}{I_{\mathrm{n}}} \cdot \Delta T_{\mathrm{n}}(p, v, \mathrm{SZA}). \tag{4.7}$$

   This step is done for both the direct and diffuse radiation components. There is no SZA-dependence for the diffuse component. The prime indicates intermediate steps.

2) Calculation of the uncertainty of $\Delta T'$ combining the "normalised" contributions from laboratory experiments (Section 4.1.3.4) stored in the LUT, and the RTM (Section 4.1.4):

$$u_{\mathrm{Exp,RTM}}(\Delta T') = \Delta T' \cdot \sqrt{\left(\frac{u(\Delta T_{\mathrm{n}})}{\Delta T_{\mathrm{n}}}\right)^2 + \left(\frac{u(I_{\mathrm{RTM}})}{I_{\mathrm{RTM}}}\right)^2}. \tag{4.8}$$

   Both components under the square root are statistically independent.

3) 'Conversion' of the uncertainties of measured $p$ and $v$ in the actual radiosonde profile to temperature uncertainties by multiplication with the sensitivities stored in the LUTs:

$$u_{p,v,\mathrm{n}}(\Delta T') = \left|\frac{\partial(\Delta T')}{\partial(p,v)}\right|_{\mathrm{n}} \cdot u(p,v). \tag{4.9}$$

4) The sensitivities are given in 'normalised' form as well. Therefore $u_{p,v,\mathrm{n}}(\Delta T')$ is scaled back with the altitude-dependent factor $f_{\mathrm{sc}}(z) = I_{\mathrm{RTM}}(z)/I_{\mathrm{n}}$:

$$u_{p,v}(\Delta T') = u_{p,v,\mathrm{n}}(\Delta T') \cdot f_{\mathrm{sc}}. \tag{4.10}$$

5) The uncertainty components in Eqs. (4.8) and (4.10) are combined:

$$u_{\mathrm{dir|dif}}(\Delta T') = \sqrt{u_p^2(\Delta T') + u_v^2(\Delta T') + u_{\mathrm{Exp,RTM}}^2(\Delta T')}. \tag{4.11}$$

The subscript "dir|dif" in Eq. (4.11) indicates that the steps in Eqs. (4.7) to (4.11) are done separately for both the direct and diffuse radiation components $I_{\mathrm{dir}}$ and $I_{\mathrm{dif}}$ from the RTM output and the two LUTs.

The diffuse short-wave radiation is solar light scattered by air molecules and particles (e.g. clouds) as well as back-scatter from the Earth's surface (albedo). Its overall intensity is therefore closely linked to that of the direct light from the Sun. For this reason it is assumed that the uncertainties of the direct and diffuse RTM results are strongly correlated. This is taken into account in the following steps:

6) It is assumed that the direct and diffuse radiation components induce the same temperature effect per W m$^{-2}$ (Section 4.1.2.2 on page 54). During a radiosonde flight, the sensor boom is exposed to different diffuse radiation components from both above and below hemispheres, and both sum up to the overall diffuse flux. Assuming that the anisotropy of the diffuse radiation involves independence of the heating effect on the incidence angle, the radiative energy taken up by sensor boom is independent on the actual boom angle relative to the vertical, and there is also no dependency on the horizontal orientation (sonde rotation). Thus, the direct and diffuse radiative heating effects overlap, and the combination of the two components (both given with Eq. (4.7) is considered as the overall altitude-dependent sensor heating $\Delta T_{\mathrm{rad}}$ and is equivalent to the correction amount:

$$\Delta T_{\mathrm{rad}} = \Delta T'_{\mathrm{dir}} + \Delta T'_{\mathrm{dif}}. \tag{4.12}$$

7) Accordingly, the two uncertainty components for the RTM-modelled direct and diffuse radiation components calculated with Eq. (4.11) are combined, taking into account their correlation (assumed as fully correlated according to a correlation factor of 1). Thus, in addition to the two terms from Eq. (4.11), a correlation term arises (see *JCGM*, 2008, page 21):

$$u(\Delta T_{\mathrm{rad}}) = \sqrt{u^2(\Delta T'_{\mathrm{dir}}) + u^2(\Delta T'_{\mathrm{dif}}) + 2 \cdot \frac{\partial(\Delta T'_{\mathrm{dir}})}{\partial I_{\mathrm{dir}}} u(I_{\mathrm{dir}}) \cdot \frac{\partial(\Delta T'_{\mathrm{dif}})}{\partial I_{\mathrm{dif}}} u(I_{\mathrm{dif}})}, \tag{4.13}$$

with the sensitivities derived from Eq. (4.7) as

$$\frac{\partial(\Delta T'_{\mathrm{dir}})}{\partial I_{\mathrm{dir}}} = \frac{\Delta T_{\mathrm{n,dir}}}{I_{\mathrm{n,dir}}}, \qquad \frac{\partial(\Delta T'_{\mathrm{dif}})}{\partial I_{\mathrm{dif}}} = \frac{\Delta T_{\mathrm{n,dif}}}{I_{\mathrm{n,dif}}}. \tag{4.14}$$

Figure 4.10 shows an example for the solar radiation correction, together with an analysis of the uncertainty components. The correction amount in the troposphere (0.10 K to 0.25 K) is low but significant, and increases to about 0.9 K in that case at the top of the profile. The uncertainty in the troposphere is enhanced as a result of the cloud scenarios applied in the RTM simulations (Section 4.1.4.7).

Oscillations a few km in height can be identified in the upper part of the correction profile. This is attributed mainly to atmospheric gravity waves, and may – depending on the state of the atmosphere – in some soundings be a very prominent feature. Because ventilation is essentially derived from the GPS-based ascent speed (see Section 4.4.4), i.e. relative to the vertical coordinate and not relative to the ambient air which can move vertically, the calculated ventilation speed may locally deviate from the true situation. In case of the presence of gravity waves this

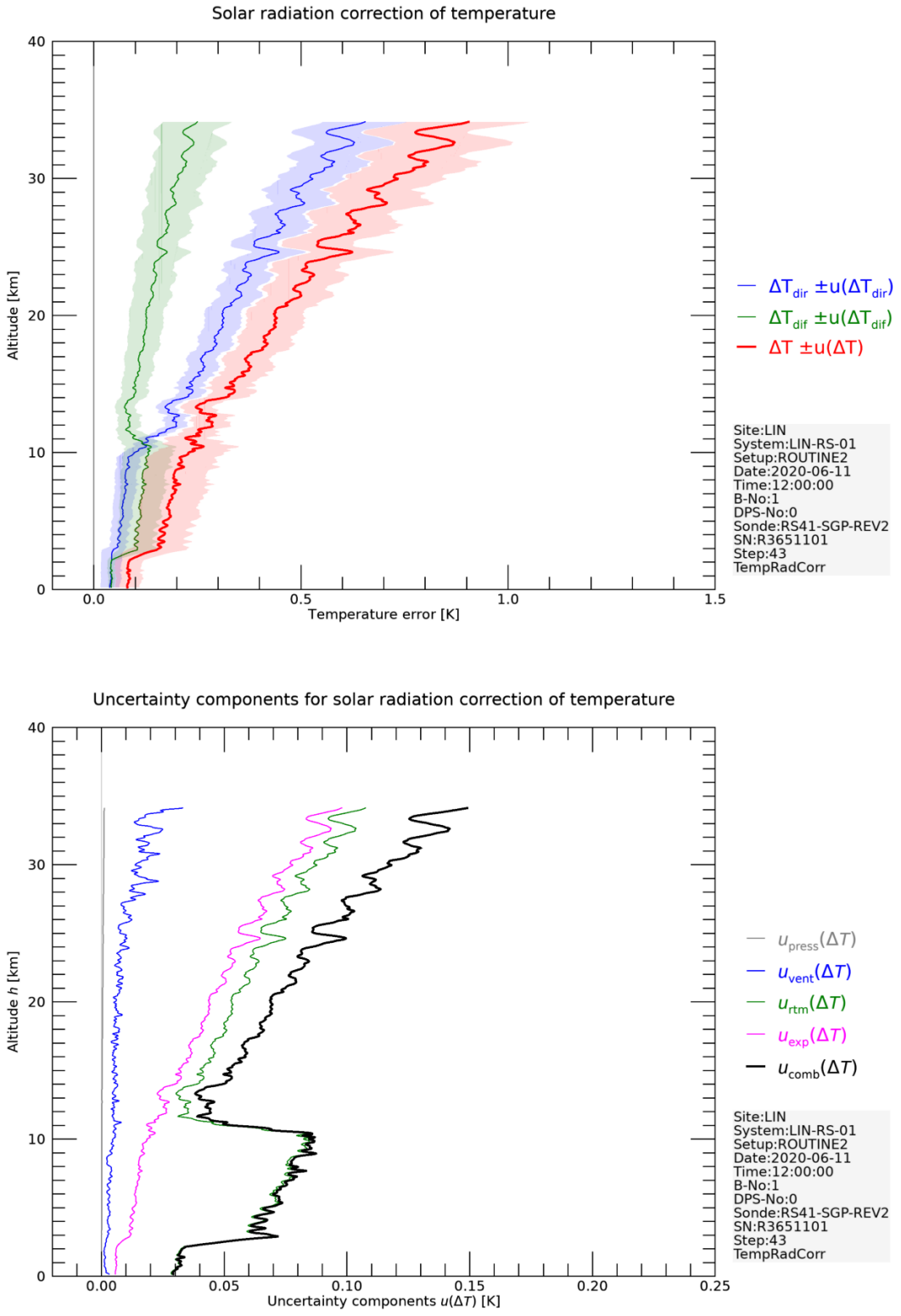


**Figure 4.10:** Top: Example profile for the amount of correction for temperature in sounding due to solar sensor heating (red curve including uncertainty ($k$=1) as shaded area). The proportions due to the diffuse and direct radiation components are shown with the green and blue curves. Bottom: Uncertainty components ($k$=1).

produces oscillations. These pattern in turn are imprinted in the final temperature correction because ventilation goes into the correction formula. Such effects are not corrected for in the current version of the RS41-GDP.

## 4.2 Time-lag for humidity measurements

### 4.2.1 Time-lag effect and correction approach

The Vaisala RS41 radiosonde uses a capacitive sensor to measure relative humidity. A hydrophilic porous polymer material as a thin film between two electrodes forms a plate capacitor. Water molecules exchange between the free moist air and the pores of the polymer matrix by diffusion. Adsorption or desorption of the molecules on the surface of the porous material changes the effective dielectric constant of the polymer and therefore its electrical capacitance, which is the actual measurement signal used to derive the relative humidity of the air.

The rates of adsorption and desorption as well as the diffusion slow down considerably with decreasing sensor temperature. That is, with decreasing temperatures, the sensor responses increasingly slower to changes of humidity during the flight. As a result the measured humidity profile is a smoothed (low-pass filtered) and time-lagged reflection of the true humidity profile. The effect is particularly noticeable if the radiosonde passes strong vertical humidity gradients in the upper troposphere and tropopause where atmospheric temperatures are low. The time lag can be experimentally measured, and based on the results, a correction to be applied in the post-flight processing can be derived.

Ideally, the temporal response behaviour of the sensor can be described with a single time constant. For an instantaneous, i.e. step-wise change of relative humidity of the air from one humidity level $U_0$ to another level $U_\infty$ at time $t = 0$, this time constant is the reciprocal of the time the sensor readings take to reach 63.2 % of that step. The humidity measured after the step evolves according to a converging curve of the form

$$U(t) = U_\infty - (U_\infty - U_0) \cdot \exp\left(-\frac{t}{\tau}\right). \tag{4.15}$$

The time constant is $1/\tau$. Accordingly is $\tau$ the '63%'-response time, i.e. the time to reach the portion $(1 - 1/e)$ of the step. Equation (4.15) is the solution of the growth-law equation which describes the time evolution of the (measured) humidity driven by the difference to the "true" ambient humidity $U_\infty$:

$$\frac{dU}{dt} = \frac{1}{\tau}(U_\infty - U(t)). \tag{4.16}$$

On the discrete time grid $t_j$ of the RS41 profiles, using $U_\infty \to U_\mathrm{a}$ and $U \to U_\mathrm{m}$, the evolution of the measured value $U_\mathrm{m}$ within each time step $\Delta t = t_i - t_{i-1} = 1\,\mathrm{s}$ can be modelled with the above described approach:

$$U_\mathrm{m}(t_i) = U_\mathrm{a}(t_i) - [U_\mathrm{a}(t_i) - U_\mathrm{m}(t_{i-1})] \cdot \exp\left(-\frac{\Delta t}{\tau}\right). \tag{4.17}$$

Given the measured points $U_{\mathrm{m},j}$ and appropriate estimates of the response times $\tau_j$, the ambient

("true") relative humidity in air $U_{\mathrm{a}}$ can be estimated by solving Eq. (4.17) for each time step (see *Miloshevich et al.*, 2004):

$$U_{\mathrm{a}}(t_i) = \frac{U_{\mathrm{m}}(t_i) - \left[U_{\mathrm{m}}(t_{i-1}) \cdot \exp\left(-\frac{\Delta t}{\tau_i}\right)\right]}{1 - \exp\left(-\frac{\Delta t)}{\tau_i}\right)}. \tag{4.18}$$

The actual point-by-point time-lag correction is then

$$\Delta U(t_i) = U_{\mathrm{a}}(t_i) - U_{\mathrm{m}}(t_i) = [U_{\mathrm{m}}(t_i) - U_{\mathrm{m}}(t_{i-1})] \frac{\exp\left(-\frac{\Delta t}{\tau_i}\right)}{1 - \exp\left(-\frac{\Delta t}{\tau_i}\right)}. \tag{4.19}$$

### 4.2.2 Experiment for time-lag measurements

The temporal response of the RS41 humidity sensor to changes in relative humidity is investigated with laboratory measurements. At various temperature levels, the sensor booms of two RS41 radiosondes are exposed to a steady air flow in which step changes of relative humidity are created. From the continuous radiosonde data records the characteristic response times $\tau$ are determined by fitting Eq. (4.15) to the data sections that cover the response periods following the step changes. The experiments are carried out at ambient pressure. A parameterisation of the characteristic time $\tau$ with temperature is derived based on the results.

The response times are determined with respect to the 'internal' relative humidity (calibrated raw data), which is lower than the actual humidity in the air stream (or the atmosphere) because of the operation of the RS41 humidity sensor at a temperature of about 5 K above ambient air (Section 2.1.3.2). Accordingly, the time-lag correction as part of the GRUAN processing consists of two steps: a) the actual correction based on 'internal' humidity and temperature data (Eq. 4.19), b) conversion of the relative humidity to free atmospheric conditions, i.e. to the GRUAN-corrected temperature from the 'normal' or 'external' RS41 temperature sensor.

#### 4.2.2.1 Setup description

The experiments have been conducted at the Meteorological Observatory Lindenberg (Deutscher Wetterdienst) in 2015. Fig. 4.11 shows the setup schematically.

Two RS41 radiosondes are tested simultaneously. The sensor booms are installed in cylindrical test cells (KF16 steel tubes, 15 mm inner diameter), which are arranged inside a Feutron climate chamber (370 litre) for temperature control. The cells are flushed with a continuous stream of air, which is driven by compressed dry nitrogen gas (purity 5.0) from outside the chamber through a 6 mm inner diameter stainless steel tubing. After adjustment of the $N_2$ gas to the chamber temperature by running through a ∼10 m long cooling coil, the flow splits into two branches, one of which passes a humidifier. The humidifier is able to increase relative humidity of the $N_2$-gas from virtually zero to ∼50 % at −10 °C and ∼25 % at −65 °C. Each of the dry and humid air streams is directed to one of the test cells. By manual 90°-switches of a valve, which

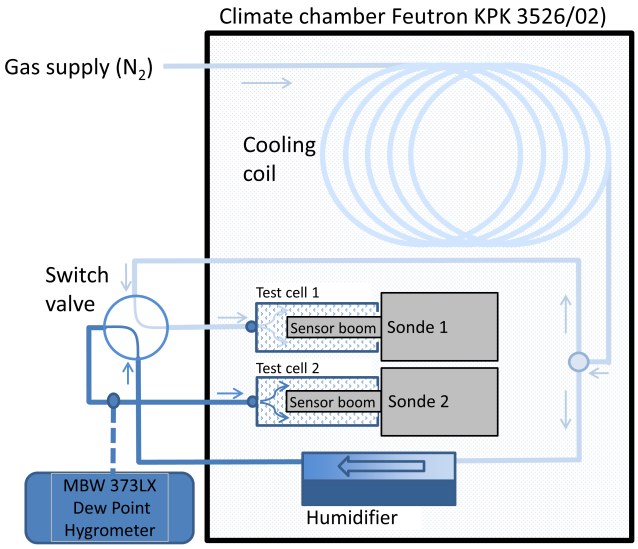


**Figure 4.11:** Scheme of the experimental setup for relative humidity time-lag measurements.

is mounted outside the chamber housing, step-like humidity changes are created in the two air flow branches, alternating for the two sondes.

The efficiency of the humidifier and hence the value of relative humidity in the humid branch of the air flow is not actively controlled. The humidity can in principle be checked (MBW 373LX dew point hygrometer). However, due to its slow response in the range of minutes, the hygrometer can not be used as reference for the humidity (changes) in the air flow.

After cooling of the chamber volume to the desired minimum temperature, the temperature control is switched off. During the subsequent slow self-warming of the chamber at active ventilation, which lasts for several hours, the actual time-lag measurements are performed by switching the valve at appropriate intervals. A temperature range between −70 °C and −10 °C is covered. This procedure of repeated measurements at increasing temperatures is chosen to suppress ice formation at the inner walls of the supply lines and thus to avoid potential water vapour contamination from sublimated ice. The radiosonde data are continuously recorded and visualised during operation with the sounding operation software.

The setup for time-lag measurements at the Meteorological Observatory Lindenberg is currently being further developed. The design of the measurement cells that house the radiosonde sensor booms, the efficiency of the humidifier, and the air flow system including the arrangement of the valves will be optimised. A different temperature regime, which uses constant temperature levels will be used, with the aim to improve temperature and moisture stability and lower the uncertainties.

## 4.2.3 Data evaluation and time-lag correction

### 4.2.3.1 Determination of response times

Fig. 4.12 shows an example of the humidity sensor response to a step-like change of relative humidity from low to high humidity state and back. The time of valve switching to the high humidity state can be easily identified in the lower panel with the rising flank of the continuous

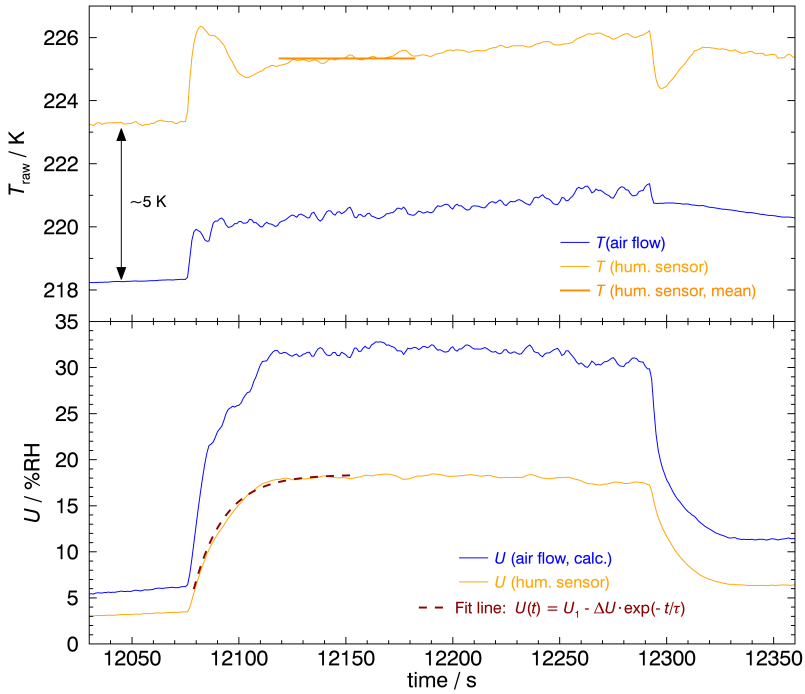


**Figure 4.12:** Example for the step response of the humidity sensor at ~225 K (–48 °C). The section includes the time of switching to elevated relative humidity (12 075 s), and back to low values (12 293 s). The dashed line is the regression curve fitted to the dry-to-humid step with the fit parameter $\tau$ representing the response time (inverse of time constant). The temperature the actual time constant is related to is indicated with the orange bar in the upper panel.

humidity data. After about 200 s in this example, the valve is switched back and the state with low humidity is restored. As can be seen in the upper panel, valve switching not only changes humidity, but also causes certain temperature changes of the air stream hitting the radiosonde sensors. This temperature variability is due to the experiment design. Especially, the valve and the connected tubes, which are installed outside the chamber, are to certain extent influenced by the laboratory air despite insulation. This might be the main reason for temperature variations in the air flow connected to valve switching. The temperature of the humidity sensor is subject to some overshooting directly after switching. This is probably caused by the RS41 PID control of the heating element for the humidity sensor.

It is assumed that the temperature measured on the sensor chip in the period immediately after switching the valve is the temperature that determines the response behaviour of the humidity sensor and hence the time constant. Consequently, this is the temperature the time constant (or response time, respectively) is set in relation to in the evaluation. The (undesired) variation of temperature associated with each humidity step is included in the estimate of the temperature uncertainty. Thus the combined temperature uncertainty is calculated with

$$u(T) = \sqrt{u^2_{T,\mathrm{step}} + u^2_{T,\mathrm{plateau}} + u^2_{T,\mathrm{pre}} + u^2_{T,\mathrm{cal}}}), \tag{4.20}$$

where $u_{T,\mathrm{step}} = (T_{\mathrm{plateau}} - T_{\mathrm{pre}})/(2\sqrt{3})$ is the dominant contribution, which accounts for the temperature variance that is connected with the valve switches. Uncertainties can reach 1 K to 2 K.

Equation (4.15) is used to determine time constants (or '63 %'-response times $\tau$ as inverse of the time constants, respectively) for the ascending flanks of pre-selected humidity steps. The data sections or time intervals to which the equation is fitted generally enclose the majority of the ascending part and the beginning of the plateau, see the dashed line in the lower panel of Fig. 4.12 as an example.

The uncertainty of $\tau$ is mainly associated with the degree to which the shape of the measured ascending flanks can be represented by the model. In order to take this type of variability into account, Eq. (4.15) is fitted to the raw humidity data three times for each humidity step, each with the same starting point close to the foot of the step, however enclosing different amounts of data points towards the plateau into account. Deviations from a 'perfect' realisation of the humidity steps generally tend to overestimate $\tau$, because 'memory' effects caused by humidity adsorption and desorption at the inner surfaces of the tubing and valve as well as turbulent mixing of the air flow within the test cells may be responsible for certain smoothing of the step signal. For that reason, the smallest estimated $\tau$ from the three regression lines is taken as the value associated with each humidity step. However, as a rough estimate for the uncertainty connected to this approach, the usual standard deviation of the response times from those three fits is assigned. With this, the preliminary uncertainty of $\tau$ from the data fitting procedure is

$$u(\tau) = \sqrt{\sigma^2_{\tau,(3\,\mathrm{fits})} + \sum_{i=1}^{3} \left(u_{\tau,\mathrm{fit,i}}\right)^2}, \tag{4.21}$$

where $\sigma_{\tau,(3\,\mathrm{fits})}$ stands for the standard deviation calculated over the three estimated $\tau$, and $u_{\tau,\mathrm{fit,i}}$ denote the formal standard uncertainties of the fit parameters.

#### 4.2.3.2 Sensor response time as function of temperature

In Fig. 4.13 the response times from the analysis of the individual humidity steps are plotted against the temperature of the humidity sensor. An exponential model curve is fitted to the data (green line):

$$\tau(T) = a \cdot \exp\big(b \cdot (T - T_0)\big), \tag{4.22}$$

where the fit parameter $a$ formally denotes the response time at $T_0 = 0\,^{\circ}\mathrm{C}$, and $b$ the 'decay' constant of $\tau$ with respect to temperature. Data points shown in light grey were excluded from the regression. Criteria for the exclusion were exceptionally large 'error' bars due to large standard deviations of $\tau$ derived from the three fits to the step response, as well as points which 'obviously' do not fit to the overall relation for unknown or unidentified reasons (outliers). Most of the excluded data points were generally on the 'top' side of the scatter, also for the above mentioned reason of possible smoothing of humidity steps.

The data points for calculating the regression line were weighted according to the inverse squares of their combined uncertainties (shown as vertical bars in Fig. 4.13. These combined uncertainties in $\tau$ include the preliminary uncertainties as given in Eq. (4.21) as well as the total uncertainties for temperature (Eq. 4.20). The temperature uncertainties were converted to uncertainties in $\tau$ by multiplying $u(T)$ with the sensitivity, i.e. the slope of the model line, which was estimated from a preceding unweighted fit to the data using Eq. (4.15).

Extensive measurements of the time-lag for the humidity sensor of the RS41 with a substantially

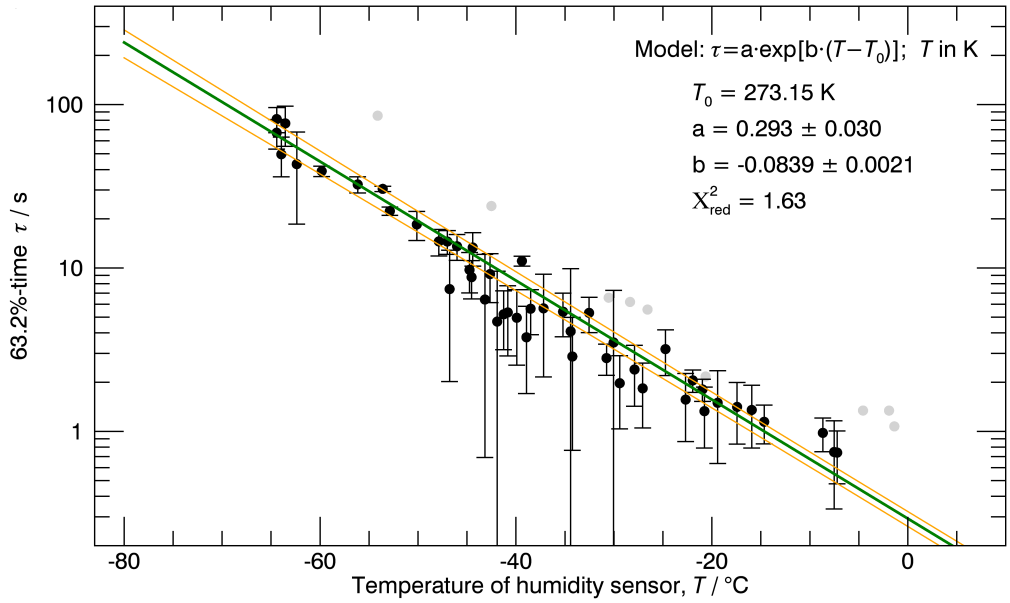


**Figure 4.13:** Response times vs. temperature of the humidity sensor. The green line depicts the exponential model to the data; the yellow lines denote the 1-$\sigma$ model uncertainty according to the given 1-$\sigma$ parameter uncertainties. Greyed out data points were excluded from the regression.

improved experimental setup are currently underway. Instead of a continuous slow temperature increase over the course of the measurements, selected constant temperature levels are set to establish more stable conditions. The new measurements will include both increasing and decreasing humidity steps, unlike the results in Fig. 4.13, for the estimation of the 63 % response time $\tau$. The results will be implemented in a subsequent version of the RS41-GDP.

#### 4.2.3.3 Implementation of time-lag correction

The humidity correction with respect to the response time refers to the measured raw humidity $U_\mathrm{m}$ at the actual 'internal' temperature of the continuously heated humidity sensor $T_\mathrm{int}$ in °C. Based on the above described experiments, the following function is used to calculate the 63 % time $\tau$:

$$\tau = a \cdot \exp(b \cdot T_\mathrm{int}), \tag{4.23}$$

with coefficients $a = 0.293$ and $b = -0.084$.

The corresponding uncertainty $u(\tau)$ (in s) is estimated with Eq. (4.24) using the parameter uncertainties $u(a) = 0.030$ and $u(b) = 0.002$:

$$u(\tau) = \tau \sqrt{\left(1/a \cdot u(a)\right)^2 + \left(T_\mathrm{int} \cdot u(b)\right)^2}, \tag{4.24}$$

however, a possible correlation between $a$ and $b$ is not taken into account.

The actual time-lag corrected relative humidity $U_{\mathrm{c},j}$ is calculated from the sensor measurements

$U_{c,j}$ for each time step $\Delta t_i = t_i - t_{i-1}$ (*Miloshevich et al.*, 2004) with

$$U_{c,i} = \frac{U_{m,i} - U_{m,i-1} \exp\left(\frac{-\Delta t_i}{\tau_i}\right)}{1 - \exp\left(\frac{-\Delta t_i}{\tau_i}\right)}. \tag{4.25}$$

The correction aims at amplifying natural atmospheric (vertical) humidity fluctuations detected in the measured profile, and thus at recovering the "true" profile. However, also noise and random fluctuations in the measured data are amplified and superimpose the corrected profile. This effect may be considerable, in particular at altitudes with overall large correction amounts. This necessitates smoothing of the time-lag corrected relative humidity profile which is done using a Gaussian-shaped kernel with a variable length related to the value of $\tau$ (see Appendix A.3). The uncertainty $u_{sm}(U_c)$ related to this smoothing is calculated using Eq. A.13 (method 1), and is considered random (uncorrelated); refer to Appendix A.3 on page 158.

Another uncertainty component $u_\tau(U_c)$ comes from sensor response time (see Eq. 4.24):

$$u_\tau(U_{c,i}) = \left|\frac{\partial U_{c,i}}{\partial \tau}\right| \cdot u(\tau_i) = \left|\frac{\Delta t_i \cdot \exp\left(-\frac{\Delta t_i}{\tau_i}\right) \cdot (U_i - U_{i-1})}{\left(1 - \exp\left(-\frac{\Delta t_i}{\tau_i}\right)\right)^2 \tau_i^2}\right| \cdot u(\tau_i). \tag{4.26}$$

This uncertainty component is considered temporally correlated, because the timelag correction algorithm is based on a unique set of experimental data. Since the $u_\tau(U_{c,i})$ generally show strong noise, the profile of uncertainties is smoothed with a similar procedure as for the actual time-lag corrected relative humidity profile.

The two combine to the standard uncertainty of the time-lag corrected internal humidity measured by the sensor:

$$u_{tl}(U_c) = \sqrt{u_\tau^2(U_c) + u_{sm}^2(U_c)}. \tag{4.27}$$

## 4.3 Pressure measurements with sensor (RS41-SGP)

The pressure sensor on board the RS41 radiosonde is briefly described in Section 2.1.3.3. The processing of the pressure and the uncertainty estimation are carried out in the following steps:

- Manufacturer-prescribed ground check and correction,
- GRUAN ground check,
- Smoothing.

The processing of pressure is shown in an overview scheme in Fig. 4.14 and explained in the following paragraphs.

**Manufacturer-prescribed ground check and correction** The correction of the pressure sensor onboard the RS41 is performed after comparison with a reference barometer during

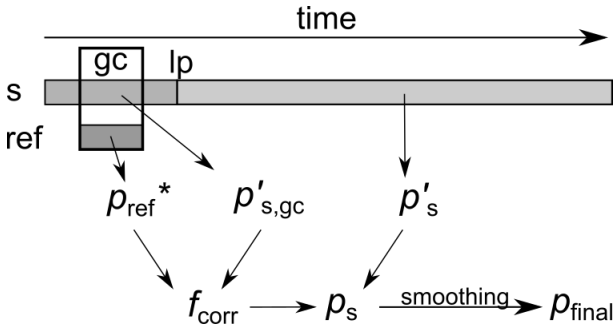


**Figure 4.14:** Scheme of the pressure processing in the GDPS. "s" indicates pressure observations with the radiosonde onboard sensor; "ref" - with the reference sensor during the ground check procedure ("gc"). "lp" denotes the time of launch of the sounding.

the manufacturer-prescribed ground check (gc) procedure before the launch. The correction is performed in two steps. Firstly, the ratio of the values of the reference sensor ($p_{\mathrm{ref}}*$) and the original RS41 sensor reading during the ground check ($p'_{\mathrm{s,gc}}$) is calculated:

$$f_{\mathrm{corr}} = \frac{p_{\mathrm{ref}}*}{p'_{\mathrm{s,gc}}}. \tag{4.28}$$

The reference pressure is measured either automatically during the ground check with the built-in pressure sensor in the RI41-B device, or, if the RI41 variant without pressure sensor is used for the check (*Vaisala*, 2021b), by manually reading the station barometer at the time of the check.

Secondly, after completion of the radiosounding, the observed raw pressure profile is corrected in the processing by applying the correction factor $f_{\mathrm{corr}}$:

$$p_{\mathrm{s}} = p'_{\mathrm{s}} \cdot f_{\mathrm{corr}}, \tag{4.29}$$

where $p_{\mathrm{s}}$ is the sensor pressure further used in the next steps, and $p'_{\mathrm{s}}$ is the original profile data. The pressure correction restores the factory calibration, and no uncertainty is introduced.

An example of the correction $p_{\mathrm{s}} - p'_{\mathrm{s}}$ is shown in Fig. 4.15 for a sounding on 24 June 2016, 12 UTC, at Lindenberg Observatory.

**Manufacturer-independent ground-check** GRUAN recommends an additional manufacturer-independent ground check (gc). After the manufacturer-prescribed ground check and before launch, the radiosonde pressure is compared with an appropriate reference sensor at surface pressure and under controlled conditions. The check can be performed over a period of several minutes in a chamber, e.g. SHC, a shelter, or a hut. The measured deviation $\Delta p$, averaged over the duration of the check, is used to evaluate the sonde readings, taking the measurement uncertainties into account. If a significant deviation is detected, an uncertainty component is added (see below).

The difference $\Delta p$ between the corrected sensor pressure $p_{\mathrm{s}}$ and the pressure from the reference

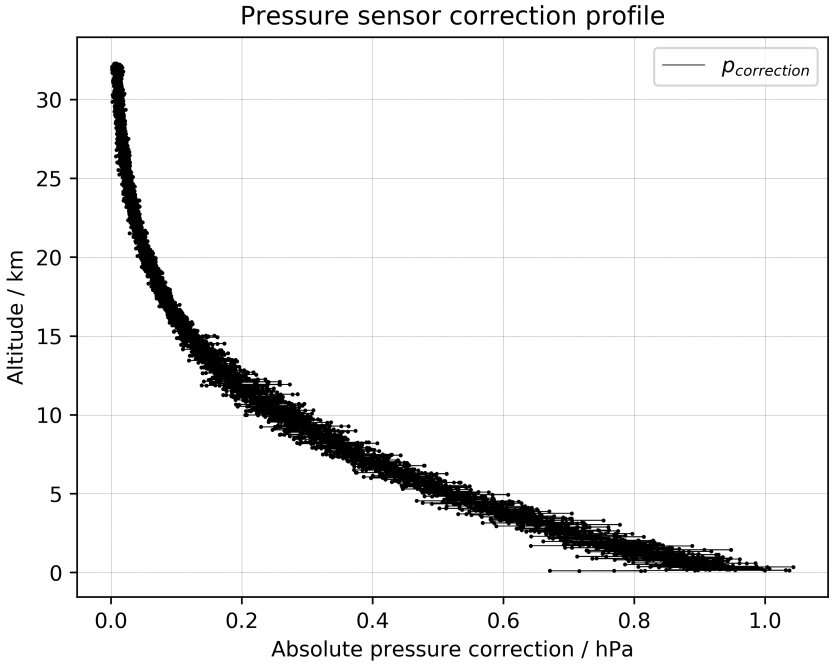


**Figure 4.15:** Correction of pressure sensor readings, based on ground check reference pressure sensor and smoothing. Profile for 24 June 2016, 12 UTC, at Lindenberg Observatory.

barometer $p_{\mathrm{ref}}^{\mathrm{G}}$ during the GRUAN ground check procedure is:

$$\Delta p = p_{\mathrm{s}} - p_{\mathrm{ref}}^{\mathrm{G}}, \tag{4.30}$$

with the superscript "G" standing for "GRUAN". The uncertainty of this difference is estimated as:

$$u(\Delta p) = \sqrt{u^2(p_{\mathrm{ref}}^{\mathrm{G}}) + u^2(p_{\mathrm{s}})}, \tag{4.31}$$

with

$$\begin{aligned} u(p_{\mathrm{s}}) &= \sqrt{u^2(\overline{p_{\mathrm{s}}}) + u_{\mathrm{cal,V}}^2(p_{\mathrm{s}})}, \\ u(p_{\mathrm{ref}}^{\mathrm{G}}) &= \sqrt{u^2(\overline{p_{\mathrm{ref}}^{\mathrm{G}}}) + u_{\mathrm{cal}}^2(p_{\mathrm{ref}}^{\mathrm{G}})}, \end{aligned} \tag{4.32}$$

where

- $u(\overline{p_{\mathrm{s}}})$ is the uncertainty of the mean of the radiosonde pressure sensor readings during the ground check,
- $u_{\mathrm{cal,V}}(p)$ is the absolute calibration uncertainty of the pressure sensor provided by Vaisala (see Appendix A.1.3),
- $u(\overline{p_{\mathrm{ref}}^{\mathrm{G}}})$ is the uncertainty of the mean of the reference sensor measurement during the ground check,
- $u_{\mathrm{cal}}(p_{\mathrm{ref}}^{\mathrm{G}})$ the uncertainty of the reference sensor, set to a value of 0.1 hPa ($k = 1$).

The uncertainty of the mean of the radiosonde pressure sensor during ground check, $u(\overline{p_\mathrm{s}})$, is obtained as the standard deviation of the pressure sensor readings divided by the square root of the number of recorded data points. The uncertainty of the mean of the reference sensor measurement during the ground check, $u(\overline{p_\mathrm{ref}})$, is calculated in a similar way as $u(\overline{p_\mathrm{s}})$. The two contributions from both averaged values to the final $u(\Delta p)$ are small, whereas the two calibration-related uncertainties dominate.

Using these uncertainties, the obtained pressure values are checked for consistency with the following test, which is similar to that for the temperature and relative humidity ground checks in the SHC (Section 3.2.3.1 and 3.2.3.3, respectively):

$$K = \frac{\Delta p}{u(\Delta p)}. \tag{4.33}$$

If $K \leq 1$, the measured pressure from the radiosonde sensor is consistent with the reference pressure, and the pressure uncertainty is set equal to the manufacturer-provided calibration uncertainty, i.e. no uncertainty related to the GRUAN ground check is added:

$$u_\mathrm{cal}(p_\mathrm{s}) = u_\mathrm{cal,V}(p_\mathrm{s}). \tag{4.34}$$

If $K > 1$, i.e. the measured pressure is not consistent with the reference, the uncertainty $u(p_\mathrm{s})$ is set equal to the measured pressure difference $\Delta p$. However, a fixed upper limit is set for this increased uncertainty (right side of Eq. 4.35). Here, $\sigma_p = 0.049\,\mathrm{hPa}$ is the result of a statistical evaluation of GRUAN ground checks at various GRUAN stations over several years:

$$u_\mathrm{cal}(p_\mathrm{s}) = \Delta p \leq \sqrt{u^2_\mathrm{cal,V}(p_\mathrm{s}) + \sigma_p^2}. \tag{4.35}$$

The above described procedure of a manufacturer-independent ground check of the pressure sensor is currently implemented at only a few GRUAN sites. At stations that use the RS41-SGP model but do not routinely perform such a check, the overall pre-launch uncertainty of the sensor pressure for the GDP is fixed with the above defined boundary value:

$$u_\mathrm{cal}(p_\mathrm{s}) = \sqrt{u^2_\mathrm{cal,V}(p_\mathrm{s}) + \sigma_p^2}. \tag{4.36}$$

The uncertainty propagation for the RS41 sensor pressure is visualised in Fig. 6.4 in Section 6.2.3. The scheme also depicts how the uncertainties are treated with regard to their correlation type (see Section 6.1):

$$\begin{aligned} u_\mathrm{tcor}(p_\mathrm{s}) &= u_\mathrm{cal}(p_\mathrm{s}) \\ u_\mathrm{ucor}(p_\mathrm{s}) &= u_\mathrm{sm}(p_\mathrm{s}), \end{aligned} \tag{4.37}$$

with $u_\mathrm{sm}(p_\mathrm{s})$ described in the next paragraph. 'tcor' means "full" correlation in time (including "full" correlation in the vertical with respect to a single radiosonde profile), and 'ucor' stands for uncorrelated uncertainty. These components are saved in separate columns in the GDP files.

**Smoothing** To obtain the final pressure ($p_\mathrm{s}$) from the RS41 sensor, the corrected raw pressure $p_\mathrm{s}$ is smoothed using a Gaussian smoothing kernel with a length of 15 points and extrapo-

lation at the edges of the profiles (see more information on smoothing in Appendix A.3). The uncertainty introduced by this smoothing is considered of uncorrelated nature.

**Overall uncertainty of pressure from sensor** The pre-launch overall calibration uncertainty and the contribution from smoothing are combined to the final uncertainty of the pressure measurement with the RS41-SGP build-in sensor:

$$u(p_\mathrm{s}) = \sqrt{u^2_\mathrm{cal}(p_\mathrm{s}) + u^2_\mathrm{sm}(p_\mathrm{s})}. \tag{4.38}$$

Both components are presented exemplary in Fig. 4.16 as the equivalent (un)correlated components $u_\mathrm{tcor}(p_\mathrm{s})$ and $u_\mathrm{ucor}(p_\mathrm{s})$, according to Eq. (4.37). The correlated ground preparation-related uncertainty is dominating, while the uncorrelated uncertainty due to the smoothing is smaller and adds some variability to the final uncertainty. A summary of the linking of uncertainties of the pressure sensor measurements is presented in the flow chart in Fig. 6.4.

Although both the pressure measured with the physical sensor and pressure derived from the GPS measurements (Section 4.4.2) are stored in separate columns in the GDP files, the GPS-derived pressure is considered as the main pressure product.

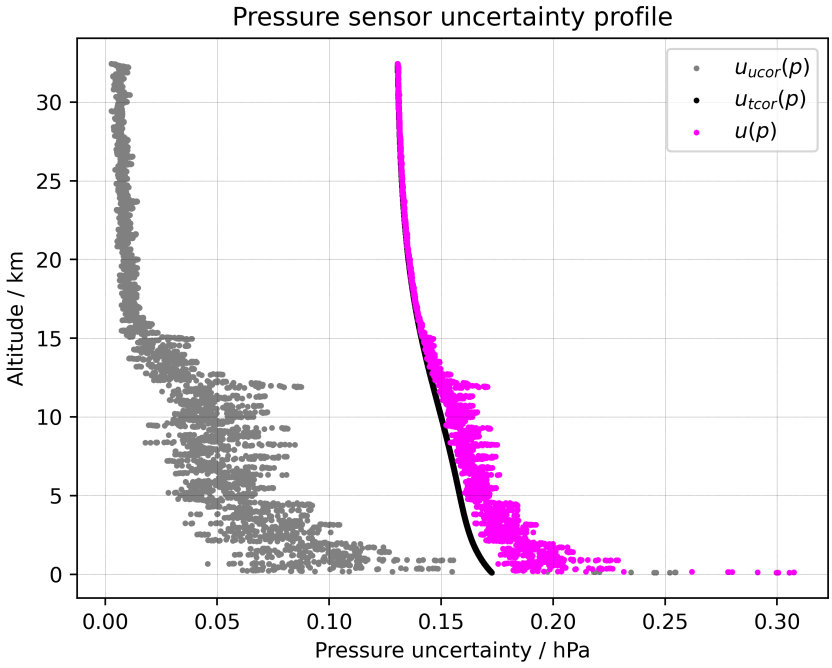


**Figure 4.16:** Profile of uncertainty of pressure from sensor ($k = 1$) for 24 June 2016, 12 UTC, at Lindenberg Observatory.

## 4.4 Evaluation of GPS and GPS-derived variables

**Note:** The uncertainties described in this section are based on the analysis of the Vaisala products, as received from the radiosonde. The GRUAN LC has not reprocessed the GPS data to provide better defined uncertainties. Thus the presented approach for uncertainty estimation of GPS derived parameters is to be improved in the next versions of the RS41 GRUAN data product.

### 4.4.1 Uncertainty in GPS measurements

The technical implementation of the positioning in the RS41/SPS311 observation system is briefly described in Section 2.1.3.4. There are two independent contributions to the uncertainty in the positioning of the radiosonde in flight:

- Uncertainty of the position of the stand-alone radiosonde,
- Uncertainty of the position of the ground-based GPS receiver, providing differential corrections.

The differential corrections of the radiosonde coordinates are implemented on a pseudorange level. Pseudoranges are the estimated distances between the satellites and the receiver, described in depth in Appendix D.1. Thus the uncertainty of the differential corrections is incorporated into the stand-alone uncertainty of the radiosonde. The uncertainties related to the ground station are associated with its absolute location and the uncertainties of the used geoid model. In order to estimate the uncertainty of the stand-alone radiosonde position, a static monitoring experiment was conveyed, described in Section 4.4.1.1.

Due to the geometry of the GPS satellites in orbit (discussed in Appendix D.2) and the position of the receivers on-board the radiosonde and in the SPS, an equivalency in the uncertainty of the two horizontal coordinates can be postulated. As a result, the uncertainties of the vertical coordinates are discussed separately from the horizontal coordinates.

#### 4.4.1.1 Experimental determination of the uncorrelated positioning uncertainties

In order to identify the uncertainty of the position of the stand-alone radiosonde, an experiment was conducted at the GRUAN site in Lindenberg (Germany) on 5 October 2020. A single RS41 radiosonde was attached to a 30 m-mast with no obstacles around it and a clear horizon. The readings from the radiosonde were recorded with applied differential corrections to the final product.

The top panel in Fig. 4.17 shows the full data set, collected over 3 h. The altitude measurements are normally distributed. The middle panel shows a section of the data with superimposed smoothed mean and standard deviation of the residuals. The zoomed-in section indicates that although the data is normally distributed, it is not random, and a distinct systematic pattern is observed, i.e. a strong local correlation. Using the obtained standard deviation from the whole data set would clearly overestimate the uncertainty of the altitude measurement. The bottom

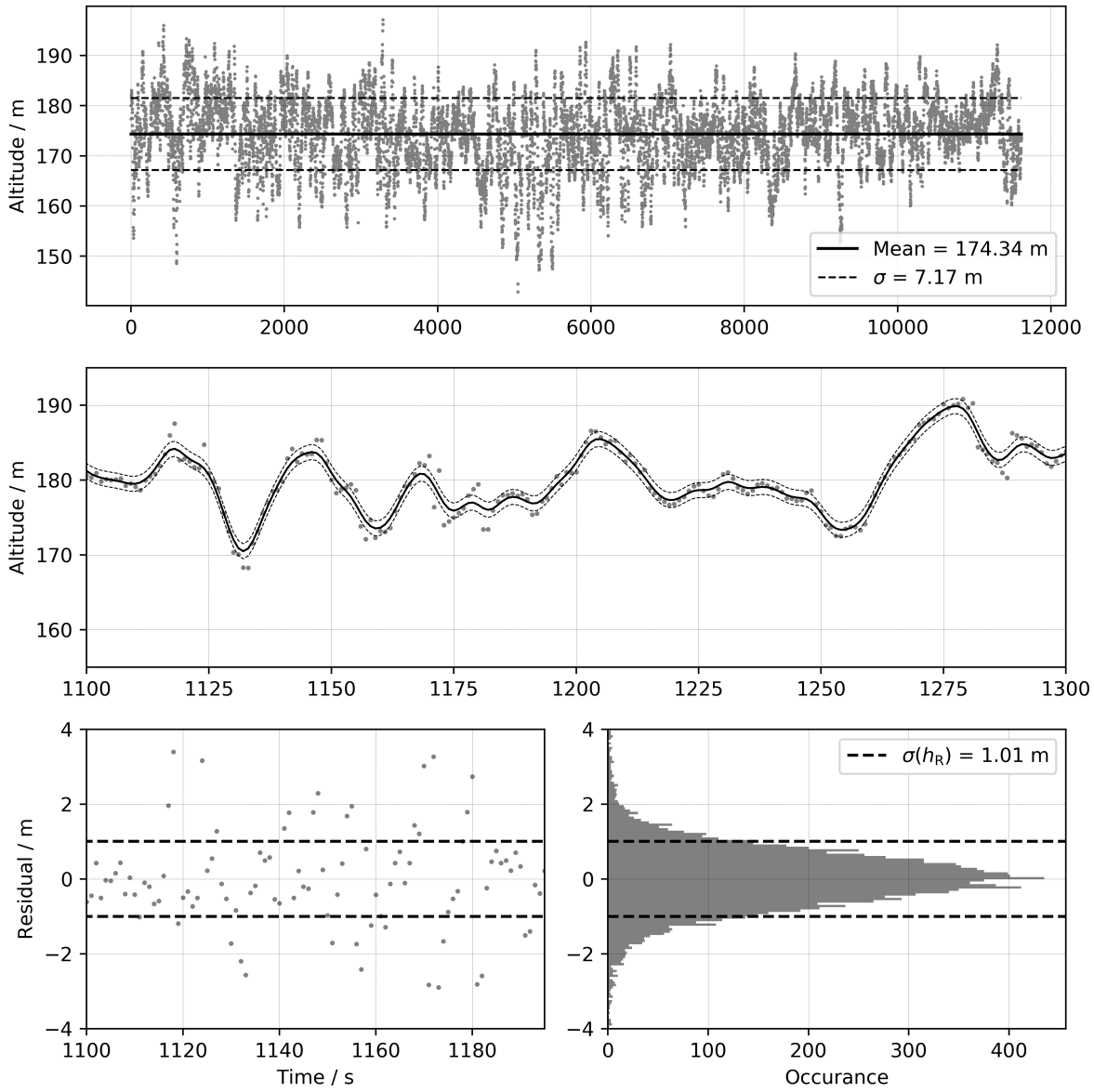


**Figure 4.17:** Record of altitude measurements from a RS41 radiosonde, attached to a static mast. Top: full dataset, collected over 3 h. Middle: section of data with superimposed smoothed mean average. Bottom: left - residuals with residual standard deviation, right - residual distribution with standard deviation of residuals over the whole 3 h observation period.

left panel shows the residuals from the middle panel. These residuals are normally distributed (bottom right panel) and are random.

The uncertainty $\sigma(h_{\mathrm{R}})$ of the measured altitude from GPS is taken as the standard deviation of the smoothed residuals from the experimental data (Fig. 4.17, bottom), where $\mathrm{R}$ stands for "radiosonde". For altitude this value is ≈1 m. This base measurement of the random uncertainty component for altitude is used for all processed RS41 data. A further analysis justifying this value can be found in Appendix D.1. Although a single constant value is assigned as uncertainty,

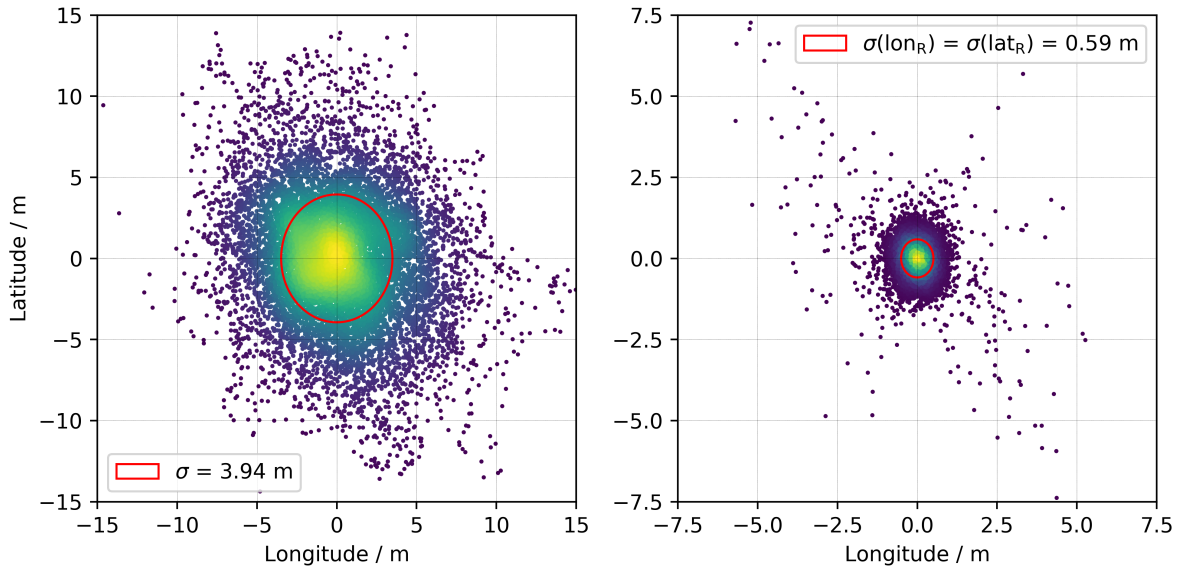


**Figure 4.18:** Ground plots of horizontal coordinate anomalies from mean, collected over 3 h during the static RS41 experiment. The colours represent point densities with yellow indicating highest concentration and blue lowest. The red circles show the standard deviation, similar to the dashed lines in Figure 4.17, bottom. Left: full raw observations of latitude and longitude during static experiment. Right: residuals of latitude and longitude after removal of systematic behaviour. Both plots show the equivalency in the spread of horizontal coordinates. Note the different scaling between the two plots.

it is not correlated throughout the profile:

$$u_{\mathrm{ucor}}(h_{\mathrm{R}}) = \sigma(h_{\mathrm{R}}) = 1.0\,\mathrm{m}. \tag{4.39}$$

The uncertainty of the horizontal position can be determined using similar assumptions as for the estimation of the uncertainty of the vertical position. The horizontal coordinates are converted from degrees to meters through the formulations given in Eqs. (A.17) and (A.18). The observed standard deviations of the residuals for latitude and longitude are virtually identical (see Fig. 4.18), thus $\sigma(\phi_{\mathrm{R}}) = \sigma(\lambda_{\mathrm{R}}) = 0.6\,\mathrm{m}$. This value is not far from the underlying presumption that the horizontal uncertainties are half as large as the vertical ones. Thus the random (uncorrelated) uncertainty component of the GPS-derived horizontal position data of the radiosonde can be estimated to be:

$$\begin{aligned} u_{\mathrm{ucor}}(\lambda_{\mathrm{R}}) &= \sigma(\lambda_{\mathrm{R}}) = 0.6\,\mathrm{m}, \\ u_{\mathrm{ucor}}(\phi_{\mathrm{R}}) &= \sigma(\phi_{\mathrm{R}}) = 0.6\,\mathrm{m}. \end{aligned} \tag{4.40}$$

The acquired values for altitude, latitude and longitude uncertainties from this static experiment are a first attempt to quantify these uncertainties. It is assumed for the time being that these values apply regardless of altitude and geographical position. A further analysis justifying these values can be found in Appendix D.1. Further investigations into the uncorrelated uncertainties

of altitude, latitude and longitude will be carried out beyond the completion of this document.

#### 4.4.1.2 Correlated uncertainty of the vertical position of the radiosonde

There are three independent factors, further contributing to the uncertainty of the height determined from GPS positioning data:

- Accuracy of the positioning of the u-blox 6 receiver on-board the radiosonde,
- Uncertainty of the position of the ground-based GPS antenna,
- Uncertainty of the EGM2008 geoid.

All of these factors influence all radiosonde profiles consistently, regardless of the location and time of the radiosonde. Thus they contribute to the correlated uncertainty of the vertical position of the radiosonde.

The technical documentation of the u-blox chip states a vertical accuracy of 5 m (*ublox*, 2013a). This value $u_{\mathrm{ublox}}(h_{\mathrm{R}})$, where "$R$" stands for "Radiosonde", is multiplied with the Vertical Dilution of Precision (VDOP) measurements from the radiosonde to acquire the u-blox uncertainty for each data point. Dilution of Precision is described in Appendix D.2.

The uncertainty of the installation height of the ground-based GPS antenna, $u_{\mathrm{pos}}(h_{\mathrm{SPS}})$ is expected to be within 0.2 m, since the antenna is firmly anchored to the ground.

The height above mean sea level in the RS41 GDP is calculated in relation to the EGM2008 Earth gravity model. This geoid includes data from both ground-based geodetic observations as well as from the GRACE/GOCE satellite missions. The uncertainty in height of the EGM2008 geoid contributes as a systematic error. A global study of the EGM2008 concludes that the range of uncertainties of this Earth gravity model is between 0 m and 0.45 m with a maximum in the Himalaya region (*Pavlis et al.*, 2012). The geoid-related uncertainty $u_{\mathrm{geoid}}(h_{\mathrm{SPS}})$ used in the RS41 GDP is set to be equal to 0.5 m for all regions of the world for simplicity.

The combined uncertainty of height related to the fixed position of the ground-based GPS station and to the u-blox receiver on-board the RS41 radiosonde is:

$$u_{\mathrm{tcor}}(h_{\mathrm{R}}) = \sqrt{\mathrm{VDOP}^2 \cdot u^2_{\mathrm{ublox}}(h_{\mathrm{R}}) + u^2_{\mathrm{geoid}}(h_{\mathrm{SPS}}) + u^2_{\mathrm{pos}}(h_{\mathrm{SPS}})}. \tag{4.41}$$

This uncertainty is fully correlated throughout a single profile and is correlated through time, which is why it is included as time correlated ('tcor') in the GDP.

#### 4.4.1.3 Correlated uncertainty of the horizontal position for the radiosonde

Unlike the correlated components of the vertical position uncertainty, the correlated uncertainties in the horizontal direction consist of only two components:

- Accuracy of the positioning of the u-blox 6 receiver,
- Uncertainty of the position of the ground-based GPS antenna.

The technical documentation of the u-blox 6 receiver (*ublox*, 2013a) states a horizontal accuracy of the acquired position of 2.5 m. This value is multiplied with the Horizontal Dilution of

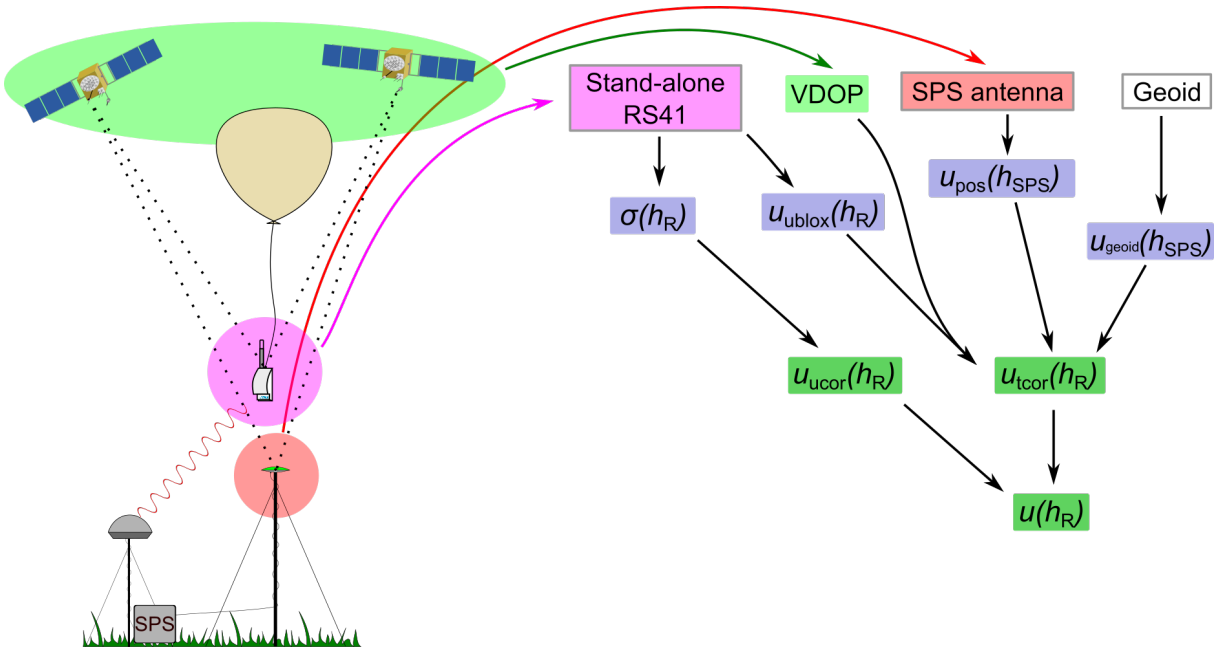


**Figure 4.19:** Scheme of the parameter dependencies in calculating height uncertainties. The parameters in the blue boxes are intermediate, while the parameters in the green boxes are provided in the GDP.

Precision (HDOP) (see Appendix D.2) measurement profiles in order to calculate this correlated uncertainty component.

The antenna horizontal coordinate uncertainty is independent of the EGM2008 uncertainty, since the geoid provides corrections for the vertical coordinates of the positioning. Due to the geometry of the GPS satellites in orbit and the position of any receiver in close proximity to the Earth surface, the horizontal position uncertainties can be assumed to be half as large as the vertical ones:

$$u_{\mathrm{pos}}(\lambda_{\mathrm{SPS}}) = u_{\mathrm{pos}}(\phi_{\mathrm{SPS}}) = u_{\mathrm{pos}}(h_{\mathrm{SPS}})/2 = 0.1\,\mathrm{m}. \tag{4.42}$$

Thus the uncertainties of the horizontal coordinates with an assigned full correlation in time (including full vertical correlation within a profile) are:

$$\begin{aligned} u_{\mathrm{tcor}}(\lambda_{\mathrm{R}}) &= \sqrt{\mathrm{HDOP}^2 \cdot u^2_{\mathrm{ublox}}(\lambda_{\mathrm{R}}) + u^2_{\mathrm{pos}}(\lambda_{\mathrm{SPS}})} \\ u_{\mathrm{tcor}}(\phi_{\mathrm{R}}) &= \sqrt{\mathrm{HDOP}^2 \cdot u^2_{\mathrm{ublox}}(\phi_{\mathrm{R}}) + u^2_{\mathrm{pos}}(\phi_{\mathrm{SPS}})}, \end{aligned} \tag{4.43}$$

where $R$ stands for "Radiosonde".

#### 4.4.1.4 Full position uncertainties

The radiosonde altitude uncertainty $u(h_{\mathrm{R}})$ (see Fig. 4.19 and example profile in Fig. 4.20)

$$u(h_{\mathrm{R}}) = \sqrt{u^2_{\mathrm{tcor}}(h_{\mathrm{R}}) + u^2_{\mathrm{ucor}}(h_{\mathrm{R}})} \tag{4.44}$$

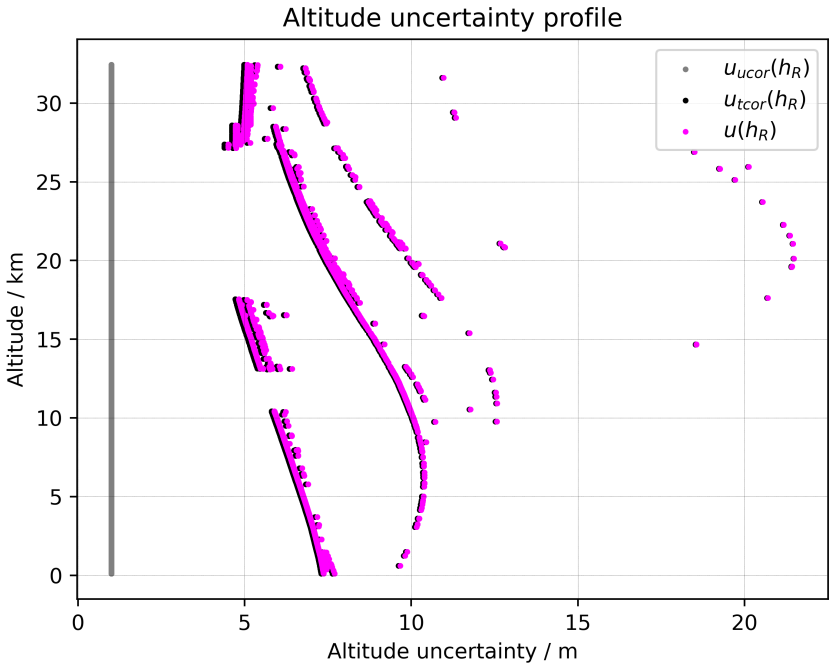


**Figure 4.20:** Altitude uncertainty ($k = 1$) components profile for 24 June 2016, 12 UTC, at Lindenberg Observatory. The black points indicate the correlated altitude uncertainty, the gray line the uncorrelated, and the magenta the total altitude uncertainty, calculated from GPS. The structural pattern, visible in the correlated and total altitude uncertainties, are caused by the VDOP profile pattern.

includes the uncertainty parameters of both WGS84 height uncertainty and the uncertainty of the altitude above Mean Sea Level (MSL). In order to calculate the uncertainty of the WGS84 height, the $u_{\mathrm{geoid}}(h_{\mathrm{SPS}})$ term has to be omitted. The impact of this term is very small and $u_{\mathrm{MSL}}(h_{\mathrm{R}})$ and $u_{\mathrm{WGS84}}(h_{\mathrm{R}})$ are of similar amount.

The full horizontal uncertainties are calculated similarly to the vertical uncertainty:

$$u(\lambda_{\mathrm{R}}) = \sqrt{u^2_{\mathrm{tcor}}(\lambda_{\mathrm{R}}) + u^2_{\mathrm{ucor}}(\lambda_{\mathrm{R}})}, \tag{4.45}$$

$$u(\phi_{\mathrm{R}}) = \sqrt{u^2_{\mathrm{tcor}}(\phi_{\mathrm{R}}) + u^2_{\mathrm{ucor}}(\phi_{\mathrm{R}})}, \tag{4.46}$$

where “R” stands for “Radiosonde”.

#### 4.4.1.5 Geopotential height uncertainty

The uncertainty of the geopotential height $u(Z)$ is closely linked (virtually identical) to that of the altitude:

$$u(Z) = \left(\frac{R_{\mathrm{e}}}{R_{\mathrm{e}} + h}\right)^2 \cdot u(h), \tag{4.47}$$

with $R_e$ the radius of the Earth and $h$ the altitude.

## 4.4.2 GPS-based pressure

### 4.4.2.1 Calculation of pressure from height measurement

The pressure observations are derived from GPS-height measurements using the barometric formula in iterations. For any height point $i$ in the radiosonde profile:

$$p_i = p_{i-1} \exp\left(\frac{-M_a \cdot g_i \cdot \Delta h_i}{R_u \cdot T_{v,i}}\right) = p_{i-1} \exp\left(\frac{-g_i \cdot \Delta h_i}{R_d \cdot T_{v,i}}\right), \tag{4.48}$$

where

- $M_a = 0.028\,96\,\mathrm{kg\,mol^{-1}}$ is the molar mass of dry air,
- $R_u = 8.3143\,\mathrm{J\,mol^{-1}\,K^{-1}}$ is the (molar) gas constant of dry air,
- $R_d = R_u/M_a = 287.052\,\mathrm{J\,kg^{-1}\,K^{-1}}$ is the specific gas constant of dry air,
- $p_i$ and $p_{i-1}$ is the pressure at points $i$ and $i-1$, respectively,
- $g_i$ is the gravity acceleration at point $i$,
- $T_{v,i}$ is the virtual temperature of the actual layer,
- $\Delta h_i$ is the height difference:

$$\Delta h_i = h_i - h_{i-1}, \tag{4.49}$$

where $h_{i-1}$ and $h_i$ are the heights of the data points at iteration $i-1$ and $i$, respectively. That is:

$$p_i = p_0 \cdot \exp\left(-\frac{1}{R_d}\sum_{j=1}^{i}\frac{g_j(h_j - h_{j-1})}{T_{v,j}}\right). \tag{4.50}$$

The virtual temperature is the temperature that dry air would have if its pressure and density were equal to those of a given sample of moist air. It allows the use of the dry-air equation of state for moist air, except with $T$ replaced by $T_v$ (https://glossary.ametsoc.org). The virtual temperature is calculated with:

$$T_{v,i} = \frac{T_i}{1 - \frac{e_i}{p_i}(1-\epsilon)}, \tag{4.51}$$

where

- $e$ is the partial pressure of water vapour, calculated from the relative humidity measurement and Hyland-Wexler formulation for the saturation water vapour pressure (see Appendix A.2),
- $T$ is the measured temperature,
- $p$ is the pressure,
- $\epsilon = 0.622$ is the ratio $M_w/M_a$ of the molar masses of dry air and water vapour, respectively.

The calculated pressure is initialised with the surface pressure measured with a barometer at the station, and, if present, the height difference between the launch site and the barometer height for the derivation of the launch point pressure, again using the barometric formula:

$$p_0 = p_{\mathrm{sb}} \exp\left(\frac{-g_0 \cdot \Delta h_{\mathrm{sb}}}{R_{\mathrm{d}} \cdot T_{\mathrm{v}}}\right), \tag{4.52}$$

where

- $p_0$ is the pressure of the launch point, as observed by the radiosonde,
- $p_{\mathrm{sb}}$ is the surface pressure measured with the station barometer,
- $\Delta h_{\mathrm{sb}}$ is the height difference between the launch point and the station barometer.

Since the pressure is dependent on the virtual temperature, and the virtual temperature is in turn dependent on the pressure (see Figure 4.21), the calculation of the pressure and virtual temperature has in principle to be iterative.

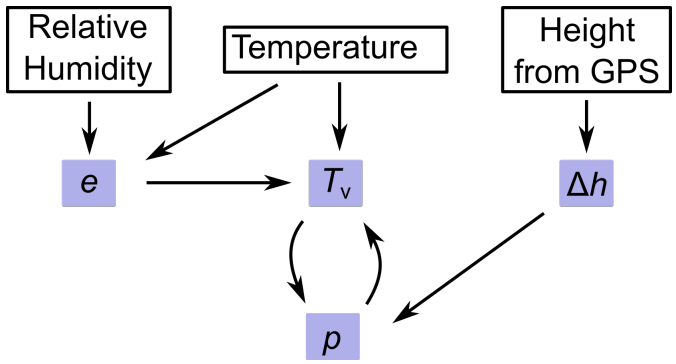


**Figure 4.21:** Basic structure of the parameter dependencies in calculating pressure from height.

#### 4.4.2.2 Uncertainty of pressure from GPS-height

Based on Eq. (4.50), the overall uncertainty of pressure is calculated at each height $i$ with the following expression, where $p_0$ is the pressure at the lowermost point of the radiosonde profile (launch point), and $h_j$ and $T_{\mathrm{v},j}$ the altitudes and virtual temperatures at each profile point up to the actual height $i$, respectively:

$$u(p_i) = p_i \cdot \left\{ \left(\frac{u(p_0)}{p_0}\right)^2 + \left(\frac{g_1}{R_{\mathrm{d}} T_{\mathrm{v},1}} u(h_0)\right)^2 + \left(\frac{g_i}{R_{\mathrm{d}} T_{\mathrm{v},i}} \sigma(h_i)\right)^2 + \sum_{j=1}^{i-1} \left[\frac{1}{R_{\mathrm{d}}} \left(\frac{g_{j+1}}{T_{\mathrm{v},j+1}} - \frac{g_j}{T_{\mathrm{v},j}}\right) u(h_j)\right]^2 + \sum_{j=1}^{i} \left[\frac{g_j (h_j - h_{j-1})}{R_{\mathrm{d}} T_{\mathrm{v},j}^2} u(T_{\mathrm{v},j})\right]^2 \right\}^{1/2}. \tag{4.53}$$

The derivation of this uncertainty formulation including a further analysis of the uncertainty of the pressure at the launch point $u(p_0)$ is described in Appendix D.3, and the components are visualised in Fig. 6.3.

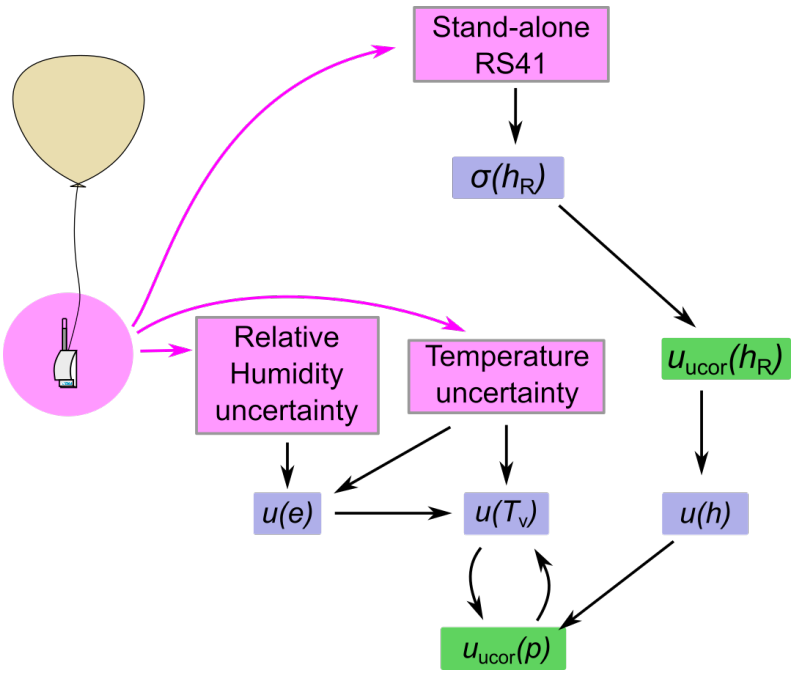


**Figure 4.22:** Schematic of the parameter dependencies in calculating uncorrelated pressure uncertainties. The parameters in the blue boxes are intermediate, while the parameters in the green boxes are provided in the GDP.

The uncertainty of $T_\mathrm{v}$ (Eq. 4.51) is mostly dependent on the uncertainty of the measured temperature. The uncertainty terms related to the water vapour pressure $e(T)$ and absolute pressure $p$ do not contribute significantly. Thus, in Eq. (4.53), the term containing $u(T_{\mathrm{v},j})$ is about two orders of magnitude smaller than the uncertainty contributions from the height steps ($u(h_i)$), and plays therefore a subordinate role (see Fig. D.4). Nevertheless, the equation used to estimate the uncertainty of the virtual temperature is given here for completeness:

$$u(T_{\mathrm{v},i}) = \sqrt{\left(\frac{p_i}{p_i - e_i\alpha}u(T_i)\right)^2 + \left(\frac{p_i T_i \alpha}{(p_i - e_i\alpha)^2}u(e_i)\right)^2 + \left(\frac{-e_i T_i \alpha}{(p_i - e_i\alpha)^2}u(p_i)\right)^2}, \quad (4.54)$$

with $\alpha = (1 - \epsilon)$. For each point in the profile, the water vapour partial pressure is calculated with $e = U \cdot e_\mathrm{s}(T)$, and its uncertainty $u(e)$ is determined by the measurement uncertainties for relative humidity and temperature (see Eq. 4.79 in Section 4.5.2 ):

$$u(e) = \sqrt{\left(e_\mathrm{s}(T) \cdot u(U)\right)^2 + \left(U\frac{\partial e_\mathrm{s}}{\partial T} \cdot u(T)\right)^2}, \quad (4.55)$$

with relative humidity $U$ (dimensionless), and $e_\mathrm{s}(T)$ the saturation water vapour pressure (Section A.2).

**Correlated and uncorrelated components** The uncertainty components in Eq. (4.53), including $u(p_0)$ in Eq. (D.7), are assigned correlation properties as follows (see also Section 6.1):

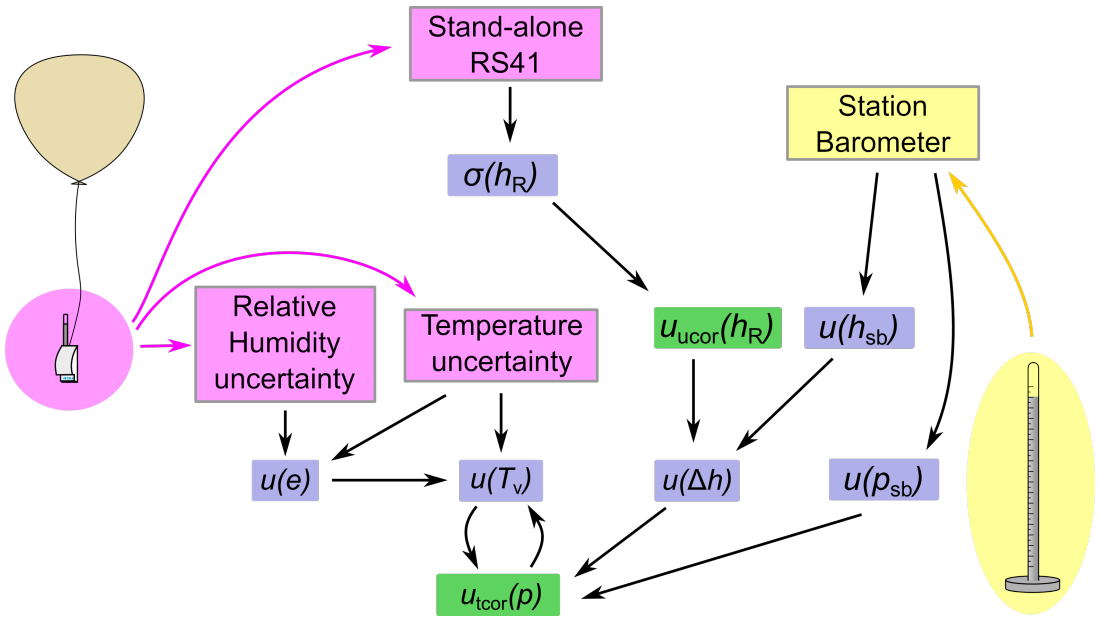


**Figure 4.23:** Scheme of the parameter dependencies in calculating correlated pressure uncertainties. The parameters in the blue boxes are intermediate, while the parameters in the green boxes are provided in the GDP.

- Uncorrelated ('ucor'): The random uncertainty components of the GPS-measured heights in the actual profile $\sigma(h_0)$, $u(h_i)$, $u(h_j)$ (Eq. 4.39), and the (virtual) temperature $u(T_{\mathrm{v},j})$,
- Fully correlated in time ('tcor'), including in the vertical within single profiles: Surface pressure reading and installation height of the reference barometer at the site of the actual radiosounding, $u(p_{\mathrm{sb}})$, $u(h_{\mathrm{sb}})$, and the VDOP-related systematic component of the GPS measurements for the launch point height, $u(h_0)$.

Thus, the overall uncorrelated uncertainty for pressure from GPS (see Fig. 4.22) is

$$u^2_{\mathrm{ucor}}(p_i) = p_i^2 \cdot \left\{ \frac{1}{R_{\mathrm{d}}^2} \left[ \left( \frac{-g_0}{T_{\mathrm{v},0}} \right)^2 + \left( \frac{g_1}{T_{\mathrm{v},1}} \right)^2 \right] \sigma^2(h_0) + \left( \frac{g_i}{R_{\mathrm{d}} T_{\mathrm{v},i}} \sigma(h_i) \right)^2 + \sum_{j=1}^{i-1} \left[ \frac{1}{R_{\mathrm{d}}} \left( \frac{g_{j+1}}{T_{\mathrm{v},j+1}} - \frac{g_j}{T_{\mathrm{v},j}} \right) \sigma(h_j) \right]^2 + \sum_{j=1}^{i} \left[ \frac{g_j (h_j - h_{j-1})}{R_{\mathrm{d}} T_{\mathrm{v},j}^2} u(T_{\mathrm{v},j}) \right]^2 \right\}. \quad (4.56)$$

The overall correlated uncertainty for pressure from GPS (see Fig. 4.23) is

$$u^2_{\mathrm{tcor}}(p_i) = p_i^2 \cdot \left\{ \left( \frac{u(p_{\mathrm{sb}})}{p_{\mathrm{sb}}} \right)^2 + \frac{1}{R_{\mathrm{d}}^2} \left[ \left( \frac{-g_0}{T_{\mathrm{v},0}} \right)^2 + \left( \frac{g_1}{T_{\mathrm{v},1}} \right)^2 \right] u'^2(h_0) + \left( \frac{g_0}{R_{\mathrm{d}} T_{\mathrm{v},0}} u(h_{\mathrm{sb}}) \right)^2 \right\}. \quad (4.57)$$

The above two uncertainty components are stored in the NetCDF GDP product files as columns

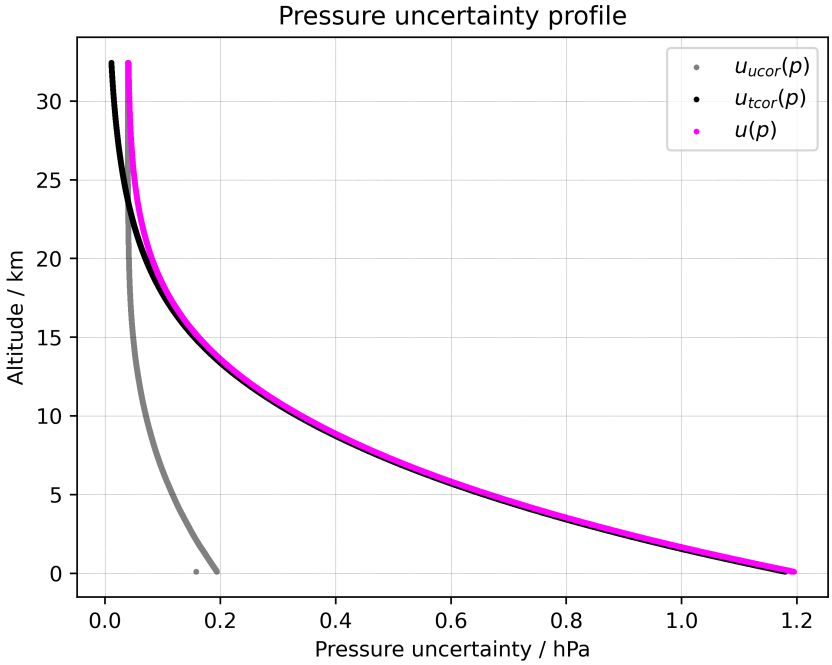


**Figure 4.24:** Profiles of uncertainty components for pressure calculated from GPS ($k = 1$) height measurements on 24 June 2016, 12 UTC, at Lindenberg Observatory. The black curve indicates the correlated component, the grey curve the uncorrelated, and the magenta the combination of the two.

'press_gnss_uc_ucor' and 'press_gnss_uc_tcor', respectively. The total uncertainty profile of the pressure is the combination of the correlated and uncorrelated uncertainties (see also example profile in Fig. 4.24 and statistics in Fig. 4.25):

$$u(p_i) = \sqrt{u^2_{\mathrm{tcor}}(p_i) + u^2_{\mathrm{ucor}}(p_i)}. \tag{4.58}$$

The primary reason of the latitude-dependent distribution of uncertainties observed in Fig. 4.25 is the inhomogeneity in the distribution of GPS satellites above the stations. The inclination of the GPS orbits is 55°, which means that in the equatorial regions GPS satellites can be observed from all azimuth and elevation angles, while in the polar regions no satellites can be observed directly above the radiosonde, leading to larger positional uncertainty and larger pressure uncertainty.

## 4.4.3 Wind speed and wind direction

### 4.4.3.1 Derivation of wind parameters from horizontal coordinates

The horizontal coordinates, which are part of the raw data measured by the RS41 radiosonde, are stored in units of degrees. They are converted into units of metres before calculation of wind speed and wind direction. Transformation equations in a simplified form can be found in

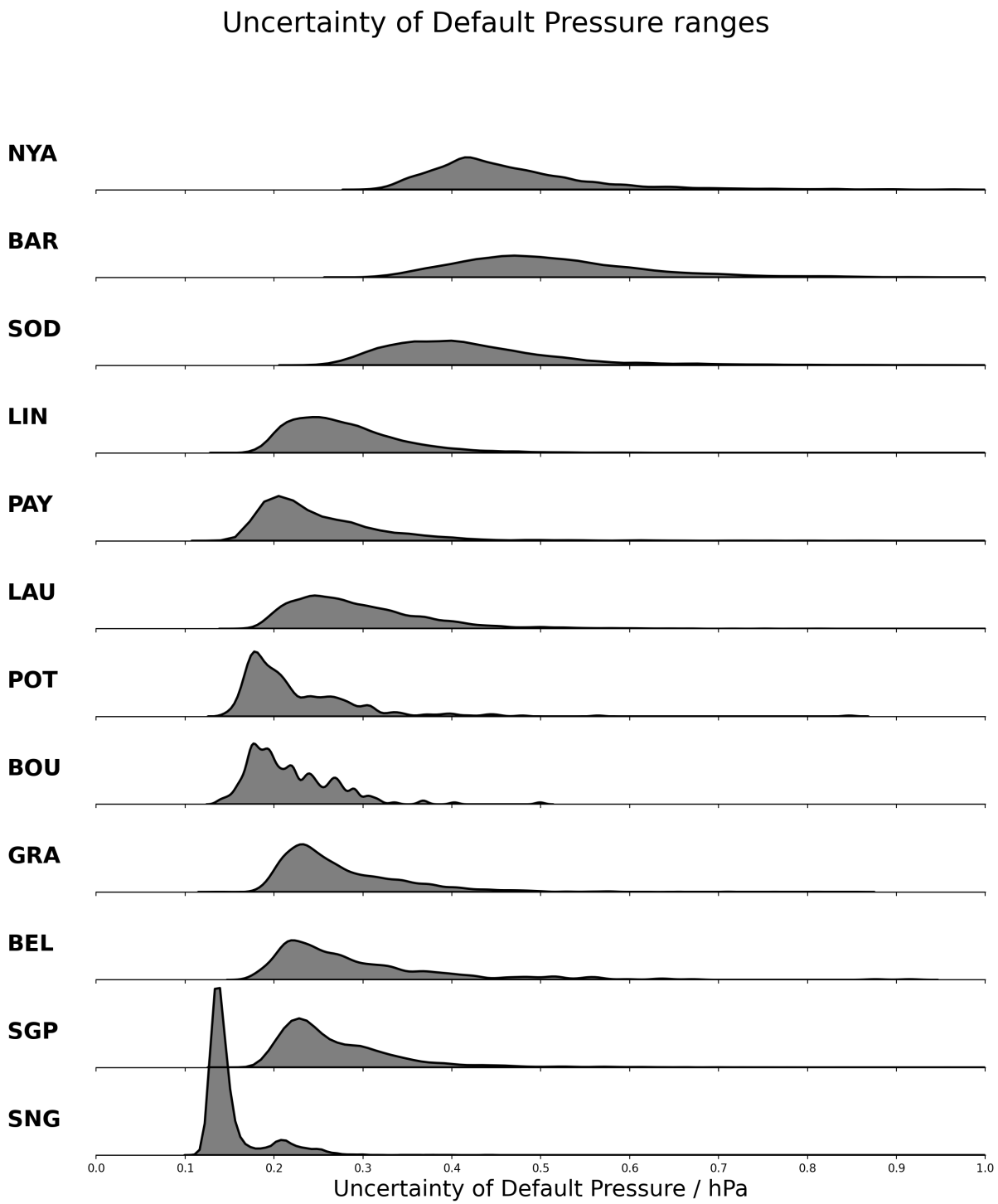


**Figure 4.25:** Uncertainty distributions ($k = 1$) for GPS-derived pressure for RS41-GDP 2016-2021. The 3-letter GRUAN station abbreviations are listed on the left with the closest to the poles station Ny-Ålesund (NYA) at the top and the closest to the equator station Singapore (SNG) at the bottom. The mean uncertainties for pressure range from less than 0.1 hPa to about 0.5 hPa.

Appendix A.4. The zonal ($u_\mathrm{w}$) and meridional ($v_\mathrm{w}$) wind components can then be calculated from the changes of the (transformed) horizontal coordinates along the balloon trajectory (with $\Delta$ denoting differences between consecutive points in the measured profile):

$$\begin{aligned} u_\mathrm{w} &= \frac{\Delta\phi}{\Delta t}, \\ v_\mathrm{w} &= \frac{\Delta\lambda}{\Delta t}. \end{aligned} \tag{4.59}$$

The zonal and meridional wind components are the components of the horizontal wind vector:

$$\vec{w}_\mathrm{hor} = [u_\mathrm{w}, v_\mathrm{w}]. \tag{4.60}$$

The horizontal wind speed $w_\mathrm{hor}$ in $\mathrm{m\,s^{-1}}$ and wind direction $\theta$ in angular degree are calculated from the zonal and meridional wind components:

$$w_\mathrm{hor} = \sqrt{u_\mathrm{w}^2 + v_\mathrm{w}^2}, \tag{4.61}$$

$$\theta = 90° - \left(\frac{180°}{\pi}\right) \arctan(u_\mathrm{w}, v_\mathrm{w}). \tag{4.62}$$

Negative values for $\theta$ from Eq. (4.62) are corrected by addition of a value of 360°, so that $\theta$ is within the interval of 0° to 360°.

#### 4.4.3.2 Uncertainty of wind speed and wind direction

The uncertainties of the horizontal wind speed ($w_\mathrm{hor}$) and direction ($\theta$) consist of uncorrelated components only. The two sources of these uncertainties are the components related to the GPS measurements and the components derived from smoothing of the wind data.

**Contribution from GPS measurements** The uncertainty of the zonal and meridional wind components are calculated from the uncorrelated uncertainties of the latitude and longitude. Since these are predetermined and the same for both latitude and longitude for all profiles (Section 4.4.1.1), the uncertainty of the wind components is also static for the complete profiles:

$$\begin{aligned} u(u_\mathrm{w}) &= \sqrt{2} \cdot u_\mathrm{ucor}(\phi_\mathrm{R}) \approx 0.85\,\mathrm{m\,s^{-1}}, \\ u(v_\mathrm{w}) &= \sqrt{2} \cdot u_\mathrm{ucor}(\lambda_\mathrm{R}) \approx 0.85\,\mathrm{m\,s^{-1}}. \end{aligned} \tag{4.63}$$

The uncertainty for the absolute wind speed is again constant and independent of its value. According to Eq. (4.61), and using $u(u_\mathrm{w}) = u(v_\mathrm{w}) := u(w_\mathrm{hor,comp})$:

$$
\begin{aligned}
u_{\mathrm{GPS}}(w_{\mathrm{hor}}) =& \frac{\sqrt{u_{\mathrm{w}}^2 \cdot u^2(u_{\mathrm{w}}) + v_{\mathrm{w}}^2 \cdot u^2(v_{\mathrm{w}})}}{w_{\mathrm{hor}}} \\
=& u(w_{\mathrm{hor,comp}}) \cdot \underbrace{\frac{\sqrt{u_{\mathrm{w}}^2 + v_{\mathrm{w}}^2}}{w_{\mathrm{hor}}}}_{=1} \approx 0.85\,\mathrm{m\,s^{-1}}.
\end{aligned}
\tag{4.64}
$$

The wind direction uncertainty in degrees is calculated using

$$
\begin{aligned}
u_{\mathrm{GPS}}(\theta) =& \frac{180^\circ}{\pi} \frac{\sqrt{u_{\mathrm{w}}^2 \cdot u^2(v_{\mathrm{w}}) + v_{\mathrm{w}}^2 \cdot u^2(u_{\mathrm{w}})}}{w_{\mathrm{hor}}^2} \\
=& \frac{180^\circ}{\pi} \cdot \frac{u(w_{\mathrm{hor,comp}})}{w_{\mathrm{hor}}}.
\end{aligned}
\tag{4.65}
$$

The second line in Eq. (4.65) again holds for the static estimate of the uncorrelated horizontal position uncertainty.

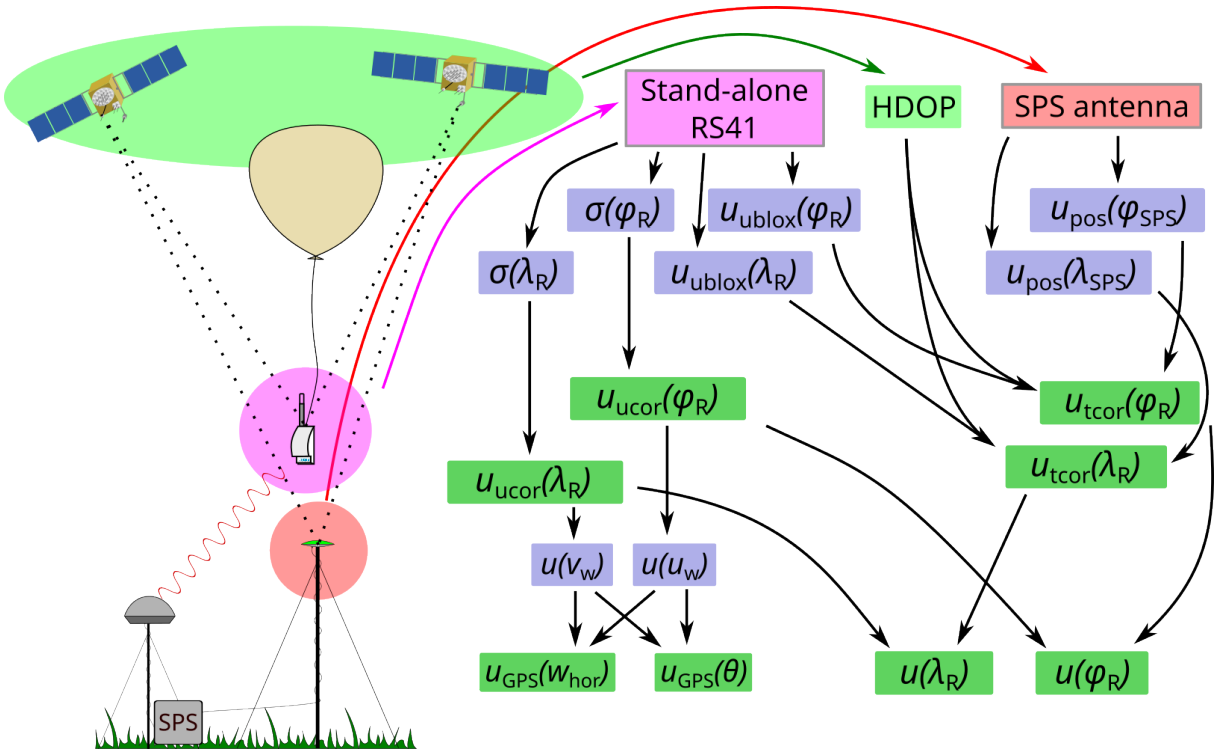


**Figure 4.26:** Scheme of wind direction and wind speed uncertainty derivation from GPS positioning measurements. The final wind component uncertainties are dependent on the GPS measurements onboard the radiosonde, the observations from the ground station, and on the satellite geometry in the GPS constellation. Dark green boxes indicate values exported in the GDP files, blue boxes contain intermediate steps data.

**Contribution from smoothing** The final wind direction and wind speed are derived from the smoothed data sets of the horizontal wind components ($v_\mathrm{w}$, $u_\mathrm{w}$). The smoothing is performed with a kernel size of 30 s, the values at the edges of the profiles are mirrored (for details on the smoothing procedures see Appendix A.3). The residuals between the wind direction and wind speed calculated from the raw and smoothed data are used to estimate the smoothing uncertainty components ($u_\mathrm{sm}(w_\mathrm{hor})$ and $u_\mathrm{sm}(\theta)$). These uncertainties are considered uncorrelated.

**Combined uncertainties** The final combined uncertainties of wind speed (see also Figure 4.27) and direction are derived as follows:

$$\begin{aligned} u(w_\mathrm{hor}) &= u_\mathrm{ucor}(w_\mathrm{hor}) = \sqrt{u^2_\mathrm{GPS}(w_\mathrm{hor}) + u^2_\mathrm{sm}(w_\mathrm{hor})} \\ u(\theta) &= u_\mathrm{ucor}(\theta) = \sqrt{u^2_\mathrm{GPS}(\theta) + u^2_\mathrm{sm}(\theta)}. \end{aligned} \tag{4.66}$$

Theoretically, if both wind speed components would approach zero, the wind speed uncertainty becomes undetermined (both the numerator and the denominator in the general term (first line) of Eq. (4.64) approach zero). Consequently, in such a case also the wind direction is undefined, as well as its uncertainty. A value of 180° is then assigned as a top limit for the wind direction uncertainty. Such conditions occur very rarely.

### 4.4.4 Ventilation

Ventilation speed, represented by the absolute speed of the radiosonde relative to the ambient air, is estimated for each point in the profile in m s$^{-1}$. It is an important input parameter for the solar radiation correction of the temperature measurement (see Section 4.1.1, e.g. Eq. 4.2), because the ventilation, i.e. the combined effect of air speed and density (or pressure), determines the cooling rate of the solar heated sensor. The ventilation speed is derived from two sources:

- the vertical speed of the ascent,
- lateral components due to the pendulum motion.

GPS data are the basis to calculate position changes at the temporal resolution of the sonde measurements, and from that the two ventilation components.

The position changes are measured with the sonde's GPS receiver relative to the Earth's surface (the WGS84 reference ellipsoid). They are used to determine horizontal wind speed and direction (see Section 4.4.3) under the assumption that the balloon essentially follows the horizontal wind during the ascent and – because it then 'sees' an essentially resting air column – rises vertically with respect to that column. Ventilation is thus caused both by the (horizontally shifting) ascent as a vertical component, and by the pendulum movement of the sonde around the ascent as a horizontal component. To determine the latter, the 'mean' wind is subtracted from the high-resolution horizontal position data, which resolves the pendulum, by appropriate smoothing and evaluation of the residuals (see below). However, vertical larger-scale movements of the surrounding air, as for example vertical wind components connected to convection or gravity waves, cannot be corrected for without elaborate analyses. As such they are included

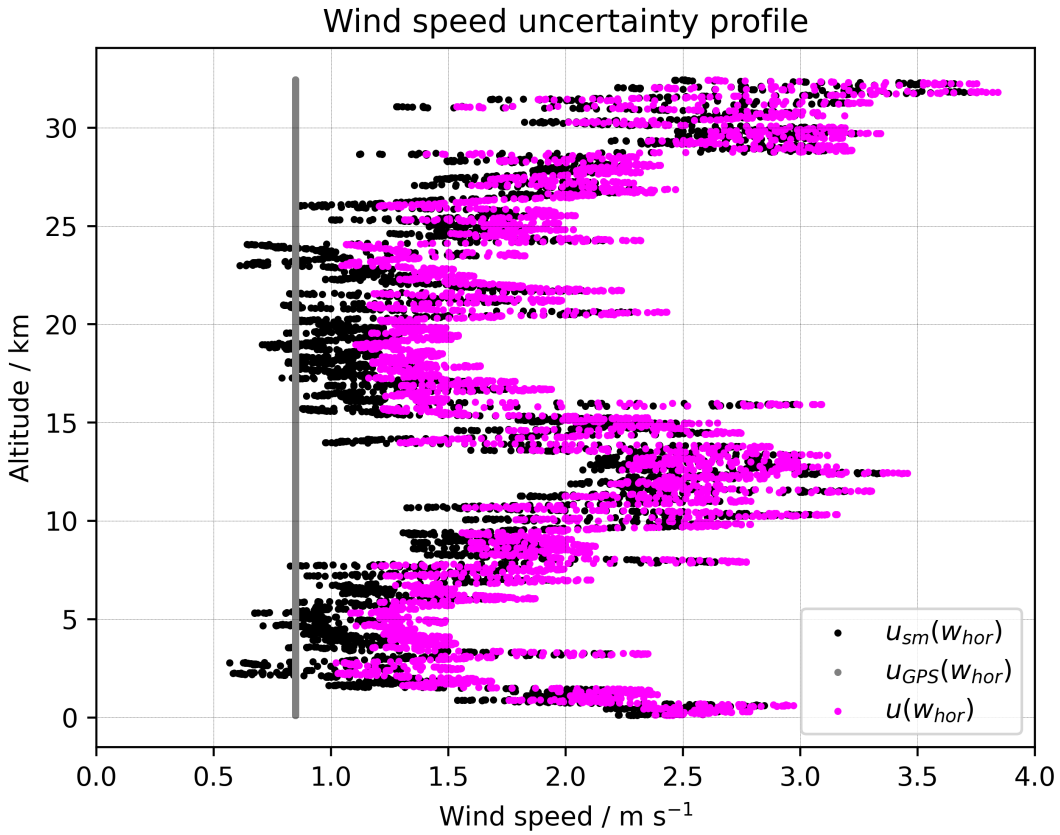


**Figure 4.27:** Wind speed uncertainty components. Both the $u_{\mathrm{GPS}}(w_{\mathrm{hor}})$ and $u_{\mathrm{sm}}(w_{\mathrm{hor}})$ are uncorrelated. Profile for 24 June 2016, 12 UTC, at Lindenberg Observatory, $k = 1$.

in the calculated vertical ventilation component although they are not part of the true vertical air speed, and may thus lead to over- or underestimation of the overall ventilation in the respective altitude ranges.

**Estimate of ventilation** The ascent speed is calculated from the measured altitude changes and represents the vertical component of the ventilation:

$$v_{\mathrm{asc},i} = \frac{h_i - h_{i-1}}{t_i - t_{i-1}}. \tag{4.67}$$

The so calculated direct ascent speed profile shows some noise, to which the noise from the sonde's GPS receiver contributes. The noise is suppressed by smoothing using a running mean with a Gaussian-shaped kernel with a length of 61 data points (=61 s, width = $2\sigma \approx 23$ s).

The horizontal component of the ventilation speed is associated with the pendulum movement ($\approx$60 m string length for most of the GRUAN soundings). It is derived from the measured horizontal change of position data. This is achieved by separately smoothing longitude and latitude data using a Gaussian kernel with a total length of 21 s. Such a low-pass filtering should essentially smooth out the $\approx$15 s pendulum oscillation that is connected to the string

length. The distances between the measured and smoothed horizontal positions are considered as the pendulum-related displacements ($\Delta$) with regard to the actual horizontal component of the ascent trajectory:

$$\Delta\phi = \phi - \phi_{\mathrm{sm}}, \qquad \Delta\lambda = \lambda - \lambda_{\mathrm{sm}}, \tag{4.68}$$

with $\phi$ and $\lambda$ the latitude and longitude in degrees, respectively.

For estimation of the ventilation in m s$^{-1}$, the displacements (or residuals) need to be converted to meters beforehand by multiplying with appropriate conversion factors $f_\phi$ and $f_\lambda$, respectively. These factors are calculated using an algorithm of *Vincenty* (1975), which is based on the WGS84 ellipsoid adjusted to the average height of the two horizontal positions in the profile with which the current ventilation is to be determined. For illustration or comparison purposes, simpler expressions are given in Appendix A.4, which can be used for such calculations with only marginally greater uncertainties.

With this, the absolute point-by-point horizontal ventilation is given by the distance between the displacements of the two points, i.e. by the vectorial sum of $D\phi'_i = \Delta\phi'_i - \Delta\phi'_{i-1}$ and $D\lambda'_i = \Delta\lambda'_i - \Delta\lambda'_{i-1}$:

$$v_{\mathrm{hor},i} = \frac{\sqrt{(D\phi'_i)^2 + (D\lambda'_i)^2}}{(t_i - t_{i-1})}. \tag{4.69}$$

The prime indicates that longitude and latitude are in metres. The result is again smoothed using a moving average with a 61 s Gaussian-shaped kernel. For the absolute ventilation (as a smoothed profile in m s$^{-1}$), the horizontal and the ascent-related components are combined:

$$v_{\mathrm{abs}} = \sqrt{v_{\mathrm{hor}}^2 + v_{\mathrm{asc}}^2}. \tag{4.70}$$

**Uncertainty of ventilation** For the uncertainty estimate of $v_{\mathrm{abs}}$, two contributions for both the horizontal and ascent-connected components are included, each of which is considered as uncorrelated: A component connected to absolute uncertainties of the GPS positioning, and a component from low-pass smoothing of the high-resolution positioning data (or the derived horizontal and vertical velocity components, respectively).

The random parts of the variability in GPS-positioning was experimentally determined once for the RS41 (Section 4.4.1.1) as $u_{\mathrm{alt}} = 1\,\mathrm{m}$ and $u_\phi = u_\lambda := u_{\mathrm{hor}} = 0.6\,\mathrm{m}$ for the vertical (altitude) and horizontal (longitude/latitude) components, respectively, and assumed to be representative for the entire profile. In that case the uncertainties for the horizontal and vertical ventilation due to the positioning are

$$u_{\mathrm{pos}}(v_{\mathrm{hor},i}) = \frac{\sqrt{2}\cdot u_{\mathrm{hor}}}{(t_i - t_{i-1})} \tag{4.71}$$

(according to Eq. 4.69) and

$$u_{\mathrm{pos}}(v_{\mathrm{asc},i}) = \frac{\sqrt{2}\cdot u_{\mathrm{alt}}}{(t_i - t_{i-1})} \tag{4.72}$$

according to Eq. (4.67). Each of the two is then combined with the contributions from low-pass

filtering (Appendix A.3):

$$\begin{aligned} u(v_{\mathrm{hor},i}) &= \sqrt{u^2_{\mathrm{pos}}(v_{\mathrm{hor},i}) + u^2_{\mathrm{sm}}(v_{\mathrm{hor},i})} \\ u(v_{\mathrm{asc},i}) &= \sqrt{u^2_{\mathrm{pos}}(v_{\mathrm{asc},i}) + u^2_{\mathrm{sm}}(v_{\mathrm{asc},i})}. \end{aligned} \tag{4.73}$$

Based on Eq. (4.70), the overall uncertainty of the absolute ventilation at each point $i$ in the actual profile is then:

$$u(v_{\mathrm{abs}}) = \frac{1}{v_{\mathrm{abs}}} \cdot \sqrt{\big(v_{\mathrm{asc}} \cdot u(v_{\mathrm{asc}})\big)^2 + \big(v_{\mathrm{hor}} \cdot u(v_{\mathrm{hor}})\big)^2}. \tag{4.74}$$

The uncertainty of the overall ventilation is uncorrelated and clearly determined by the value $u_{\mathrm{alt}}$ taken as random uncertainty component of the GPS altitude. As relative uncertainty it is in the order of 20 %.

## 4.5 Humidity-related variables

### 4.5.1 Conversion of relative humidity

**Calculation of relative humidity in ambient air** The temperature $T_{\mathrm{int}}$ of the RS41 humidity sensor is kept above that of ambient air ($T_{\mathrm{air}}$) at a constant offset of about 5 K. This is achieved through controlled heating with a heating element located on the humidity chip close to the polymer sensor and the 'internal' PT1000 temperature sensor also located on the chip. That is, since the sensor measures relative humidity at an elevated temperature, humidity has to be converted to the 'true' humidity in ambient air according to the temperature difference between air and sensor. This is done using the *Hyland and Wexler* (1983) formulation for saturation water vapour pressure $e_{\mathrm{s}}$ (see Section 4.5.2 and Appendix A.2). With the definitions of the dew point and the relative humidity ($e = U \cdot e_{\mathrm{s}}$, with $U$ as ratio with value between 0 and 1),

$$e_{\mathrm{d}} = e_{\mathrm{s}}(T_{\mathrm{d}}) = U_i \cdot e_{\mathrm{s}}(T_i) \tag{4.75}$$

applies for each temperature $T_i$ higher than $T_{\mathrm{d}}$. Here, $e_{\mathrm{d}}$ is the water vapour pressure at the dew point $T_{\mathrm{d}}$. Due to the independence of the dew point from temperature changes of an air parcel (as long as there are no phase transitions) follows for the 'internal' and air temperature and humidity during a humidity measurement with the RS41 radiosonde: $U_{\mathrm{int}} \cdot e_{\mathrm{s}}(T_{\mathrm{int}}) = U_{\mathrm{air}} \cdot e_{\mathrm{s}}(T_{\mathrm{air}})$, i.e.,

$$U_{\mathrm{air}} = \frac{e_{\mathrm{s}}(T_{\mathrm{int}})}{e_{\mathrm{s}}(T_{\mathrm{air}})} \cdot U_{\mathrm{int}}(T_{\mathrm{int}}). \tag{4.76}$$

**Uncertainty** Assuming independence of the uncertainties for $e_s(T_{int})$, $e_s(T_{air})$, and $U_{int}(T_{int})$, the combined uncertainty is calculated as

$$u(U_{air}) = |U_{air}| \cdot \sqrt{\left(\frac{u\left(e_s(T_{int})\right)}{e_s(T_{int})}\right)^2 + \left(\frac{u\left(e_s(T_{air})\right)}{e_s(T_{air})}\right)^2 + \left(\frac{u\left(U_{int}(T_{int})\right)}{U_{int}(T_{int})}\right)^2}. \tag{4.77}$$

Absolute values for $U_{air}$ are used in Eq. (4.77) to account for the possible occurrence of negative measured values at low humidities around 0 %.

### 4.5.2 Water vapour partial pressure

The water vapour partial pressure in Pa can be calculated with

$$e = U \cdot e_s(T), \tag{4.78}$$

with $U$ the (measured) relative humidity (dimensionless), and $e_s(T)$ the temperature dependent vapour pressure at saturation. For the RS41 GDP, the formulation of *Hyland and Wexler* (1983) (see Appendix A.2) is used for calculation of $e_s(T)$ with unit Pa.

The uncertainty of the vapour pressure in Pa is calculated by combining the measurement uncertainties for temperature and relative humidity $u(T)$ and $u(U)$ :

$$u(e) = \sqrt{\left(e_s(T) \cdot u(U)\right)^2 + \left(U\frac{\partial e_s(T)}{\partial T} \cdot u(T)\right)^2}, \tag{4.79}$$

with $\frac{\partial e_s(T)}{\partial T}$ the temperature sensitivity of the Hyland and Wexler relationship (Appendix A.2).

### 4.5.3 Integrated Water Vapour (IWV)

**Calculation of IWV** The Integrated Water Vapour (IWV) is the total amount of water vapour integrated over the air column, i.e. the integrated mass per unit area:

$$\mathrm{IWV} = \int_0^\infty \rho_w(z)\, dz, \tag{4.80}$$

with $\rho_w$ the water vapour density.

The IWV is equivalent to Total Column Water Vapour (TCWV), used by the modelling and satellite observation communities. There is another metric, alongside IWV, for the measurement of the total amount of water vapour in a vertical column of air, namely Precipitable Water Vapour (PWV) (sometimes called Precipitable Water (PW)). They are related to each other according to

$$\mathrm{PWV} = \frac{\mathrm{IWV}}{\rho_{lw}}, \tag{4.81}$$

where $\rho_{lw} \approx 1000\,\mathrm{kg\,m^{-3}}$ is the density of liquid water. The exact density is dependent on the temperature of the water and has a maximum at about 4 °C. IWV by definition is measured in

$\mathrm{kg\,m^{-2}}$, representing the mass of the water vapour in a column of air with base of $1\,\mathrm{m^2}$, while PWV is measured in mm, indicating the height of the condensed water vapour, precipitated as liquid water. The absolute values of IWV and PWV are numerically approximately equal.

IWV is calculated in the GDP as the sum of the water content in the layers between consecutive measurement points in the radiosonde profile. More than 99 % of the total water content is present below the tropopause. Thus, with burst altitudes in the middle of the stratosphere, radiosondes practically record the total water content in the atmospheric column.

IWV is calculated by summing the water mass in all layers from the ground to the $i$-th data point of the profile using the (measured) partial pressure of water vapour $e_j = U_j \cdot e_\mathrm{s}(T_j)$:

$$\mathrm{IWV}_i = \sum_{j=1}^{i} \rho_{\mathrm{w},j}(h_j - h_{j-1}) = \frac{1}{R_\mathrm{w}} \cdot \sum_{j=1}^{i} \frac{U_j\, e_\mathrm{s}(T_j)}{T_j}(h_j - h_{j-1}), \tag{4.82}$$

with $U_j$ the measured relative humidity, $e_s(T_j)$ the saturation vapour pressure over water, and $T_j$ the measured ambient air temperature in K. $R_\mathrm{w} = R/M_\mathrm{w} = 461.523\,\mathrm{J\,kg^{-1}\,K^{-1}}$ is the specific gas constant of water vapour, with $R = 8.3145\,\mathrm{J\,mol^{-1}\,K^{-1}}$ the universal gas constant, and $M_\mathrm{w} = 18.0153\,\mathrm{g\,mol^{-1}}$ the molecular mass of water. The water vapour density is proportional to the vapour pressure (assuming water vapour an ideal gas), and is thus given with the relative humidity measurement:

$$\rho_\mathrm{w} = \frac{e_\mathrm{w}(T)}{R_\mathrm{w} T} = \frac{U \cdot e_\mathrm{s}(T)}{R_\mathrm{w} T}. \tag{4.83}$$

**Uncertainty of IWV** With the water vapour density as function of the measured relative humidity and temperature (Eq. 4.83), and assuming that the latter two do not correlate, the uncertainty of $\rho_\mathrm{w}$ at each observation point $j$ is calculated according to Gaussian uncertainty propagation with

$$u(\rho_{\mathrm{w},j}) = \rho_{\mathrm{w},j} \sqrt{\left(\frac{u(U_j)}{U_j}\right)^2 + \left[\left(\frac{T_j}{e_{\mathrm{s},j}} S_{e_\mathrm{s},j} - 1\right)\frac{u(T_j)}{T_j}\right]^2}, \tag{4.84}$$

with $S_{e_\mathrm{s},j} = \frac{\partial e_{\mathrm{s},j}}{\partial T_j}$ the sensitivity of the saturation water vapour to temperature, i.e. the first derivative of the Hyland and Wexler formula. The humidity measurement (first term under the square root) by far dominates $u(\rho_{\mathrm{w},j})$.

The uncertainties $u(\rho_{\mathrm{w},j})$ and $u(h_j)$ both contribute to the overall uncertainty of the summed water content (Eq. 4.82). As described in Section 4.4.1.1, the random component of altitude has been experimentally determined once. The resulting uncertainty $\sigma(h_\mathrm{R})$ (here $\sigma(h_\mathrm{R})$ is $u_\mathrm{ucor}(h_R) = 1\,\mathrm{m}$ from Eq. 4.39) is assumed to be constant and representative for the entire altitude range of the radiosonde profile. The uncertainty of $\mathrm{IWV}_i$ is then calculated with

$$u(\mathrm{IWV}_i) = \sqrt{\left(\sum_{j=1}^{i}(h_j - h_{j-1}) \cdot u(\rho_{\mathrm{w},j})\right)^2 + \left(\rho_{\mathrm{w},1}^2 + \rho_{\mathrm{w},i}^2 + \sum_{j=2}^{i-1}(\rho_{\mathrm{w},j} - \rho_{\mathrm{w},j-1})^2\right)\sigma^2(h_\mathrm{R})}. \tag{4.85}$$

The uncertainty of the relative humidity is mainly given by the uncertainties from manufac-

turer calibration and ground check procedures (except for a profile section around the cold tropopause, where the sensor time lag contribution is significant, see Section 4.2.3). Humidity is therefore considered as 'fully' correlated over the entire profile. The first term under the square root in Eq. (4.85) describes the uncertainty contribution from vapour density, which is in turn essentially given by the uncertainty of relative humidity ($u(U_i)$ in Eq. 4.84), and thus takes the assumed full correlation into account. This is expressed in the fact that

$$\sum_{j=1}^{i}\Big((h_j - h_{j-1}) \cdot u(\rho_{\mathrm{w},j})\Big)^2 = \left(\sum_{j=1}^{i}(h_j - h_{j-1}) \cdot u(\rho_{\mathrm{w},j})\right)^2 \tag{4.86}$$

for full correlation of the $\rho_{\mathrm{w},j}$ (see *JCGM*, 2008, p. 21).

For a better understanding, an example sounding is shown in Fig. 4.28, as well as statistics of uncertainty in the network in Fig. 4.29. The IWV statistics show smaller values in polar areas and larger values in the Equator region.

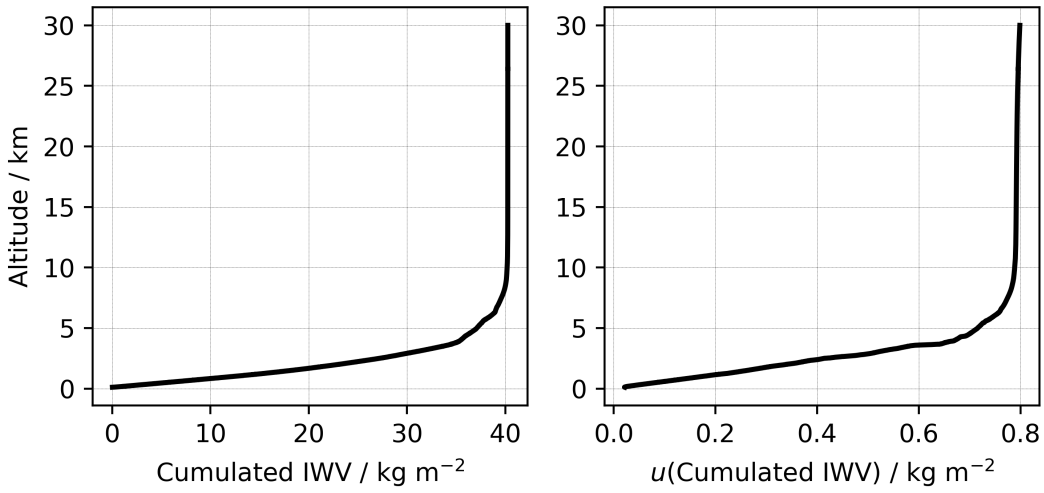


**Figure 4.28:** Cumulative IWV ('ciwv' variable in GDP) and uncertainty ($k = 1$) from a mid-latitude station in summer.

## 4.5.4 Water vapour mixing ratio

**Mass mixing ratio** The water vapour mixing ratio is usually defined as the ratio of the mass of water vapour molecules to the mass of dry air. With the ideal gas law it can be expressed in terms of pressure:

$$r = \frac{M_\mathrm{w}}{M_\mathrm{a}} \cdot \frac{e}{p - e}, \tag{4.87}$$

with $M_\mathrm{w} = 18.0153\,\mathrm{g\,mol^{-1}}$ the molar mass of water, and $M_\mathrm{a} = 28.9644\,\mathrm{g\,mol^{-1}}$ the molar mass of dry air. The unit is $\mathrm{kg\,kg^{-1}}$, or $\mathrm{ppm} = 10^{-6}\,\mathrm{kg\,kg^{-1}}$.

The uncertainty of the mass mixing ratio is determined by the uncertainties of the total atmospheric pressure $u(p)$ and the water vapour pressure $u(e)$ (via the relative humidity and

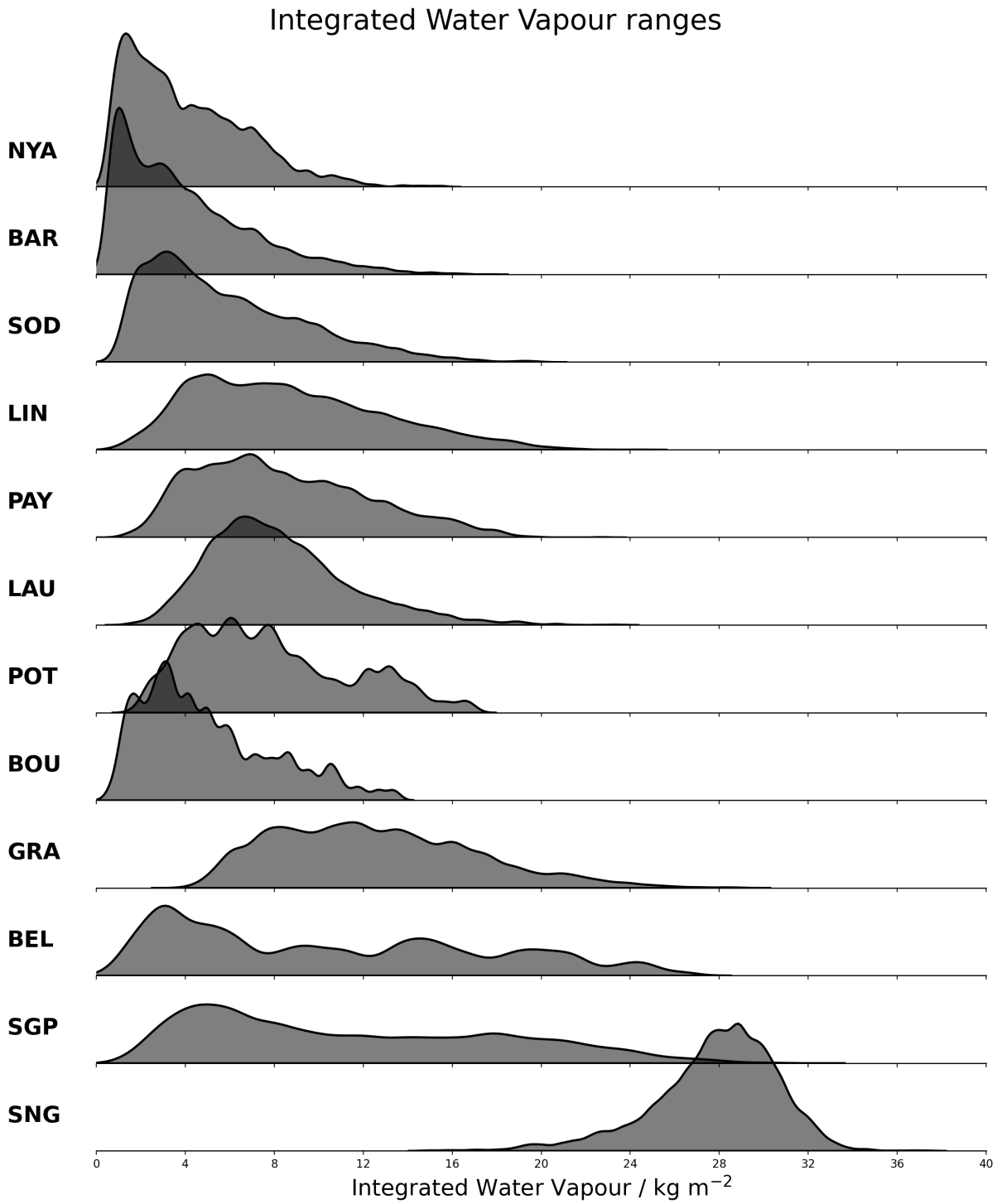


**Figure 4.29:** IWV ranges from the RS41-GDP for 2016-2021. The 3-letter GRUAN station abbreviations are listed on the left with the closest to the poles station Ny-Ålesund (NYA) at the top and the closest to the equator station Singapore (SNG) at the bottom. The mean uncertainties for IWV range from less than 0.5 kg m$^{-2}$ to more than 1.5 kg m$^{-2}$.

temperature dependent saturation vapour pressure, Eq. 4.79), and is calculated with

$$u(r) = \frac{r\,p}{p-e}\sqrt{\left(\frac{u(e)}{e}\right)^2 + \left(\frac{u(p)}{p}\right)^2}, \tag{4.88}$$

assuming that $u(p)$ and $u(e)$ are uncorrelated. The main contribution to $u(r)$ is the uncertainty of the relative humidity measurement through Eq. (4.79).

**Volume mixing ratio** The mixing ratio can also be expressed as volume mixing ratio (also called the molar mixing ratio). It is the number of moles of water vapour divided by the number of moles of moist air, which is equivalent to the volume of water vapour divided by the volume of moist air when assuming ideal gasses. With the ideal gas law it can be expressed with the pressure ratio:

$$x_v = \frac{e}{p}. \tag{4.89}$$

The unit is mol mol$^{-1}$ or m$^3$ m$^{-3}$, however, for handy figures of typical atmospheric water vapour mixing ratios, the unit $\mathrm{ppmv} = 10^{-6}\,\mathrm{m}^3\,\mathrm{m}^{-3}$ is preferably used. Note the added 'v' in the unit and as subscript in $x_\mathrm{v}$ to avoid confusion with the numerically different mass mixing ratio. The uncertainty is computed with

$$u(x_\mathrm{v}) = x_\mathrm{v}\sqrt{\left(\frac{u(e)}{e}\right)^2 + \left(\frac{u(p)}{p}\right)^2}, \tag{4.90}$$

with $u(e)$ given in Eq. (4.79).

### 4.5.5 Dew point and frost point temperature

From the relative humidity measurement, the water vapour partial pressure $e(T)$ at the actual temperature $T$ can be calculated using the definition of relative humidity, Eq. (4.78):

$$e(T) = U \cdot e_\mathrm{s}(T),$$

with $e_\mathrm{s}(T)$ the (empirical) expression describing the temperature dependence of saturation vapour pressure (Eq. A.4). The dew point $T_\mathrm{d}$ is defined as the temperature to which a given air parcel must be cooled at constant pressure and constant water vapour content in order for saturation to occur (https://glossary.ametsoc.org/wiki/Dewpoint). This implies

$$e(T) = e_\mathrm{s}(T_\mathrm{d}), \tag{4.91}$$

so that the dew point (and equivalently the frost point) can be determined from an inversion of $e_\mathrm{s}(T_\mathrm{d})$. This inversion is done numerically by interpolating $T_\mathrm{d}$ from a Look-Up Table (LUT) containing pre-calculated values for $e_\mathrm{s}(T_\mathrm{d})$ in 0.05 K steps for the temperature range of 100 K to 350 K. The interpolation is performed linearly in terms of the logarithm of the water vapour pressure.

The same procedure is used for the uncertainty estimate of $T_\mathrm{d}$. Using the uncertainty of the

water vapour partial pressure (Eq. 4.79), $u(T_\mathrm{d})$ is approximated by 'transferring' the uncertainty interval for vapour pressure into an uncertainty interval for $u(T_\mathrm{d})$:

$$u(T_\mathrm{d}) = \frac{|T_\mathrm{d}\left(e + u(e)\right) - T_\mathrm{d}\left(e - u(e)\right)|}{2\sqrt{3}}. \tag{4.92}$$

# 5 Traceability

In the International Vocabulary of Metrology (VIM) (*JCGM*, 2012), metrological traceability is defined as 'property of a measurement result whereby the result can be related to a reference through a documented unbroken chain of calibrations, each contributing to the measurement uncertainty'. The sequence of measurement standards and calibrations that is used to relate a measurement result to a reference is called the metrological traceability chain. With this chain all measurement results are traceable to the International System of Units (SI).

This chapter collects information on the traceability of the physical sensors for temperature, relative humidity, and pressure used on the RS41 radiosonde. Some information is given also for the GPS receiver.

RS41 radiosondes are calibrated against production working standards. The calibration validity period of those standards is 6 to 12 months depending on the reference type and parameter. Information of production working standards is recorded in a special database. The information includes standard type, manufacturer, serial number, Vaisala ID, calibration validity period, calibration history, and some other relevant data. The calibration automation in the production checks the status of applied working standards from the database and prevents the use of standards with expired calibrations. This guarantees that all factory working standards are regularly calibrated according to defined intervals.

The production working standards for pressure, temperature and humidity are calibrated in Vaisala's internal Measurement Standards Laboratory (MSL) against laboratory working standards. MSL is an ISO 17025 accredited laboratory. Accreditation includes regular calibration of MSL working and primary standards at the national laboratory level. The procedures and methods of MSL are fully compliant with the standard, and the laboratory is assessed by the Finnish Accreditation Service (FINAS) on a yearly basis. MBW chilled mirror reference standards are calibrated regularly outside Vaisala in a national level laboratory or ISO 17025 accredited laboratory.

Following this unbroken chain of calibrations with appropriate calibration validity periods and due to the adopted quality control procedures, RS41 calibrations are fully traceable to SI units.

## 5.1 Temperature

Temperature sensors are calibrated in Vaisala's own calibration facilities in measurement chambers specially designed for the RS41 sonde. The temperature calibration of RS41 is traceable to SI units (Fig. 5.1). Currently, Accumac AM1612 and Fluke 5606 Pt-100 Platinum Resistance Thermometers (PRTs) are used as reference temperature instruments. The calibration uncertainty of the reference instrument is (0.021 to 0.023) K ($k = 2$). The calibration interval is half a year for new sensors, and one year after a period of one year.

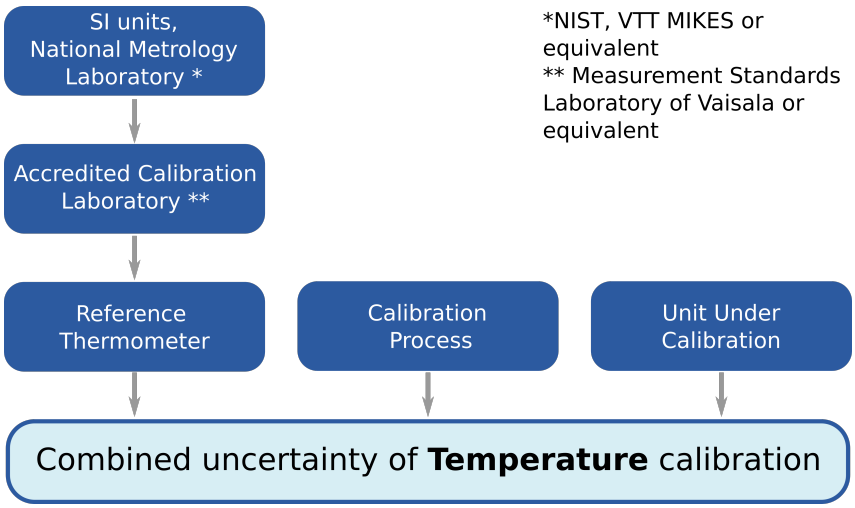


**Figure 5.1:** Chain of traceability and uncertainty components in RS41 temperature calibration (reproduced from *Vaisala*, 2017d).

For GRUAN soundings, a manufacturer-independent ground check for temperature is recommended. For manual soundings, this is realised with the Standard Humidity Chamber (SHC) (see Section 3.2.3). During the 100 %-check of the indication of the humidity sensor, the temperature in the SHC is also measured and either read once by the operator, or recorded continuously with an automatic data acquisition system. The used temperature sensor should be of high quality and traceable to the SI.

The RS41 temperature data in daytime soundings are corrected for solar radiative heating in the GRUAN processing. The correction is based on laboratory measurements of the solar effect (see Section 4.1 and *von Rohden et al.*, 2022). All sensors arranged in the setup that significantly contribute to the uncertainty of the experimental results (namely sensors for temperature, pressure, irradiance, and the determination of ventilation speed) are calibrated in accredited laboratories and are therefore traceable to national or international references.

## 5.2 Relative humidity

Special measurement chambers designed by the manufacturer are used for humidity calibration. The calculated relative humidity during calibration is based on SI-traceable measurements of ambient temperature, dew point, and pressure (Fig. 5.2).

Reference instruments for temperature during humidity calibration are Accumac AM1612 and Fluke 5606 Pt-100 PRTs, with calibration uncertainties of (0.021 to 0.023) K ($k = 2$), and a calibration interval of half a year for new sensors, and every year after the first year.

Dew point reference instruments are the Vaisala Dewpoint Transmitter DMT143, with a calibration uncertainty of 0.6 K ($k = 1$) and a calibration interval of two years, and the MBW 373 LHX, with a calibration uncertainty of (0.16 to 0.18) K ($k = 2$) and a calibration interval of one year.

The pressure reference device for the radiosonde humidity calibration is the Vaisala Digital Barometer PTU300. It has a calibration uncertainty of 0.07 hPa ($k = 2$) and is calibrated every

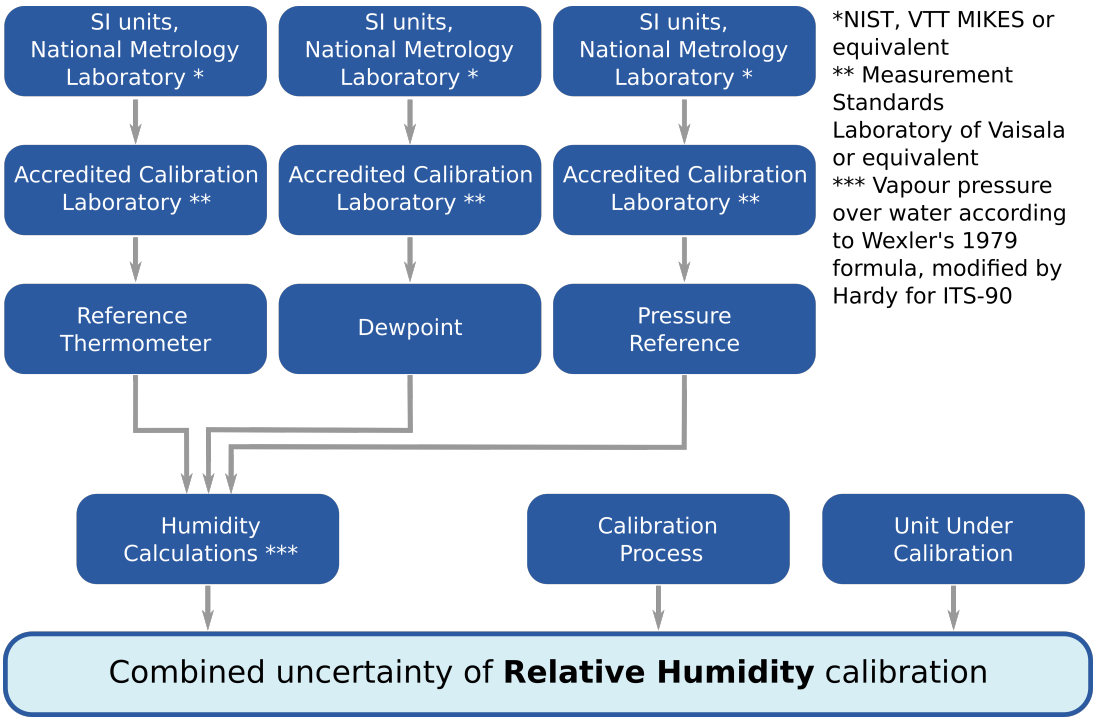


**Figure 5.2:** Chain of traceability and uncertainty components in RS41 humidity calibration (reproduced from *Vaisala*, 2017d).

6 months.

For calculation of relative humidity, Wexler's formula modified by *Hardy* (1998) is used for the water vapour pressure over water.

The manufacturer-prescribed ground check using the RS41 ground check device includes a reconditioning by controlled heating of the humidity sensor, where possible contaminants are removed and a humidity level of 0 % should be established (Section 2.2) as a reference point. This procedure is required to fully restore the original factory calibration, i.e. to remove possible biases which may have occurred during storage and transport. Thus, the 0 % relative humidity reference point assures traceability because it is realised in a way similar to a natural principle.

The subsequent GRUAN-100 % check in the SHC (see Section 3.2.3) provides direct traceability to the SI by using a basic physical principle when realising the 100 % relative humidity value at a second independent reference point.

## 5.3 Pressure sensor

The calibration of pressure sensors used in the RS41-SGP model is conducted in specially designed measurement chambers at the manufacturer. The calibration reference sensors are traceable to the SI (Fig. 5.3). The reference pressure instrument used for radiosonde pressure calibration is Fluke pressure reference monitor RPM4. It is calibrated with an uncertainty of 0.08 hPa ($k = 2$) at 6 month intervals.

For the manufacturer-prescribed ground check of the RS41-SGP radiosonde, the RI41-B ground

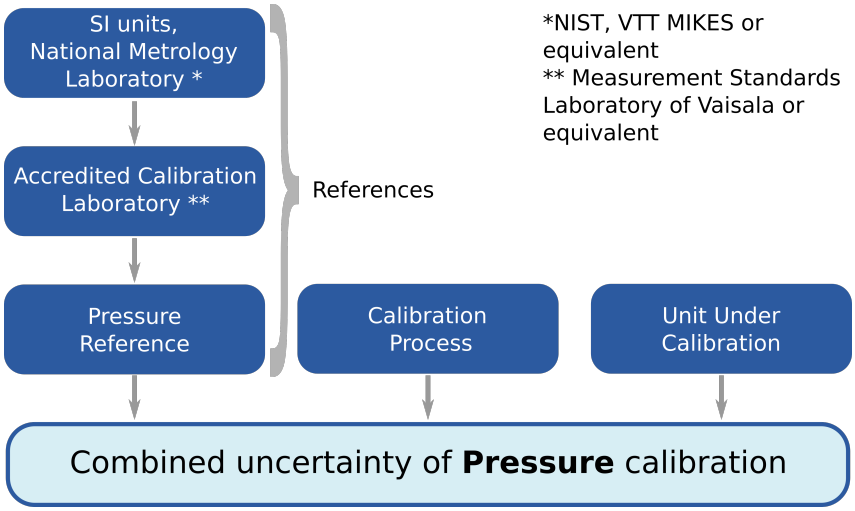


**Figure 5.3:** Chain of traceability and uncertainty components in RS41 pressure calibration (reproduced from *Vaisala*, 2017d, 2014).

check device with in-build reference high-precision barometer should be used. The reference sensor module in the RI41-B is Class-A calibrated and traceable to NIST. Its uncertainty is 0.15 hPa, and the long-term stability is 0.1 hPa per year. If another reference (e.g. the station barometer) is used for comparison during the pressure ground check the traceability must be ensured by use of a calibrated instrument.

When using a RS41-SG model without pressure sensor, the GDP for pressure is based on GPS data, however the the profile is still tied to the surface pressure at the launch point. That is, the traceability is given by measuring the ground pressure with the calibrated station barometer.

## 5.4 GPS receiver

The information in this section is taken mainly from *Matsakis et al.* (2018).

The SI primary reference for time is the Coordinated Universal Time (UTC). UTC is computed by the International Bureau of Weights and Measures (French: Bureau International des Poids et Mesures) (BIPM) in France by performing a weighted average of data collected from local time scales located at more than 70 timing laboratories. UTC is defined through its difference with the local time scales of the laboratories in the standard. The monthly *Circular T*, produced by the BIPM, provides the uncertainty between UTC and the local time standards in each of the timekeeping laboratories.

United States Naval Observatory (USNO) is the source of UTC for the Department of Defence and by extension of GPS. GPS has its own time scale, known as GPS time. The satellites broadcast parameters in subframe 4 of the GPS navigation message that receivers can apply to convert GPS time to a prediction of UTC (USNO). The GPS time predictions of UTC at USNO are within 0.5 ns, which in terms of length is approximately 14 cm. The GPS time on board the satellites are updated through the GPS control segment with corrections to each satellite clock calculated and then further transmitted to the users within the GPS message. GPS time is intended only for positioning and does not include leap seconds. A receiver can obtain the

UTC correction parameters from any satellite, but should use the satellite whose information was most recently refreshed.

The transition from time standard to distances is done within the World Geodetic System 1984 (WGS84). The WGS84 postulates the speed of light to be 299 792 458 m $s^{-1}$.

The calibration of the GPS receiver on board the RS41 radiosonde is done through the synchronisation of the receiver clock during the process of primary acquisition. The documented root mean square error of the installed u-blox receiver stability over time is 30 ns, which in terms of length is approximately 10 m (*ublox*, 2013a).

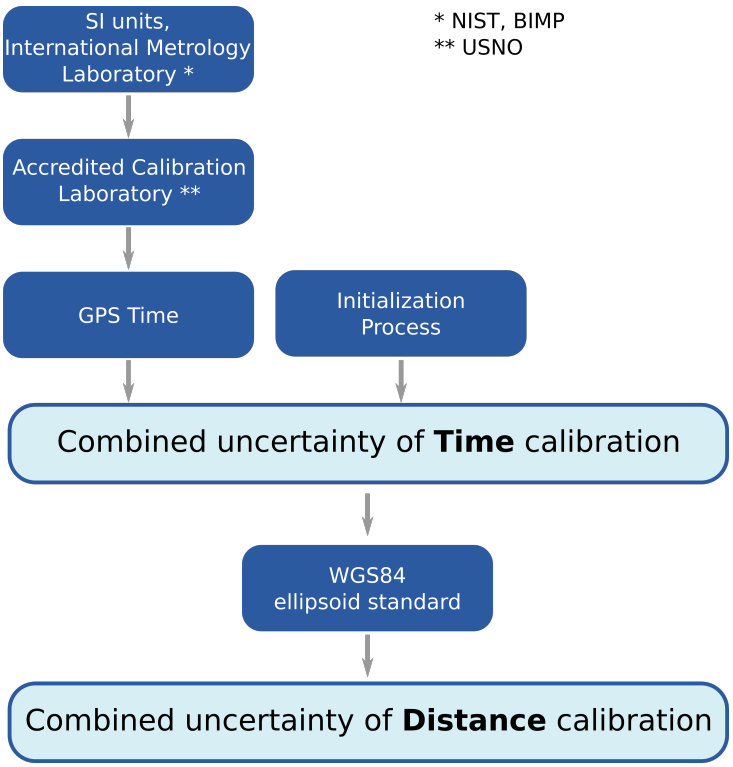


**Figure 5.4:** Chain of traceability and uncertainty components in RS41 time and distances calibration.

# 6 Combination of uncertainties

This chapter summarises information on the propagation of measurement uncertainties, and the combination of uncertainty components for temperature, relative humidity, and pressure. The uncertainty propagation for each of these measurement parameters is visualised in a separate diagram (Figs. 6.1 to 6.4). The diagrams represent the order in which various uncertainty components, resulting from the steps in the data processing for the RS41-GDP.1 data product, contribute to the uncertainty budget.

The primary intention of the diagrams is to provide an overview of the error propagation, and to illustrate the connectivity between the individual uncertainty components. However, the diagrams do not provide a quantitative representation of the uncertainty budgets. They depict source and intermediate uncertainty components (shown in red-framed boxes), and the paths along which these components propagate and combine with other components into the final uncertainties (shown in double framed red-coloured boxes). The connecting pathways are indicated with black solid lines. Relevant formulas or expressions describing uncertainty combinations are included in the diagrams.

## 6.1 Correlations of uncertainties

A correlation property is assigned to each uncertainty component that contributes to the combined total uncertainty of the measurement parameter in question. Three correlation types are used: 'uncorrelated' (subscript 'ucor'), 'spatially correlated' ('scor'), and 'temporally correlated' ('tcor'):

- 'Uncorrelated' means that the uncertainties of the individual data points are treated as independent (random), i.e. no correlation exists.
- 'Spatially correlated' means that the uncertainties of the individual data points within a single sounding profile are correlated, but that there is no correlation with the uncertainties of data from other soundings. The degree of correlation is assumed to be 'full' according to a Pearson correlation coefficient of $r = 1$.
- 'Temporally correlated' means that the uncertainties are correlated amongst separate profiles that have been measured at different times and/or locations (sites). An example is the calibration uncertainty of a sensor, which is performed by the manufacturer and applies to any measured data point in the same way. The degree of the temporal correlation is assumed to be 'full' according to a Pearson correlation coefficient of $r = 1$. The assignment of a temporal correlation automatically includes a the spatial (vertical) correlation. To illustrate this: consider the analysis of a time series of a parameter after averaging (gridding) over a certain altitude range. If the uncertainty of the parameter is temporally correlated, the spatial correlation must be taken into account when calculating the layer

means.

The classification of the correlation types is specified ‘by hand’, based on evidence or experience. The classification is not based on calculations or comprehensive covariance analyses, because of the complex interrelations between the variables and the high processing efforts required to collect suitable information about their actual degree of correlation. Thus, the term “correlation” is not used here in a strictly mathematical or stochastic sense. Instead, it means a simple categorisation in which uncertainty components are defined as either systematic (with the two subcategories with regard to time and space) or random, depending on which of the categories they tend to fall into.

The provision of correlated and uncorrelated uncertainty components enables the user to take correlations into account when combining uncertainties, at least at the coarse level of the described classification. That is, individual uncertainty components in the budget can be rearranged and re-combined according to the above categories. This allows more realistic estimates to be made for the overall or combined uncertainties of variables of interest.

In the charts presented in Figs. 6.1, 6.2, 6.3, and 6.4, the colour of the boxes surrounding uncertainties indicate the correlation types: red for temporally correlated, green for spatially correlated, and blue for uncorrelated.

The classification of the correlation types for the uncertainty components is consistent, meaning that when combining these, i.e. calculating of the square root of the sum of the squares of the complete set of correlated and uncorrelated components, the result is equal to the original combined uncertainty of the variable:

$$u = \sqrt{u_{\text{ucor}}^2 + u_{\text{scor}}^2 + u_{\text{tcor}}^2}. \tag{6.1}$$

The final combined ‘correlated’ uncertainty components are marked in the charts with purple dashed boxes and arranged at the bottom, and the connecting paths are represented by purple dashed lines.

The values of the ‘correlated’ and ‘uncorrelated’ uncertainties are saved in the data files of the GDP in separate columns. They can be recognised by the designations ‘ucor’, ‘tcor’, and ‘scor’ in the column names (Appendix A.2 in *Sommer et al.*, 2022).

## 6.2 Uncertainty combination

### 6.2.1 Temperature

Fig. 6.1 shows a chart scheme describing the sources and propagation of uncertainties that are included in the calculation of the uncertainty of the air temperature measurement in the GDP. More detailed discussions of the components included in this scheme can be found in the following sections of this document:

- Manufacturer calibration: Section 3.2.1.1 and Appendix A.1.1,
- Manufacturer prescribed ground check: Section 3.2.2,
- GRUAN SHC-ground check: Section 3.2.3.1,

- Combined pre-launch uncertainty: Section 3.2.3.2,
- Radiative Transfer Model (RTM): Section 4.1.4.7,
- Pressure derived from GPS: Section 4.4.2.2,
- Pressure measured with sensor: Section 2.1.3.3,
- Ventilation during ascent: Section 4.4.4,
- Solar radiation correction: Section 4.1.5,
- Smoothing: Appendix A.3.

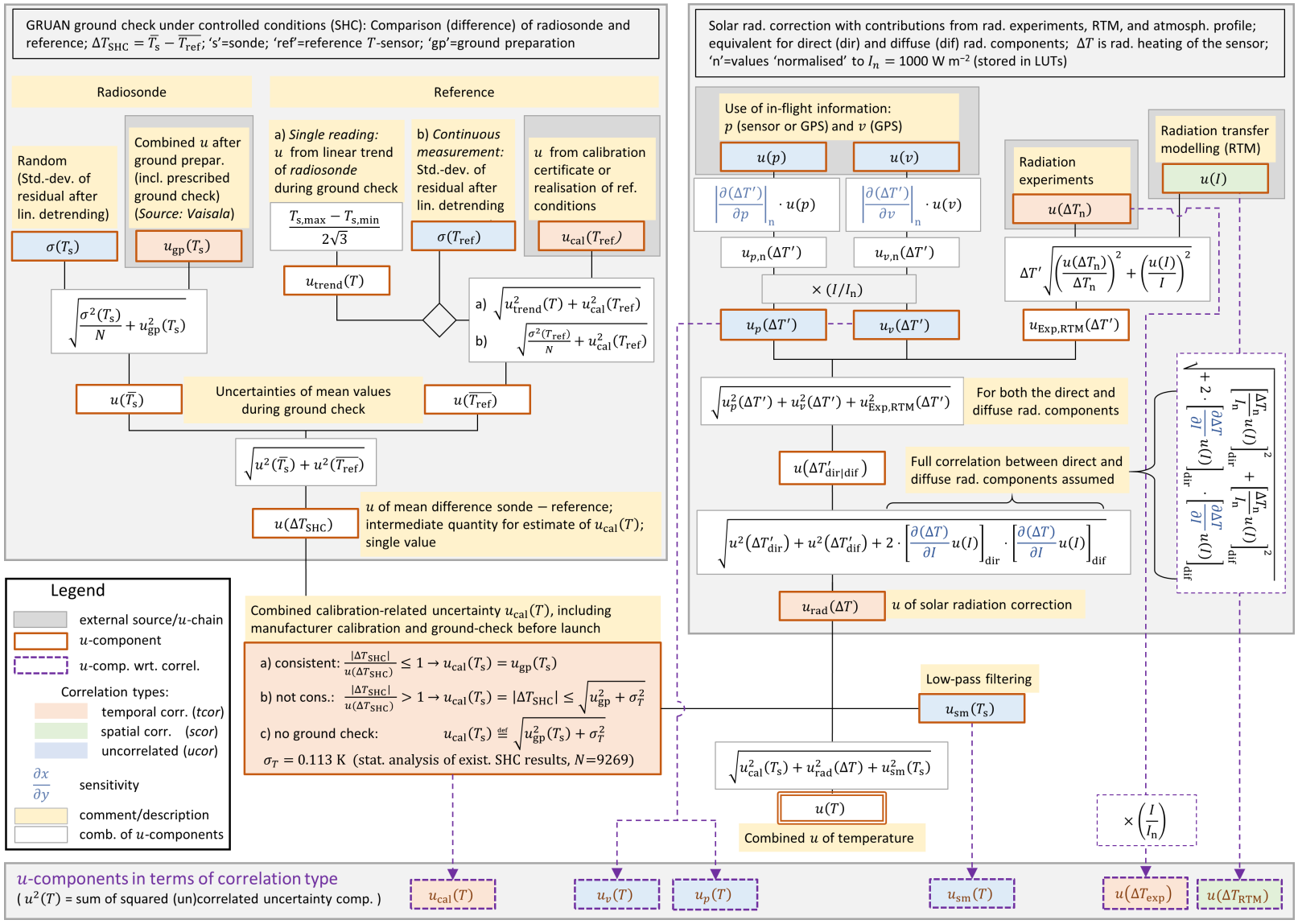


**Figure 6.1:** Combination of uncertainty components of temperature in the GDP for the Vaisala RS41 radiosonde (version RS41-GDP.1).

### 6.2.2 Relative humidity

Fig. 6.2 shows a chart scheme describing the sources and propagation of uncertainties that are included in the calculation of the uncertainty of the relative humidity measurement in the GDP. More detailed discussions of the components included in this scheme can be found in the following sections of this document:

- Manufacturer calibration of rel. humidity sensor: Section 3.2.1.2 and Appendix A.1.2,
- Manufacturer calibration of temperature sensor at humidity sensor chip (the same as for the regular temperature sensor): Section 3.2.1.1 and Appendix A.1.1,
- Manufacturer prescribed ground check: Section 3.2.2,
- Uncertainty of air temperature measurement in flight: Section 6.2.1
- Combined pre-launch uncertainty: Section 3.2.3.4,
- GRUAN SHC-ground check: Section 3.2.3.3,
- Time-lag of relative humidity sensor: Section 4.2.3,
- Smoothing: Appendix A.3.

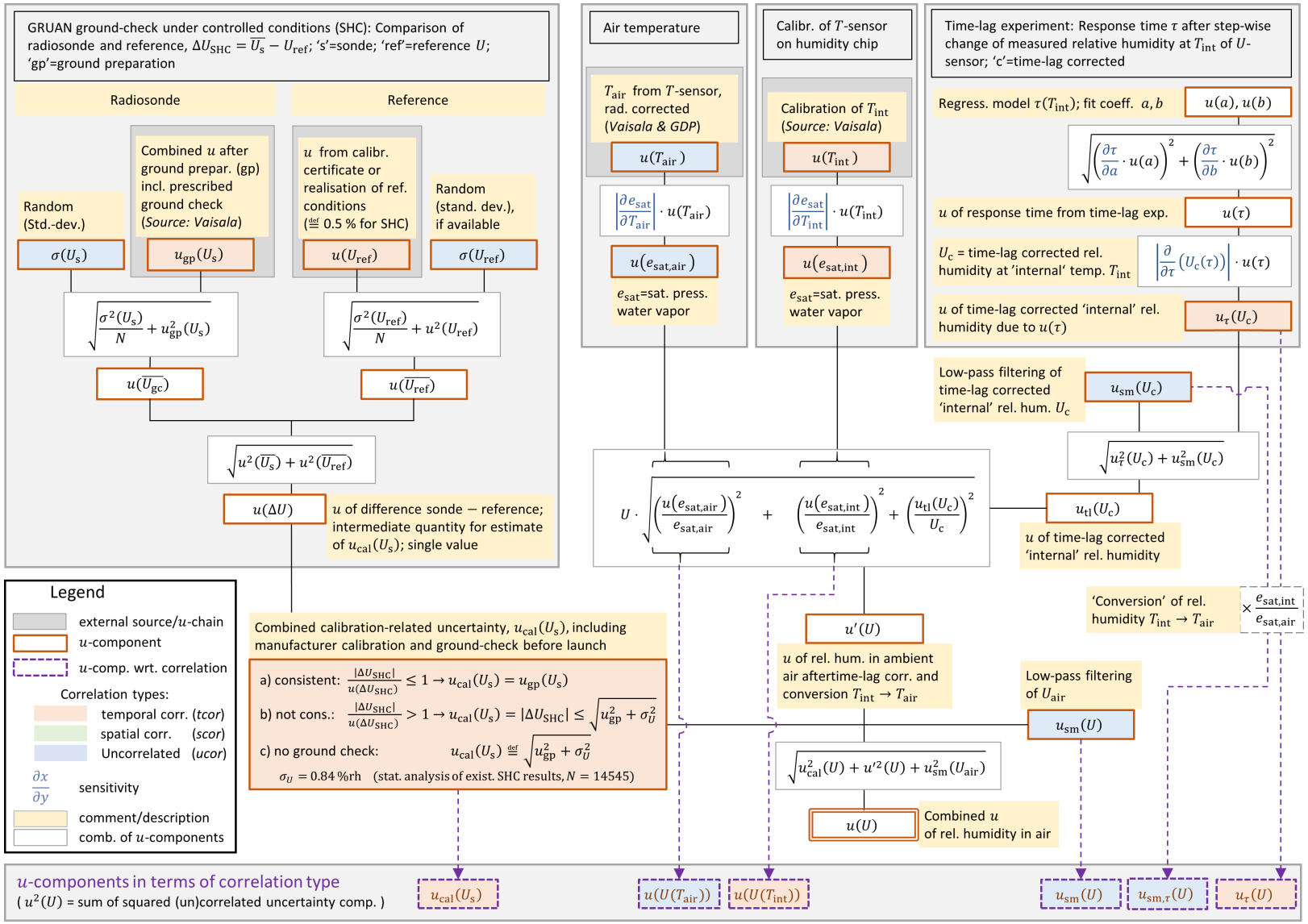


**Figure 6.2:** Combination of uncertainty components of relative humidity in the GDP for the Vaisala RS41 radiosonde (version RS41-GDP.1).

### 6.2.3 Pressure

**GPS derived pressure** Figure 6.3 shows a chart scheme describing the sources and propagation of uncertainties included in the calculation of the uncertainty of pressure that is derived from GPS altitude measurements. More detailed discussions of the components included in this scheme can be found in the following sections of this document:

- Uncertainties related to GPS altitude measurements (random and systematic components) and virtual temperature: Section 4.4.2.2
- A summarising description including the uncertainty of the 'reference' pressure at the launch altitude $u(p_0)$ can be found in Appendix D.3

**Pressure measured with sensor** Figure 6.4 shows a chart scheme describing the sources and propagation of uncertainties that are included in the calculation of the uncertainty of pressure measured with the physical sensor in case of sounding with the RS41-SGP radiosonde model. More detailed discussions of the components included in this scheme can be found in the following sections of this document:

- Calibration at manufacturer and pressure correction after manufacturer-prescribed ground check (RI41) (no uncertainty contribution): Section 3.2.1.3, Appendix A.1.3, Fig. 3.11
- GRUAN SHC-ground check: Section 4.3,
- Smoothing: Appendix A.3.

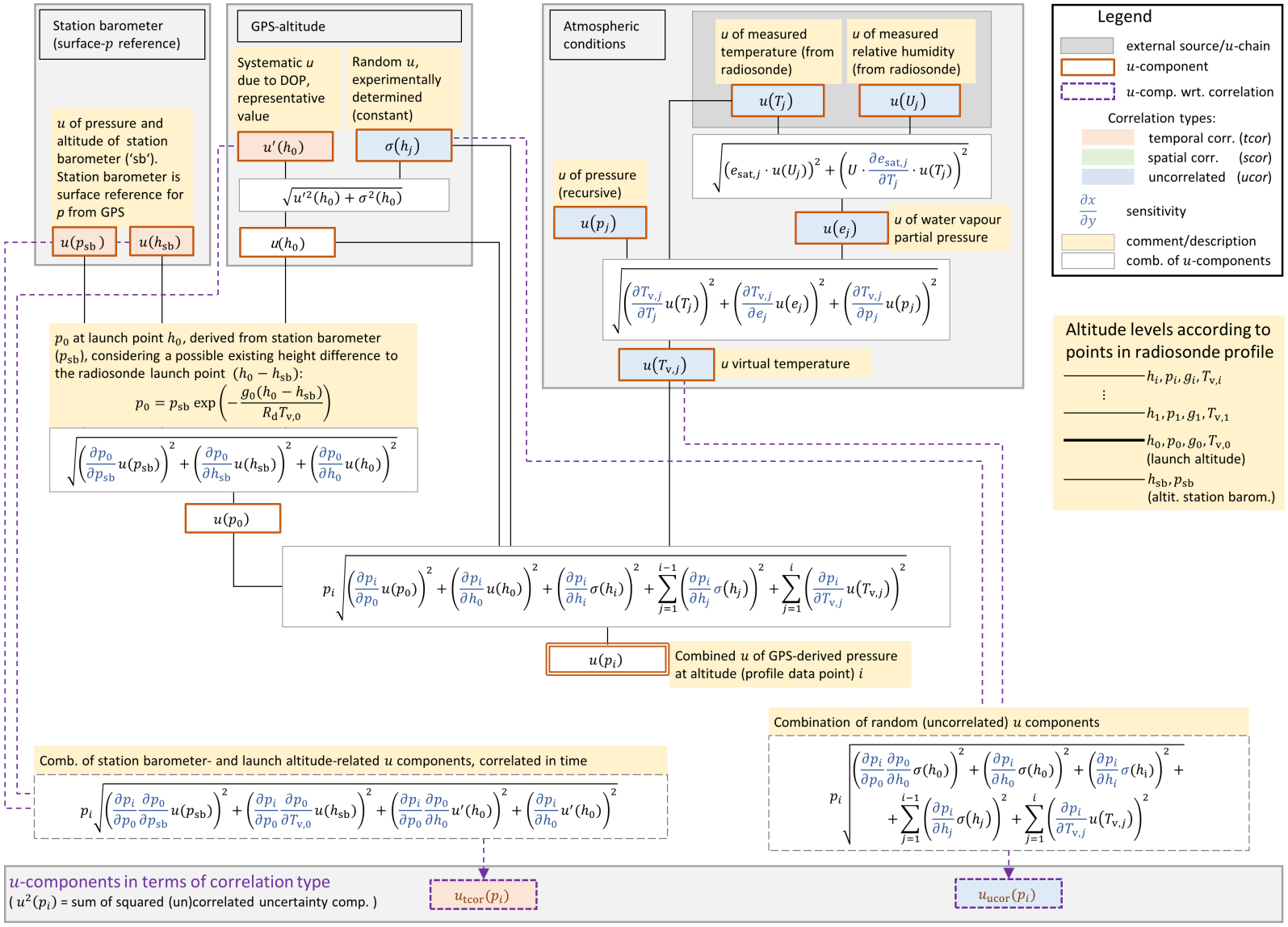


**Figure 6.3:** Combin. of uncert. components for GPS-derived pressure in the GDP for the Vaisala RS41 radiosonde (version RS41-GDP.1).

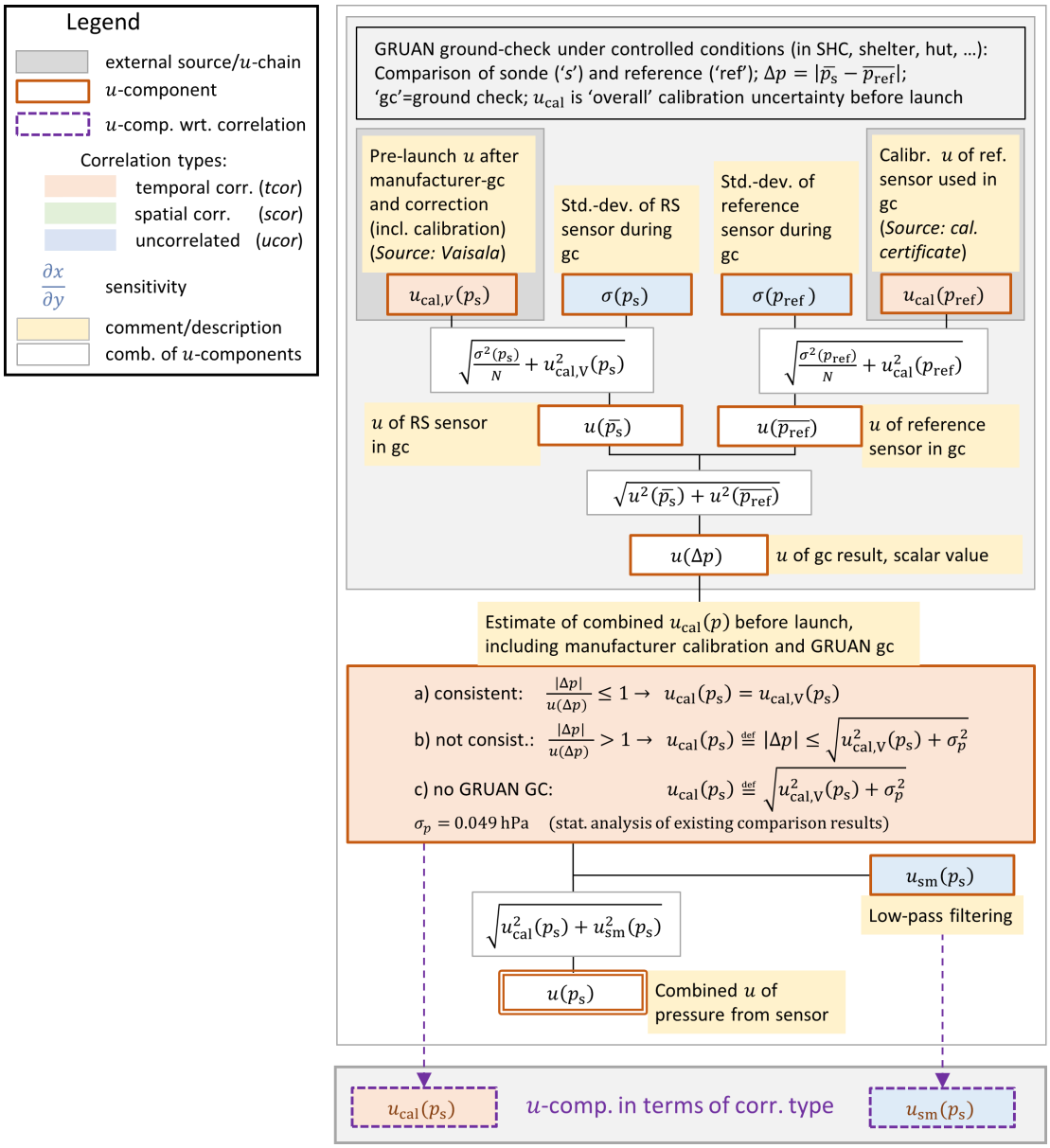


**Figure 6.4:** Combination of uncertainties for pressure measured with pressure sensor in the GDP (version RS41-GDP.1).

# 7 GRUAN Data Product (GDP)

The software for the processing of the raw data and creation of the GRUAN Data Product (GDP) for the RS41 radiosonde was developed at the GRUAN Lead Centre, and the GRUAN Lead Centre is also the executive Processing Centre (PC). A brief overview of the processing system is given in Section 7.1, including a flowchart illustrating the basic working structure. Details of the workflow are listed in Appendix B.1. Section 7.2 describes the naming and format of the input data files. The individual steps of the processing are briefly explained in Section 7.3, grouped by variables. Section 7.4 gives an outlook to a future data quality assessment, to be implemented by coordinated efforts of the Quality Task Force (QTF) and Task Team (TT) Radiosondes.

The processing produces various output files that are described in some detail in Section 7.5. In order to place the RS41 data processing within the larger framework of GRUAN, the GRUAN RS41 data management is explained in Section 7.6. Data management includes all GRUAN-relevant steps after the completion of the sounding, including the transfer of the product data to the users.

## 7.1 General overview of the processing system

The GRUAN Data Processing System for radiosondes (GDPS) is a modular system for processing of radiosonde sounding data in GRUAN. Its design is generic to facilitate the creation of official GRUAN data products for various radiosonde types. The processing handles calibrated raw data from the individual sensors of the radiosonde as well as metadata (from the GMDB or separate input files).

The development started in 2014 based on a review and analysis of the existing GRUAN processing software for the predecessor radiosonde RS92 (RS92-GDP.2, see *Sommer et al.*, 2021), which was developed earlier at the Lead Centre and became the first GRUAN-certified data product. A number of extended criteria was defined for the new system, which essentially meant a redevelopment of the software:

- *Detailed configuration*: base system, processing steps, input and output,
- *Clear structure*: clear and orderly structure of processing steps,
- *Flexible names*: mapping of names of variables (data) and attributes (metadata); definitions of variables at module level,
- *Usable offline*: preferably no external dependencies, e.g. on server Application Programming Interfaces (APIs),
- *Modular and extensible*: flexible number of processing modules, modules arbitrarily expandable, universal module design,

- *Generic*: easy adaptation to any radiosonde type or other in-situ instruments, and
- *Stable*: robust and secure processing, capable of being integrated into a batch processing system.

Further capabilities include:

- Optional concurrent generation of analysis plots,
- Creation of an extensive log file,
- Default output in NetCDF version 4 file format (incl. compression),
- Use of XML and INI files for individual configuration of modules and processing steps,
- Version management, logging of all changes (especially in the modules), and
- Optional comparison with other available data (e.g. manufacturer product).

Figure 7.1 contains a flowchart showing an outline of the workflow of the processing system. The modular and generic design allows easy adaption to changing requirements. A more detailed view is documented in Appendix B.1. The processing system (GDPS) will be fully described in a separate document (*Sommer and von Rohden*, 2023, in preparation).

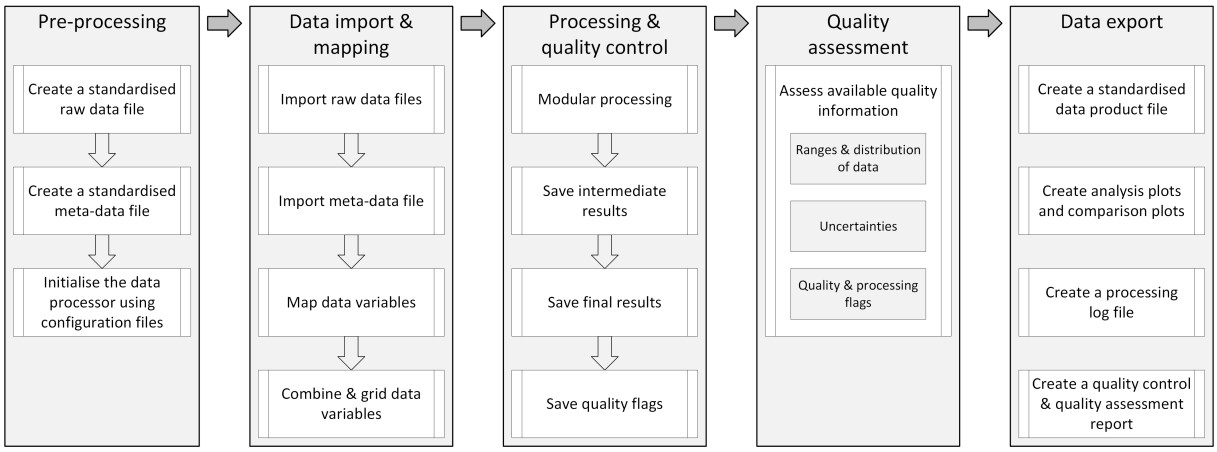


**Figure 7.1:** Basic structure of the GRUAN Data Processing System for radiosondes (GDPS).

## 7.2 Input data

The RS41 processing ingests data from three sources: raw data, metadata, and results from external reference sensors during ground checks (if available). It was important to use few file formats in a standardised form. The three sources and its formats are

- NetCDF file (GNC-RAW), converted from Vaisala's proprietary MWX data format – see Sections 7.2.1 and 7.2.2,
- Metadata from the GMDB (MD) – see Section 7.2.3,
- Ground check reference sensor data (not standardised yet) – see Section 7.2.4.

These data sources or file formats are described in more detail below.

### 7.2.1 Original MW41 sounding archive file (MWX)

The Vaisala ground system MW41 used for soundings with the RS41 radiosonde exports the data of a sounding in MWX format. The format is called a sounding archive because it contains the complete set of information for a sounding. Among other things it contains the following:

- Original frames transmitted by the radiosonde,
- Original and converted raw data for all parameters,
- Vaisala data product results for all parameters,
- Results of the ground checks,
- Sonde-specific settings,
- Log of the sounding events, and
- Configuration of the MW41 system.

A MWX file is basically a packed file (ZIP) containing a number of XML files. Each XML file is the result of an export (dump) from a database table with the same name. The automatically generated, unique sounding ID serves as the only filter. Depending on the configuration of the MW41 system, the MWX files contain different numbers of XML tables. The number and structures of the available tables has changed with time through further development at the manufacturer. Undocumented changes in the structure of the input data files, especially renamed or removed tables, may cause problems in automatic data processing systems. However, the GRUAN processing is able to overcome such issues to a certain extent.

An actual list of XML tables including information on their contents (columns and column names, data types, units and descriptions) can be found in the MW41 system documentation (Appendix A in *Vaisala*, 2020d). A list of accessible MW41 tables is also given in Appendix E.2 of this document.

The following tables are used for the GRUAN processing:

- RawPtu – **required** data table as source INT1 – raw data of pressure, temperature and humidity (see Table E.1)
- GpsResults – **required** data table as source INT2 – results of GNSS (GPS) measurements (see Table E.2)
- GpsRawMeasurements – **required** data table as source INT3 – raw data of GNSS (GPS) measurements (see Table E.3)
- GSupport – *recommended* data table as source INT4 (*In principle it is required. However, MW41 does not provide this table at a number of sites. In such cases, a workaround is implemented.*) – internal temperature and humidity raw data of heated humidity sensor (see Table E.4)
- PtuResults – *optional* data table as source INT5 – Vaisala data product for pressure, temperature and humidity (see Table E.5)
- SynchronizedSoundingData – *optional* data table as source INT6 – full Vaisala results as basis for standard exports, e.g. BUFR messages (see Table E.6)
- Soundings – **required** meta-data table as meta-data attributes – general meta-data related

to the sounding (see Table E.7)

- Radiosondes – **required** meta-data table as meta-data attributes – meta-data related to the used radiosonde (see Table E.8)
- GCCORRECTIONS – **required** meta-data table as meta-data attributes – ground check results used to correct/adjust raw data (see Table E.9)
- SurfaceObservations – **required** meta-data as meta-data attributes – weather conditions at launch site at launch time (see Table E.10)

**Note:** The GDPS does not directly read original MWX files for input. It only works with converted NetCDF files. Please see next Section 7.2.2.

### 7.2.2 Converted as NetCDF file (GNC-RAW)

In order to detach the GDPS as much as possible from proprietary file formats, the original files are converted into NetCDF before use. The original content and structures (tables, columns, metadata) are preserved as far as possible. This "GRUAN NetCDF Raw Data Format for Radiosondes" (GNC-RAW) is a generic format. Raw data of any type, including Vaisala's current format (MWX) and predecessor format (DC3DB), can be used as source. Thus, to limit the complexity, GDPS's import ability is restricted to NetCDF. The format is documented in *Sommer* (2023b, in preparation). The original names and formats of the tables, columns and meta data can be assigned by proper configuration.

### 7.2.3 Metadata (MD) from GMDB

Beside the information contained in the MWX file, data from the GRUAN Meta-data Data Base (GMDB) is included in the processing of each profile. The GMDB is a central repository for the complete set of GRUAN metadata to be collected with all measurement activities. It is developed and managed by the GRUAN Lead Centre and operated since more than 10 years. It provides various information e.g. on:

- Site, measurement systems and instrumentation,
- Setup, rig composition (e.g. additional sondes or instruments, balloon type, string length),
- Ground conditions, ground checks (if performed),
- Measurements, files, data products and processing.

The continuous change and expansion of the database requires a robust, automatised but flexible method of access during processing. Therefore a transfer file with a simple structure (key/value pairs) was developed to export metadata from the database. Depending on the complexity of the sounding setup, the file can contain hundreds of lines. As an example, the following listing presents some lines of such a Meta-Data (MD) file:

```
1 File.Type                                    = GMDB Export File
2 File.TypeVersion                             = 0.1
3 Measurement.Balloon.FillingWeight            = 450 g
4 Measurement.Balloon.Gas                      = Helium
```

```
Measurement.Balloon.Key                          = TA600
Measurement.Checks.0.Id                          = 167841
Measurement.Checks.0.p.RefPressure               = 986.36 hPa
Measurement.Checks.0.p.SensorPressure            = 985.2217 hPa
Measurement.Id                                   = 118279
Measurement.InternalKey                          = 222
Measurement.IsExperiment                         = no
Measurement.MainSonde.Check_1.CheckDate          = 2020-02-25T04:27:16.680Z
Measurement.MainSonde.Check_1.CheckType          = GC-RI41
Measurement.MainSonde.Check_1.ToolSN             = M4150012
Measurement.MainSonde.Check_1.ToolType           = DC-RI41-B
Measurement.MainSonde.Check_1.p.RefPressure      = 986.36 hPa
Measurement.MainSonde.Check_1.p.SensorPressure = 985.2217 hPa
Measurement.MainSonde.Key                        = RS41-SGP-REV2
Measurement.MainSonde.Manufacturer               = Vaisala (VAISALA)
Measurement.MainSonde.SerialNumber               = R2820034
Measurement.MainSonde.p.AttachmentType           = free hanging
Measurement.MainSonde.p.CoverMaterial            = styrofoam
Measurement.MainSonde.p.Weight                   = 84 g
Measurement.p.WeatherCondition.Comment           = after rain
Measurement.p.WeatherCondition.Pressure          = 985.1194 hPa
```

The example shows that the keys can be composed of several grouping levels. The current structure of the MD file is documented in Appendix E.1.

### 7.2.4 Data from external sensors during ground checks

Another data source for the processing are data from external (reference) sensors measured during ground checks. Several station-specific file formats are still supported (currently for NYA, GVN and LIN). However, work is being done within GRUAN towards a standardisation of the data format.

The actual used formats are simple text files with the following characteristics:

- (Optional) header with metadata, which is marked accordingly (e.g. line starting with '#'),
- Metadata given line by line as key/value pairs to enable automatic reading (keys must be unique),
- Data table with a single title line and any number of data lines,
- Title line with (unique) column names,
- The data table's first column contains the time (UTC) of the measurement (e.g. full ISO time stamp '2020-11-02T09:43:21.521Z'),
- The data table contains one or more columns with measurement values from one or more external sensors, and
- The data table may contain columns with flags indicating the time period of the ground check (e.g. 0 or 1).

Ideally, the measurement data from the external sensors should be provided with at least the same temporal resolution as that of the RS41 radiosonde (1 s).

**Note:** The need for standardisation for these files is pointed out here once again. This adds to the flexibility of the GDPS and increases the ability to process other radiosonde models in the future. Therefore, a proposal for a standardisation needs to be worked out timely and then submitted to the "Task Team Radiosondes" and the "Task Team Sites" for discussion.

### 7.2.5 Gridding and merging of input data

Using the main data source (table "RawPtu" in the MWX file) the time data column is analysed first and used to create a regular grid (e.g. 1 s). The time-related variables and all other tables are then re-arranged to that constant time grid. In a further step, the various tables are synchronised such that the profile data of all files and tables are given on the same time grid.

### 7.2.6 Additional resources directly accessed by the processing modules

During the processing, several modules directly access information stored in resource files which are available as so-called SAV files. These are binary IDL files containing pre-evaluated data, e.g. in the form of look-up tables.

Some of the modules call external programmes. In the RS41 GDP this is used to run on call the code of a radiation transfer model as part of the radiation correction for daytime temperature data (Section 4.1.4).

**Note:** The use of NetCDF instead of SAV files is envisaged for future GDP versions to reduce dependency on other programming languages.

## 7.3 Processing steps

The processing of the RS41 data consists of approximately 80 individual steps which are worked through sequentially. The steps can be assigned to different groups. A summarising list of the steps can be found in Appendix C.1. The list provides basic information including the name and version of the processing module used for the actual step.

To give an overview, the steps are briefly outlined in the following subsections in the order of processing. The most important steps are described in detail in Chapter 4.

### 7.3.1 Initialisation and preparation

First, various preparatory steps are carried out, in particular the processing initialisation. A number of attributes (scalar values used in the processing) are initialised with default values from the configuration file (for details see *Sommer and von Rohden*, 2023, in preparation).

This ensures that these attributes are always assigned appropriate values in case they are not provided in the metadata. The extensive list of metadata provided by the GMDB is analysed and the relevant values are read into the processing. Several variables (e.g. latitude, longitude) are initialised if they are not already provided by the input files. This step is applied only in specific cases, e.g. if input data tables are not available.

Currently, the table 'GSupport' (INT4) is considered necessary for processing. The table contains temperature and humidity raw data of the heated humidity sensor which are used in the the processing steps for relative humidity. However, at several GRUAN sites, this table is not continuously produced or provided by the MW41 system due to the manufacturer's configuration. In such cases a workaround takes effect in the processing that restores the values based on manufacturer-calculated ambient humidity data from the 'RawPtu' table and assuming a constant (5 K) offset for the temperature of the humidity sensor.

## 7.3.2 Pre-check and ground checks

### 7.3.2.1 Pre-check input variables

Before starting a processing, a series of tests and checks with regard to data quality and consistency is performed with the input variables of all data channels (see the example in Figure 7.2). In a first step, data with indefinite values are identified. Then a test of the range covered by the finite values is carried out. Values outside the valid (physically meaningful) range, which is predefined for each variable, are removed by setting them NaN. Furthermore, a test can be carried out for larger data ranges with unexpected zero values (0.0) which indicate corrupt data in some situations. If present, they are set to NaN as well. A further test detects outliers. Two techniques are available. One compares the deviation of the actual data point from the local mean with a pre-defined multiple of the standard deviation of that mean (positive and negative deviations can be treated separately). The other evaluates the standard deviation of the local gradient of the profile (or time series). An outlier is identified if a specific value of that gradient is exceeded. Detected outliers are set to NaN, independent of the method. Next, the distribution of the missing values (NaN) is examined, i.e. the lengths and locations of gaps in the profile. In RS41-GDP.1, gaps with a length of up to 10 points (10 seconds) are interpolated. An allocation of uncertainties associated with interpolation is planned for a later GDP version, based on a procedure that was recently developed for temperature (*Fassò et al.*, 2020).

### 7.3.2.2 Analysis of ground checks

For an RS41 sounding, up to three ground checks can be analysed, depending on the actual site's practice: the manufacturer's mandatory check using the RI41 ground check device, an independent indoor ground check using the SHC, and another independent ground check performed outdoors in a ventilated hut or a similar environment.

The ground checks are performed to test the calibration of the sensors at a single point. The check results are used in different ways. The RI41 check provided by the manufacturer is used, among other things, to adjust the pressure sensor.

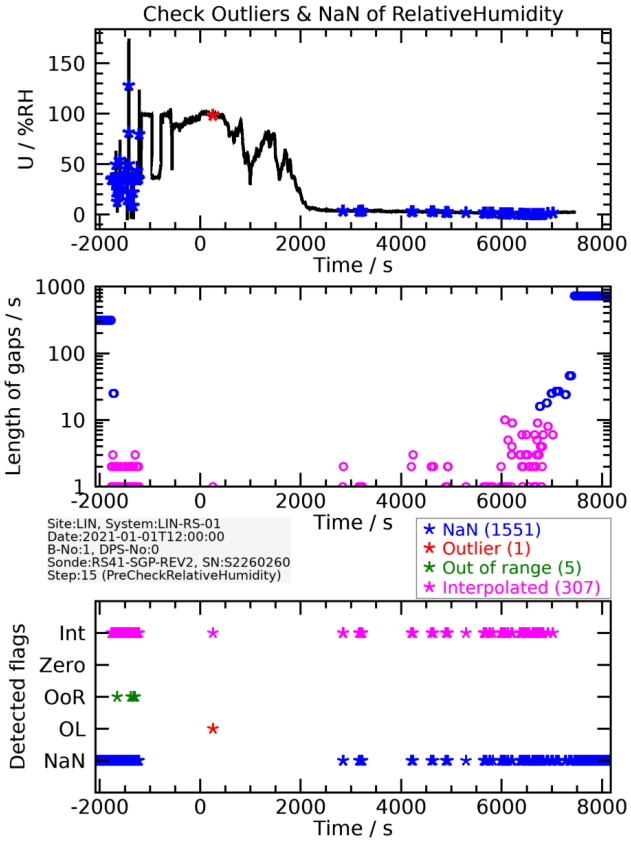


**Figure 7.2:** Example of a pre-check of raw input data for relative humidity.

**RI41** During the ground check with the RI41, the pressure is examined only if the radiosonde is equipped with a pressure sensor. Either the internal pressure sensor of the RI41-B or an external barometer is used as reference pressure sensor.

**SHC** The SHC ground check data are routinely analysed. The procedure is able to analyse checks for relative humidity (at 100 %), temperature and pressure. In a first step, the temporal section in the continuous data in which the Ground Check (GC) took place is automatically detected. If available, existing further information. e.g. flags, is included. If measurements from external sensors (reference sensors for humidity, temperature, pressure) are available, these are included in the evaluation as well. Alternatively, representative (mean) values are used for the reference. Figure 7.3 shows an example of such an automatic detection of the ground check period. The absolute humidity (∼100 %RH) or the stability of the temperature signal are used as criteria to identify the ground check period in the radiosonde data.

Two examples of the analysis results of the actual GC period in the SHC are given in Fig. 7.4. Further information on the evaluation of the GC data and the integration into the processing is given in Section 3.2.3 for temperature and relative humidity, and in Section 4.3 for pressure.

**SHELTER** The analysis of the ground check by means of 'SHELTER' is similar to that of a SHC. The term 'SHELTER' summarises ground checks, which are carried out under out-

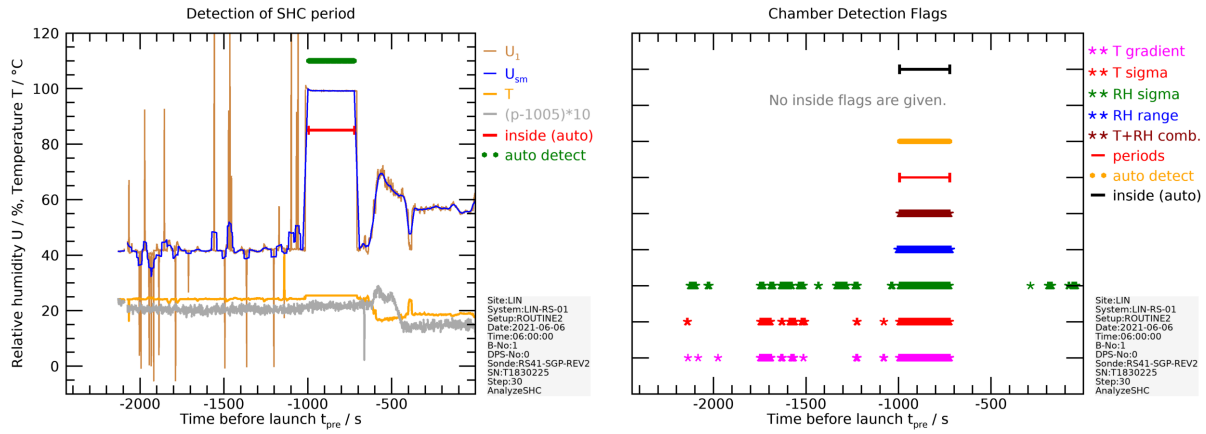


**Figure 7.3:** Example of automatic detection of a SHC ground check period.

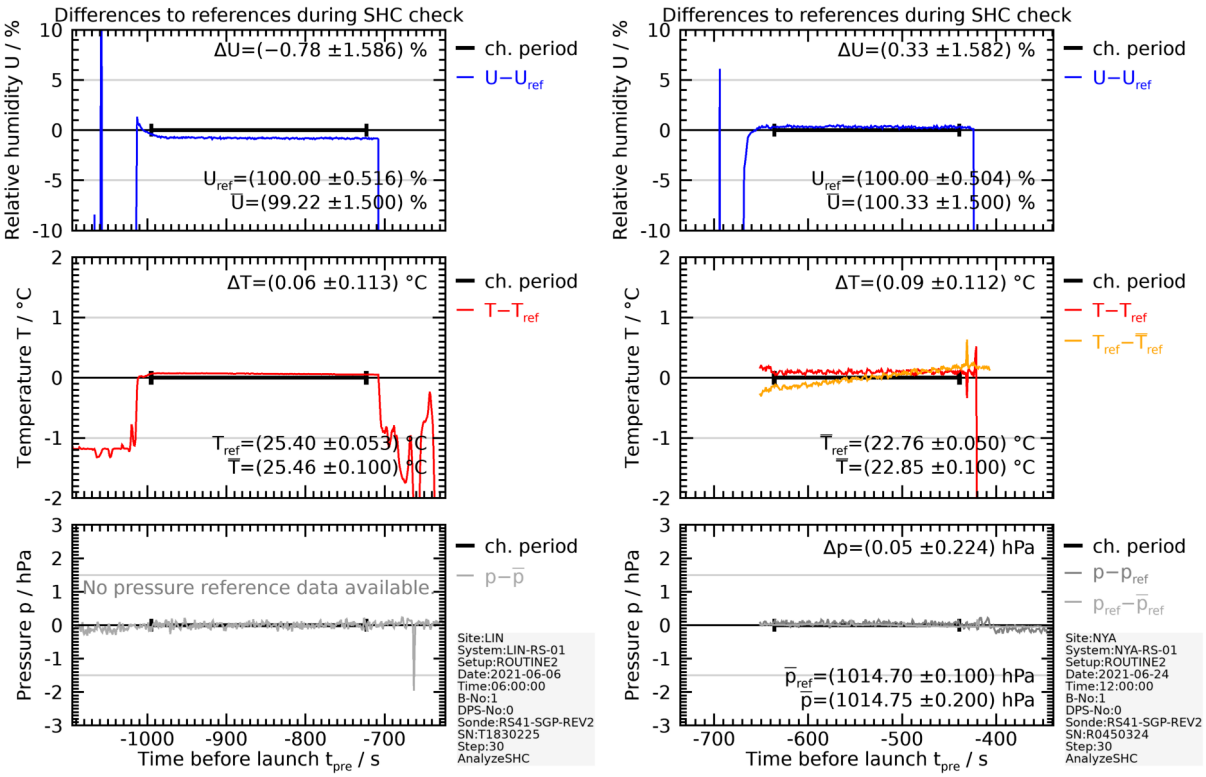


**Figure 7.4:** Two examples of data analysis (difference between radiosonde and reference) of a SHC ground check period.

door conditions immediately before launch. The radiosondes are placed either in a protecting (weather) hut or similar shelter, or simply under the open sky, with the external sensors placed next to it. However, measurements are often unstable under such conditions, which may impede the correct automatic identification of the GC time period in the continuous data record. Thus, in such cases of absence of reliable reference sensor data, no information from the GC can be included in the processing.

**Long-term analyses** Figure 7.5 shows the results of long-term analyses of the GCs for relative humidity and temperature over the period 2014 to 2020. Such analyses are valuable for disclosing possible inconsistencies, jumps, or trends in the calibrated raw data. Changes in the production or calibration procedures at the manufacturer as well as changes in the ground procedures at the sounding sites may be the cause of such inconsistencies. This proves the importance of performing GCs and the recording and collection of metadata for assurance of data quality on the long-term.

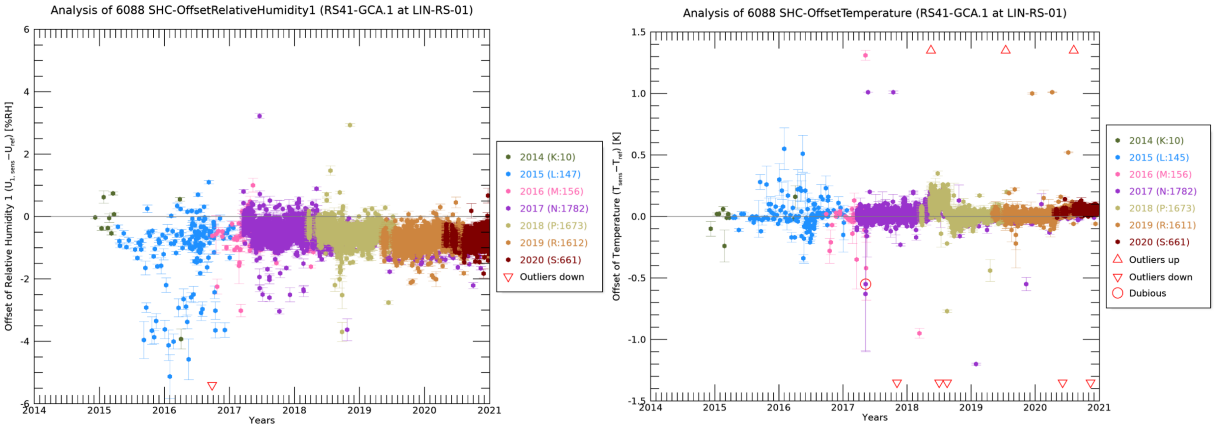


**Figure 7.5:** Long-term analysis (2014 to 2020) of SHC ground check results at the GRUAN site Lindenberg for relative humidity and temperature.

## 7.3.3 Location coordinates, altitude and wind

### Calculation of WGS84 position from Cartesian coordinates

The measured GPS data (longitude, latitude, and altitude) are stored in the designated data tables in relation to both the WGS84 ellipsoid as well as in Cartesian coordinates (xyz) with the centre of the Earth as origin. The RS41 GDP processes WGS84 data. In case position data are available in Cartesian coordinates only, which may occur under certain circumstances, they are transformed to WGS84 before use.

### Fixed GNSS position at site

The MW41 ground system includes a stationary GPS or GNSS antenna. From analyses of time series of its position measurements, apparent position variations (uncertainties), in particular

for the WGS84 altitude, are derived, which are the result of a variable satellite constellation as well as changing atmospheric properties.

### Acceleration of gravity

Acceleration due to gravity is used in various steps of the processing. Its slight change with altitude is taken into account. The formula used is documented in Appendix A.5.

### Difference between geoid and WGS84

The height above mean sea level in the RS41-GDP is related to the geoid defined in the Earth gravity model EGM2008 (see Section 4.4.1.2). This geoid (surfaces of the same gravitational potential) is provided in a Look-Up Table (LUT) with a resolution of $0.1° \times 0.1°$. Figure 7.6 shows a map of the deviations to the WGS84, which is used to transfer the measured GPS data to EGM2008 altitudes.

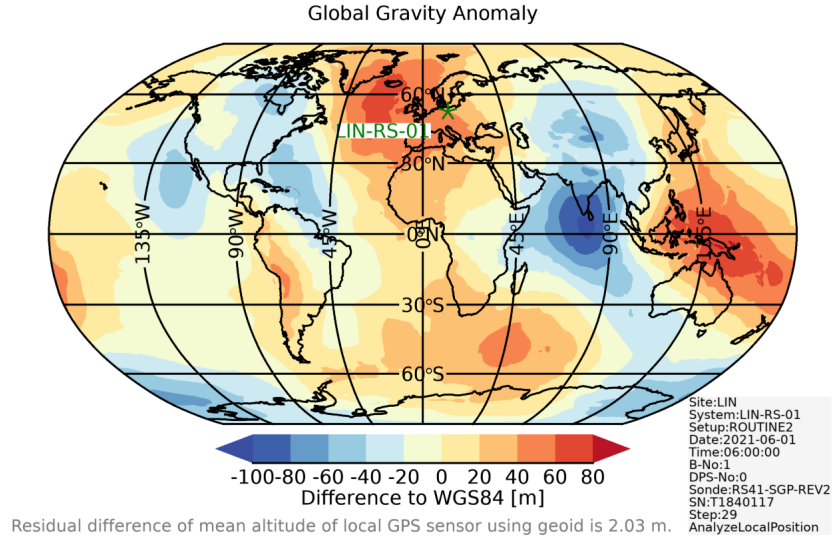


**Figure 7.6:** Difference between the geoid EGM2008 (which represents the mean sea level) and the GPS ellipsoid WGS84.

### Estimation of uncertainty of altitude

The uncertainty of the altitude depends mainly on the quality of the GPS measurements. The evaluated uncertainty of the GPS altitude (WGS84) is transferred into uncertainties of the altitude variables used in the processing (altitude above mean sea level and geopotential height). See Section 4.4.1.2 ‘Correlated uncertainty of the vertical position of the radiosonde’ for details.

### Uncertainty of latitude and longitude

The uncertainty of the horizontal position (latitude and longitude) depends mainly on the quality of the GPS measurements. See Section 4.4.1.3 ‘Correlated uncertainty of the horizontal position for the radiosonde’ for details.

### Calculate ventilation

The ventilation, i.e. the absolute speed of the radiosonde relative to the ambient air, is an important input variable for calculating the correction of the solar radiation error of the temperature measurement. It is estimated by combining the ascent speed estimates from GPS altitude changes as the main component with another component associated with horizontal fluctuations (pendulum movements) during ascent. A detailed description can be found in Section 4.4.4 ‘Ventilation’. Figure 7.7 shows an example of the so estimated ventilation.

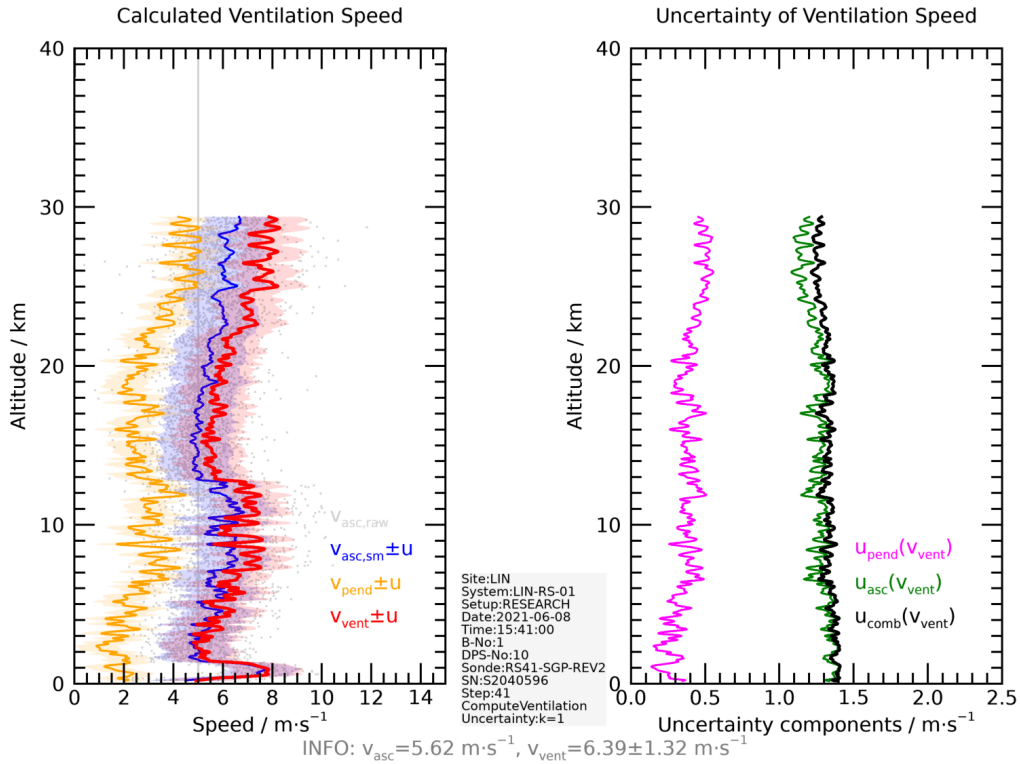


**Figure 7.7:** Example of calculated ventilation at GRUAN site Lindenberg.

### Wind retrieval

Horizontal wind components and from that wind speed and wind direction are calculated from horizontal position changes. The overall uncertainties are composed of the uncertainties of the GPS position data and the uncertainty that can be attributed to the pendulum movement. Figure 7.8 shows example profiles for wind components, wind speed, and wind direction including

uncertainties. Figure 7.9 shows sections of wind speed and wind direction (raw and smoothed) close to launch (ground) and balloon burst (stratosphere). Section 4.4.3 ‘Wind speed and wind direction’ provides more details.

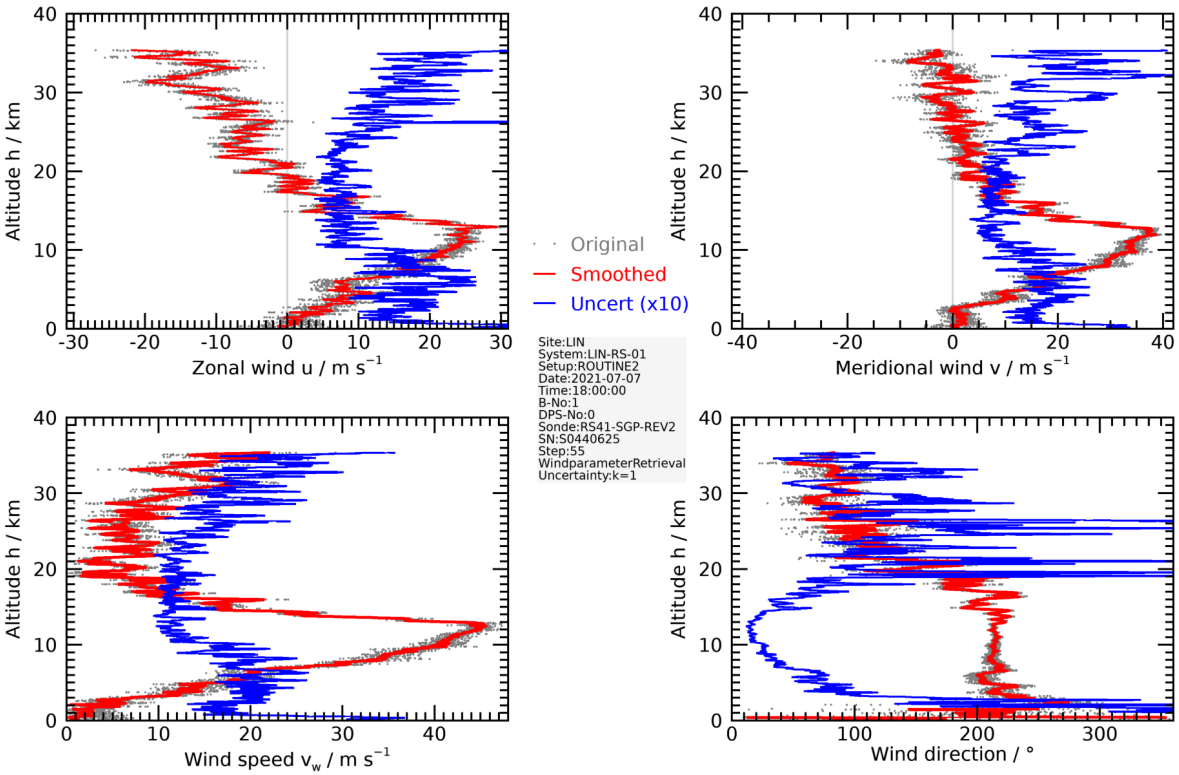


**Figure 7.8:** Example of a wind retrieval at GRUAN site Lindenberg.

## 7.3.4 Pressure

The processing steps related to the pressure sensor of RS41-SGP are documented in Section 4.3.

### Apply correction of pressure sensor

The pressure sensor is checked during the preparation of the radiosonde using the RI41 ground check device (see Section 3.2.2). It is recommended to use the RI41-B version of the device with integrated pressure sensor. Alternatively, another pressure sensor, e.g. a station barometer, can be used as reference. The first part ‘Pressure correction’ of Section 4.3 describes how the adjustment of pressure raw data is performed.

### Estimate calibration uncertainty of pressure sensor

Information on the pre-launch uncertainty of the pressure sensor is given by the manufacturer (Vaisala) and evaluated here as calibration uncertainty for the processing. This includes uncer-

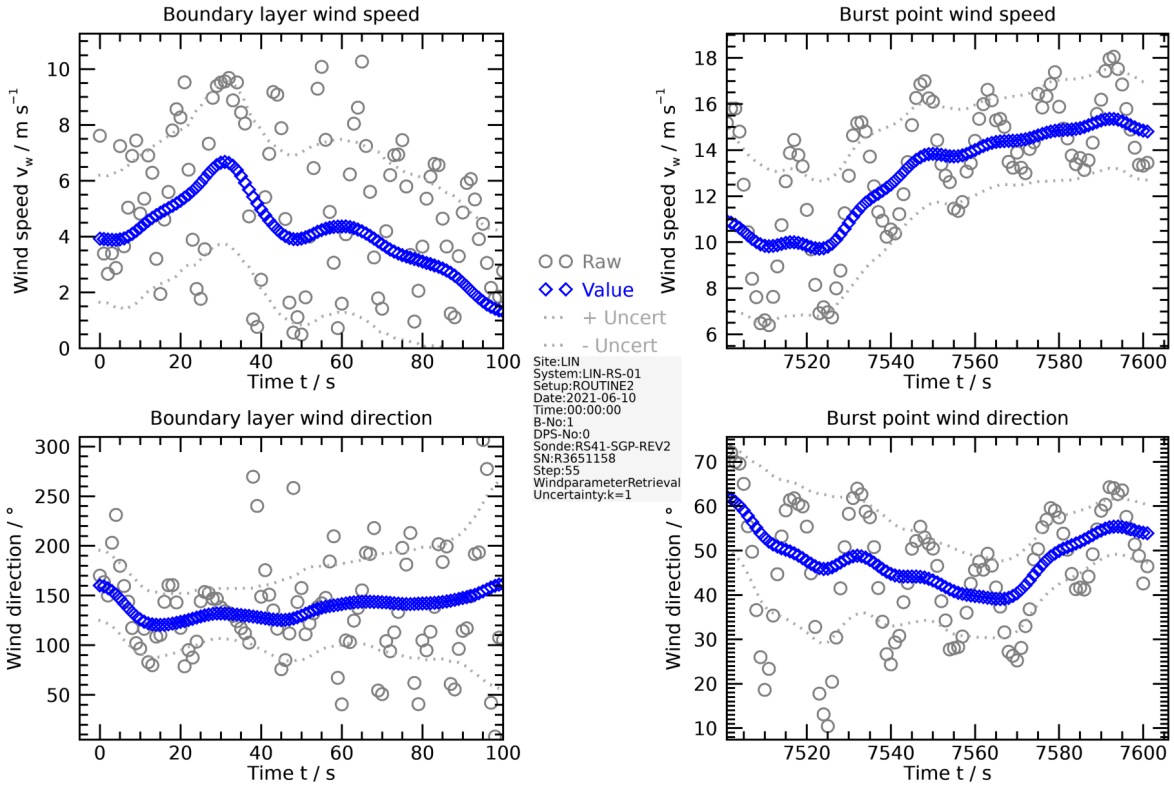


**Figure 7.9:** Example of wind speed and direction shortly after balloon launch and shortly before balloon burst.

tainties of the original calibration at the manufacturer as well a storing and transport-related components. See Section 3.2.1.3 and Appendix A.1.3 for more details.

### Smooth sensor pressure

The pressure values are smoothed to reduce noise. Based on the residual an uncorrelated (ucor) uncertainty is derived. Appendix A.3 provides general information on the smoothing procedure.

### Finalise sensor pressure

The module summarises the individual uncertainties and additionally stores uncertainty components with regard to their correlation properties (ucor, scor, tcor). Also, the difference in pressure between raw values and the final product is calculated and saved with the subscript ‘corr’.

### Calculate pressure based on GNSS altitude

Independent of a pressure measurement with a physical sensor, the pressure at a certain altitude is calculated using the barometric altitude formula, based on the ground pressure and taking the

actual temperature and humidity profile into account. See Section 4.4.2 for more details.

#### Source of final pressure in GDP

The pressure measured by the sensor and the pressure derived from GNSS data are completely independent. Although the quality of both products for pressure are comparable (see example in Fig. 7.10), the GNSS-based pressure is used as the final product in the GDP; there is no combination of the two. The reason for this is that the majority of RS41 sondes launched in GRUAN are not equipped with a pressure sensor, and there is a general tendency to use models without a sensor due to the improved quality of Global Navigation Satellite System (GNSS)-based pressure and also for cost reasons.

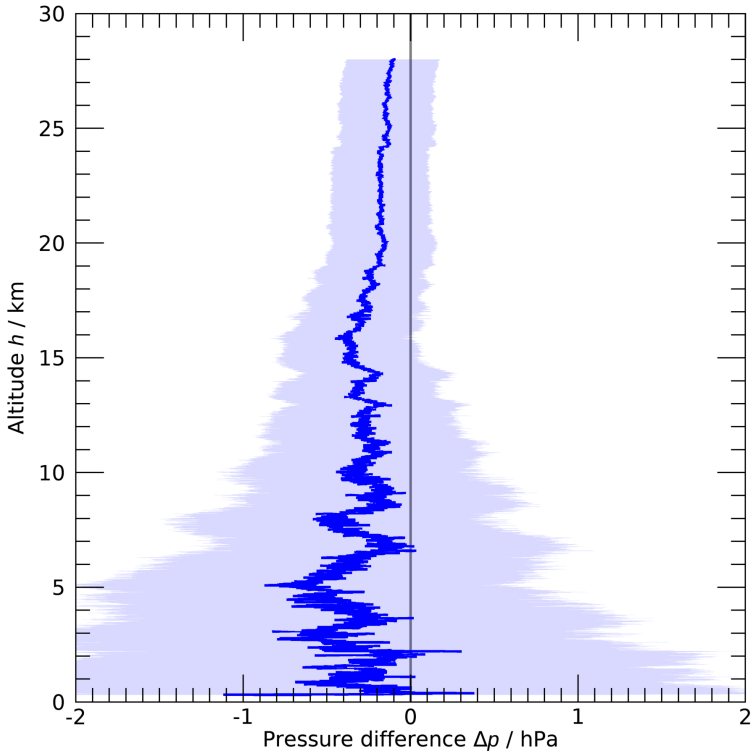


**Figure 7.10:** Example of the difference between profiles of pressure measured with sensor and calculated from GPS data. The shaded area indicates the uncertainty ($k = 1$) of the difference. Data as of 7 July 2022, 11:30 UTC, at Lamont site (SGP).

### 7.3.5 Temperature

#### Estimate calibration uncertainty of temperature sensor

Information on the uncertainty of the temperature sensor after performing the ground preparations (i.e. immediately before launch) is given by the manufacturer (Vaisala) and evaluated here as calibration uncertainty for the processing. This includes contributions from the original

calibration and other components as well as a storage-related uncertainty. Section 3.2.1.1 and Appendix A.1.2 present more information on this.

### Cloud detection

As approach for a rough characterisation of the cloud situation, the measured humidity is compared with the calculated saturation humidity (over both water and ice). Measured values very close to or exceeding saturation humidity indicate cloud passage during the ascent. However, due to the local character of the measurements, no definite statements can be made with regard to larger spatial scales covering the entire trajectory of the sounding. For that reason, this information is visualised only in the evaluation plots (see Section 7.3.7) produced during processing as marks in the profiles where clouds may be present, but it is not used any further. Figure 7.11 shows an example of such a 'cloud detection'.

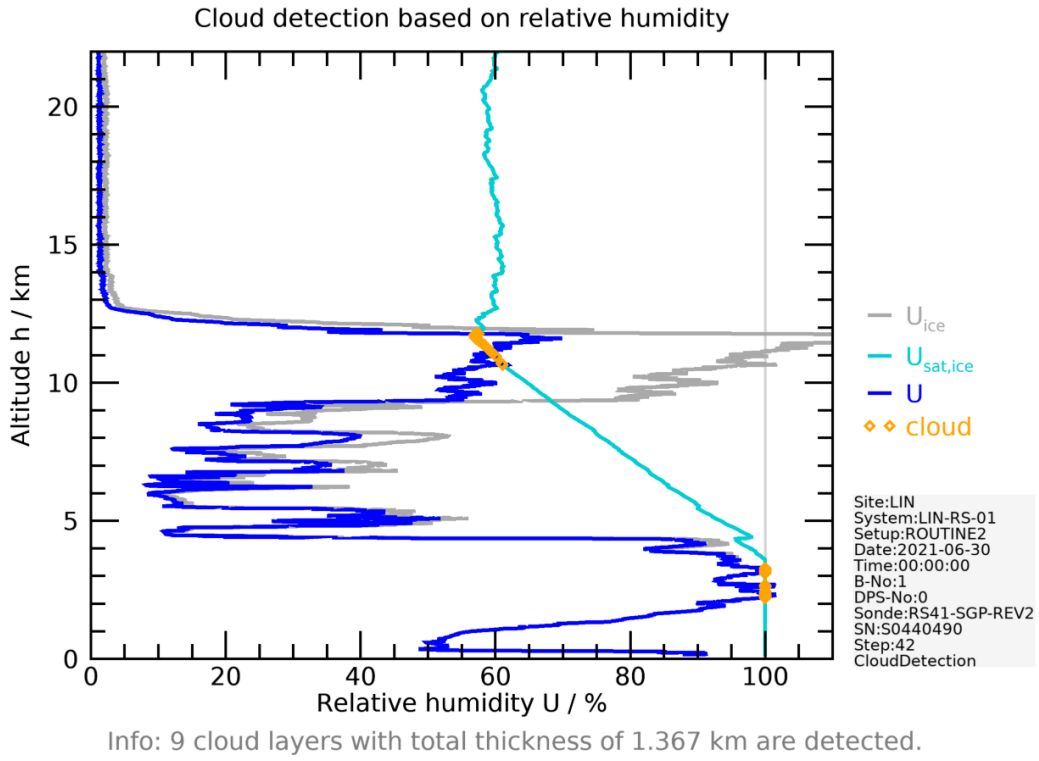


**Figure 7.11:** Example of a 'cloud detection'.

### Calculate position of sun

The position of the Sun is calculated for each point of the profile, and from that the Sun elevation angle, which is used as parameter for the solar radiation correction of the temperature measurements. No significant uncertainties are introduced with the used algorithm (see Section 4.1.4.4).

#### Simulation of solar radiation

The shortwave solar radiation is estimated vertically resolved using a radiative transfer model. Due to the absence of suitable information on cloud cover and albedo at the time and place of the actual sounding their contributions to the overall radiation are estimated by simulating the radiation using appropriate cloud scenarios and using representative albedo values from available data sets. These two contribute most to the uncertainty of the modelled radiation. Section 4.1.4 provides details.

#### Calculate and apply temperature radiation correction

For daytime flights, this step calculates and applies a correction of the temperature measurement to compensate for the solar radiative sensor heating, including uncertainty estimates. The correction algorithm is based on experimental results and on launch-individual modelling of the solar radiation. Detailed descriptions can be found in Section 4.1.5 and in *von Rohden et al.* (2022).

#### Smooth temperature

A low-pass filter is applied to the temperature profile to smooth fluctuations smaller than those caused by sonde orientation changes (spinning and pendulum motion), which takes effect especially in daytime flights as a result of the solar irradiation. The filter length is 15 s at daytime and 7 s at nighttime. An uncorrelated ('ucor') uncertainty is derived from the residual. General information on the algorithms used for smoothing procedures can be found in Appendix A.3.

#### Finalise temperature

As a final step, the uncertainty components evaluated in previous steps are combined. Additionally, combined uncertainties in terms of their correlation properties are evaluated and saved, i.e. uncorrelated ('ucor'), vertically correlated within a profile ('scor'), and temporally correlated ('tcor'). Both types of uncertainties (source-related and correlation-related) are presented in an example from the GRUAN site Lindenberg in Figure 7.12. Also, the total difference in temperature between the raw and the final product data is calculated and stored with subscript 'corr'.

### 7.3.6 Humidity

#### Estimate calibration uncertainty of humidity sensor

This step evaluates manufacturer-provided information on uncertainties of relative humidity readings after manufacturer-prescribed ground checks. This includes uncertainties from the factory calibration and storage as well as components introduced by the conversion of the measured 'internal' relative humidity at the temperature of the heated sensor chip to the ambient

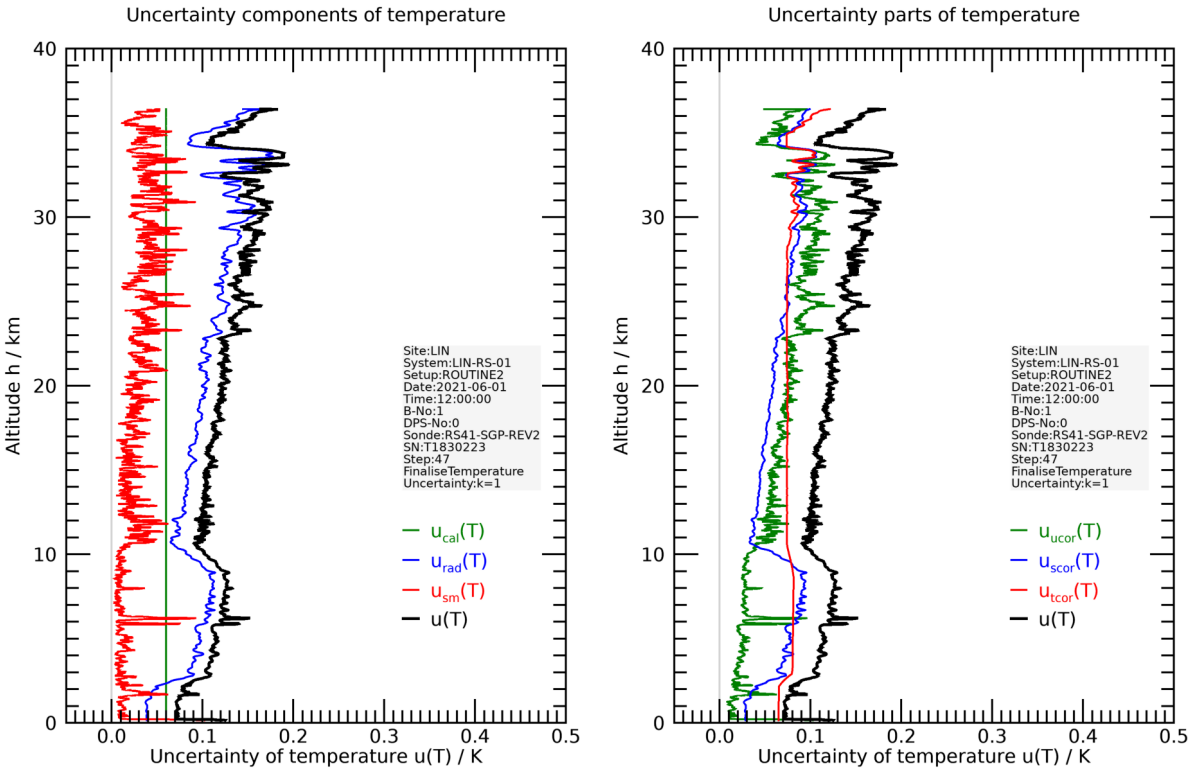


**Figure 7.12:** Example of uncertainty components and combined uncertainty for temperature. Left: Source-based components; Right: components ('parts') with respect to the correlation properties. Values given for $k = 1$.

conditions. The overall pre-launch uncertainty is called calibration uncertainty. Details can be found in Section 3.2.1.2.

### Time-lag correction

An important systematic error for relative humidity is caused by the slow response of the sensor at low temperature. The time-lag measured in laboratory experiments. From that a correction algorithm is derived and applied within this step during the processing of the raw humidity profiles. With the correction procedure, also noise components in the raw data are amplified which superimpose the time-lag corrected profile. This amplified noise, which can be significant in profile sections with low temperatures, is largely removed by a smoothing filter with a variable (temperature dependent) window length. The smoothing adds to the overall uncertainty of the corrected relative humidity. Figure 7.13 demonstrates the time-lag correction for a sounding at a tropical site. See Section 4.2.1 and especially Section 4.2.3.3 therein for detailed explanations.

### Retrieve relative humidity in ambient air from measurements with heated humidity sensor

The raw data of the humidity measurement refer to the temperature of the actively heated sensor. Within this processing step, the 'internal' humidity is converted to that at the temperature of the

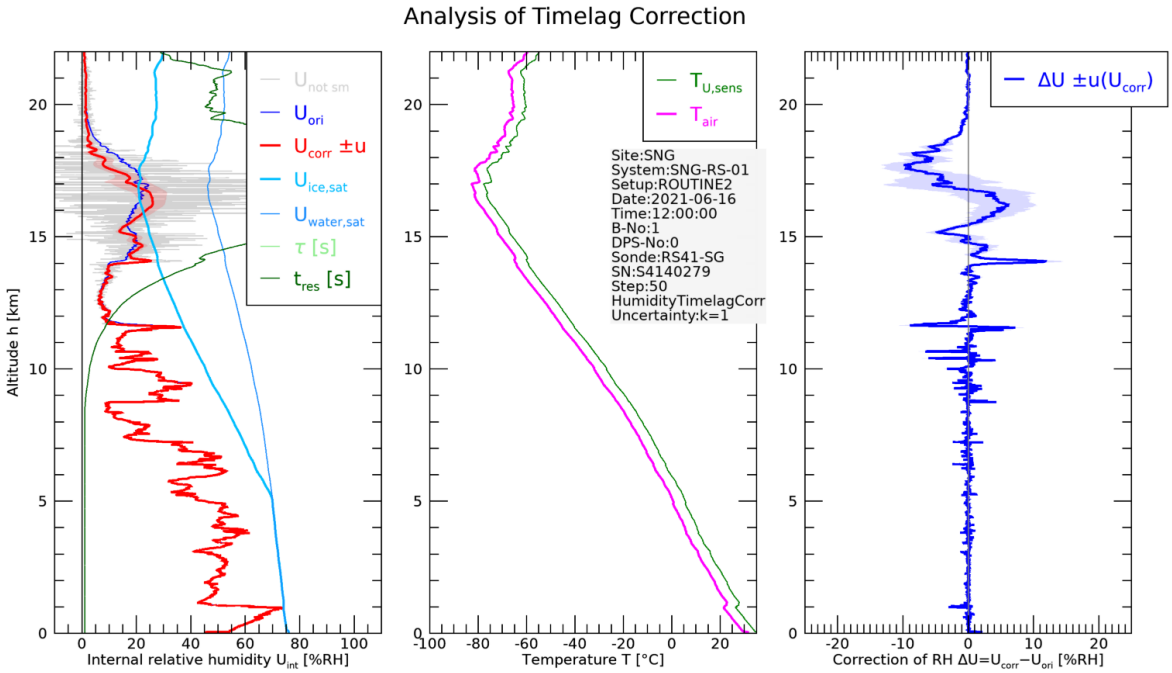


**Figure 7.13:** Example of time-lag correction analysis at the tropical GRUAN site Singapore.

ambient air, and the associated uncertainties are evaluated. Section 4.5.1 gives a more detailed description and Figure 7.14 illustrates the results by example.

### Smooth humidity

A final smoothing (Appendix A.3) with a window length of 7 points is applied to the humidity data, which takes effect primarily at higher temperatures where the sensor response is not significantly slowed down (no time-lag) and therefore the time-lag correction's own smoothing (see above) is not effective.

### Finalise humidity

In the final step for relative humidity, the uncertainty components are combined. Furthermore, combined uncorrelated ('ucor'), vertically correlated within a profile ('scor'), and temporally correlated ('tcor') uncertainties are evaluated and saved. The total difference of the raw humidity converted to ambient temperature and the final product data (see right panel in Fig. 7.13) is calculated and saved in the GDP with subscript 'corr'.

### Calculation of other variables expressing atmospheric water vapour content

For comparison purposes, e.g. with results from other instruments, the relative humidity is converted into several other quantities that express the water vapour content, including the full set

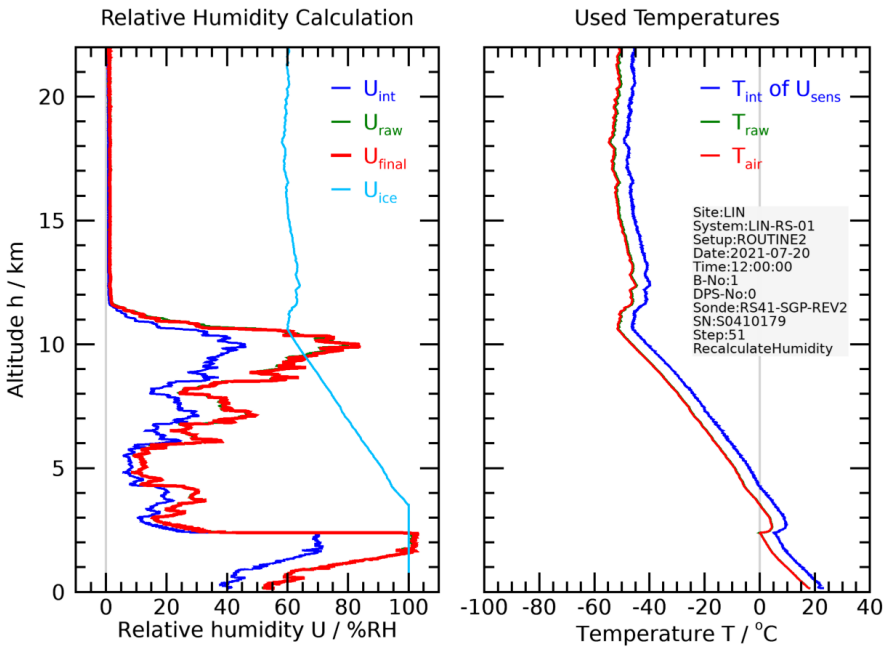


**Figure 7.14:** Derivation of relative humidity of air from measurements with the actively heated humidity sensor (example from the GRUAN site Lindenberg). $U_{\text{int}}$: 'internal' raw data; $U_{\text{raw}}$: 'converted' raw data after smoothing; $U_{\text{final}}$: GDP humidity; $U_{\text{ice}}$: saturation humidity over ice.

of uncertainty components. The following water vapour-related variables are provided:

- dp – dew point temperature (Section 4.5.5)
- wvmr_mass – water vapour mass mixing ratio (Section 4.5.4)
- wvmr_vol – water vapour volume mixing ratio (Section 4.5.4)
- wvpp – water vapour partial pressure (Section 4.5.2)
- wvsp – water vapour saturation pressure (Appendix A.2)

#### Calculate integrated column of water vapour

From the relative humidity profile, the total or integrated amount of water vapour is determined including uncertainty estimate. See Section 4.5.3 for further description.

### 7.3.7 Comparisons and evaluation plots

During the processing of each radiosonde profile, graphical representations of some of the results can optionally be generated and saved as image files. They are intended as quick looks for evaluation and comparison purposes. The plot generation is controlled via processing initialisation.

### Create plots of profiles

In this part of the processing, plots of vertical profiles of measured or calculated variables are created. The plots include the following quantities:

- temperature,
- relative humidity and water vapour mixing ratio,
- wind speed and wind direction,
- zonal and meridional wind components,
- ascent speed and pressure.

They are generated in two versions, one with the data shown in the original vertical resolution, and a second showing 500 m vertical averages. Example plots for the water vapour mixing ratio are presented in Figure 7.15.

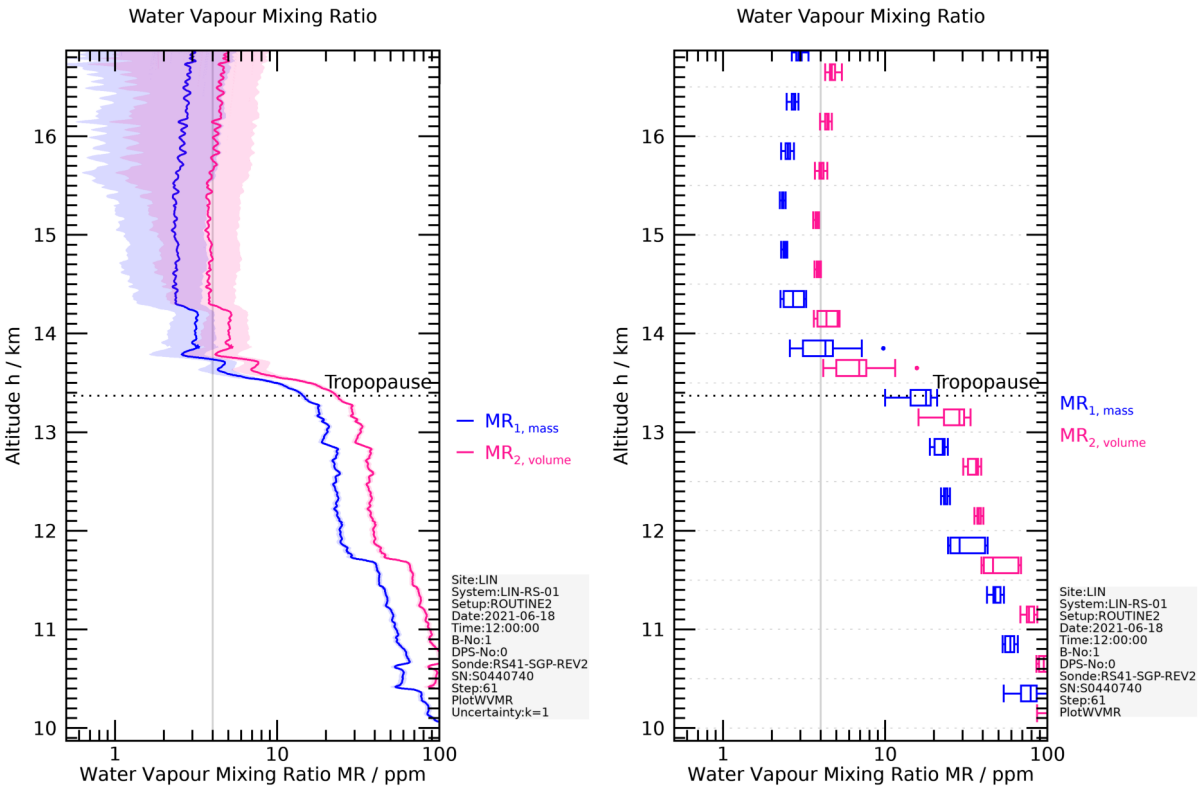


**Figure 7.15:** Profile plots (original resolution and 500 m-gridded), exemplary for the water vapour mixing ratio.

### Create comparison plots

In addition to the profile plots, a series of comparison plots is generated showing the differences between the Vaisala and the GRUAN data product. Comparison plots are available for the most important variables:

- pressure (GNSS), sensor pressure,

- temperature,
- relative humidity,
- wind speed, wind direction, ascent speed,
- geopotential height, altitude (WGS84), altitude above MSL.

Examples for pressure and temperature are presented in Figure 7.16.

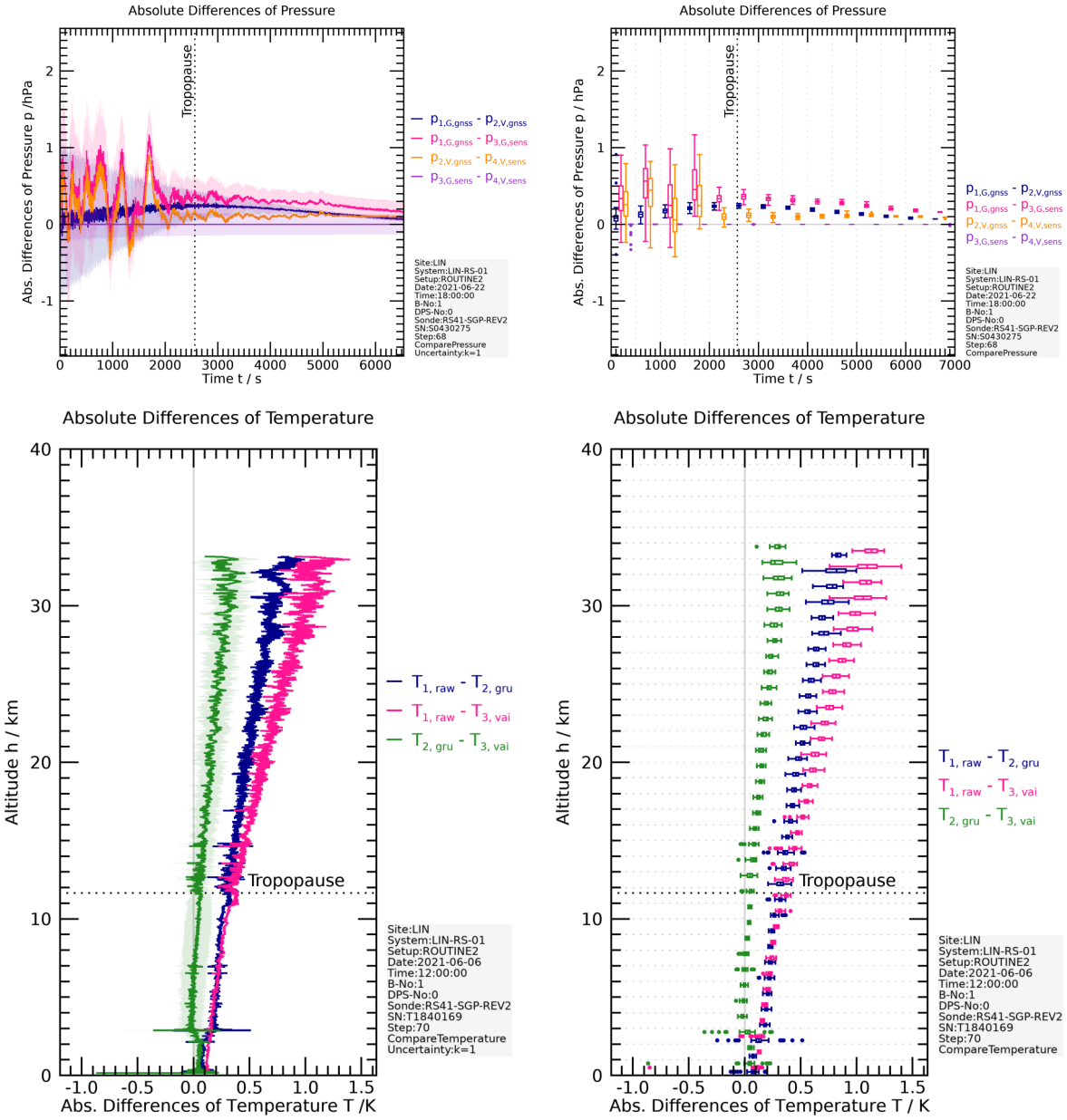


**Figure 7.16:** Comparison plots (original resolution and gridded), examples for pressure and temperature.

## 7.3.8 Further variables and retrievals

### Detection of launch point and burst point

The time axis is the primary reference axis for all measured or derived variables in a sounding. The actual profile starts at the time of the release of the rig at the dedicated launch altitude. This time mark separates the pre-launch period at the ground from the actual ascent data. Thus, a precise determination of the launch time is vital, especially for pressure derived from the GPS measurements, which uses the ground pressure measured with the station barometer as reference point.

Two different methods of launch point detection are used, one using data from the pressure sensor on-board the radiosonde (if available), and another using the GPS altitude data. Figure 7.17 shows examples of the two methods. The sensor-based determination is more accurate and robust due to the better stability of the sensor pressure measurements, whereas the GPS signal at the ground is prone to considerable fluctuations or noise, dependent on the surroundings of the launch site, e.g. the presence of buildings or if auto-launchers are used. Thus, at sites using sondes without pressure sensor, the detection algorithm may be unable to (precisely) determine the launch time.

The time of balloon burst, which marks the upper end of the profile and separates the ascent from descent, is determined with a separate algorithm.

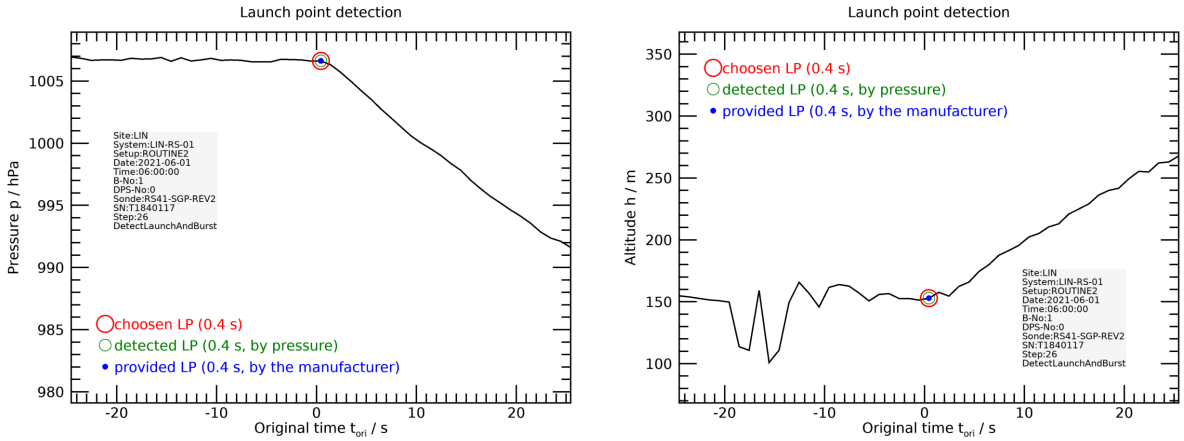


**Figure 7.17:** Example of launch detection based on pressure and altitude (GPS) data.

> **Note:** The automatic launch point detection as routine part of the GRUAN processing entails a potential source of error with respect to the assignment of the pressure axis, especially for radiosondes without pressure sensor.

### Detect tropopause using WMO definition

Using the GRUAN processed data, the WMO tropopause altitude is determined in this step based on the criteria given in the WMO definition. Figure 7.18 shows the result of the WMO tropopause detection in two examples.

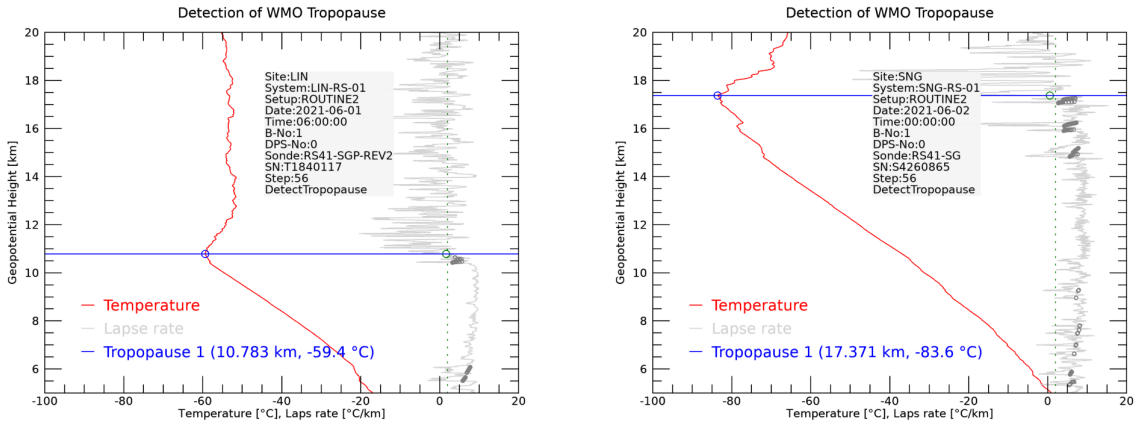


**Figure 7.18:** Examples of detecting the WMO tropopause at two GRUAN sites Lindenberg and Singapore.

### Sectioning profiles

The processed data of each radiosonde record are divided into sections according to different phases of the sounding. These partially overlapping sections are bounded by the (time) positions of the launch point, the tropopause, and the burst point. The sections, also called bands, are flagged accordingly. The following bands are defined:

- **ascent** – ascending radiosonde,
- **descent** – descending radiosonde (not part of result files),
- **flight** – any data in flight (after launch and before landing),
- **tropoasc** – ascending radiosonde in troposphere (below tropopause),
- **stratoasc** – ascending radiosonde in stratosphere (above tropopause),
- **utlsasc** – ascending radiosonde in UTLS (between 2 km below and 2 km above tropopause).

Figure 7.19 shows an example of the distribution of the bands.

### Finalise the data product including meta-data and product information

In the final step of the processing, the metadata collected from the GMDB and previous processing steps are compiled and saved.

## 7.4 Quality assessment

The GRUAN Data Product in the current version RS41-GDP.1 provides corrected radiosonde data based on independent sensor characterisations and with comprehensive estimates of measurement uncertainty components and their combination. The product files are extended to include extensive meta data. This creates a high degree of transparency and applicability.

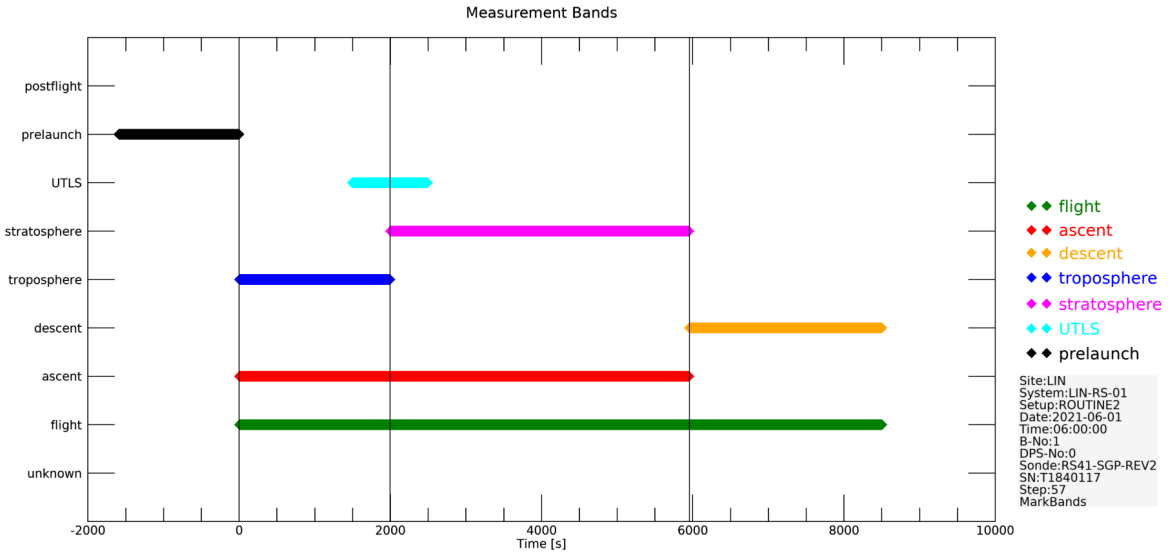


**Figure 7.19:** Example of the distribution of flags according to the definitions of profile sections (bands).

The GDP generation is fully automated, and there are no "manual" checks. During processing, data integrity is monitored, especially the incoming raw data is subjected to extensive automatic checks. A number of problems with regard to missing or erroneous data are identified and the processing is able to deal with them and avoid terminations. However, problems, for which there is no detection and treatment so far, can in principle lead to corresponding erroneous data or data of degraded quality in the GDP data. This applies in particular to unrecognised issues with regard to the quality of the original raw data.

Efforts have been made in GRUAN to establish criteria for a standardised quality assessment of radiosonde data. However, these criteria have not yet been determined and are subject to ongoing discussions within GRUAN. Therefore, the GDP in version RS41-GDP.1 does not contain a final quality assessment. The user may carry out his own quality assessment based on the extensive information available in the GDP files.

> **Note:** A comprehensive quality assessment is not implemented yet in version RS41-GDP.1 of the GDP.

The quality assessment criteria should be defined universally such that they can be included in the future processing of any radiosonde model. The GRUAN Lead Centre, the Quality Task Force and the Task Team on Radiosondes should be involved in this coordination process. The final criteria should be independently published within the GRUAN documentation.

The criteria for a quality assessment of the RS41 GDP may include (but is not restricted to) the following:

- Burst point height
- Frequency of data gaps

- Plausibility of estimated uncertainties
- Evaluation of the ground checks (RI41, SHC, SHELTER)
- Inconsistencies between original MWX file and metadata in GMDB
- Contamination (information from meta-data or detected?)
- Extreme conditions (outside certain value ranges)

Separate assessments for:

- Parameter ($p$, $T$, $U$, wind speed, wind direction, ...)
- Sections of the sounding (ground checks, boundary layer, troposphere, UTLS, stratosphere)
- Sounding as a whole

The result of an evaluation could be represented using the traffic light system:

- green – within the optimal range (everything OK)
- yellow – within an extended range (usable with restrictions)
- red – Outside the extended area (results do not meet requirements)

## 7.5 Output of the processing

### 7.5.1 File content of GDP

The file format of the NetCDF files of the RS41-GDP.1 is described in detail in the supporting document "User Guide of the RS41 GRUAN Data Product Version 1 (RS41-GDP.1)" (*Sommer et al.*, 2022). GRUAN strives for uniformity of product file structures for all radiosonde data products as far as possible. The product files in general support the Climate and Forecast (CF) metadata conventions for NetCDF files. The following data are contained:

- Groups of metadata:
  - General attributes following the CF conventions,
  - Product and file,
  - Site, measurement system and measurement setup,
  - Measurement (event) and surface observations,
  - Instrumentation: ground system, main sonde, telemetry sonde,
  - Ground checks: RI41, SHC, SHELTER;
- Groups of variables:
  - Time, altitude, position,
  - Pressure, temperature, relative humidity,
  - Other humidity measures, wind,

- Supplementary variables,
- Raw data, flags related to raw data variables.

### 7.5.2 Log file

For each sounding a comprehensive log file is generated during the processing. It contains detailed information about the procedures for each step of the processing. In case of errors, aborts, and other problems, the log file can be used as a starting point for troubleshooting. The log file is stored separately from the actual result file. Its content is imported into the GMDB for evaluation at any time.

### 7.5.3 Data analysis plots

During processing, a number of plots (as PNG images) are generated for an initial visual assessment of the product data. Currently these analysis plots are available for internal use at the LC only. It is planned to make them freely accessible to the GRUAN community in future.

## 7.6 Data management in GRUAN

An overview of the data flow, including the relevant services and institutions, is presented in Figure 7.20. The GRUAN data management, i.e. the interaction between the elements in that scheme, is organised and monitored by the LC.

The essential data flow components in GRUAN are listed in summary below and are described in more detail in the following sections:

- **Collection** – measurement data collected by sites and submitted to LC (Section 7.6.1),
- **Converting** – original data files converted to a standardised format (Section 7.6.2),
- **Processing** – processing and re-processing of converted data, i.e. creation of the GDP, (Section 7.6.4), carried out by a processing centre (Section 7.6.3)
- **Archiving** – main data archive for all levels of GRUAN radiosonde data managed by the LC (Section 7.6.5),
- **Distribution** – provision of product files designated distribution points (Section 7.6.6), and
- **Monitoring** – data flow monitoring generally performed by the LC (Section 7.6.7).

### 7.6.1 Data collection

The Vaisala RS41 radiosonde is used by many of the GRUAN sites. It is launched as operational sonde in routine single soundings, as the main or telemetry sonde in combination with other sondes or instruments (e.g. ECC ozone sonde), or in comparison flights with other radiosondes.

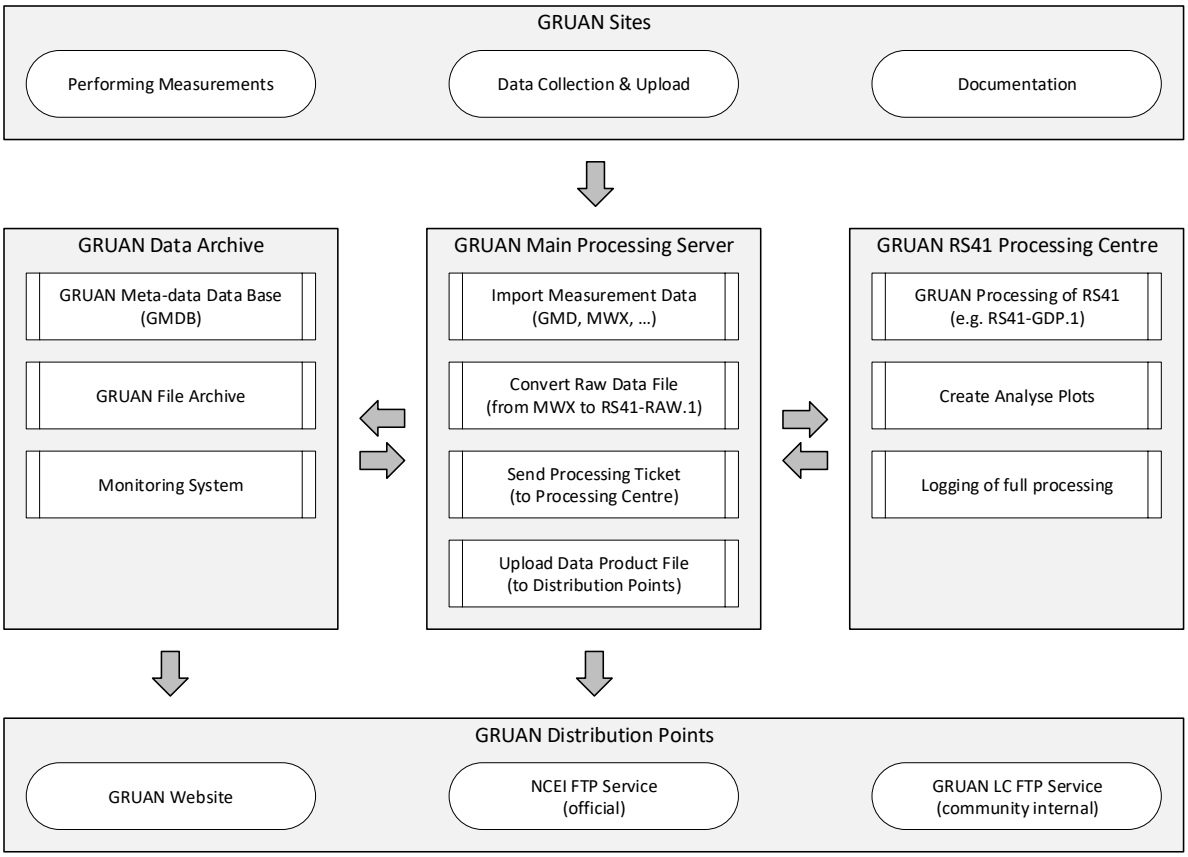


**Figure 7.20:** GRUAN RS41 data flow (single soundings or combined soundings with other instruments).

All radiosonde data in GRUAN are imported into the GRUAN archive (located at the GRUAN Lead Centre) via a standardised procedure. This procedure uses two main components:

- a GMD file (GRUAN Meta-Data file) – an XML file that follows a specific XML schema, and
- an FTP server with a specific internal structure for easy data delivery from the GRUAN sites.

Regular instrument comparison measurements make up a significant part of GRUAN's activities, which includes a comprehensive documentation of the setups. Therefore, the GMD files are designed to record technical information and meta-data of all instruments combined in complex sounding configurations. Information from ground checks can be logged in the GMD files as well. Associated data files are named (linked), e.g raw data files, but also others such as pictures.

The structure and capabilities of GMD files is described in *Sommer* (2023a, in preparation).

In order to generate GMD files, the GRUAN LC provides the GRUAN sites with two software programs. One is the "RsLaunchClient", which provides a user interface for manual input of radiosonde launch information. The other is the command line program "gtRsl", which is optimised for automatic data delivery, e.g. for autolauncher. More documentation for both tools can be found in GRUAN-TN-3 (*Sommer*, 2014) and GRUAN-TN-6 (*Sommer*, 2020b),

respectively.

### 7.6.2 Converting of MWX to NetCDF

At the Lead Centre, incoming MWX files are usually converted into NetCDF files in a timely manner with an automatic procedure. This procedure accepts the different manufacturer raw data formats as input, including Vaisala's earlier DC3DB files. The structure of the generated NetCDF files is designed for permanent archiving of radiosonde raw data. The format is called "GRUAN NetCDF Radiosonde Raw Data" (GNC-RAW) and is described in detail in *Sommer* (2023b, in preparation). The Lead Centre developed the freely accessible software tool "gt92", which can be used for the conversion. The tool is described in GRUAN-TN-11 (*Sommer*, 2020a).

With the conversion as a pre-step, the data input to the GRUAN Data Processing System for radiosondes (GDPS) can be limited to only the NetCDF format, which helps to reduce the complexity in that regard.

The use of NetCDF is justified by the universality of the format. That is, the converted and archived radiosonde data can easily be used with other software systems, as NetCDF libraries are available for many platforms.

### 7.6.3 The Processing Centre (PC)

In accordance with the agreements in GRUAN, a Processing Centre (PC) had to be established for RS41 soundings. The GRUAN Lead Centre at the Lindenberg Meteorological Observatory (Germany) of the Deutscher Wetterdienst (DWD) agreed to take over this task permanently. This was an obvious choice, since the Lead Centre has been acting as the Processing Centre for the Vaisala RS92 radiosonde for many years. Also the development of the data product for the RS41 took place there.

The PC's tasks include:

- The data processing of the RS41 radiosoundings performed at all GRUAN sites,
- Archiving of the data product files (all versions),
- Re-processing of the archived data in case of version updates of the data product,
- Use and archiving of stable versions of various software tools (source code, documentation),
- Monitoring of the processing with feedback to the sites (e.g. monthly statistics, problem cases, ...).

### 7.6.4 Processing and reprocessing

RS41 soundings are processed by the PC generally within approximately 2 h of data upload. Since GRUAN is not a real-time network but a climate observation network, no significant effort has been put into the permanent availability (e.g. fail-safe, redundancy, etc.) of the processing service. Immediate processing of newly incoming data is therefore not guaranteed,

especially in case of processing errors. After the problem has been solved and the service has been reactivated, the processing of the data accumulated up to that point is continued. Attention is given to ensuring that there is a high degree of certainty that no loss of files (especially raw data and metadata) will occur.

With the release of a new version of the data product, the archived RS41 soundings are re-processed sequentially, starting with the most recent sounding. During such a batch processing, which may take several months due to the high number of archived soundings, the parallel routine processings of actual profiles may temporarily take some more time, e.g. up to 6 h, due to the higher utilisation of the system. Reprocessing of an existing data set for each new product version runs in the same way with regard to preparation and duration.

In case of a problem with the processing of a sounding, which may occur for a number of reasons, the processing of that sounding is restarted at a later time as a first measure. This can lead to success if the termination was for a technical reason, e.g. a temporally broken connection to the database. In case of continued errors after a defined number of further attempts (3 to 5), the current sounding is classified as faulty and not processed further.

During the processing of a sounding the following files are created and stored:

- A result NetCDF file (GNC-DATA) – including permanent storage in file archive,
- A series of analysis plots (approx. 100) – currently only temporary storage is provided, and
- A log file – including permanent storage in database.

### 7.6.5 Archiving of raw data and data product files

#### Archiving of raw data

The GRUAN Lead Centre is primarily responsible for archiving the raw data. In general it is advisable, however, to save a backup copy at the Processing Centre. In case of the RS41 this does not apply because of the organisational identity of LC and PC.

The original raw data files (MWX) as well as raw data files converted to the NetCDF format (GNC-RAW) are stored at the GRUAN LC in a file archive. The data are stored redundantly at DWD in Offenbach (Germany), and a backup is stored at CIAO/IMAA/CNR in Italy. Local archiving of the original raw data at the GRUAN sites is expected.

#### Archiving of data products

The data products can be re-generated from the raw data at any time by re-processing. For this reason, the high archiving standard as for raw data is in principle not required. However, since for the RS41 radiosonde the GRUAN Lead Centre takes over the role of the Processing Centre, the archiving of the product files takes place in the same way as for the raw data. That means that data product files (GNC-DATA) of all product versions are permanently saved at the GRUAN LC, with redundant storage at DWD in Offenbach (Germany) and at CIAO/IMAA/CNR in Italy.

### 7.6.6 Distribution of data products

The data product files are made available via different access paths. These paths are subject to change from time to time, but this will be kept up to date on the GRUAN website. The actual information is available in the section "Dataset details and ordering" on the web page https://www.gruan.org/data/data-products/gdp/rs41-gdp-1. In addition, the GRUAN Lead Centre (LC) (gruan.lc@dwd.de) can be contacted for more specific access. All data is made available a short time after processing, so that the entire data set is constantly growing.

### 7.6.7 Monitoring and feedback

The monitoring and feedback activities consist of:

- [regular] weekly update of general launch statistic on website
- [regular] daily update of data flow plots on website
- [sporadic] monthly update of data product statistic on website
- [planned] weekly email to each GRUAN site with statistics about data flow and processing of radiosoundings.

**General launch statistic** On the GRUAN website the statistics of soundings with radiosondes and other in-situ instruments are presented in the form of charts and tables (see https://www.gruan.org/data/measurements/sonde-launches). These statistics are updated weekly. Figure 7.21 presents example charts showing the frequency of RS41 soundings for each GRUAN site and the network total, respectively.

**Data flow plots** On the GRUAN website the current data flow (last 30 days) from GRUAN sites to the Lead Centre are presented as plots (see https://www.gruan.org/data/measurements/current-data-flow). These plots are updated daily. Figure 7.22 gives an example for the sequence of launches performed at a single site.

**Data product statistic** On the GRUAN website the processing status of the GDPs are presented as plots (see https://www.gruan.org/data/data-products/data-availability). These statistics are updated occasionally (e.g. monthly). Figure 7.23 shows as an example the processing status of the RS41-GDP.1 for the whole network and for one GRUAN site.

**Processing terminations** The following list shows events that are certain to cause termination of the actually processed sounding so that no product file for this sounding is created. There is no further categorisation or standardisation of such events so far.

- Issues related to input data:
  - One of the required tables 'RawPtu' (INT1) or 'GpsResults' (INT2) or 'GpsRawMeasurements' (INT3) (see Section 7.2.1) is not available
  - Irregularities or non-constancy of the time grid in the main data tables

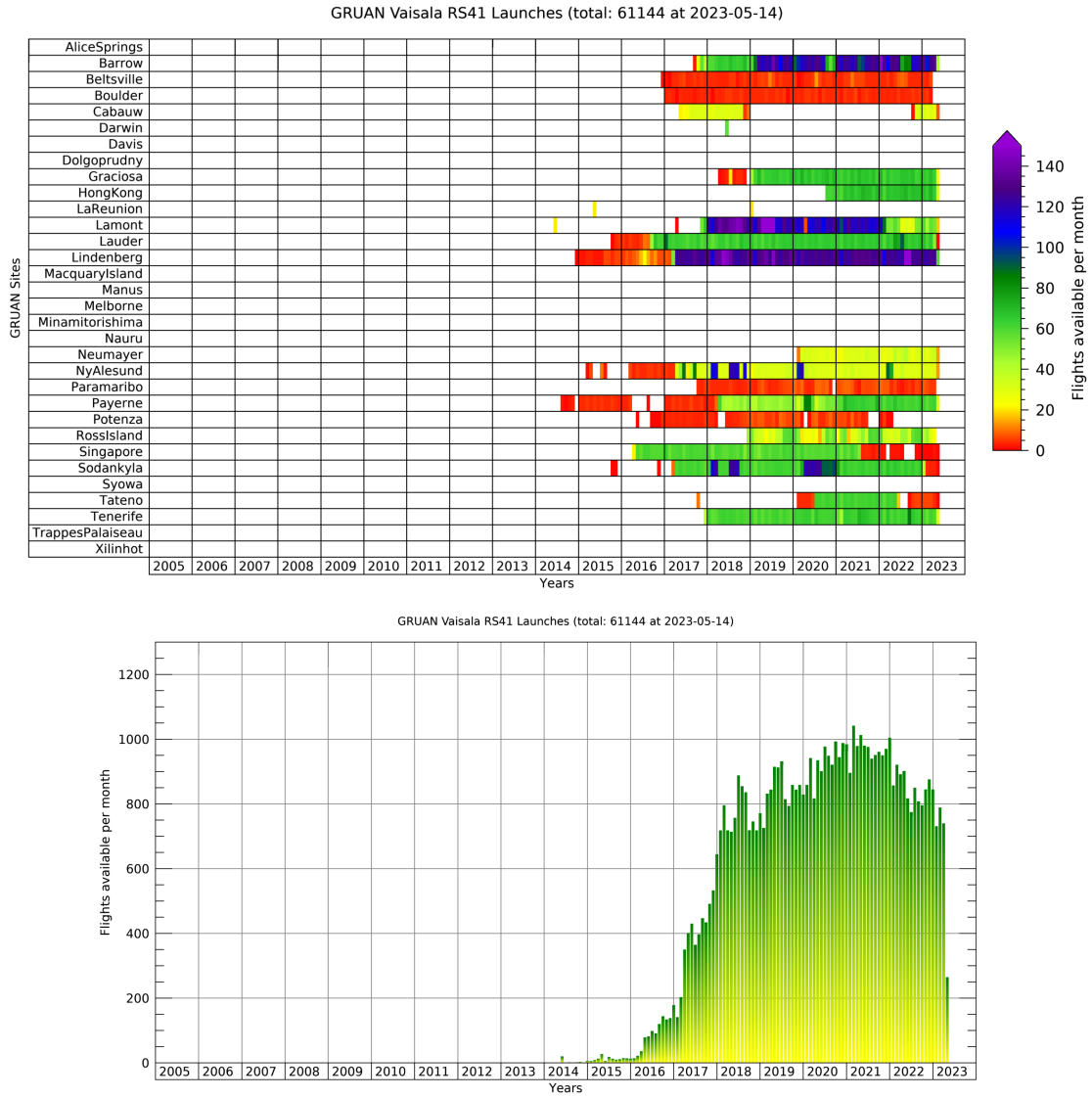


**Figure 7.21:** Examples of long-term launch statistics of RS41 soundings in GRUAN.

  - Not enough data points available (lower limit set to 1000)
- Errors related to launch point detection:
  - Measurement-derived and given launch site altitude inconsistent
  - Inconsistent pressure from radiosonde and reference barometer at launch site
  - Pressure or altitude data not available (NaN) around launch time
  - Automatic detection of launch and burst point failed for any reason
- Other issues:
  - Sounding scheduled for processing was updated (in data base) in the meantime

**Note:** As a consequence of processing aborts, the GRUAN station could be notified. However, this is not yet implemented. Also the concrete reason for the error would have to be detected (automatically) and stored in the database.

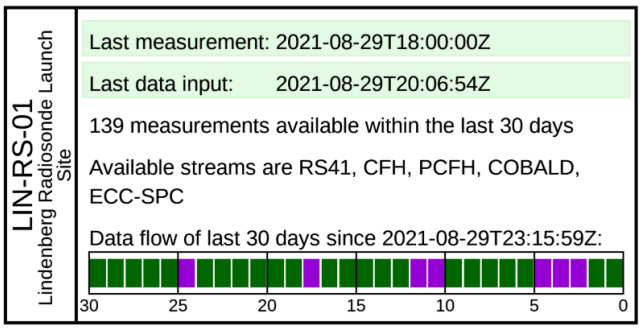


**Figure 7.22:** Example plot of data flow at GRUAN site Lindenberg. The general state of the data flow is coded via the background colours in the upper area: green – current data available, yellow – no data submitted for more than a month, orange – no data submitted over 3 months, red – no data submitted for more than a year, grey – no data submitted yet. The number of collected daily measurements are coded in the lower area with the coloured markers: purple – 5 or more, dark green – 4, green - 3 or 2, yellow-green – 1, white – none.

During the development of the data product, attention was paid to eliminating as many errors as possible. However, in addition to the defined cancellation criteria, new (previously unknown) errors may occur in the processing in the future. These should also be analysed in the future and (if possible) eliminated.


**Figure 7.23:** Example plots of data product statistic of RS41-GDP.1 for 2022.

# Appendix

# A Collection of relevant formulas and algorithms

## A.1 Manufacturer calibration uncertainties

### A.1.1 Temperature

Combined uncertainty ($k = 1$) after sensor calibration over the temperature range is shown in *Vaisala* (2017d) and Fig. 3.8 in Section 3.2.1, including the uncertainty of the mathematically formulated sensor model, i.e. terms like sensor linearity and sensor model fit to the calibration points:

$$u_{\text{cal,s}}(T) = c_0 + c_1 T + c_2 T^2 + c_3 T^3 + c_4 T^4, \tag{A.1}$$

with coefficients

$$\begin{aligned} c_0 &= \phantom{-}3.0537 \times 10^{-2} \\ c_1 &= \phantom{-}1.3011 \times 10^{-4} \\ c_2 &= \phantom{-}2.1843 \times 10^{-6} \\ c_3 &= -6.6082 \times 10^{-9} \\ c_4 &= -6.1354 \times 10^{-11} \end{aligned}$$

and $T$ in °C.

### A.1.2 Humidity

The combined uncertainty ($k = 1$) after sensor calibration is provided by the manufacturer as function of relative humidity, see *Vaisala* (2017d) and Fig. 3.9 for $k = 1$:

$$u_{\text{cal,s}}(U) = c_0 + c_1 U + c_2 U^2 + c_3 U^3, \tag{A.2}$$

with coefficients

$$\begin{aligned} c_0 &= \phantom{-}4.6854 \times 10^{-2} \\ c_1 &= \phantom{-}2.9560 \times 10^{-3} \\ c_2 &= \phantom{-}1.0586 \times 10^{-5} \\ c_3 &= -7.0354 \times 10^{-8} \end{aligned}$$

and $U$ in %RH.

Table A.1 lists combined uncertainties after ground preparation (i.e. sensor reconditioning and the zero humidity check have been performed at room conditions) as function of relative humidity and air temperature, provided by Vaisala (see Fig. 3.2 in *Vaisala*, 2017c). They include the uncertainties of the measured air temperature and of the built-in temperature sensor on the integrated humidity chip. They are visualised in Fig. 3.10 and used as overall calibration uncertainties in the data processing after fitting 3rd-degree polynomials.

**Table A.1:** RS41 uncertainty for relative humidity after ground preparations for $k = 1$ in %RH as function of humidity and for different temperature levels.

| U/%RH \| T/°C | −80 | −60 | −40 | −20 | 0 | 20 | 40 | 60 |
|---|---|---|---|---|---|---|---|---|
| 0 | 1.15 | 0.67 | 0.39 | 0.24 | 0.17 | 0.20 | 0.33 | 0.52 |
| 10 | 1.27 | 0.77 | 0.49 | 0.34 | 0.28 | 0.30 | 0.41 | 0.59 |
| 20 | 1.42 | 0.90 | 0.60 | 0.45 | 0.37 | 0.38 | 0.48 | 0.65 |
| 30 | 1.59 | 1.04 | 0.71 | 0.55 | 0.45 | 0.46 | 0.55 | 0.70 |
| 40 | 1.75 | 1.17 | 0.83 | 0.64 | 0.52 | 0.54 | 0.61 | 0.76 |
| 50 | 1.93 | 1.31 | 0.94 | 0.74 | 0.60 | 0.61 | 0.68 | 0.82 |
| 60 | | 1.45 | 1.05 | 0.84 | 0.67 | 0.68 | 0.74 | 0.87 |
| 70 | | | 1.17 | 0.94 | 0.75 | 0.75 | 0.80 | 0.92 |
| 80 | | | | 1.04 | 0.82 | 0.82 | 0.86 | 0.96 |
| 90 | | | | | 0.90 | 0.88 | 0.91 | 0.99 |
| 100 | | | | | 0.97 | 0.94 | 0.95 | 1.01 |

### A.1.3 Pressure

The combined calibration uncertainty ($k = 1$) for pressure measurement after ground preparation (see Fig. 3.11) is given as

$$u_{\mathrm{cal}}(p) = c_0 + c_1 p + c_2 p^2 + c_3 p^3, \tag{A.3}$$

with coefficients

$$\begin{aligned} c_0 &= \phantom{-}1.200 \times 10^{-1} \\ c_1 &= \phantom{-}1.125 \times 10^{-4} \\ c_2 &= -1.498 \times 10^{-7} \\ c_3 &= \phantom{-}8.246 \times 10^{-11} \end{aligned}$$

and $p$ in hPa.

## A.2 Saturation vapour pressure for water

The Hyland-Wexler formulation (*Hyland and Wexler*, 1983) is used for the RS41 GDP for calculation of the saturation pressure of water vapour over liquid water:

$$e_{\mathrm{s}}(T) = \exp\left(\frac{c_1}{T} + c_2 + c_3 T + c_4 T^2 + c_5 T^3 + c_6 \ln(T)\right), \tag{A.4}$$

with $T$ the temperature of the layer in K, and the polynomial coefficients

$$\begin{aligned} c_1 &= -5.800\,220\,6 \times 10^{3} \\ c_2 &= \phantom{-}1.391\,499\,3 \\ c_3 &= -4.864\,023\,9 \times 10^{-2} \\ c_4 &= \phantom{-}4.176\,476\,8 \times 10^{-5} \\ c_5 &= -1.445\,209\,3 \times 10^{-8} \\ c_6 &= \phantom{-}6.545\,967\,3 \end{aligned}$$

The partial pressure of water vapour in Pa is then derived from $e = U \cdot e_s$, with $U$ given in relative units (dimensionless).

The first derivative to temperature (sensitivity, used in Eq. 4.79) is:

$$\frac{\partial e_\mathrm{s}}{\partial T} = e_\mathrm{s} \cdot \left( \frac{-c_1}{T^2} + c_3 + 2c_4 T + 3c_5 T^2 + \frac{c_6}{T} \right), \tag{A.5}$$

with $e_\mathrm{s}$ the saturation vapour pressure in Eq. (A.4).

## A.3 Smoothing algorithm

Smoothing is part of the processing for creation of the GRUAN data product. It is used, among others, for removing statistical variation (noise) from the data, but also to reduce known non-random unnatural structures that are created by the sounding itself, such as those connected to the intrinsic motion of the radiosonde (pendulum and spinning).

Smoothing is carried out by moving an averaging window (kernel) of appropriate size and shape point-by-point over the data series (convolution), equivalent to low-pass filtering. The kernel describes the weights with which the data points within the smoothing window are included in the averaging. It is chosen symmetrical around the central point.

For the current GDP, non-uniform Gaussian-shaped kernels are used for most of the smoothing procedures. Different kernel widths, expressed as number of the regular 1 s-data points, are used to match the respective variables, i.e. to achieve different appropriate smoothing strengths. Figure A.1 shows examples of these Gaussian-like kernels.

For practical reasons, an odd number $N$ for the kernel width is advantageous for the representation of a symmetrical kernel

$$N = 2M + 1, \tag{A.6}$$

with $M \geq 1$ defining the width $N$. The cut-off frequency $f_\mathrm{c}$ is the frequency at which the filter transfer function has the value 1/2, or where the signal attenuation is –3.01 dB, and therefore defines the resolution of the smoothed data. It is given by the inverse kernel width:

$$f_\mathrm{c} = N^{-1}. \tag{A.7}$$

Beside the width, the function used in the processing to calculate the Gaussian-distributed kernel weights expects as defining parameter the half width of the Gaussian at its turning points (equivalent to the standard deviation). To make sure that the filter has an attenuation of –3.01 dB

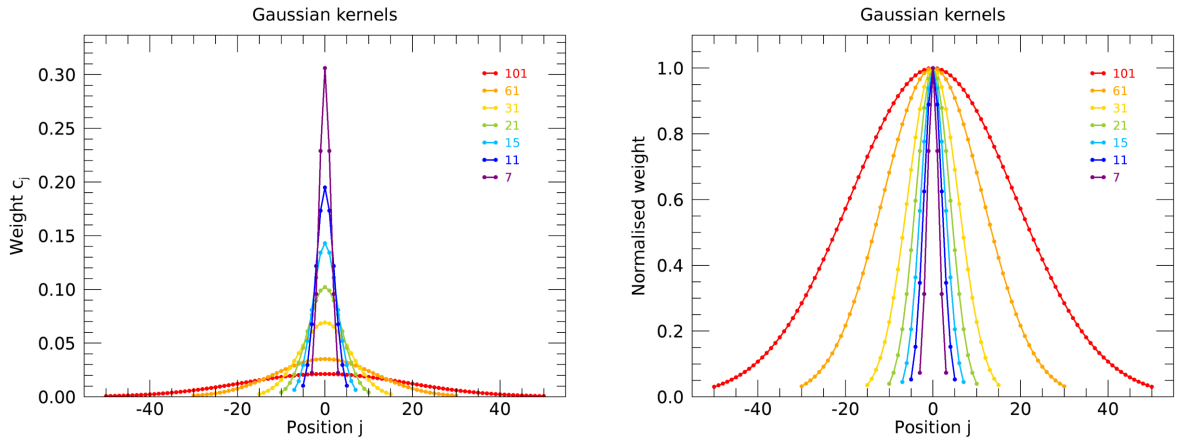


**Figure A.1:** Used Gaussian-like smoothing kernels of different lengths (data points or seconds, see legend). Left: plotted as normalised weights. Right: Normalised to the same maximum value (1.0) for better visual comparability of the kernel shapes.

at the cut-off frequency $f_c$, this parameter is defined as

$$\sigma_g = \frac{\sqrt{\frac{\ln 2}{2}}}{\pi \cdot f_c}. \tag{A.8}$$

In principle, other filter types than a Gaussian can be used and are available as option in the processing, e.g. a simple box-car or a digital filter. However, they play a negligible role in the current implementation of the data product.

The smoothed data points $\bar{s}_i$ at each position in the profile (time series) are calculated as weighted means with:

$$\bar{s}_i = \sum_{j=-M}^{M} c_j \cdot s_{i+j}, \tag{A.9}$$

where the $c_j$ are normalised Gaussian-distributed weighting coefficients:

$$\sum_{j=-M}^{M} c_j = 1. \tag{A.10}$$

The effective sample size $N'$ denotes the effective number of data points relevant for the smoothing. For a Gaussian kernel it is smaller than the actual number of points $N$, because points with low weights contribute less to the mean. We use a formula developed by *Kish* (1965) for estimating $N'$:

$$N' = \left( \sum_{j=-M}^{M} c_j^2 \right)^{-1}. \tag{A.11}$$

The scatter of the data (standard deviation), divided by $\sqrt{N}$, is usually used as estimate for the uncertainty of a simple arithmetic mean. Equivalently, an uncertainty $u(\bar{s}_i)$ has to be attributed

to the kernel-smoothed means $\bar{s}_i$. Three options were considered for the RS41-processing:

1) Derivation from the weighted standard deviation over the actual window length,
2) An empirical estimate using a block averaging procedure, and
3) Derivation from the standard deviation of the residuals (original minus smoothed profile).

In preliminary ALPHA or BETA versions for RS41, as well as in the existing RS92-GDP.2 data product (*Dirksen et al.*, 2014), **method 1** was used. The (weighted) standard deviation $\sigma_i$ for the running mean $\bar{s}_i$ in (Eq. A.9) is defined as

$$\sigma_i = \sqrt{\left(\frac{N'_i}{N'_i - 1}\right) \sum_{j=-M}^{M} c_j \cdot (s_{i+j} - \bar{s}_i)^2}. \tag{A.12}$$

The uncertainty of the weighted mean, $u(\bar{s}_i)$, is then estimated as:

$$u(\bar{s}_i) = \frac{\sigma_i}{\sqrt{N'_i}}. \tag{A.13}$$

A drawback of that simple estimate is that low-frequency or trend components in the profile, which rather reflect natural variations or gradients on large scales (e.g. the tropospheric temperature lapse), may significantly contribute and lead to overestimates of the uncertainty.

**Method 2** Block averaging is a numerical method to estimate the uncertainty (standard deviation) of a sample mean of quasi-stationary data which takes local auto-correlation into account. An according algorithm was developed and tested for use in the processing. However, the computing effort is significantly higher than for the other methods, which has discouraged its use in RS41-GDP.1.

For the current version of the RS41 data product, **method 3** – unweighted standard deviation of residuals – was chosen. The residual $r_i$ after subtracting the smoothed profile from the original is

$$r_i = \Delta s_i = s_i - \bar{s}_i. \tag{A.14}$$

The uncertainty of the smoothed data is then estimated as simple standard deviation of the mean over the residuals in the local interval $(-M ... + M)$:

$$u(\bar{s}_i) = \sqrt{\left(\frac{1}{N-1}\right) \sum_{j=-M}^{M} (r_{i+j} - \bar{r}_i)^2}, \tag{A.15}$$

with the local mean of the residual

$$\bar{r}_i = \sum_{j=-M}^{M} \frac{1}{2M+1} \cdot r_{i+j}. \tag{A.16}$$

The advantage of this method is that large-scale fluctuations or trends should contribute less.

It is noted here that smoothing, i.e. averaging over a limited interval in the profile around the current data point, leads to a local 'vertical' correlation of the smoothed values on the grid (1 s) of the original data. This correlation is removed as soon as points of the smoothed profile

are viewed on a vertical grid that is coarser than the actual resolution of the smoothed profile (Eq. A.7). Such a local correlation is not taken into account in the smoothing-based estimates of uncorrelated uncertainty components (Section 6.1) because the size of the smoothing window is small in comparison to the whole radiosonde profile and also in comparison to most resolvable vertical structure in the atmosphere.

The symmetry of the smoothing window around the central point requires special treatment at both ends of the profiles, where the window would move beyond the range of available data. The original data series is extended at the ends by half the kernel length such that enough data are available to calculate smoothed values also at the first and last position of the original profile. The GDPS offers different selectable methods to extend the profiles, which are:

- *NAN* – extension with NaN values,
- *ZERO* – extension with zero values (0.0),
- *NO* – do nothing,
- *WRAP* – extension with original values from the opposite end,
- *TRUNCATE* – extension with the value of the last/first data point in the original profile,
- *MIRROR* – extension with original data mirrored at the last/first point of the original profile,
- *EXTRAPOL* – extension with linearly extrapolated values.

Only MIRROR and EXTRAPOL are actually used in the RS41 processing.

Missing data (identified by NaN values) may be present in the raw data profiles. They are already filled by linear interpolation in an earlier processing step, given the gap lengths do not exceed 10 points (10 s). Larger gaps are not treated in that step and therefore remain in the profile. If such a gap is encountered by the running window in the smoothing procedure, the window slides into that gap, similar to the effect at the profile ends. That is, the number of data points included in the actual smoothing, and hence the number of weighting coefficients decreases. Therefore, the remaining weighting coefficients are re-normalised according to Eq. (A.10) before performing the actual convolution (smoothing). Otherwise the smoothed value would be underestimated. This procedure is applied as long as at least one non-NaN data point is covered by the smoothing window when moving over the actual gap (otherwise the convolution produces NaN). However, smoothing does not fill any missing data, i.e. once the centre of the smoothing window matches the first grid point in the gap, the original NaN are kept. Thus, gaps larger than 10 points may occasionally occur in processed profiles, and users should be aware of this.

## A.4 Conversion of GPS-position data

The conversion of GPS positions from degree longitude and latitude values to geometric meters is implemented in RS41-GDP.1 using the following not so simple algorithm.

We use the following steps to convert latitude $\phi$ and longitude $\lambda$ from degrees into meters. In a first step the three dimensional geodetic measurement between two positions measured in reference to a specified ellipsoid (WGS84) are calculated. This calculation is performed by first computing a new ellipsoid by expanding or contracting the reference ellipsoid such that the new

**Table A.2:** List of all variable-related smoothing configurations

| Variable | Shape | $N$ ($N'$) | Edge | Uncertainty | Comment |
|---|---|---|---|---|---|
| wind | GF | 31 (20.286) | MIRROR | RESIDUAL | |
| ventilation | GF | 21 (13.745), 61 (39.914) | MIRROR, EXTRAPOL | WEIGHTED | special handling, see Section 4.4.4 |
| pressure | GF | 15 (9.820) | EXTRAPOL | RESIDUAL | |
| temperature | GF | 15 (9.820) | EXTRAPOL | RESIDUAL | switch between day and night; kernel length at night is 7 (4.592) |
| humidity (TL) | GF | 1 (1.000) – 1500 (981.5) | NAN | WEIGHTED | special handling, see Section 4.2.3.3 |
| humidity | GF | 7 (4.592) | EXTRAPOL | RESIDUAL | |

ellipsoid passes through the average elevation of the two positions. A geodetic curve across the new ellipsoid is calculated. The point-to-point distance is calculated as the hypotenuse of a right triangle where the length of one side is the ellipsoidal distance and the other is the difference in elevation. We use an own implementation of Thaddeus Vincenty's algorithms to solve the direct and inverse geodetic problems. See Vincenty's original publication on the NOAA website (http://www.ngs.noaa.gov/PUBS_LIB/inverse.pdf).

An approach using simpler formulas but providing with sufficient accuracy (between approx. 0.0 % at surface and 0.5 % at 30.0 km altitude) is given with the following expressions (see e.g. *Bugayevskiy and Snyder*, 1995; *Snyder*, 1987). In Eq. (A.17), $f_\phi$ represents the metric distance per degree latitude as function of latitude:

$$f_\phi = c_1 + c_2 \cdot \cos(2\phi) + c_3 \cdot \cos(4\phi) + c_4 \cdot \cos(6\phi), \tag{A.17}$$

where

$$\begin{aligned} c_1 &= \phantom{-}1.111\,329\,2 \times 10^5 \\ c_2 &= -5.5982 \times 10^2 \\ c_3 &= \phantom{-}1.175 \\ c_4 &= -2.3 \times 10^{-3} \end{aligned}$$

are the coefficients in terms of the WGS84 ellipsoid, and latitude $\phi$ in radians. Small position differences, e.g. two consecutive points in a radiosonde profile or the residual after smoothing a profile of horizontal radiosonde position data, can be converted from degree to metres by simply applying this conversion factor to these differences, without taking the latitude dependence into account.

Similarly, the metric distance per degree longitude as function of longitude can be approximated using

$$f_\lambda = c_1 \cdot \cos(\lambda) + c_2 \cdot \cos(3\lambda) + c_3 \cdot \cos(5\lambda), \tag{A.18}$$

with coefficients

$$\begin{aligned} c_1 &= \phantom{-}1.114\,128\,4 \times 10^{5} \\ c_2 &= -9.35 \times 10^{1} \\ c_3 &= \phantom{-}1.18 \times 10^{-1} \end{aligned}$$

These expressions are valid for the Earth's surface and do not take the (small) dependence on altitude into account, which in principle takes effect during radiosoundings. However, the deviations are small. Relative differences between this approximation and the more elaborate approach implemented in the RS41 data processing are for both latitude and longitude less than 1 ‰ at the surface and reach about 5 ‰ at 30 km altitude.

## A.5 Gravitational acceleration

The gravitational acceleration $g$ depending on the latitude $\phi$ and the altitude $h$ is calculated using following formula (see https://en.wikipedia.org/wiki/Theoretical_gravity#WELMEC_formula):

$$g(\phi, h) = \left(c_1 + c_2 \cdot \sin^2(\phi) + c_3 \cdot \sin^2(2\phi)\right) \cdot c_4 + c_5 \cdot h \tag{A.19}$$

where

$$\begin{aligned} c_1 &= \phantom{-}1.0 \\ c_2 &= \phantom{-}5.3024 \times 10^{-3} \\ c_3 &= -5.8 \times 10^{-6} \\ c_4 &= \phantom{-}9.780\,318 \\ c_5 &= -3.085 \times 10^{-6} \end{aligned}$$

and the units of $c_4$ and $c_5$ are $\mathrm{m\,s^{-2}}$ and $\mathrm{s^{-2}}$ respectively.

# B Additional information about processing system

## B.1 Details of workflow of the processing system

In the following a more detailed view of the implemented workflow of the processing system is presented. See also Figure 7.1 in Section 7.1 which shows this workflow as scheme.

Run the GDPS (see Section 7.1)
↦ function “gruan_GDPS_run”

1) Read INI file “runCfg*.ini”
2) Initialise logging system
   ↦ functions “gruan_LOG_*”
3) Start main processing routine
   ↦ function “gruan_GDPS_process”
   - **Part 1: Initialisation**
     - check and interpret configuration (e.g. paths, plotting, general)
     - read processing structure “proc_*.xml”
       ↦ function “gruan_GDPS_readProcessingXml”
     - read repository description “Repository_*.xml”
       ↦ function “gruan_GDPS_readRepositoryXml”
   - **Part 2: Read data sources** (see Section 7.2)
     ↦ function “gruan_GDPS_readSources”
     - Read file information from configuration file “process_case*.ini”
     - Read input files (loop with all input files)
       - Read file: GNC-RAW (MWX, DC3DB), CSV (EXT, REF), MD (GMDB)
         ⇒ Optional connection to GMDB if MD file not available
         ↦ function “gruan_GMDB_getInfoAboutMeasurement”
       - Import data variables (columns of a table)
       - Import meta-data attributes
       - Use filter rules (if defined) to filter rows of data table
       - Mapping of imported data fields
       - Convert data type of data fields (if necessary)

↦ function “gruan_GDPS_convertFieldValue”

· Make time axis steady and regular (grid, e.g. 1 second)
↦ function “gruan_DP_fitDataInGridTable”

* Combine all data sources including time synchronisation
↦ function “gruan_DP_combineDataSources”

– **Part 3: Prepare processing steps**

* Prepare channels
* Prepare processing steps (loop with all steps)
  · Read and check module description “mod*.xml”
  ↦ function “gruan_GDPS_readModuleXml”
  · Check input attributes and variables
  ↦ function “gruan_GDPS_checkModule”
  · Check output attributes and variables
  ↦ function “gruan_GDPS_checkModule”
  · Read configuration file related to module “modCfg*.ini”, check attributes and parse values
  ↦ functions “gruan_GDPS_readModuleConfig”, “gruan_GDPS_checkModuleConfig”, “gruan_GDPS_parseModuleConfig”

– **Part 4: Run processing**

* Pre-processing ⇒ Process instructions of full processing (moment=‘pre’)
↦ function “gruan_GDPS_processInstructions”
* Initialise channel stack list with source variables
* Process steps (loop with all steps)
  · Process instructions of step (moment=‘block’)
  ↦ function “gruan_GDPS_processInstructions”
  · Mapping of all input variables and attributes
  · Pre-define all output variables and attributes
  · Prepare general information and configuration for processing module
  · Process instructions of step (moment=‘pre’)
  ↦ function “gruan_GDPS_processInstructions”
  · Run module ⇒ **Run real processing step** (see Section 7.3)
  ↦ functions “gruan_GDPS_mod*”
  · Check and save all output attributes and variables
  · Process instructions of step (moment=‘post’)
  ↦ function “gruan_GDPS_processInstructions”
* Post-processing ⇒ Process instructions of full processing (moment=‘post’)
↦ function “gruan_GDPS_processInstructions”

  - **Part 5: Save output files** (see Section 7.5)
    ↦ function “gruan_GDPS_writeOutputFiles”

4) Dump results and messages (optional)

5) Terminate program

The workflow refers not only to relevant functions in the IDL source code of the GDPS but also to various configuration and initialisation files. These are essential for the GDPS and are therefore briefly mentioned here for completeness:

**runCfg_RS41-GDP.1.ini** – Main configuration file for the GDPS

**modCfg_RS41-GDP.1.ini** – Configuation file for all processing modules

**strDef_RS41-GDP.1.ini** – Configuration file for the radiation simulations using the Streamer RTM

**proc_RS41-GDP.1.xml** – Definition file of whole processing

**outFile_RS41-GDP.1__1.0.xml** – Definition file of the output file of the GDP

**Repository_DevelopmentAll.xml** – Definition file of the repository of modules

**mod<name>__<version>.xml** – Definition files of each module

The full processing system (GDPS) is described in detail in *Sommer and von Rohden* (2023, in preparation).

# C Documentation of processing steps and related processing modules

## C.1 Processing steps

**Table C.1:** List of all processing steps of **RS41-GDP.1** with used modules and short descriptions

| Nº | Name | Module & Version & Comments |
|---|---|---|
| *Preparation and pre-checks (see Section 7.3.2)* | | |
| 1 | InitRelevantAttributes | modInitAttributes (v0.3.1, 2018-08-21), initialisation of some relevant attributes |
| 2 | ExtractGmdbMetadata | modExtractGmdbMetadata (v0.1.5, 2020-05-12), extract (import) all relevant metadata from GMDB metadata file |
| 3 | InitLatitude | modInitVariable (v0.2.2, 2018-09-14), init channel latitude if no input data available |
| 4 | InitLongitude | modInitVariable (v0.2.2, 2018-09-14), init channel longitude if no input data available |
| 5 | PreCheckSondeX | modDetectNanAndOutlier (v0.3.13, 2020-11-23), pre-check of channel 'SondeX' which includes outlier detection, gap detection, interpolation of small gaps, and more |
| 6 | PreCheckSondeY | modDetectNanAndOutlier (v0.3.13, 2020-11-23), pre-check of channel 'SondeY' … |
| 7 | PreCheckSondeZ | modDetectNanAndOutlier (v0.3.13, 2020-11-23), pre-check of channel 'SondeZ' … |
| 8 | ComputePosition | modComputePosition (v0.4.6, 2020-10-02), calculate WGS84 position (lat/lon/alt) from cartesian coordiates (x/y/z) |
| 9 | PreCheckAltitude | modDetectNanAndOutlier (v0.3.13, 2020-11-23), pre-check of channel 'Altitude' … |

*This table is continued on the next page.*

Table C.1 – *Continued from previous page*

| № | Name | Module & Version & Comments |
|---|---|---|
| 10 | PreCheckLatitude | modDetectNanAndOutlier (v0.3.13, 2020-11-23), pre-check of channel 'Latitude' … |
| 11 | PreCheckLongitude | modDetectNanAndOutlier (v0.3.13, 2020-11-23), pre-check of channel 'Longitude' … |
| 12 | PreCheckLocalAltitude | modDetectNanAndOutlier (v0.3.13, 2020-11-23), pre-check of channel 'AltitudeLocal' … |
| 13 | PreCheckLocalLatitude | modDetectNanAndOutlier (v0.3.13, 2020-11-23), pre-check of channel 'LatitudeLocal' … |
| 14 | PreCheckLocalLongitude | modDetectNanAndOutlier (v0.3.13, 2020-11-23), pre-check of channel 'LongitudeLocal' … |
| 15 | PreCheckRelative-Humidity | modDetectNanAndOutlier (v0.3.13, 2020-11-23), pre-check of channel 'RelativeHumidity' … |
| 16 | PreCheckTemperature | modDetectNanAndOutlier (v0.3.13, 2020-11-23), pre-check of channel 'Temperature' … |
| 17 | CalcInternalHumidity | modComputeInternalHumidity (v0.1.6, 2021-01-22), calculate a symbolic internal temperature of humidity sensor with related relative humidity if table 'GSupport' is not available |
| 18 | PreCheckIntHumidity | modDetectNanAndOutlier (v0.3.13, 2020-11-23), pre-check of channel 'IntHumidity' … |
| 19 | PreCheckIntHumidity-Temperature | modDetectNanAndOutlier (v0.3.13, 2020-11-23), pre-check of channel 'IntHumidityTemperature' … |
| 20 | ComputeWindComponents | modComputeWindComponents (v0.1.2, 2020-12-08), compute zonal and meridional wind components from Lat/Lon/Alt |
| 21 | PreCheckZonalWind | modDetectNanAndOutlier (v0.3.13, 2020-11-23), pre-check of channel 'ZonalWind' … |
| 22 | PreCheckMeridionalWind | modDetectNanAndOutlier (v0.3.13, 2020-11-23), pre-check of channel 'MeridionalWind' … |
| 23 | PreCheckPressureFrom-Sensor | modDetectNanAndOutlier (v0.3.13, 2020-11-23), pre-check of channel 'PressureFromSensor' … |
| *Ground checks and further preparations (see Section 7.3.2)* | | |
| 24 | AnalyzeRI41 | modAnalyzeGroundCheck (v0.2.5, 2018-11-07), analyse ground check data from manufacturer ground check RI41 |

*This table is continued on the next page.*

Table C.1 – *Continued from previous page*

| № | Name | Module & Version & Comments |
|---|---|---|
| 25 | CorrectPressureFrom-Sensor | modCorrectVariable (v0.1.4, 2021-09-29), apply correction to the pressure sensor data |
| 26 | DetectLaunchAndBurst | modDetectFlightPoints (v0.3.4, 2021-09-29), analyse pressure and altitude data to detect launch and burst point |
| 27 | CheckMainVariable-Availability | modCheckVariables (v0.1.0, 2021-09-09) symbolic module to provide a possibility to check variables using processing instructions |
| 28 | ComputeGravity | modComputeGravity (v0.1.8, 2021-09-24), calculate acceleration of gravity |
| 29 | ComputeGeoid | modComputeGeoid (v0.1.8, 2021-09-24), get difference between WGS84 and real geoid (mean sea level) |
| 30 | AnalyzeLocalPosition | modAnalyzeLocalPosition (v0.2.9, 2021-09-23), analyse GNSS position of local antenna at site |
| 31 | AnalyzeSHC | modAnalyzeChamber (v0.5.5, 2020-11-24), detect and analyse ground check period in SHC |
| 32 | AnalyzeShelter | modAnalyzeChamber (v0.5.5, 2020-11-24), analyse ground check period in a shelter |
| *Altitude and pressure (see Sections 7.3.3 and 7.3.4)* | | |
| 33 | LaunchPressure | modLaunchPressureAltitude (v0.3.1, 2020-11-23), analyse altitude and pressure of radiosonde and launch site at launch |
| 34 | AltitudeUncertainty | modEstimateAltitudeUncertainty (v0.1.9, 2021-05-10), estimate uncertainty of altitude WGS84, altitude above MSL and geopotential height |
| 35 | PositionUncertainty | modEstimatePositionUncertainty (v0.1.1, 2020-12-10), estimate uncertainty of position (Lat/Lon from GNSS) |
| 36 | CalibratePressure | modCalibrationUncertainty (v0.2.2, 2021-09-23), estimate calibration uncertainty of pressure sensor |
| 37 | SmoothPressureFrom-Sensor | modSmoothVariable (v0.1.9, 2021-05-26), smooth data of pressure sensor (see Appendix A.3) |
| 38 | FinalisePressure | modFinalisePressure (v0.1.4, 2020-12-07), finalise data of pressure sensor |
| 39 | ComputeGNSSPressure | modComputePressureBasedOnGNSS (v0.1.11, 2021-11-03), calculate pressure based on GNSS altitude (see Section 4.4.2) |

*This table is continued on the next page.*

Table C.1 – *Continued from previous page*

| № | Name | Module & Version & Comments |
|---|---|---|
| 40 | MergePressure | modChooseAndMergePressure (v0.1.4, 2021-09-20), choose pressure based on GNSS as default pressure variable |
| *Temperature (see Section 7.3.5)* | | |
| 41 | TemperatureCalibration | modCalibrationUncertainty (v0.2.2, 2021-09-23), estimate calibration uncertainty of temperature sensor |
| 42 | ComputeVentilation | modComputeVentilation (v0.3.13, 2021-03-05), analyse pendulum and calculate a combined ventilation from ascent speed and pendulum speed (see Section 4.4.4) |
| 43 | CloudDetection | modDetectClouds (v0.2.6, 2020-12-16), try to detect cloud layers using humidity (result is not used at moment) |
| 44 | SolarElevation | modSolarElevation (v0.4.8, 2021-01-15), calculate position of sun with all relevant angles and mark day/night/twilight |
| 45 | CalcRadiation | modComputeRadiationWithStreamer (v0.1.19, 2021-03-05; bug fix: v0.1.20, 2022-01-05), calculate solar radiation using RTM Streamer (see Section 4.1.4) |
| 46 | TempRadCorr | modTempRadiationCorrection (v0.1.11, 2021-03-09), calculate and apply temperature radiation correction (see Section 4.1.5) |
| 47 | SmoothTemperature | modSmoothVariable (v0.1.9, 2021-05-26), smooth data of temperature sensor (see Appendix A.3) |
| 48 | FinaliseTemperature | modFinaliseTemperature (v0.2.10, 2020-12-07), finalise data of temperature sensor |
| *Humidity (see Section 7.3.6)* | | |
| 49 | IntHumTempCalibration | modCalibrationUncertainty (v0.2.2, 2021-09-23), estimate calibration uncertainty of internal temperature of heated humidity sensor |
| 50 | HumidityCalibration | modCalibrationUncertainty (v0.2.2, 2021-09-23), estimate calibration uncertainty of heated humidity sensor |
| 51 | HumidityTimelagCorr | modRHTimelagCorrection (v0.4.1, 2020-10-26), calculate and apply temperature-related time-lag correction of humidity sensor (see Section 4.2.3.3) |

*This table is continued on the next page.*

Table C.1 – *Continued from previous page*

| № | Name | Module & Version & Comments |
|---|---|---|
| 52 | RecalculateHumidity | modComputeHumidity (v0.1.12, 2021-05-28), recalculate relative humidity at air temperature based on data of heated humidity sensor (see Section 4.5.1) |
| 53 | SmoothHumidity | modSmoothVariable (v0.1.9, 2021-05-26), smooth data of humidity sensor (see Appendix A.3) |
| 54 | FinaliseHumidity | modFinaliseHumidity (v0.1.8, 2020-12-07), finalise data of humidity sensor |
| 55 | CalculateAlternative-Humidity | modComputeAlternativeHumidity (v0.2.4, 2020-12-15), calculate a couple of alternative humidity variables, e.g. dew point, mixing ratio (see Section 4.5) |
| *Wind and further parameters (see e.g. Sections 7.3.3 and 7.3.8)* | | |
| 56 | WindparameterRetrieval | modWindRetrieval (v0.2.12, 2021-06-09), calculate a final retrieval of all wind variables including an estimation of uncertainty (see Section 4.4.3) |
| 57 | DetectTropopause | modDetectTropopause (v0.3.9, 2021-09-09), detect tropopause using WMO definition |
| 58 | MarkBands | modMarkBands (v0.1.3, 2020-12-10), mark data parts which are related to specific bands, e.g. ascent, troposphere |
| 59 | CalcIWV | modComputeIntegratedWaterVapour (v0.1.9, 2021-09-15), calculate integrated column of water vapour (see Section 4.5.3) |
| *Plots and comparisons (see Section 7.3.7)* | | |
| 60 | PlotTemperature | modPlotVariable (v0.1.6, 2020-11-23), plot profile of temperature |
| 61 | PlotRelativeHumidity | modPlotVariable (v0.1.6, 2020-11-23), plot profile of relative humidity |
| 62 | PlotWVMR | modPlotVariable (v0.1.6, 2020-11-23), plot water vapour mixing ratio |
| 63 | PlotWindSpeed | modPlotVariable (v0.1.6, 2020-11-23), plot wind speed |
| 64 | PlotWindDirection | modPlotVariable (v0.1.6, 2020-11-23), plot wind direction |
| 65 | PlotZonalWind | modPlotVariable (v0.1.6, 2020-11-23), plot zonal wind component |

*This table is continued on the next page.*

Table C.1 – *Continued from previous page*

| № | Name | Module & Version & Comments |
|---|---|---|
| 66 | PlotMeridionalWind | modPlotVariable (v0.1.6, 2020-11-23), plot meridional wind component |
| 67 | PlotAscentSpeed | modPlotVariable (v0.1.6, 2020-11-23), plot ascent speed |
| 68 | PlotPressure | modPlotVariable (v0.1.6, 2020-11-23), plot pressure |
| 69 | ComparePressure | modCompareVariables (v0.1.12, 2020-11-23), compare several pressure variables |
| 70 | ComparePressureFrom-Sensor | modCompareVariables (v0.1.12, 2020-11-23), compare pressure from sensor |
| 71 | CompareTemperature | modCompareVariables (v0.1.12, 2020-11-23), compare temperature |
| 72 | CompareHumidity | modCompareVariables (v0.1.12, 2020-11-23), compare relative humidity |
| 73 | CompareWindSpeed | modCompareVariables (v0.1.12, 2020-11-23), compare wind speed |
| 74 | CompareWindDirection | modCompareVariables (v0.1.12, 2020-11-23), compare wind direction |
| 75 | CompareAscentSpeed | modCompareVariables (v0.1.12, 2020-11-23), compare ascent speed |
| 76 | CompareGeopotHeight | modCompareVariables (v0.1.12, 2020-11-23), compare geopotential height |
| 77 | CompareAltitude | modCompareVariables (v0.1.12, 2020-11-23), compare altitude (WGS84) |
| 78 | CompareAltitudeMSL | modCompareVariables (v0.1.12, 2020-11-23), compare altitude above MSL |

*Finalise data product*

| | | |
|---|---|---|
| 79 | LatLonStatistics | modComputeStatistics (v0.1.0, 2021-09-03), calculate statistics (e.g. min, max) of latitude and longitude |
| 80 | PrepareProduct-Information | modPrepareProductInformation (v0.2.2, 2019-10-01), prepare information about this data product |
| 81 | PrepareMetadataFor-Output | modPrepareMetadata (v0.5.13, 2021-09-03), prepare meta-data related to the flight, system, instrument, site, … |

## C.2 Main steps related to specific variables

For each main variable, the relevant processing steps are listed below. In addition to the name of the step, the module used and the corresponding section in the configuration file for the modules ('modCfg') are also given.

### Longitude

1) **InitLongitude** – initialisation of variable longitude
   ↦ module "modInitVariable" using configuration section "init_lat"
2) **PreCheckSondeX** – raw data check of Cartesian coordinate X
   ↦ module "modDetectNaNAndOutlier" using configuration section "precheck_sondex"
3) **PreCheckSondeY** – raw data check of Cartesian coordinate Y
   ↦ module "modDetectNaNAndOutlier" using configuration section "precheck_sondey"
4) **PreCheckSondeZ** – raw data check of Cartesian coordinate Z
   ↦ module "modDetectNaNAndOutlier" using configuration section "precheck_sondez"
5) **ComputePosition** – compute position (incl. longitude) using XYZ
   ↦ module "modComputePosition" using configuration section "compute_position"
6) **PreCheckLongitude** – raw data check longitude
   ↦ module "modDetectNaNAndOutlier" using configuration section "precheck_lon"
7) **PositionUncertainty** – estimate uncertainty of position (incl. longitude)
   ↦ module "modEstimatePositionUncertainty" using configuration section "uncert_pos"

### Latitude

1) **InitLatitude** – initialisation of variable latitude
   ↦ module "modInitVariable" using configuration section "init_lon"
2) **PreCheckSondeX** – raw data check of Cartesian coordinate X
   ↦ module "modDetectNaNAndOutlier" using configuration section "precheck_sondex"
3) **PreCheckSondeY** – raw data check of Cartesian coordinate Y
   ↦ module "modDetectNaNAndOutlier" using configuration section "precheck_sondey"
4) **PreCheckSondeZ** – raw data check of Cartesian coordinate Z
   ↦ module "modDetectNaNAndOutlier" using configuration section "precheck_sondez"
5) **ComputePosition** – compute position (incl. latitude) using XYZ
   ↦ module "modComputePosition" using configuration section "compute_position"
6) **PreCheckLatitude** – raw data check of latitude
   ↦ module "modDetectNaNAndOutlier" using configuration section "precheck_lat"
7) **PositionUncertainty** – estimate uncertainty of position (incl. latitude)
   ↦ module "modEstimatePositionUncertainty" using configuration section "uncert_pos"

## Altitude

1) **PreCheckSondeX** – raw data check of Cartesian coordinate X
   ↦ module “modDetectNaNAndOutlier” using configuration section “precheck_sondex”
2) **PreCheckSondeY** – raw data check of Cartesian coordinate Y
   ↦ module “modDetectNaNAndOutlier” using configuration section “precheck_sondey”
3) **PreCheckSondeZ** – raw data check of Cartesian coordinate Z
   ↦ module “modDetectNaNAndOutlier” using configuration section “precheck_sondez”
4) **ComputePosition** – compute position (incl. altitude) using XYZ
   ↦ module “modComputePosition” using configuration section “compute_position”
5) **PreCheckAltitude** – raw data check of altitude
   ↦ module “modDetectNaNAndOutlier” using configuration section “precheck_alt”
6) **ComputeGravity** – calculate acceleration due to gravity
   ↦ module “modComputeGravity” using configuration section “compute_gravity”
7) **ComputeGeoid** – get difference between ellipsoid WGS84 and a specific geoid
   ↦ module “modComputeGeoid” using configuration section “compute_geoid”
8) **AnalyzeLocalPosition** – analyse position (incl. altitude) of GNSS antenna of station
   ↦ module “modAnalyzeLocalPosition” using configuration section “local_position”
9) **AltitudeUncertainty** – estimate uncertainty of altitude
   ↦ module “modEstimateAltitudeUncertainty” using configuration section “uncert_alt”

## Pressure (measured by sensor)

1) **PreCheckPressureFromSensor** – raw data check
   ↦ module “modDetectNaNAndOutlier” using configuration section “precheck_press_sensor”
2) **AnalyzeRI41** – analysis of ground check (ground initialisation) which was done by RI41
   ↦ module “modAnalyzeGroundCheck” using configuration section “gc_ri41”
3) **CorrectPressureFromSensor** – apply a pressure correction of pressure if ground check values are available
   ↦ module “modCorrectVariable” using configuration section “corr_press_sens”
4) **AnalyzeSHC** – optional additional ground check using a SHC and further reference sensors
   ↦ module “modAnalyzeChamber” using configuration section “shc”
5) **AnalyzeShelter** – optional additional ground check outside in a shelter using further reference sensors
   ↦ module “modAnalyzeChamber” using configuration section “shelter”
6) **CalibratePressure** – calculate calibration uncertainty of pressure
   ↦ module “modCalibrationUncertainty” using configuration section “press_cal”
7) **SmoothPressureFromSensor** – light smoothing of pressure
   ↦ module “modSmoothVariable” using configuration section “smooth_pressure_sens”
8) **FinalisePressure** – finalise all pressure related variables (incl. correction, uncertainty)
   ↦ module “modFinalisePressure” using configuration section “final_press”

## Pressure (based on GNSS)

Variable altitude is used as base variable.

1) **LaunchPressure** – check consistency of pressure and altitude at balloon launch
   ↦ module “modLaunchPressureAltitude” using configuration section “launch_pressure”
2) **ComputeGNSSPressure** – calculate pressure and geopotential height based on GNSS (GPS) data
   ↦ module “modComputePressureBasedOnGNSS” using configuration section “pressure_gnss”
3) **MergePressure** – symbolic act to choose calculated pressure as default one
   ↦ module “modChooseAndMergePressure” using configuration section “merge_pressure”

## Temperature

1) **PreCheckTemperature** – raw data check of temperature
   ↦ module “modDetectNaNAndOutlier” using configuration section “precheck_temp”
2) **AnalyzeRI41** – analysis of ground check (ground initialisation) which was done by RI41
   ↦ module “modAnalyzeGroundCheck” using configuration section “gc_ri41”
3) **AnalyzeSHC** – optional additional ground check using a SHC and further reference sensors
   ↦ module “modAnalyzeChamber” using configuration section “shc”
4) **AnalyzeShelter** – optional additional ground check outside in a shelter using further reference sensors
   ↦ module “modAnalyzeChamber” using configuration section “shelter”
5) **TemperatureCalibration** – estimate calibration uncertainty of temperature
   ↦ module “modCalibrationUncertainty” using configuration section “temp_cal”
6) **ComputeVentilation** – compute ventilation at sensor boom
   ↦ module “modComputeVentilation” using configuration section “compute_ventilation”
7) **CloudDetection** – simple ‘cloud detection’ using relative humidity
   ↦ module “modDetectClouds” using configuration section “detect_cloud”
8) **SolarElevation** – calculate position of the Sun with all relevant angles
   ↦ module “modSolarElevation” using configuration section “solar_elevation”
9) **CalcRadiation** – calculate short-wave solar radiation using the RTM Streamer
   ↦ module “modComputeRadiationWithStreamer” using configuration section “streamer”
10) **TempRadCorr** – calculate and apply radiation correction of temperature
    ↦ module “modTempRadiationCorrection” using configuration section “temp_rad_corr”
11) **SmoothTemperature** – light smoothing of temperature
    ↦ module “modSmoothVariable” using configuration section “smooth_temp”
12) **FinaliseTemperature** – finalise temperature incl. correction and uncertainty
    ↦ module “modFinaliseTemperature” using configuration section “final_temp”

## Relative humidity

1) **PreCheckRelativeHumidity** – raw data check of pre-calculated (by manufacturer) relative humidity at air temperature
   ↦ module “modDetectNaNAndOutlier” using configuration section “precheck_rh”
2) **CalcInternalHumidity** – calculate internal relative humidity and internal temperature as workaround if not available
   ↦ module “modComputeInternalHumidity” using configuration section “calc_int_rh”
3) **PreCheckIntHumidity** – raw data check of relative humidity at internal temperature
   ↦ module “modDetectNaNAndOutlier” using configuration section “precheck_inthum”
4) **PreCheckIntHumidityTemperature** – raw data check of internal temperature of humidity sensor
   ↦ module “modDetectNaNAndOutlier” using configuration section “precheck_inthumtemp”
5) **AnalyzeRI41** – analysis of ground check (ground initialisation) which was done by RI41
   ↦ module “modAnalyzeGroundCheck” using configuration section “gc_ri41”
6) **AnalyzeSHC** – optional additional ground check using a SHC and further reference sensors
   ↦ module “modAnalyzeChamber” using configuration section “shc”
7) **AnalyzeShelter** – optional additional ground check outside in a shelter using further reference sensors
   ↦ module “modAnalyzeChamber” using configuration section “shelter”
8) **IntHumTempCalibration** – estimate calibration uncertainty of internal temperature of relative humidity
   ↦ module “modCalibrationUncertainty” using configuration section “int_hum_temp_cal”
9) **HumidityCalibration** – estimate calibration uncertainty of relative humidity
   ↦ module “modCalibrationUncertainty” using configuration section “humid_cal”
10) **HumidityTimelagCorr** – apply time-lag correction of relative humidity
    ↦ module “modRHTimelagCorrection” using configuration section “rh_timelag”
11) **RecalculateHumidity** – recalculate relative humidity at air temperature
    ↦ module “modComputeHumidity” using configuration section “calc_humid”
12) **SmoothHumidity** – light smoothing of relative humidity
    ↦ module “modSmoothVariable” using configuration section “smooth_humid”
13) **FinaliseHumidity** – finalise relative humidity incl. correction and uncertainty
    ↦ module “modFinaliseHumidity” using configuration section “final_rh”
14) **CalculateAlternativeHumidity** – derive several alternative humidity variables including a transfer of uncertainties
    ↦ module “modComputeAlternativeHumidity” using configuration section “calc_humid_alt”
15) **CalcIWV** – calculate integrated column of water vapour inclusive an estimation of uncertainty
    ↦ module “modComputeIntegratedWaterVapour” using configuration section “calc_iwv”

## Wind (all details)

Variables longitude and latitude are used as base variables.

1) **ComputeWindComponents** – compute zonal and meridional wind components
   ↦ module “modComputeWindComponents” using configuration section “compute_wind_comp”
2) **PreCheckZonalWind** – raw data check of zonal wind component
   ↦ module “modDetectNaNAndOutlier” using configuration section “precheck_zonal_wind”
3) **PreCheckMeridionalWind** – raw data check of meridional wind component
   ↦ module “modDetectNaNAndOutlier” using configuration section “precheck_meridional_wind”
4) **WindparameterRetrieval** – compute a retrieval of all required wind variables including an estimation of uncertainties
   ↦ module “modWindRetrieval” using configuration section “wind_retrieval”

# D Additional discussion on GPS positioning within the RS41 system

This appendix includes additional information on the GPS observations, as implemented within the RS41 radiosonde.

## D.1 Pseudorange observations of GPS satellites

The pseudorange measurements represent the apparent signal travel distance between a GPS satellite and the RS41 GPS receiver. The receiver generates a replica of the transmitted satellite code and aligns it with the received signal. The time difference between the two codes is the apparent travel time of the signal. It is then combined with additional information from the satellite's navigation data to obtain the actual travel time from the satellite to the receiver, which is then multiplied with the speed of light to obtain the pseudorange between the satellite and the receiver. The obtained pseudorange differs from the actual distance between the transmitter and receiver, since the signal is subject to delays in the atmosphere as well as to the unknown receiver and satellite clock offsets.

The simplified pseudorange equation, describing the distance between the satellite and receiver takes the following form:

$$p_{\mathrm{r}}^{\mathrm{s}}(t) = \rho_{\mathrm{r}}^{\mathrm{s}}(t) + c(dt_{\mathrm{r}} + dt^{\mathrm{s}} + \delta t^{\mathrm{rel}}(t)) + I_{\mathrm{r}}^{\mathrm{s}}(t) + T_{\mathrm{r}}^{\mathrm{s}}(t) + \epsilon_{\mathrm{r}}^{\mathrm{s}}(t), \tag{D.1}$$

where $p_{\mathrm{r}}^{\mathrm{s}}(t)$ is the pseudorange, $\rho_{\mathrm{r}}^{\mathrm{s}}(t)$ is the actual distance between the satellite and the receiver, $dt_{\mathrm{r}}$ and $dt^{\mathrm{s}}$ are the clock offsets, $\delta t^{\mathrm{rel}}(t)$ are relativistic corrections, $I$ and $T$ are the ionospheric and tropospheric delays and $\epsilon_{\mathrm{r}}^{\mathrm{s}}(t)$ are residuals, such as antenna-related errors, instrumental delays, noise and multipath.

The raw observations, recorded by the MW-41 system, contain the "GpsRawChannelData" table, where the pseudoranges from the u-blox receiver onboard the RS41 radiosonde are stored together with the Pseudo-random Noise (PRN) identifiers of each satellite slot in the GPS constellation. The receiver has 48 channels to track satellites, but the message sent by the RS41 radiosonde to the ground station is limited to pseudoranges from up to 12 satellites.

In order to analyse the pseudorange data, a ground experiment flight simulation on 15 March 2021 was performed. Two RS41 radiosondes were mounted on a high mast with 1 m distance in between and recorded data for 1.5 h. Both radiosondes were oriented in the same direction. The observed data comprises records from a total of 16 satellites and is used to determine the stability of the measured pseudoranges. The pseudorange raw data contains receiver related artefacts, such as jumps, caused by receiver clock slips (see Fig. D.1).

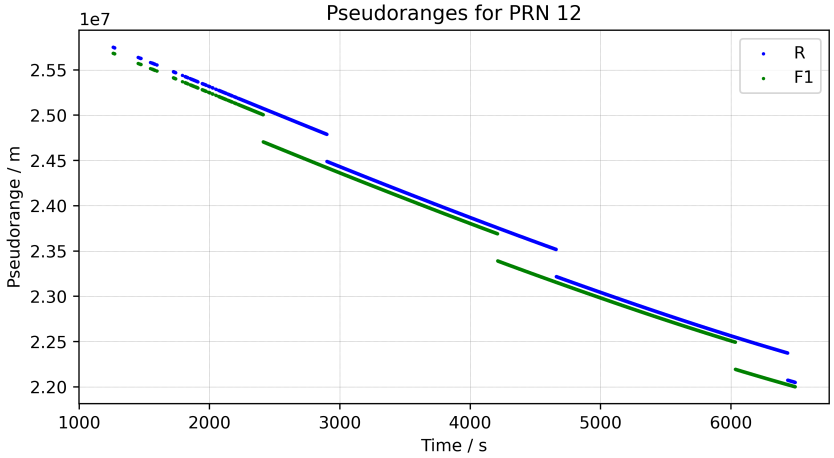


**Figure D.1:** Raw pseudorange observations from PRN 12 from a ground experiment with two RS41 sondes. The indicated pseudoranges between the satellite and the receivers are in the range of 22 000 km to 26 000 km. The jumps in the pseudorange datasets are caused by recalibrations of the receiver's clocks. Each receiver clock is recalibrated independently. The PRN 12 satellite is rising during the observation period, which is indicated by the range shortening.

The raw pseudoranges are then detrended to determine the standard deviation of the observations (see Fig. D.2). The de-trended values from both sondes are in good agreement for almost all satellites. The standard deviations of the residual pseudoranges from most satellites are within 1 m. These results are in agreement with the results for the vertical and horizontal static uncertainties for the calculated positions, presented in Section 4.4.1.1. The difference between the 'R' and 'F1' radiosondes demonstrates, that each of these two ground stations synchronises its time with the GPS time independently. If both radiosondes were equipped with atomic clocks, or the data was reprocessed with IGS orbits and clocks, these PRN differences and jumps would not appear.

The location data, available in the final product are not GRUAN-reprocessed. The analysis of the pseudorange data was conducted to validate the static receiver experiments described in Section 4.4.1.1. The pseudorange observations from the RS41 can be used to calculate the position of the radiosonde, as well as to calculate the uncertainties (see also Appendix D.2), related to the atmospheric, instrumental and clock delays, included in the pseudorange equation.

## D.2 Dilution of Precision (DOP) measurements

The estimated position of the observer (called fix) using the GPS system is triangulated from the pseudoranges of multiple GPS satellites. There are two distinct effects, which have to be accounted for when computing the uncertainty of the positioning. The first one is the random errors, coming from the pseudorange ambiguities, briefly described in Appendix D.1. The second is the geometry of the GPS constellation during the fix.

When the satellites, used to acquire the fix, are located in a small solid angle, the intersection of their pseudoranges together with the uncertainties is much larger, than when the satellites

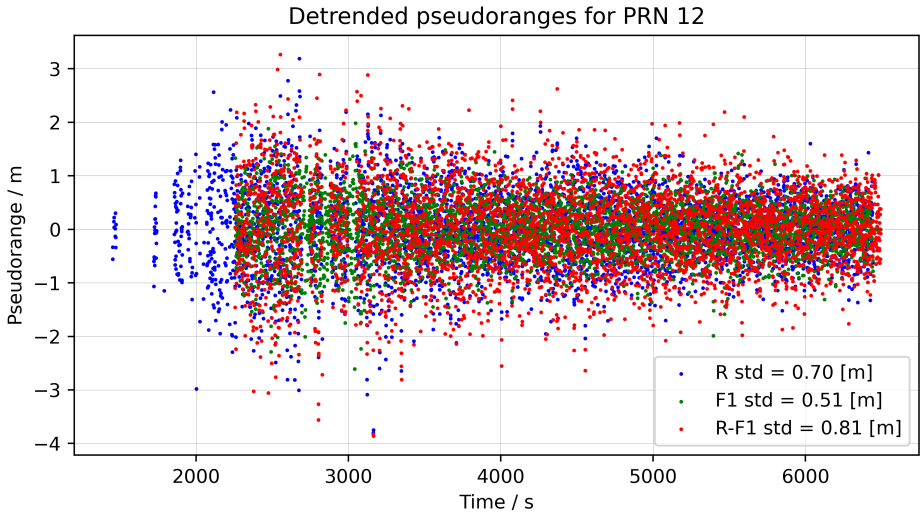


**Figure D.2:** Residuals of detrended pseudoranges from PRN 12 from a ground experiment with RS41. The observed standard deviation of the pseudoranges from both the 'R' and 'F1' SPS are within the expected.

are spread at larger solid angles (see Figure D.3). The Dilution of Precision (DOP) parameters represent the size of the intersection volume of all satellites, used for each fix.

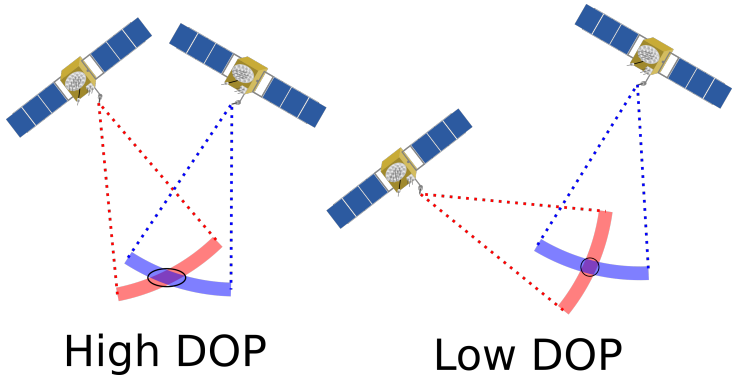


**Figure D.3:** The left scheme shows two GPS satellites, appearing from small angle from the point of view of the observer in the black circle. This is a situation with low precision of the position, when the intersection between the distances between the satellites and the observer are large, leading to high DOP. The right scheme represents large angle between the GPS satellites, when the aforementioned intersection is small, leading to higher precision and low DOP.

The u-blox chip onboard the radiosonde calculates the Dilution of Precision (DOP) parameters of the position. The DOP parameters indicate how close is the estimated uncertainty of the positioning measurement when compared to the nominal uncertainty, provided by the receiver.

There are several characteristics of the DOP, separated by direction and time:

- TDOP - time DOP,
- PDOP - position DOP, which is further divided into

- VDOP - vertical DOP,
- HDOP - horizontal DOP.

All of these DOP parameters have a minimum value of less than one, which indicates large spread between the GPS satellites, used for the position fix and a maximum value of above 5 (in practice the maximum DOP value is infinite) with an average value in the interval between 1 and 2.

## D.3 Derivation of uncertainty of pressure from GPS altitudes

For the calculation of the uncertainty of pressure from GPS height, the barometric equation can be presented as a function of the differences of all height measurements up to the point (altitude) $i$:

$$p_i = p_{i-1} \exp\left\{ \frac{-g_i(h_i - h_{i-1})}{R_\mathrm{d} T_{\mathrm{v},i}} \right\}. \tag{D.2}$$

Starting from an initial value $p_0$, which is defined separately, $p_i$ can also be formulated as a sum over all height layers:

$$p_i = p_0 \exp\left\{ \frac{-1}{R_\mathrm{d}} \left[ \frac{g_1(h_1 - h_0)}{T_{\mathrm{v},1}} + ... + \frac{g_j(h_j - h_{j-1})}{T_{\mathrm{v},j}} + ... + \frac{g_i(h_i - h_{i-1})}{T_{\mathrm{v},i}} \right] \right\}, \tag{D.3}$$

where $i \geq 1$ and $1 \leq j \leq i$. With $p_0$, $h_j$, $T_{\mathrm{v},j}$ introducing uncertainties and assuming that these uncertainties are statistically independent, the combined uncertainty is

$$u^2(p_i) = \left( \frac{\partial p_i}{\partial p_0} u(p_0) \right)^2 + \left( \frac{\partial p_i}{\partial h_0} u(h_0) \right)^2 + \left( \frac{\partial p_i}{\partial h_i} u(h_i) \right)^2 + \sum_{j=1}^{i-1} \left( \frac{\partial p_i}{\partial h_j} u(h_j) \right)^2 + \sum_{j=1}^{i} \left( \frac{\partial p_i}{\partial T_{\mathrm{v},j}} u(T_{\mathrm{v},j}) \right)^2, \tag{D.4}$$

by applying Gaussian error propagation. From that, Eq. (4.53) follows. In Eq. (D.3), $h_0$ and $h_i$ each appear once, whereas the $h_j$ with $1 \leq j \leq i$ appear twice each, which is why the terms for $h_0$ and $h_i$ are separate in Eq. (D.4). Note that the uncertainty of the GPS-based launch altitude, $u(h_0)$, consists of two components $u^2(h_0) = u'^2(h_0) + \sigma^2(h_0)$. The first is a component related to the vertical dilution of precision (VDOP) of the GPS measurement (Section D.2). It is available from Vaisala's MWX sounding file. As shown in Fig. 4.20, this component has strong systematic pattern, however may considerably vary from sounding to sounding. As estimate of the VDOP-related share of $u'(h_0)$, the median of the 100 lowermost $u'$ is taken. This launch point-related component may contribute considerably to the overall uncertainty, in the same way to each point in the profile due to its systematic nature. The second, $\sigma(h_0)$, corresponds to the random component that is experimentally determined (Section 4.4.1.1) and applies to each altitude point in the profile.

Considering a possible altitude difference of the location of a station's installed reference barometer and the launch site, $\Delta h_\mathrm{sb} = h_0 - h_\mathrm{sb}$, the pressure at the launch site is related to the pressure

of station barometer:

$$p_0 = p_{\mathrm{sb}} \exp\left(\frac{-g_0 \cdot \Delta h_{\mathrm{sb}}}{R_{\mathrm{d}} \cdot T_{\mathrm{v}}}\right), \tag{D.5}$$

with uncertainties introduced from pressure and altitude of the station barometer ($u(p_{\mathrm{sb}})$ and $u(h_{\mathrm{sb}})$, respectively), and the above two components ($u'(h_0)$ and $\sigma(h_0)$) from the GPS-based launch altitude $h_0$, with that:

$$u^2(p_0) = \left(\frac{\partial p_0}{\partial p_{\mathrm{sb}}} u(p_{\mathrm{sb}})\right)^2 + \left(\frac{\partial p_0}{\partial h_0} u'(h_0)\right)^2 + \left(\frac{\partial p_0}{\partial h_0} \sigma(h_0)\right)^2 + \left(\frac{\partial p_0}{\partial h_{\mathrm{sb}}} u(h_{\mathrm{sb}})\right)^2, \tag{D.6}$$

or in explicit form

$$u^2(p_0) = p_0^2 \cdot \left\{ \left(\frac{u(p_{\mathrm{sb}})}{(p_{\mathrm{sb}})}\right)^2 + \left(\frac{-g_0}{R_d T_{\mathrm{v},0}} u'(h_0)\right)^2 + \left(\frac{-g_0}{R_d T_{\mathrm{v},0}} \sigma(h_0)\right)^2 + \left(\frac{g_0}{R_d T_{\mathrm{v},0}} u(h_{\mathrm{sb}})\right)^2 \right\}. \tag{D.7}$$

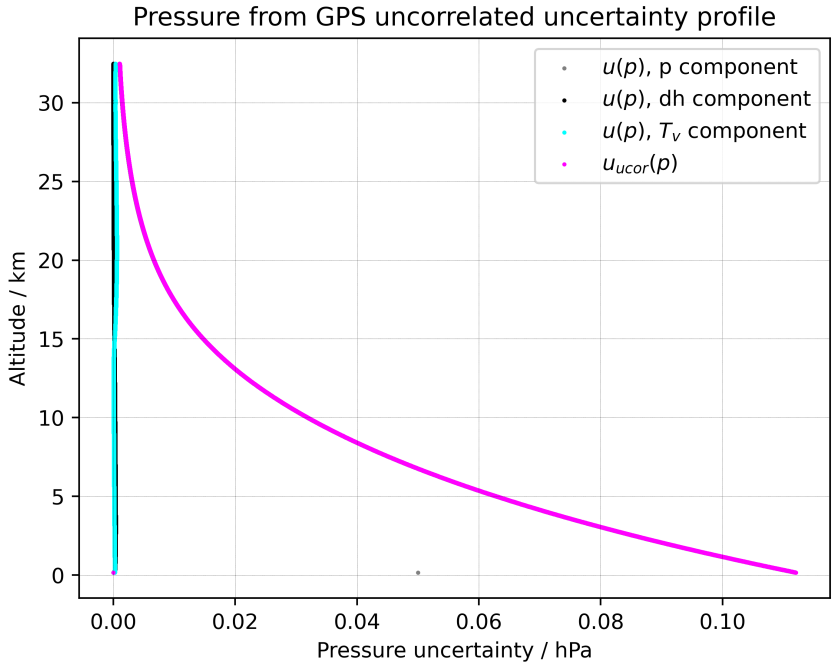


**Figure D.4:** Profiles of uncorrelated pressure uncertainty components ($k = 1$) on 24 June 2016, 12 UTC, at Lindenberg Observatory. The black curve indicates the contribution of the $\Delta h$ component, the cyan curve that of the virtual temperature, and the grey curve (covered by the magenta curve denoting the combined uncorrelated uncertainty) the dominant contribution of the pressure at launch point uncertainty.

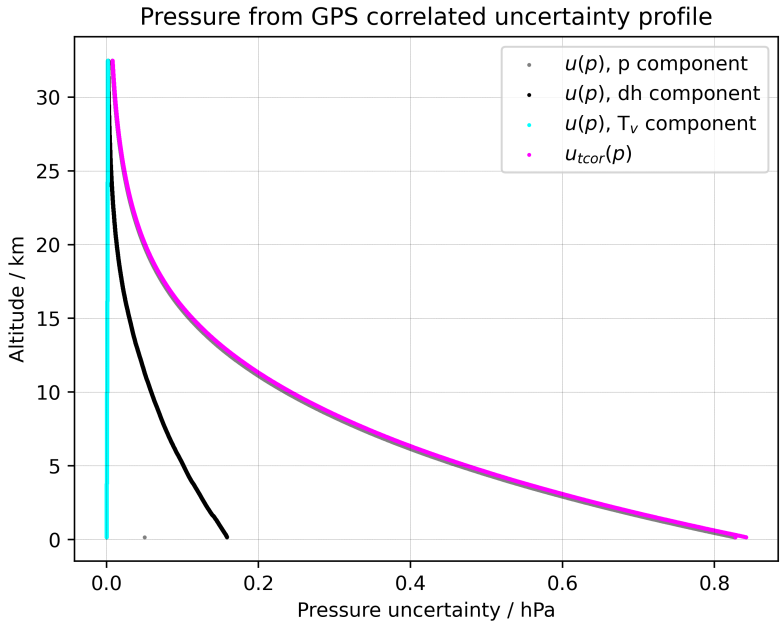


**Figure D.5:** Profiles of correlated pressure uncertainty components ($k = 1$) for 24 June 2016, 12 UTC, at Lindenberg Observatory. The black curve indicates the contribution of the $\Delta h$ component, the cyan curve that of the virtual temperature, and the grey curve the dominant contribution of the pressure at launch point uncertainty.

# E File Content

## E.1 Possible content structure of MD files

The following list shows the currently possible structure of MD files (see Section 7.2.3):

- *File* group includes attributes BaseRequest, CreatedBy, Timestamp, Type, TypeVersion
- *Measurement* group includes subgroups and attributes BalloonNo, Equipment, Id, InternalKey, IsExperiment, IsOld, IsTest, IssueDate, OldId, Operator, ScheduleDate, Status, Version, and a list of properties starting with p.
  - *Balloon* group includes attributes FillingWeight, Gas, Key, Manufacturer, Several
  - *BaseFile* group includes attributes ArchiveFileId, DpsPartId, DpsPartNo, Id, Name, Size, Type
  - *BaseProductItem* group includes attributes ArchiveFileId, DpsPartId, DpsPartNo, FullKey, Id, Name, Product, Type, Version
  - *Checks* contains a list of all checks stored with a number (0., 1., ...). Each check includes attributes CheckDate, CheckType, CheckedPartId, CheckedSN, CheckedType, CheckedPartNo, Id, ToolPartId, ToolPartNo, ToolSN, ToolType, and a list of properties starting with p.
  - *Dps* group includes attributes Family, Key, Manufacturer, MsaKey, Name, PartId, PartNo, SerialNumber, Type, and a list of properties starting with p.
  - *Equipment* group includes attributes FullStringLength, GrossWeight, Payload
  - *Files* contains a list of all files stored with a number (0., 1., ...). Each file includes attributes ArchiveFileId, DpsPartId, DpsPartNo, Id, Name, Size, Type
  - *MainSonde* group includes attributes Family, IsExperiment, Key, Name, Manufacturer, PartId, PartNo, SerialNumber, Type, and a list of properties starting with p.
    - List of all *checks* are stored with a special group (*Check_1*, *Check_2*, ...). Each check includes attributes CheckDate, CheckType, ToolPartId, ToolSN, ToolPartNo, ToolType, and a list of properties starting with p.
  - *Parachute* group includes attributes Diameter, Key, Several
  - *Parts* contains a list of all parts stored with a number (0., 1., ...). Each part includes attributes Id, Instrument, InstrumentFamily, InstrumentName, InstrumentType, Manufacturer, MsaKey, SerialNumber, (SondePartIds), (DpsPartIds), Type, and a list of properties starting with p.
  - *ProductItems* contains a list of all product items stored with a number (0., 1., ...).

Each product item includes attributes ArchiveFileId, DpsPartId, DpsPartNo, Id, Name, Product, Type, Version

  - *Rig* group includes attributes Key, Several
  - *TelemetrySonde* group includes attributes Family, Key, Manufacturer, Name, PartId, PartNo, SerialNumber, Type, and a list of properties starting with p.
  - *Unwinder* group includes attributes Key, Length, Several
- *Setup* group includes attributes Id, Key, Name, TypeKey, TypeName
- *Station* group includes attributes Altitude, Id, Key, Latitude, Longitude, Name, OperatedBy, WmoCode, WmoName
- *System* group includes attributes Altitude, Id, Key, Latitude, Longitude, Name, OperatedBy, Type

## E.2 Available tables in Zipped MW41 sounding archive file (MWX) files

List of tables which can be contained in a MWX file, documented in MW41 Technical Reference. Only some of these tables are included by default:

- *AdditionalSensorData* – [data] Contains additional sensor data from the radiosonde.
- *AdditionalSoundingInformation* – [md] Contains additional sounding information used for flight summary.
- *AutosondeEventCustomData* –
- *AutosondeEvents* –
- *CalculatedOzone* – [data] Contains calculated ozone data (ozone layer data with pressure correction applied).
- *GCCORRECTIONS* – [md] Contains ground check corrections. (see Table E.9)
- *GSupport* – [data] Contains raw data of heated humidity sensor. (see Table E.4)
- *GpsRawChannelData* – [data] Contains radiosonde-specific information on the tracked satellites.
- *GpsRawMeasurements* – [data] Contains GPS raw measurements (both local and remote). (see Table E.3)
- *GpsResults* – [data] Contains GPS result data from any type of GPS calculation. (see Table E.2)
- *GroundCheckValues* – [md]
- *IonoCorrections* – [data, internal] Contains ionosphere correction parameters.
- *MessageCounters* – Contains message send counter data.
- *MessageInformation* – Contains message information data.

- *MessageParameters* – Contains sounding-specific parameters for message generation.
- *MessageTransmissionInfo* – Contains message transmission information.
- *MessageTransmissionLog* – Contains information about each message transmission.
- *OifParameters* – [md] Contains OIF92 or OIF411 ozone parameters.
- *OzoneResults* – [md] Contains the ozone results (summary of calculated ozone data).
- *PtuResults* – [data] Contains the sounding's PTU results. (see Table E.5)
- *RadioDiagnostics* – [data] Contains software radio diagnostics data.
- *Radiosondes* – [md] Contains information about the found radiosondes. (see Table E.8)
- *RawOzone* – [data] Contains raw ozone data (ozone layer data without pressure correction).
- *RawPtu* – [data] Contains raw PTU results. (see Table E.1)
- *RdfResult* – [data] Contains RDF results.
- *RS92SpecialSensorData* – [data] Contains RS92 special sensor data.
- *SatelliteOrbit* – [data] Contains satellite ephemeris or almanac data.
- *SatelliteStatus* – [data] Contains information on satellites tracked by local and radiosonde GPS receivers.
- *SignificantLevels* – Contains significant level information.
- *SoundingMetadata* – [md] Contains metadata values that were related to the sounding.
- *SoundingParameters* – [md] Contains parameter values that were used in the sounding.
- *Soundings* – [md] Contains general information about a sounding. (see Table E.7)
- *StabilityIndex* – [md]
- *StdPressureLevels* – Contain standard pressure levels.
- *SurfaceObservations* – [md] Contains surface observations data. (see Table E.10)
- *SurfaceWeather* – [md] Contains AWS surface weather observation data.
- *SynchronizedSoundingData* – [data] Contains synchronized sounding data. Wind and height are interpolated to PTU time. (see Table E.6)
- *SystemEvents* – [md] Contains sounding's system events.
- *TelemetryData* – [data] Contains radiosonde's telemetry frame.
- *VersionInfo* – Contains the device's version data.
- *WindResults* – [data] Contain filtered wind values.

List of general columns, which are part of most tables:

- *SoundingIdPk* – Randomly generated, unique sounding ID.
- *DataSrvTime* – Data server timestamp [yyyy-MM-dd HH:mm:ss.fff].
- *RadioRxTimePk* – Radiosonde time [s].

**Note:** Missing values are designated differently depending on the data type. In case of numbers (double, integer) the following number is mostly used: '-32768'. In the case of other data types, such as string, the designation 'NULL' occurs, among others.

## E.3 Details of relevant tables in Zipped MW41 sounding archive file (MWX) files

In the following, detailed descriptions of the tables, which are used in the GRUAN processing, are listed:

- *INT1* – Data table 'RawPtu' is mandatory, and the processing stops if not available, see Table E.1
- *INT2* – Data table 'GpsResults' is mandatory, and the processing stops if not available, see Table E.2
- *INT3* – Data table 'GpsRawMeasurements' is mandatory, and the processing stops if not available, see Table E.3
- *INT4* – Data table 'GSupport' is required, but a workaround is implemented if not available, see Table E.4
- *INT5* – Data table 'PtuResults' is optional, and is only used to create comparison plots, see Table E.5
- *INT6* – Data table 'SynchronizedSoundingData' is optional, and is only used to create comparison plots, see Table E.6
- Meta-data table 'Soundings' is mandatory, see Table E.7
- Meta-data table 'Radiosondes' is mandatory, see Table E.8
- Meta-data table 'GCCORRECTIONS' is mandatory, see Table E.9
- Meta-data table 'SurfaceObservations' is mandatory, see Table E.10

**Table E.1:** List of all data columns of table **RawPtu** (INT1) of a MWX file.

| № | Name | Type | Unit | Description |
|---|---|---|---|---|
| 1 | SoundingIdPk | string | – | Randomly generated, unique sounding ID. |
| 2 | RadioRxTimePk | double | s | Radio time [s]. |
| 3 | DataSrvTime | dateTime | – | Data server timestamp [yyyy-MM-dd HH:mm:ss.fff]. |
| 4 | Pressure | double | hPa | Pressure [hPa]. |
| 5 | Temperature | double | K | Temperature [Kelvin] |

*This table is continued on the next page.*

Table E.1 – *Continued from previous page*

| № | Name | Type | Unit | Description |
|---|---|---|---|---|
| 6 | Humidity1 | double | % | **RS92**: Humidity values of sensor 1 [%]. **RS41**: Humidity value of sensor [%]. |
| 7 | Humidity2 | double | % | **RS92**: Humidity values of sensor 2 [%]. **RS41**: Missing data. |
| 8 | AscentRate | double | m/s | Ascent rate [m/s]. |
| 9 | PressureOk | boolean | – | Pressure quality indicator. True if value is OK. |
| 10 | TemperatureOk | boolean | – | Humidity quality indicator. True if value is OK. |
| 11 | HumidityOk | boolean | – | Temperature quality indicator. True if value is OK. |

**Table E.2:** List of all data columns of table **GpsResults** (INT2) of a MWX file.

| № | Name | Type | Unit | Description |
|---|---|---|---|---|
| 1 | SoundingIdPk | string | – | Randomly generated, unique sounding ID. |
| 2 | RadioRxTimePk | double | s | Radio time [s]. |
| 3 | DataSrvTime | dateTime | – | Data server timestamp [yyyy-MM-dd HH:mm:ss.fff]. |
| 4 | GpsWeek | integer | w | GPS week. |
| 5 | GpsSeconds | double | s | GPS seconds. |
| 6 | GeometricHeight-FromSeaLevel | double | m | Geometric height from sea level [m]. |
| 7 | GeopotHeight | double | m | Geopotential height [m]. |
| 8 | ClockDrift | double | s | Remote clock drift [s]. |
| 9 | PosResidual | double | m | Position residual. |
| 10 | VelResidual | double | m/s | Velocity residual. |
| 11 | VelocityNorth | double | m/s | Radiosonde north velocity. |
| 12 | VelocityEast | double | m/s | Radiosonde east velocity. |
| 13 | VelocityUp | double | m/s | Radiosonde up velocity. |

*This table is continued on the next page.*

Table E.2 – *Continued from previous page*

| Nº | Name | Type | Unit | Description |
|---|---|---|---|---|
| 14 | WindSolutionStatus | integer | – | Wind solution status:<br>**0** = Undefined,<br>**1** = NoMeasurementData,<br>**2** = BadSigma4d,<br>**3** = TooFewSatellites,<br>**4** = IterationFailed,<br>**5** = GpsStationPositionNot-Initialized,<br>**6** = PreviousResult,<br>**7** = CalculationFailed,<br>**8** = Autonomous,<br>**9** = Differential,<br>**10** = Generated |
| 15 | Wgs84Latitude | double | deg_N | Radiosonde WGS84 latitude position. |
| 16 | Wgs84Longitude | double | deg_E | Radiosonde WGS84 longitude position. |
| 17 | Wgs84Altitude | double | m | Radiosonde WGS84 altitude position. |
| 18 | Wgs84X | double | m | Radiosonde X position. |
| 19 | Wgs84Y | double | m | Radiosonde Y position. |
| 20 | Wgs84Z | double | m | Radiosonde Z position. |
| 21 | NeuNorth | double | m | Radiosonde north distance from the station position. |
| 22 | NeuEast | double | m | Radiosonde east distance from the station position. |
| 23 | NeuUp | double | m | Radiosonde up distance from the station position. |
| 24 | HDOP | double | – | Horizontal dilution of precision. |
| 25 | VDOP | double | – | Vertical dilution of precision. |
| 26 | PDOP | double | – | Position dilution of precision. |
| 27 | TDOP | double | – | Time dilution of precision. |
| 28 | GDOP | double | – | Geometry dilution of precision. |

**Table E.3:** List of all data columns of table **GpsRawMeasurements** (INT3) of a MWX file.

| № | Name | Type | Unit | Description |
|---|---|---|---|---|
| 1 | SoundingIdPk | string | – | Randomly generated, unique sounding ID. |
| 2 | RadioRxTimePk | double | s | Radio time [s]. |
| 3 | ReceiverRolePk | string | – | Specifies the role of the receiver in calculation (Local or Remote). |
| 4 | ReceiverType | string | – | Specifies the possible types of GPS receiver: AstechG12, VaisalaRS92, SiRF, uBlox4, uBlox5, uBlox6, Unknown |
| 5 | DataSrvTime | dateTime | – | Data server timestamp [yyyy-MM-dd HH:mm:ss.fff]. |
| 6 | GpsWeek | integer | w | GPS week. |
| 7 | GpsSeconds | double | s | GPS seconds. |
| 8 | Wgs84Latitude | double | deg_N | Radiosonde WGS84 latitude position. |
| 9 | Wgs84Longitude | double | deg_E | Radiosonde WGS84 longitude position. |
| 10 | Wgs84Altitude | double | m | Radiosonde WGS84 altitude position. |
| 11 | VelocityX | double | m/s | X velocity in XYZ coordinates. |
| 12 | VelocityY | double | m/s | Y velocity in XYZ coordinates. |
| 13 | VelocityZ | double | m/s | Z velocity in XYZ coordinates. |
| 14 | NumberOf-SatellitesUsed | integer | – | Number of satellites used in calculation. |
| 15 | PosAccuracy-Estimate | double | – | Position accuracy estimate. |
| 16 | PDop | double | – | Position dilution of precision. |
| 17 | Gain | integer | – | Gain read from message UBX-MON PT. |

**Table E.4:** List of all data columns of table **GSupport** (INT4) of a MWX file.

| № | Name | Type | Unit | Description |
|---|---|---|---|---|
| 1 | SoundingIdPk | string | – | Randomly generated, unique sounding ID. |
| 2 | RadioRxTimePk | double | s | Radio time [s]. |
| 3 | DataSrvTime | dateTime | – | Data server timestamp [yyyy-MM-dd HH:mm:ss.fff]. |
| 4 | GU | double | % | Internal humidity of heated sensor. |
| 5 | GUT | double | K | Internal temperature of heated humidity sensor. |

**Table E.5:** List of all data columns of table **PtuResults** (INT5) of a MWX file.

| № | Name | Type | Unit | Description |
|---|---|---|---|---|
| 1 | SoundingIdPk | string | – | Randomly generated, unique sounding ID. |
| 2 | RadioRxTimePk | double | s | Radio time [s]. |
| 3 | DataSrvTime | dateTime | – | Data server timestamp [yyyy-MM-dd HH:mm:ss.fff]. |
| 4 | SensorPressure | double | hPa | Sensor pressure [hPa]. |
| 5 | PressureFromHeight | double | hPa | Pressure calculated from height [hPa]. |
| 6 | Temperature | double | K | Temperature [K] |
| 7 | Humidity | double | % | Humidity [%] |
| 8 | Height | double | m | Height [m] |
| 9 | HeightFromGps | double | m | Height from GPS [m] |

*This table is continued on the next page.*

Table E.5 – *Continued from previous page*

| Nº | Name | Type | Unit | Description |
|---|---|---|---|---|
| 10 | Status | integer | – | Status flags:<br>**0x100000** = PressureReady,<br>**0x200000** = HeightReady,<br>**0x300000** = PressureAndHeight-Ready,<br>**0x40000** = TemperatureReady,<br>**0x80000** = HumidityReady,<br>**0xF0000** = PtuAndHeightReady,<br>**1** = PressureInterpolated,<br>**2** = HeightInterpolated,<br>**4** = TemperatureInterpolated,<br>**8** = HumdityInterpolated,<br>**16** = TelemetryBreak,<br>**32** = AdiabticCheckFailed,<br>**64** = PressureFromHeight-Interpolated |

**Table E.6:** List of all data columns of table **SynchronizedSoundingData** (INT6) of a MWX file.

| Nº | Name | Type | Unit | Description |
|---|---|---|---|---|
| 1 | SoundingIdPk | string | – | Randomly generated, unique sounding ID. |
| 2 | RadioRxTimePk | double | s | Radio time [s]. |
| 3 | DataSrvTime | dateTime | – | Data server timestamp [yyyy-MM-dd HH:mm:ss.fff]. |
| 4 | Pressure | double | hPa | Pressure [hPa] |
| 5 | Temperature | double | K | Temperature [Kelvin] |
| 6 | Humidity | double | % | Humidity [%] |
| 7 | WindDir | double | deg | Meteorological wind direction (opposite to air molecule movement) [deg]. |
| 8 | WindSpeed | double | m/s | Wind speed [m/s]. |
| 9 | WindNorth | double | m/s | Wind speed (molecule movement) north component [m/s]. |

*This table is continued on the next page.*

Table E.6 – *Continued from previous page*

| № | Name | Type | Unit | Description |
|---|---|---|---|---|
| 10 | WindEast | double | m/s | Wind speed (molecule movement) east component [m/s]. |
| 11 | Height | double | gpm | Geopotential height calculated from PTU or measured height [gpm]. (following height columns were available in earlier versions: HeightFromPtu, HeightFromGps) |
| 12 | GeometricHeight | double | m | Geometric height calculated from PTU or measured height [m]. |
| 13 | PtuStatus | integer | – | PTU status flags: **1** = PressureInterpolated, **2** = HeightInterpolated, **4** = TemperatuInterpolated, **8** = HumdityInterpolated, **16** = TelemetryBreak, **32** = AdiabaticCheckFailed, **64** = PressureFromHeightInterpolated |
| 14 | WindInterpolated | boolean | – | Wind status. If true, wind is marked as interpolated. |
| 15 | Latitude | double | deg_N | Radiosonde latitude [deg]. |
| 16 | Longitude | double | deg_E | Radiosonde longitude [deg]. |
| 17 | North | double | m | Radiosonde north distance [m]. |
| 18 | East | double | m | Radiosonde east distance [m]. |
| 19 | Up | double | m | Radiosonde up distance [m]. |
| 20 | Altitude | double | m | Radiosonde WGS84 altitude [m]. |
| 21 | Dropping | integer | – | True if data is from a dropping (descending) sounding. |

**Table E.7:** List of data columns of table **Soundings** of a MWX file. This table contains metadata, that means one row for one sounding.

| № | Name | Type | Unit | Description |
|---|---|---|---|---|
| 1 | IdPk | string | – | Randomly generated, unique sounding ID. |

*This table is continued on the next page.*

Table E.7 – *Continued from previous page*

| Nº | Name | Type | Unit | Description |
|---|---|---|---|---|
| 2 | BeginTime | dateTime | – | Beginning of sounding in UTC time (time of launch when launch has happened) [yyyy-MM-dd HH:mm:ss.fff]. |
| 3 | LaunchTime | double | s | Sounding launch radio time [s]. |
| 4 | Duration | double | s | Sounding duration [s]. |
| 5 | ArchiveRecalculationTime | dateTime | – | |
| 6 | Height | double | gpm | Station geopotential height [gpm]. |
| 7 | Altitude | double | m | Station geometric altitude from mean sea level [m]. |
| 7 | Latitude | double | deg_N | Station latitude [deg]. |
| 8 | Longitude | double | deg_E | Station longitude [deg]. |
| 9 | RadioResetTime | dateTime | – | UTC time of radio time reset [yyyy-MM-dd HH:mm:ss.fff] |
| 10 | MinPressure | double | hPa | Sounding's minimum pressure [hPa]. |
| 11 | MaxAltitude | double | m | Sounding's maximum altitude [m]. |
| 12 | AscentRate | double | m/s | Sounding's average ascent rate [m/s]. |
| 13 | AscentRateSurfaceTo400hPa | double | m/s | |
| 14 | AscentRate400hPaToTermination | double | m/s | |

*This table is continued on the next page.*

Table E.7 – *Continued from previous page*

| Nº | Name | Type | Unit | Description |
|---|---|---|---|---|
| 15 | ReasonForTermination | integer | – | Reason for sounding termination:<br>**0** = Unknown,<br>**1** = IncreasingPressure,<br>**2** = ManualStop,<br>**3** = BatteryLow,<br>**4** = KillerTimeOut,<br>**5** = TemperatureSensorFailure,<br>**6** = PressureSensorFailure,<br>**7** = HumiditySensorFailure,<br>**8** = SondeSignalLost,<br>**9** = UnknownRadiosonde,<br>**10** = PtuFilteringStopped,<br>**11** = HumidityTemperatureSensorFailure,<br>**12** = PreparationFailed,<br>**13** = SondeDisonnected,<br>**14** = SystemShutdown,<br>**15** = UnsupportedRadiosonde,<br>**16** = PtuSensorFailure,<br>**17** = RadioFailure |
| 16 | FailureReason | integer | – | Reason for sounding failure flags:<br>**0x00** = Unknown or no failure,<br>**0x01** = In-built functional temperature check failed,<br>**0x02** = In-built functional humidity check failed,<br>**0x04** = Ground check pressure difference limit was exceeded,<br>**0x08** = Ground check temperature difference limit was exceeded,<br>**0x10** = Ground check humidity difference limit was exceeded,<br>**0x20** = Other failure reported by radiosonde,<br>**0x40** = Preparation initialisation failed,<br>**0x80** = Radiosonde was disconnected before end of preparation,<br>**0x100** = Radio signal lost,<br>**0x200** = Support for used radiosonde requires a license which the system does not have. |

*This table is continued on the next page.*

Table E.7 – *Continued from previous page*

| Nº | Name | Type | Unit | Description |
|---|---|---|---|---|
| 17 | FailureDetails | string | – | Details about the sounding failure. |
| 18 | TelemetryNoiselevel | double | – | Average telemetry noise level. |
| 19 | MeanSatellite-TrackCount | double | – | Mean satellite track count. |
| 22 | AltitudeOffset | double | m | Launch site altitude offset [m]. |
| 23 | DirectionOffset | double | deg | Launch site direction offset [deg]. |
| 24 | DistanceOffset | double | m | Launch site distance offset [m]. |
| 25 | SoftwareVersion | string | – | Software version of the system performing the sounding. |
| 26 | AltitudeConfidence | integer | – | Altitude confidence value for the sounding. |
| 27 | StationName | string | – | Sounding station name. |
| 28 | SystemName | string | – | Sounding system name. |
| 29 | BarometerOffset | double | m | Barometer offset from the station height [m]. |
| 30 | GpsAntennaOffset | double | m | GPS antenna offset from the station height [m]. |
| 31 | ContinueDescending | boolean | – | If true, continues sounding with descending data. |
| 32 | SsdRate | integer | s | Synchronized sounding data rate [s]. |
| 33 | Status | integer | – | Successful sounding criteria check result flags:<br>**0** = Ok,<br>**1** = PressureNotReached,<br>**2** = HeightNotReached,<br>**4** = TimeNotReached,<br>**8** = WindNotContinuous,<br>**16** = PressureNotContinuous,<br>**32** = TemperatureNotContinuous,<br>**64** = HumidityNotContinuous |
| 34 | SpecialSensorType | integer | – | Special sensor type:<br>**0** = None,<br>**1** = Generic,<br>**2** = Ozone |

*This table is continued on the next page.*

Table E.7 – *Continued from previous page*

| № | Name | Type | Unit | Description |
|---|---|---|---|---|
| 35 | IsSimulated | boolean | – | True, if sounding is simulated from the UI. |
| 37 | PtuFindingType | string | – | PTU finding type: CompHeightFromPtu, CompPressureFromGpsHeightAndTu |
| 38 | SoundingType | string | – | |

**Table E.8:** List of all data columns of table **Radiosondes** of a MWX file. This table contains metadata, that means one row for one sounding.

| № | Name | Type | Unit | Description |
|---|---|---|---|---|
| 1 | SoundingIdPk | string | – | Randomly generated, unique sounding ID. |
| 2 | SerialNbr | string | – | Serial number. |
| 3 | SondeTypeFk | integer | – | Radiosonde type. |
| 4 | SondeFamily | string | – | Radiosonde family:<br>**0** = Undefined,<br>**1** = RS92,<br>**2** = RS41 |
| 5 | Eeprom | binary | – | Radiosonde EEPROM data. |
| 6 | Compatibility-Number | double | – | Radiosonde ground equipment minimum version number. |
| 7 | Configuration-Number | double | – | Radiosonde configuration number. |
| 8 | Frequency | double | MHz | Radiosonde frequency [MHz]. |
| 9 | WindFindingType | string | – | Wind finding type (e.g. ccGPS). |

**Table E.9:** List of all data columns of table **GCCORRECTIONS** of a MWX file. This table contains metadata, that means one (to three) row(s) for one sounding.

| № | Name | Type | Unit | Description |
|---|---|---|---|---|
| 1 | SoundingIdPk | string | – | Randomly generated, unique sounding ID. |

*This table is continued on the next page.*

Table E.9 – *Continued from previous page*

| № | Name | Type | Unit | Description |
|---|---|---|---|---|
| 2 | DataSrvTimePk | dateTime | – | Data server timestamp [yyyy-MM-ddHH:mm:ss.fff]. |
| 3 | PressureReference | double | hPa | Pressure reference [hPa]. |
| 4 | Temperature-Reference | double | K | Temperature reference [K]. |
| 5 | HumidityReference | double | % | Humidity reference [%]. |
| 6 | UserPressure-Reference | double | hPa | User-set pressure reference [hPa]. |
| 7 | UserTemperature-Reference | double | K | User-set temperature reference [K]. |
| 8 | UserHumidity-Reference | double | % | User-set humidity reference [%]. |
| 9 | SondePressure | double | hPa | Radiosonde pressure [hPa]. |
| 10 | SondeTemperature | double | K | Radiosonde temperature [K]. |
| 11 | SondeHumidity1 | double | % | Radiosonde humidity 1 [%]. |
| 12 | SondeHumidity2 | double | % | Radiosonde humidity 2 [%]. |
| 13 | PressureDiffLimit | double | hPa | Limit for pressure correction [hPa]. |
| 14 | TemperatureDiff-Limit | double | deg | Limit for temperature correction [degrees]. |
| 15 | HumidityDiffLimit | double | % | Limit for humidity correction [%]. |

**Table E.10:** List of all data columns of table **SurfaceObservations** of a MWX file. This table contains metadata, that means one row for one sounding.

| № | Name | Type | Unit | Description |
|---|---|---|---|---|
| 1 | SoundingIdPk | string | – | Randomly generated, unique sounding ID. |
| 2 | DataSrvTimePk | dateTime | – | Data server timestamp [yyyy-MM-ddHH:mm:ss.fff]. |
| 3 | Pressure | double | hPa | Pressure [hPa]. |
| 4 | LaunchSitePressure | double | hPa | Launch site pressure [hPa]. |
| 5 | Temperature | double | K | Temperature [K]. |

*This table is continued on the next page.*

Table E.10 – *Continued from previous page*

| № | Name | Type | Unit | Description |
|---|---|---|---|---|
| 6 | Humidity | double | % | Humidity [%]. |
| 7 | WindDirection | double | deg | Wind direction [deg]. |
| 8 | WindSpeed | double | m/s | Wind speed [m/s]. |
| 9 | CloudGroup | string | – | WMO cloud group for TEMP and BUFR. |
| 10 | SpecialGroup1 | string | – | Optional special group 1 for weather messages. |
| 11 | SpecialGroup2 | string | – | Optional special group 2 for weather messages. |
| 12 | AsapStatus | integer | – | ASAP status for TEMP SHIP. |
| 13 | SeaWater-Temperature | double | K | Temperature of sea water for TEMP SHIP. |
| 14 | Source | integer | – | Surface observation source:<br>**0** = Manual,<br>**1** = Radiosonde,<br>**2** = AWS |
| 15 | Mode | integer | – | Surface observation mode:<br>**0** = AWS auto,<br>**1** = AWS manual before release,<br>**2** = AWS manual after release,<br>**3** = Radiosonde manual,<br>**4** = Radiosonde auto,<br>**5** = Manual before release,<br>**6** = Manual after release |
| 16 | WeatherCode | string | – | Optional weather code WWWW. |
| 17 | Previous-Temperature | double | K | Optional previous temperature [K]. |
| 18 | Dewpoint-Temperature | double | K | Optional surface dewpoint temperature [K]. |
| 19 | WetBulb-Temperature | double | K | Optional surface wet-bulb temperature [K]. |
| 20 | DryBulb-Temperature | double | K | Optional surface dry-bulb temperature [K]. |

# Nomenclature

| | |
|---|---|
| $\Delta p$ | Pressure difference, hPa, Eq. (4.30), p. 78 |
| $\Delta p_{\mathrm{GC}}$ | Pressure difference detected during manufacturer ground check, hPa, p. 31 |
| $\Delta T$ | Radiative heating of temperature sensor, K, p. 54 |
| $\Delta T_{\mathrm{GC}}$ | Temperature difference detected during manufacturer ground check, K, p. 31 |
| $\Delta U$ | Correction of relative humidity due to sensor time lag, %RH, Eq. (4.19), p. 71 |
| $\Delta U_{\mathrm{GC}}$ | Relative humidity difference detected during manufacturer ground check, %RH, p. 31 |
| $\epsilon_r$ | Effective dielectric constant, $\mathrm{F\,m^{-1}}$, Eq. (2.1), p. 20 |
| $\lambda$ | Longitude, °, Eq. (4.68), p. 97 |
| $\lambda_{\mathrm{R}}$ | GPS-derived longitude, °, Eq. (4.40), p. 83 |
| IWV | Integrated water vapour, $\mathrm{kg\,m^{-2}}$, Eq. (4.80), p. 99 |
| PWV | Precipitable water vapour, mm, Eq. (4.81), p. 99 |
| SZA | Sun Zenith Angle, °, Eq. (4.7), p. 67 |
| $\phi$ | Latitude, °, p. 61 |
| $\phi_{\mathrm{R}}$ | GPS-derived latitude, °, Eq. (4.40), p. 83 |
| $\rho_{\mathrm{lw}}$ | Density of liquid water, $\mathrm{kg\,m^{-3}}$, Eq. (4.81), p. 99 |
| $\rho_{\mathrm{w}}$ | Water vapour density, $\mathrm{kg\,m^{-3}}$, Eq. (4.80), p. 99 |
| $\sigma$ | Standard deviation, Eq. (3.3), p. 43 |
| $\tau$ | '63 %'-response time (humidity sensor), s, Eq. (4.20), p. 74 |
| $\theta$ | Horizontal wind direction, °, p. 93 |
| $\vec{w}_{\mathrm{hor}}$ | Horizontal wind vector, $\mathrm{m\,s^{-1}}$, Eq. (4.60), p. 93 |
| $e$ | Water vapour pressure, Pa, Eq. (2.2), p. 21 |
| $e_{\mathrm{d}}$ | Vapour pressure at the dew point, Pa, Eq. (2.2), p. 21 |
| $e_{\mathrm{s}}$ | Saturation vapour pressure, Pa, Eq. (2.2), p. 21 |
| $f_\lambda$ | Factor to convert longitude from degree to meter, m/°, p. 97 |
| $f_{\mathrm{sc}}$ | Altitude-dependent scaling factor, Eq. (4.10), p. 67 |
| $f_\phi$ | Factor to convert latitude from degree to meter, m/°, p. 97 |
| $g$ | Gravitational acceleration, $\mathrm{m\,s^{-2}}$, Eq. (4.48), p. 87 |
| $g_0$ | Gravitational acceleration at the launch point, $\mathrm{m\,s^{-2}}$, Eq. (4.56), p. 90 |
| $h$ | Height (geometric or geopotential, see context), m, Eq. (4.53), p. 88 |
| $h_0$ | Height at the launch point, m, Eq. (4.53), p. 88 |
| $h_{\mathrm{R}}$ | GPS-derived altitude, m, Eq. (4.39), p. 83 |
| $I$ | Irradiance, $\mathrm{W\,m^{-2}}$, p. 54 |
| $I_{\mathrm{dif}}$ | Simulated diffuse radiation flux, $\mathrm{W\,m^{-2}}$, Eq. (4.4), p. 66 |
| $I_{\mathrm{dir}}$ | Simulated direct radiation flux, $\mathrm{W\,m^{-2}}$, Eq. (4.4), p. 66 |
| $I_{\mathrm{eff}}$ | Irradiance at location of temperature sensor, $\mathrm{W\,m^{-2}}$, Eq. (4.0), p. 55 |
| $I_{\mathrm{n}}$ | Normalised irradiance ($1000\,\mathrm{W\,m^{-2}}$), Eq. (4.7), p. 67 |

| | |
|---|---|
| $I_{\mathrm{RTM}}$ | Modelled irradiance from the Streamer Radiative Transfer Model (RTM), W m$^{-2}$, Eq. (4.7), p. 67 |
| $k$ | Coverage factor, Eq. (1.1), p. 14 |
| $M_{\mathrm{a}}$ | Molar mass of dry air, g mol$^{-1}$, Eq. (4.48), p. 87 |
| $M_{\mathrm{w}}$ | Molar mass of water, g mol$^{-1}$, Eq. (4.87), p. 101 |
| $N$ | Number of data points included, Eq. (3.3), p. 43 |
| $p$ | Pressure, hPa or Pa |
| $p_{\mathrm{s}}$ | Pressure from radiosonde sensor during sounding, hPa, Eq. (4.29), p. 77 |
| $r$ | Water vapour mass mixing ratio, kg kg$^{-1}$, Eq. (4.87), p. 101 |
| $R_{\mathrm{e}}$ | Earth radius, m, Eq. (4.47), p. 87 |
| $R_{\mathrm{d}}$ | Specific gas constant of dry air, J kg$^{-1}$ K$^{-1}$, Eq. (4.48), p. 87 |
| $R_{\mathrm{u}}$ | Molar gas constant of dry air, J mol$^{-1}$ K$^{-1}$, Eq. (4.48), p. 87 |
| $T$ | Temperature, °C or K |
| $t$ | Time, s, Eq. (4.1), p. 58 |
| $T_0$ | Temperature at ice point (0 °C), Eq. (4.22), p. 74 |
| $T_{\mathrm{d}}$ | Dew point temperature, K or °C, Eq. (2.2), p. 21 |
| $T_{\mathrm{int}}$ | Internal temperature of the heated humidity sensor, °C, Eq. (4.23), p. 75 |
| $T_{\mathrm{R}}$ | Rotation period, s, Eq. (4.0), p. 55 |
| $T_{\mathrm{v}}$ | Virtual temperature, K, Eq. (4.51), p. 87 |
| $U$ | Relative humidity, %RH or rel. units |
| $u$ | Measurement uncertainty; within the GDP generally to be taken as standard uncertainty assuming normal distribution of the measured quantity values. Information on the origin of an uncertainty will be indicated by appropriate subscripts. |
| $U_{\mathrm{air}}$ | Relative humidity of air, %RH, Eq. (4.76), p. 98 |
| $u_{\mathrm{cal}}$ | Calibration and ground check related uncertainty (Section 6) |
| $U_{\mathrm{int}}$ | Internal relative humidity at internal temperature of heated humidity sensor, %RH, Eq. (4.76), p. 98 |
| $u_{\mathrm{scor}}$ | Spatially correlated uncertainty (Section 6.1) |
| $u_{\mathrm{sm}}$ | Uncertainty related to smoothing (Section 6 and Appendix A.3) |
| $u_{\mathrm{tcor}}$ | Temporally correlated uncertainty (Section 6.1) |
| $u_{\mathrm{ucor}}$ | Uncorrelated uncertainty (Section 6.1) |
| $u_{\mathrm{gp}}$ | Combined uncertainty after ground preparation, p. 38 |
| $u_{\mathrm{w}}$ | Zonal wind component (no uncertainty!), m s$^{-1}$, Eq. (4.59), p. 93 |
| $v$ | Ventilation speed (total air speed at which the radiosonde is ventilated), m s$^{-1}$, Eq. (4.0), p. 55 |
| $v_{\mathrm{w}}$ | Meridional wind component, m s$^{-1}$, Eq. (4.59), p. 93 |
| $w_{\mathrm{hor}}$ | Horizontal wind speed, m s$^{-1}$, Eq. (4.61), p. 93 |
| $x_v$ | Volume mixing ratio, also pressure ratio, m$^3$ m$^{-3}$, Eq. (4.89), p. 103 |
| $z$ | Altitude, m, Eq. (4.10), p. 67 |

# Acronyms

| | |
|---|---|
| **Apache** | Apache Software Foundation |
| **API** | Application Programming Interface |
| **ASCII** | American Standard Code for Information Interchange |
| **BUFR** | Binary Universal Form for the Representation of meteorological data |
| **BIPM** | International Bureau of Weights and Measures (French: Bureau International des Poids et Mesures) |
| **CIAO** | CNR-IMAA Atmospheric Observatory |
| **CF** | Climate and Forecast |
| **CNR** | National Research Council, Italy |
| **DC3DB** | Vaisala DigiCora3 Data Base file format |
| **DOP** | Dilution of Precision |
| **DWD** | Deutscher Wetterdienst |
| **ECC** | Electrochemical Concentration Cell |
| **ECV** | Essential Climate Variable |
| **EGM96** | Earth Gravitational Model 1996 |
| **EGM2008** | Earth Gravitational Model 2008 |
| **EPS** | Expanded Polystyrene |
| **FTP** | File Transfer Protocol |
| **GC** | Ground Check |
| **GCOS** | Global Climate Observing System |
| **GDP** | GRUAN Data Product |
| **GDPS** | GRUAN Data Processing System for radiosondes |
| **GMD** | GRUAN Meta-Data |
| **GMDB** | GRUAN Meta-data Data Base |
| **GNSS** | Global Navigation Satellite System |
| **GPS** | Global Positioning System |
| **GRUAN** | GCOS Reference Upper-Air Network |
| **GUM** | Guide to the Expression of Uncertainty in Measurement |
| **GTS** | Global Telecommunication System |
| **GUAN** | GCOS Upper-Air Network |
| **HDOP** | Horizontal Dilution of Precision |
| **IBM** | International Business Machines Corporation |
| **ID** | Identifier |
| **IDL** | Interactive Data Language |
| **IGS** | International GNSS Service |
| **IMAA** | Institute of Methodologies for Environmental Analysis |
| **ISO** | International Organization for Standardization |
| **ITS-90** | International Temperature Scale of 1990 |
| **IWV** | Integrated Water Vapour |

| | |
|---|---|
| **IronPython** | Python programming language for the .NET Framework |
| **LAN** | Local Area Network |
| **LC** | Lead Centre |
| **LAN** | Local Area Network |
| **LDA** | Laser Doppler Anemometry |
| **LUT** | Look-Up Table |
| **MD** | Meta-Data |
| **MSL** | Mean Sea Level |
| **MWX** | Zipped MW41 sounding archive file |
| **NaN** | Not a Number |
| **NetCDF** | Network Common Data Format |
| **NFC** | Near Field Communication |
| **NIST** | National Institute of Standards and Technologies |
| **NOAA** | National Oceanic and Atmospheric Administration |
| **NWF** | National Weather Forecast |
| **OIF411** | Vaisala Ozone Interface RS41 |
| **PC** | Processing Centre |
| **PID** | Proportional Integral Derivative |
| **PNG** | Portable Network Graphics |
| **PRT** | Platinum Resistance Thermometer |
| **PRN** | Pseudo-random Noise |
| **PWV** | Precipitable Water Vapour |
| **PW** | Precipitable Water |
| **QTF** | Quality Task Force |
| **RSA411** | Vaisala Ozone Interface Kit RS41 |
| **RTM** | Radiative Transfer Model |
| **SHC** | Standard Humidity Chamber |
| **SI** | International System of Units |
| **SISTER** | Simulator for Investigation of Solar Temperature Error of Radiosondes |
| **SPS** | Signal Processing System |
| **SZA** | Sun Zenith Angle |
| **TCWV** | Total Column Water Vapour |
| **TT** | Task Team |
| **USB** | Universal Serial Bus |
| **USNO** | United States Naval Observatory |
| **UTC** | Coordinated Universal Time |
| **UTLS** | Upper Troposphere / Lower Stratosphere |
| **VDOP** | Vertical Dilution of Precision |
| **VIM** | International Vocabulary of Metrology |
| **WGS84** | World Geodetic System 1984 |
| **WMO** | World Meteorological Organization |
| **XML** | Extensible Markup Language |

# Bibliography

Bodeker, G. E., *et al.*, Reference Upper-Air Observations for Climate: From Concept to Reality, *Bulletin of the American Meteorological Society*, **97**(1), 123–135, https://doi.org/10.1175/BAMS-D-14-00072.1, 2016, ISSN 0003-0007.

Bugayevskiy, L. and J. Snyder, *Map Projections – A Reference Manual* (CRC Press, 1995), 1st edition, ISBN 9780429159848, 352 pp., https://doi.org/10.1201/b16431.

Dirksen, R. J., *et al.*, Reference quality upper-air measurements: GRUAN data processing for the Vaisala RS92 radiosonde, *Atmospheric Measurement Techniques*, **7**, 4463–4490, https://doi.org/10.5194/amt-7-4463-2014, 2014.

Fassò, A., M. Sommer, and C. von Rohden, Interpolation uncertainty of atmospheric temperature profiles, *Atmospheric Measurement Techniques*, **13**(12), 6445–6458, https://doi.org/10.5194/amt-13-6445-2020, 2020, URL https://amt.copernicus.org/articles/13/6445/2020/.

GCOS-134, GRUAN Implementation Plan 2009–2013, Technical report, GCOS, WMO Integrated Global Observing System (WIGOS), 2009, URL https://library.wmo.int/opac/doc_num.php?explnum_id=3847, WMO/TD No. 1506.

GCOS-170, The GCOS Reference Upper-Air Network (GRUAN) Manual, Technical report, GCOS, WMO Integrated Global Observing System (WIGOS), 2013, URL http://library.wmo.int/pmb_ged/gcos_170.pdf, version 1.1.0.3, 2013-02.

GCOS-171, The GCOS Reference Upper-Air Network (GRUAN) Guide, Technical report, GCOS, 2013, URL https://library.wmo.int/doc_num.php?explnum_id=7196, version 1.1, 2013-03.

GCOS-226, GCOS Surface Reference Network (GSRN): Justification, requirements, siting and instrumentation options, Technical report, GCOS, WMO Integrated Global Observing System (WIGOS), 2019, URL https://library.wmo.int/doc_num.php?explnum_id=6261, WMO/TD No. 1506.

Hardy, B., ITS-90 Formulations for Vapor Pressure, Frostpoint Temperature, Dewpoint Temperature, and Enhancement Factors in the Range $-100$ to $+100$ °C, in *Proceedings of the Third International Symposium on Humidity & Moisture, Teddington, London, England, April 1998* (1998).

Hyland, R. W. and A. Wexler, Formulations for the thermodynamic properties of the saturated phases of $H_2O$ from 173.15 K to 473.15 K, *ASHRAE Transaction*, **89**(2), 500–520, 1983.

Jauhiainen, H., J. Lentonen, P. Survo, R. Lehtinen, and T. Pietari, The Implications of Vaisala's new Radiosonde RS41 on Improved in-situ Observations for Meteorological Applications, in *94th American Meteorological Society Annual Meeting, Atlanta, GA, USA* (American Meteorological Society, 2014).

JCGM, *Evaluation of measurement data – Guide to the expression of uncertainty in measurement* (JCGM, 2008), 1st edition, URL https://www.bipm.org/en/publications/guides/gum.html, last accessed: May 04, 2020.

JCGM, *The international vocabulary of metrology—basic and general concepts and associated terms (VIM), JCGM 200:2012* (JCGM, 2012), 3rd edition, URL http://www.bipm.org/en, last accessed: May 25, 2021.

Karlsson, K.-G., *et al.*, CLARA-A2: CM SAF cLoud, Albedo and surface RAdiation dataset from AVHRR data - Edition 2, Satellite Application Facility on Climate Monitoring (CM SAF), 2017, https://doi.org/10.5676/EUM_SAF_CM/CLARA_AVHRR/V002, Format: NetCDF v4, Size: 12.4 TiB.

Key, J. R. and A. J. Schweiger, Tools for atmospheric radiative transfer: Streamer and FluxNet, *Computers & Geosciences*, **24**(5), 443 – 451, https://doi.org/10.1016/S0098-3004(97)00130-1, 1998, ISSN 0098-3004.

Kish, L., *Survey Sampling* (Wiley, New York, 1965), ISBN 0-471-48900-X.

Kizu, N., *et al.*, Technical characteristics and GRUAN data processing for the Meisei RS-11G and iMS-100 radiosondes, GRUAN Technical Document 5, GRUAN, 2018, URL https://www.gruan.org/documentation/gruan/td/graun-td-5/.

Madonna, F., *et al.*, Use of automatic radiosonde launchers to measure temperature and humidity profiles from the GRUAN perspective, *Atmospheric Measurement Techniques*, **13**(7), 3621–3649, https://doi.org/10.5194/amt-13-3621-2020, 2020.

Matsakis, D., J. Levine, and M. Lombardi, Metrological and legal traceability of time signals, in *Proceedings of the 49th Annual Precise Time and Time Interval Systems and Applications Meeting*, pp. 59–71 (2018).

Miloshevich, L. M., A. Paukkunen, H. Vömel, and S. J. Oltmans, Development and Validation of a Time-Lag Correction for Vaisala Radiosonde Humidity Measurements, *Journal of Atmospheric and Oceanic Technology*, **21**(9), 1305–1327, https://doi.org/10.1175/1520-0426(2004)021¡1305:DAVOAT¿2.0.CO;2, 2004.

NOAA, Vaisala ES41 Soft & Light Assessment Report, Technical report, U.S. Department of Commerce, NOAA, NWS, 2017, prepared by Sterling Field Support Center, Ref. TP-003.00-UA-2017Rn.

Oelsner, P. and R. Tietz, GRUAN Monitor MW41 and the Vaisala RS41 Additional Sensor Interface, GRUAN Technical Note 8 (GRUAN-TN-8), GRUAN Lead Centre, 2021, URL https://www.gruan.org/documentation/gruan/tn/gruan-tn-8, v1.3 (2021-02-18).

Pavlis, N. K., S. A. Holmes, S. C. Kenyon, and J. K. Factor, The development and evaluation of the Earth Gravitational Model 2008 (EGM2008), *Journal of geophysical research: solid earth*, **117**(B4), 2012.

Reda, I. and A. Andreas, Solar position algorithm for solar radiation applications, Technical Report TP-560-34302, revised January 2008, NREL, 2003, https://doi.org/10.2172/15003974.

Reda, I. and A. Andreas, Solar position algorithm for solar radiation applications, *Solar Energy*, **76**(5), 577–589, https://doi.org/10.1016/j.solener.2003.12.003, 2004, ISSN 0038-092X.

von Rohden, C., M. Sommer, T. Naebert, V. Motuz, and R. Dirksen, Laboratory characterisation of the radiation temperature error of radiosondes and its application to the GRUAN data processing for the Vaisala RS41, *Atmospheric Measurement Techniques*, **15**, 383–405, https://doi.org/10.5194/amt-15-383-2022, 2022.

Seidel, D. J., *et al.*, Reference Upper-Air Observations for Climate: Rationale, Progress, and Plans, *Bulletin of the American Meteorological Society*, **90**(3), 361–369, https://doi.org/10.1175/2008BAMS2540.1, 2009, ISSN 0003-0007.

Snyder, J. P., *Map projections - A working manual*, volume 1395 (US Government Printing Office, 1987).

Sommer, M., User Guide for the GRUAN RsLaunchClient, GRUAN Technical Document 3 (GRUAN-TD-3), GRUAN Lead Centre, 2014, URL https://www.gruan.org/documentation/gruan/td/gruan-td-3, v0.7 (2014-02-05).

Sommer, M., Brief Description of GruanToolRs92 (gt92), GRUAN Technical Note 11 (GRUAN-TN-11), GRUAN Lead Centre, 2020a, URL https://www.gruan.org/documentation/gruan/tn/gruan-tn-11, v1.0 (2020-10-01).

Sommer, M., Brief Description of GruanToolRsLaunch (gtRsl), GRUAN Technical Note 6 (GRUAN-TN-6), GRUAN Lead Centre, 2020b, URL https://www.gruan.org/documentation/gruan/tn/gruan-tn-6, v1.0 (2020-08-24).

Sommer, M., Brief Description of GRUAN Meta-Data (GMD) Files, 2023a, DRAFT v0.1.3 (2023-06-12), in preparation.

Sommer, M., Brief Description of GRUAN NetCDF Radiosonde Raw Data Files (GNC-RAW), 2023b, DRAFT v0.1.2 (2023-06-09), in preparation.

Sommer, M., R. Dirksen, and C. von Rohden, Brief Description of the RS92 GRUAN Data Product (RS92-GDP), GRUAN Technical Document 4 (GRUAN-TD-4), GRUAN Lead Centre, 2021, URL https://www.gruan.org/documentation/gruan/td/gruan-td-4, v2.1.1 (2021-07-14).

Sommer, M. and C. von Rohden, GRUAN Data Processing System (GDPS) for Radiosoundings, 2023, DRAFT v0.1.5 (2023-05-30), in preparation.

Sommer, M., C. von Rohden, and T. Simeonov, User Guide of the RS41 GRUAN Data Product Version 1 (RS41-GDP.1), GRUAN Technical Note 13 (GRUAN-TN-13), GRUAN Lead Centre, 2022, URL https://www.gruan.org/documentation/gruan/td/gruan-tn-13, v1.0 (2022-11-21).

Survo, P., *et al.*, Atmospheric Temperature and Humidity Measurements of Vaisala Radiosonde RS41, in *WMO Technical Conference on Meteorological and Environmental Instruments and Methods of Observations. Saint Petersburg, Russian Federation, 07-09 July 2014, P3(16), IOM Report, 116*, WMO (WMO, 2014), URL https://library.wmo.int/pmb_ged/iom_116_en/Session%202/P2_7_Survo_SITraceabilityRS41Data.pdf.

ublox, NEO-6 u-blox 6 GPS Modules Data Sheet, 2013a, URL https://www.u-blox.com/sites/default/files/products/documents/NEO-6_DataSheet_%28GPS.G6-HW-09005%29.pdf.

ublox, u-blox 6 Receiver Description Including Protocol Specification, 2013b, URL https://www.u-blox.com/sites/default/files/products/documents/u-blox6_ReceiverDescrProtSpec_%28GPS.G6-SW-10018%29_Public.pdf.

Vaisala, GPS-Based Measurement of Height and Pressure with Vaisala Radiosonde RS41, White Paper Ref. B211316EN-A, Vaisala Oyj, Helsinki, Finland, 2013, URL https://www.vaisala.com/sites/default/files/documents/GPS-Based%20Measurement%20of%20Height%20and%20Pressure%20with%20Vaisala%20Radiosonde%20RS41%20White%20Paper%20B211316EN.pdf, ©Vaisala.

Vaisala, Vaisala Radiosonde RS41-SGP – Pressure Measurement Performance, White Paper Ref. B211431EN-A, Vaisala Oyj, Helsinki, Finland, 2014, ©Vaisala.

Vaisala, User's Guide – Vaisala Radiosonde RS41 Additional Sensor Interface, User Guide Ref. M211604EN-C, Vaisala Oyj, Helsinki, Finland, 2015a, ©Vaisala.

Vaisala, Vaisala Radiosonde RS41-SGP, Data Sheet Ref. B211444EN-C, Vaisala Oyj, Helsinki, Finland, 2015b, ©Vaisala.

Vaisala, Vaisala Radiosonde RS41 White Paper – Ground Check Device RI41, White Paper Ref. B211539EN-A, Vaisala Oyj, Helsinki, Finland, 2016, URL https://www.vaisala.com/sites/default/files/documents/White%20paper%20Ground%20Check%20of%20RS41%20B211539EN-A.pdf, ©Vaisala.

Vaisala, Automatic Sounding Station Vaisala AUTOSONDE®, Data Sheet Ref. B210402EN-G, Vaisala Oyj, Helsinki, Finland, 2017a, URL https://www.vaisala.com/sites/default/files/documents/AS15-Datasheet-B210402EN-G.pdf, ©Vaisala.

Vaisala, Vaisala Radiosonde RS41 Cover Improvement, White Paper Ref. B211661EN-A, Vaisala Oyj, Helsinki, Finland, 2017b, URL https://www.vaisala.com/sites/default/files/documents/Cover%20Improvement%20to%20RS41%20White%20paper%20B211661EN-A.PDF, ©Vaisala.

Vaisala, Vaisala Radiosonde RS41 Measurement Performance, White Paper Ref. B211356EN-B, Vaisala Oyj, Helsinki, Finland, 2017c, URL https://www.vaisala.com/sites/default/files/documents/WEA-MET-RS41-Performance-White-paper-B211356EN-B-LOW-v3.pdf, ©Vaisala.

Vaisala, Vaisala Radiosonde RS41 White Paper – Vaisala Radiosonde RS41 Calibration Traceability and Uncertainty, White Paper Ref. B211374EN-B, Vaisala Oyj, Helsinki, Finland, 2017d, ©Vaisala.

Vaisala, Product Description – Vaisala Automatic Sounding Station AUTOSONDE AS15, Product Description Ref. M211830EN-C, Vaisala Oyj, Helsinki, Finland, 2018a, ©Vaisala.

Vaisala, User Guide – Vaisala Radiosonde RS41-SG and RS41-SGP, User Guide Ref. M211667EN-G, Vaisala Oyj, Helsinki, Finland, 2018b, URL https://www.vaisala.com/sites/default/files/documents/Vaisala%20Radiosonde%20RS41-SG%20and%20RS41-SGP%20User%20Guide%20M211667EN-G.pdf, ©Vaisala.

Vaisala, User Guide – Ozone Sounding with Vaisala Radiosonde RS41, User Guide Ref. M211486EN-E, Vaisala Oyj, Helsinki, Finland, 2019, ©Vaisala.

Vaisala, IronPython scripts in the sounding system, 2020a, ©Vaisala.

Vaisala, Online Help – Vaisala DigiCORA® Sounding System MW41, Product Description Ref. M211428EN-W, Vaisala Oyj, Helsinki, Finland, 2020b, ©Vaisala.

Vaisala, Product Description – Vaisala DigiCORA® Sounding System MW41, Product Description Ref. M211397EN-S, Vaisala Oyj, Helsinki, Finland, 2020c, ©Vaisala.

Vaisala, Technical Reference – Vaisala DigiCORA® Sounding System MW41, Technical Reference Ref. M211415EN-Y, Vaisala Oyj, Helsinki, Finland, 2020d, ©Vaisala.

Vaisala, Vaisala Radiosonde RS41-SGP, Data Sheet Ref. B211444EN-H, Vaisala Oyj, Helsinki, Finland, 2020e, URL https://www.vaisala.com/sites/default/files/documents/RS41-SGP-Datasheet-B211444EN.pdf, ©Vaisala.

Vaisala, Automatic Sounding Station Vaisala AUTOSONDE® AS41, Data Sheet Ref. B211636EN-C, Vaisala Oyj, Helsinki, Finland, 2021a, URL https://www.vaisala.com/sites/default/files/documents/AS41-Datasheet-B211636EN.pdf, ©Vaisala.

Vaisala, Ground Check Device RI41/RI41-B, Data Sheet Ref. B211322EN-D, Vaisala Oyj, Helsinki, Finland, 2021b, URL https://www.vaisala.com/sites/default/files/documents/RI41-Datasheet-B211322EN.pdf, ©Vaisala.

Vaisala, Vaisala Sounding System MW41, Data Sheet Ref. B211221EN-K, Vaisala Oyj, Helsinki, Finland, 2021c, URL https://www.vaisala.com/sites/default/files/documents/MW41-Datasheet-B211221EN.pdf, ©Vaisala.

Vincenty, T., Direct and inverse solutions of geodesics on the ellipsoid with application of nested equations, in *Survey Review, XXII*, 176, pp. 88–93 (Directorate of Overseas Surveys of the Ministry of Overseas Development, 1975), URL http://www.ngs.noaa.gov/PUBS_LIB/inverse.pdf.

Wendell, J. and A. Jordan, iMet-1-RSB Radiosonde XDATA Protocol & Daisy Chaining, Technical report, NOAA, 2016, URL https://gml.noaa.gov/aftp/user/jordan/iMet-1-RSB%20Radiosonde%20XDATA%20Daisy%20Chaining.pdf, v1.3 (2016-01-26).